SYNTHESIS, CHARACTERIZATION, AND PURIFICATION OF CYCLIC POLYSTYRENE, POLY(ε-CAPROLACTONE), AND VARIOUS POLYETHERS

AN ABSTRACT

SUBMITTED ON THE 19TH DAY OF JULY 2019

TO THE DEPARTMENT OF CHEMISTRY

IN PARTIAL FULFILLMENT OF THE REQUIREMENTS

OF THE SCHOOL OF SCIENCE AND ENGINEERING

OF TULANE UNIVERSITY

FOR THE DEGREE OF

DOCTOR OF PHILOSOPHY

BY

FARIHAH MARYAM HAQUE

APPROVED: _____
JULIE N.L. ALBERT, Ph.D.

APPROVED: _____
BRUCE C. GIBB, Ph.D.

APPROVED: _____
JAMES P. DONAHUE, Ph.D.

APPROVED: _____
SCOTT M. GRAYSON, Ph.D.

ABSTRACT

The synthesis of cyclic polymers has become popularized due to improved synthetic chemistry increasing access to architecturally well-defined polymers. Since their discovery, many studies have been performed describing their physical properties in solution and bulk, and as confined thin films. Also, their electronic, biomedical, and self-assembly behavior has been characterized for advanced biomedical and industrial applications. Herein, some of the ongoing shortcomings within the cyclic polymer field are addressed by a detailed analysis of cyclic polymers synthesized through: 1) the copper(I)-catalyzed azide-alkyne cycloaddition (CuAAC) "click" ring closure method, and; 2) the electrophilic zwitterionic ring expansion polymerization (eZREP).

First, cyclic polystyrene synthesized via CuAAC is investigated to source potential impurities using a series of analytical tools including HPLC for fractionation and MALDI-ToF MS for characterization of the linear precursor and cyclic product. It was ascertained that the linear precursor undergoes uncatalyzed azide alkyne dimerization during storage, resulting in a linear dimer that retains an azide and alkyne group. Consequently, post-cyclization the sample has a high cyclic architectural purity with small amounts of cyclic dimers. With this same CuAAC cyclization, cyclic polycaprolactone was generated to fabricate thin films (~100 nm). The CuAAC cyclization was performed using an optimized synthesis, where the azide was coupled to the linear precursor directly prior to cyclization to minimize the opportunity for dimerization. Both the linear and cyclic polymers made

stable as-cast films, but only the cyclic polymer maintained a stable film after recrystallization as demonstrated by its resistance to dewetting. Moreover, the linear polymer dewet after recrystallization regardless of end group, suggesting that architecture provides a larger influence on thin film stability than end group effects.

Finally, towards understanding the ring expansion method, eZREP has been investigated to generate pure cyclic polyethers by polymerizing monosubstituted epoxides with $B(C_6F_5)_3$. While the major component was the cyclic structure, in most cases, there was still a contribution of impurities arising from non-cyclic structures (e.g., tadpole and linear architectures). Using primarily MALDI-ToF MS, it was ascertained that most impurities had free hydroxyl groups that could be alkynylated, "clicked" onto a solid phase azidified resin, and then filtered to remove resin-bound impurities. This allowed for a facile method of making pure cyclic materials in two reactions (i.e. polymerization and "click" scavenging purification). Finally, the origin of the impurities was further explored, elucidating that when glycidyl ether-based monomers were polymerized, there was competition between the boron coordinating with the epoxide oxygen to polymerize, and boron coordination with the ether oxygen to generate non-cyclic derivatives. The polymerization was improved by using monomers that either did not contain the glycidyl ether oxygen (e.g. alkyl groups) or adding electron withdrawing groups to deactivate the glycidyl ether oxygen, yielding greater amounts of cyclic polymer and fewer side reactions.

The goal of this work is to garner interest in cyclic polymers by increasing accessibility of these compounds by addressing the primary deficiencies of the CuAAC and eZREP methods for the synthesis of cyclic polymers, while bringing attention to the concern of cyclic polymer purity, arguably the largest concern within the cyclic polymer

community. Through these advancements, continued efforts will be made to make novel cyclic materials for unique biomedical and industrial applications.

SYNTHESIS, CHARACTERIZATION, AND PURIFICATION OF CYCLIC POLYSTYRENE, POLY(ε-CAPROLACTONE), AND VARIOUS POLYETHERS

A DISSERTATION

SUBMITTED ON THE 19TH DAY OF JULY 2019

TO THE DEPARTMENT OF CHEMISTRY

IN PARTIAL FULFILLMENT OF THE REQUIREMENTS

OF THE SCHOOL OF SCIENCE AND ENGINEERING

OF TULANE UNIVERSITY

FOR THE DEGREE OF

DOCTOR OF PHILOSOPHY

BY

FARIHAH MARYAM HAQUE

APPROVED: JULIE N.L. ALBERT, Ph.D.

APPROVED: BRUCE C. GIBB, Ph.D.

APPROVED: JAMES P. DONAHUE, Ph.D.

APPROVED: SCOTT M. GRAYSON, Ph.D.

ACKNOWLEDGEMENTS

This endeavor was very trying at times, but I am filled with gratitude for all who endured this path with me, encouraging me, even on days I doubted myself most. I must first thank my committee, Dr. Scott Grayson, Dr. Julie Albert, Dr. Bruce Gibb, and Dr. James Donahue, for believing in me and my work, and for taking a chance on me.

This feat would be impossible without my advisor, Scott. Thank you for opening my eyes to the scientific community, sharing your love of pure science, and teaching me that great science is only possible through a collective effort. You showed me that the scientific world is a complex place with vast opportunities, but through your endless advice and encouragement, you pushed me to be a better scientist with a skillset that will allow me to maneuver my future. I am thankful for all my collaborative ventures, and through your help and inspiration, I was able to realize that I am part of a larger scientific community and that is very special to me. These past years were not easy, but you continued to be our great mentor, and for that, I will always be thankful.

To my many collaborators and academic mentors, thank you for your time, patience, and energy. You have taught me the beauty and merit of working together - we are better together! Bruce, I appreciate all your support, especially this last year, providing the career advice and mentorship I needed when Scott was out. Dr. Fabienne Barroso, thank you for your mentorship and friendship. I am proud of our work and even happier that it has allowed me to come to Donostia, a city that I will always be fond of. To my

Loyola professors, a heartfelt thank you for inspiring me – you are the reason for my love of chemistry. Dr. Kurt Birdwhistell, you truly inspired me as a young scientist, especially the way you talked so fondly of grad school. I remember being a once polymer-obsessed undergrad and you told me to "broaden my horizons" – for some reason, I still carry these words with me, and while I'm still a polymer chemist, I think I managed to do that. I wish you were here for my defense; I think you would be happy with what I've done at Tulane.

To my coworkers, past and present, especially my senior colleagues Boyu, Ravi, and Karolina – thank you for your time and willingness to answer my endless questions. We stand on the shoulders of giants, and with your help, I have come this far. Molly – we started this road together, and I am proud of how we worked together this last year. Finally, I want to thank my Grayson group family including McKenna, Pelumi, Chris, Jen, Ca'ra, Joe, and Brittany and of course Erin, our lab mom. Romain, an unofficial Grayson group member, I am thankful for our friendship – you made life a little easier and more fun in the lab.

To my family, especially my parents Ma and Baba, I love you dearly. I thank you for your unwavering support and love. To my grandparents, there are no words for my gratitude for your love, kindness, and sweet endless encouragement. Grandpa, I am very sorry you cannot be here today, but I know you would be proud of me and that fills me with so much joy.

Finally, to my friends, you are my confidantes, my rock stars, and my PhD would be impossible without you. You were there for me on my good days and bad. They say it takes a village to raise a child, but I think it takes a village to earn a PhD. Kate and Andie, our meeting in college was serendipitous, but it was like our friendship was fate, and you became the sisters that I never had. Chloe (and Judy), I am lucky to have lived with you

these past years, and I'm going to miss you and the cats so much. Finally, to all my friends from Donostia, you taught me so much about friendship and sincerity, and I walk through life a little differently because of you. Cheers to more coffee breaks and mate! Last but not least, to Xavier, I have many things to thank you for, but most of all making me believe that the impossible can be possible. As life takes us forward, we move in our separate directions, but time or space can never destroy the bond we have created. I love you all so much. Thank you for being yourself and loving me the way you have.

TABLE OF CONTENTS

LIST OF TABLES

LIST OF FIGURES

LIST OF SCHEMES

LIST OF ABBREVIATIONS

AFM	Atomic force microscopy
ATRP	Atom transfer radical polymerization
BGE	Benzyl glycidyl ether
Cl-PGE	4-Chlorophenyl glycidyl ether
Cl-SO	4-Chlorostyrene oxide
CuAAC	Copper-catalyzed alkyne-azide click
Đ	Dispersity (polymer distribution)
Da	Daltons (atomic mass units, g mol^{-1})
DCM	Dichloromethane
DMAP	4-Dimethylaminopyridine
ECH	Epichlorohydrin
EDC	1-Ethyl-3-(3-dimethylaminopropyl)carbodiimide
ETD	1,2-Epoxytetradecane
eZREP	Electrophilic zwitterionic ring expansion polymerization
F-SO	4-fluorostyrene oxide
GPC	Gel permeation chromatography
HPLC	High performance liquid chromatography
MALDI-TOF	Matrix assisted laser-desorption ionization—time of flight
MS	Mass spectrometry
M_n	*Number average molecular weight*
M_w	Weight average molecular weight
[m/z]	Mass-per-charge (mass spectrometry)
NMR	Nuclear magnetic resonance spectroscopy
PBA	Poly(butyl acrylate)
pDMAEMA	poly((2-dimethylamino)ethylmethacrylate)

PCL	Poly(ε-caprolactone)
PEG	Poly(ethylene glycol)
PEI	Polyethyleneimine
PEO	Poly(ethylene oxide)
PGE	Phenyl glycidyl ether
PI	Polyisoprene
PMDETA	N,N,N′,N″,N″-Pentamethyldiethylenetriamine
PS	Polystyrene
RAFT	Reversible addition-fragmentation chain-transfer polymerization
ROP	Ring opening polymerization
SEC	Size exclusion chromatography
SO	Styrene oxide
$\mathbf{T_c}$	Crystallization temperature
$\mathbf{T_g}$	Glass transition temperature
THF	Tetrahydrofuran
$\mathbf{T_m}$	Melting temperature
ZREP	Zwitterionic ring expansion polymerization

CHAPTER 1

CYCLIC POLYMERS: UNIQUE PROPERTIES AND POTENTIAL APPLICATIONS*

1.1 ABSTRACT

Cyclic polymers are differentiated from the more common linear polymers by their ring-like structure and their lack of chain ends. Because of their cyclic topology, cyclic polymers exhibit a unique set of properties when compared to their linear or branched counterparts. While methods for preparing well-defined cyclic polymers have only been available since 1980, the extensive utilization of the cyclic topology in Nature highlights the vital role the cyclic architecture can play in imparting valuable physical properties, such as increased chemical stability or propensity towards self-assembly. This review will describe the major developments in the synthesis of cyclic polymers and provide an overview of their fundamental physical properties. In this context, preliminary studies exploring potential applications will be critically assessed, and the remaining challenges for the field delineated. The goal of this review is to define the present status of research on cyclic polymers and provide some perspective on the outlook and future potential of these unique materials.

---

*A portion of this work has been reproduced from Haque, F. and Grayson, S. Cyclic Polymers: Unique Properties and Potential Applications. *Nature Chemistry,* **under review**.

1.2 INTRODUCTION

When first prepared, cyclic polymers were considered by most to be an academic curiosity with many fascinating properties; however, their applications and commercial feasibility remained uncertain. Many of these unique properties result from their lack of chain ends, which distinguishes them from linear and branched polymers. Yet difficulties in the synthesis and purification of larger scale batches during these early investigations limited research efforts and made commercial explorations impractical. More recently, a variety of cyclic biomacromolecules have been discovered and this topology was found to impart increased stability and strengthened intramolecular interactions. The impact of these findings combined with the development of new synthetic tools has provided a renewed motivation to further explore the synthesis, physical characterization, and potential applications of cyclic polymers. In the last two decades, substantial progress has been made in the synthesis of high-purity cyclic samples, enabling more reliable physical evaluations and a better understanding of the ramifications of the cyclic topology. These synthetic advances have been largely achieved by using new, highly efficient polymerization catalysts or conjugation reactions. This ability to prepare polymer rings provides a promising, novel approach for modifying the physical properties of polymers, especially for tuning well-known materials that are prepared from conventional, cost-efficient monomers and exhibit well-studied physical properties and biodegradation. For example, the pharmacokinetics, biocompatibility, and biodegradation of many FDA-approved polyesters have been established; however, utilizing the cyclic analog provides

an additional tool for modifying their solubility, crystallinity, and degradation profile, while retaining both the biocompatibility of the polymer and the degradation products of already established materials. The discourse herein will cover the significant advances in the field of cyclic polymers, including new synthetic techniques, but focus on a critical examination of studies related to their physical and biological properties. This review will conclude by examining the remaining challenges that need to be addressed in order to realize the full potential of this promising class of polymers.

1.3 CYCLIC BIOMACROMOLECULES: OCCURRENCE AND RAMIFICATIONS

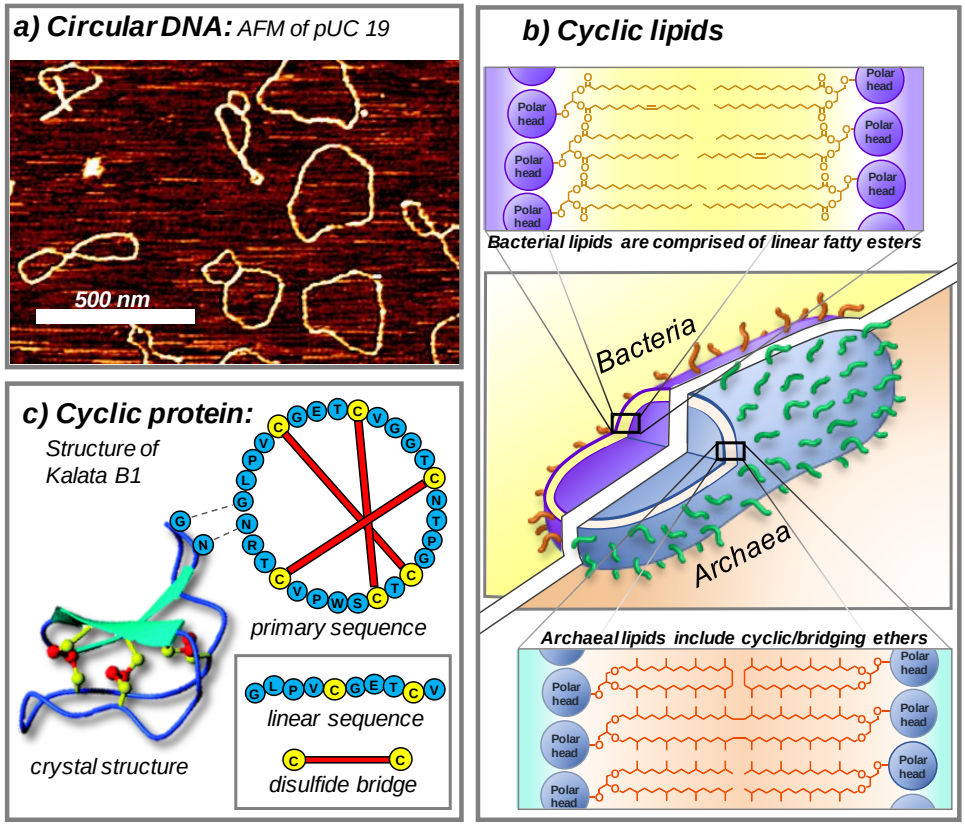

Figure 1.1. a) AFM image of circular pUC 19 DNA relaxed via treatment with Topo1;[1] b) contrast between the cyclic and bridging cyclic ether lipids in the cell walls of archaea, and the more common linear fatty esters observed in bacterial cell walls;[2] c) the cyclic crystal structure and primary sequence of kalata B1.[3]

Cyclic macromolecules have been the subject of numerous studies related to both their synthesis and physical properties. Until recently, they have been viewed as largely academic indulgences rather than materials of commercial value. However, the transformative potential of cyclic synthetic polymers as useful materials has been convincingly foreshadowed by the frequent utilization of macrocycles in Nature, including circular DNA, cyclic lipids, and cyclic peptides.

1.3.1 Cyclic DNA

The first cyclic polymer to be studied in detail was circular DNA (**Figure 1.1a**). The hypothesis that chromosomes could exhibit a cyclic form was originally proposed in 1958 by Jacob and Wollman for *E. coli*,[4] and visual confirmation of this cyclic structure was first acquired by electron microscopy images of viral DNA in 1964.[5] Since then, the topological complexity of DNA has been shown to include supercoiled, knotted, and concatenated forms of DNA,[6] each of these architectures having a distinct effect on their physical and biological properties. However, regardless of the extent of knotting, circular DNA shows enhanced stability with respect to its linear DNA analogs.[7] In fact, within the last decade, click chemistry has been employed to impart a cyclic topology on linear DNA strands, in order to improve their thermal stability and increase their resistance to enzymatic degradation.[8]

1.3.2 Cyclic lipids

In the context of lipids, it has been discovered in the last few decades that the more common linear fatty esters typically used within cell walls are often replaced with more exotic isoprenoid ethers in the case of extremophile *archaea*, presumably to enhance their stability at extreme temperature and pH.[2] In addition to swapping linear esters for linear ethers, many *archaea* incorporate into their cell walls cyclic ethers that span either the length of the lipid monolayer or in some cases the entire bilayer (**Figure 1.1b**). A strong hint of the role of these cyclic lipids was discovered while manipulating the incubation

conditions of *Methanococcus jannaschii*, isolated from submarine hydrothermal vents. Intriguingly, when the temperature of the growth conditions was increased, the proportions of the cyclic ethers incorporated within the cell walls also increased.[9] Though more research is required to fully understand the ramifications of the cyclic topology within lipid bilayers, these data suggest that the cyclic motif is utilized to enhance cell wall stability at high temperatures which in turn imparts a broader temperature range of cell viability.

1.3.3 Cyclic peptides

Similarly, cyclic peptides have demonstrated increased stability that can be attributed to both their cyclic topology and their lack of chain ends. One of the earliest cyclic peptides to be structurally characterized, kalata B1 (**Figure 1.1c**), first gained attention because of its unusual stability to boiling water when extracted from the leaves of *Oldenlandia affinis DC.*[3] Kalata B1 is among a unique class of peptide macrocycles known as cyclotides, which are stabilized by both their cyclic primary structure and by 6 cystine amino acid residues that are arranged to form three intramolecular disulfide bonds, thereby generating a "cyclic cysteine knot."[3, 10] Since its discovery, a number of other cyclic peptides have been isolated from multiple fungal, bacterial, plant and mammalian sources, confirming the importance of this topological motif in Nature.[11] The unique properties of such cyclic peptides have recently been explored to overcome some of the drawbacks that are common for peptide-based drugs,[12] including rapid metabolism, low cell permeability, low selectivity due to conformational flexibility, and insufficient

stability.[13] In one specific example, cyclic analogues of the Luteinizing Hormone-Releasing Hormone (LHRH) have been prepared as a targeted chemotherapy for hormone-dependent cancers and showed increased binding in the LHRH-I receptor relative to the linear LHRH derivative, Leuprolide. More importantly, the cyclic hormone showed exceptional stability (>68-100% intact after 30 minutes) *in vitro* while the native linear hormone LHRH and the linear Leuprolide control exhibited extensive degradation (97% degraded) under identical conditions.[14] Cyclosporin is another cyclic peptide isolated from natural sources which has proved valuable for preventing the rejection of organ transplants and has also been applied for the treatment of many autoimmune disorders including asthma and rheumatoid arthritis.[15-17] The increased thermal, chemical, and enzymatic stability observed with numerous cyclic peptides has encouraged ongoing efforts to incorporate this topology into other peptide drug designs.[12, 18-20]

While the prevalence of the cyclic topology in biological molecules has only recently been fully appreciated, it is understood that the cyclic architecture imparts specific physical properties which are critical to the improved function of these biomacromolecules. Considering the useful topology-related properties seen in Nature, the exploration of the cyclic topology in synthetic polymers seems well-justified. Until recently, the primary limitations for exploring synthetic cyclic polymers were related to synthetic scale, purity, and diversity.

1.4 SYNTHETIC TECHNIQUES

Inspired in part by the first discoveries of cyclic biomacromolecules in the 1960s, polymer chemists have invested significant efforts in developing synthetic routes to prepare cyclic polymers and explore their physical properties. The first cyclic polymers were prepared as oligomeric byproducts of condensation polymerizations. Using this ring-chain equilibrium approach, two synthetic pathways compete: the coupling of an end group on two different linear precursors to yield an unwanted larger linear polymer and the coupling of two reactive end groups on the same polymer chain to yield the desired cyclic polymer.[21] Though technically simple, such condensation reactions inherently yield materials with a high dispersity, and the cyclization product is usually a minor, low molecular weight component in a complex linear/cyclic mixture.[22] Consequently, the crude products can be poorly-defined and exhibit undesirable amounts of linear impurities, even after fractionation or other methods of purification. Since these initial synthetic efforts, three distinct approaches have evolved for the generation of cyclic polymers: the bimolecular ring closure, the unimolecular ring closure, and the ring expansion technique.

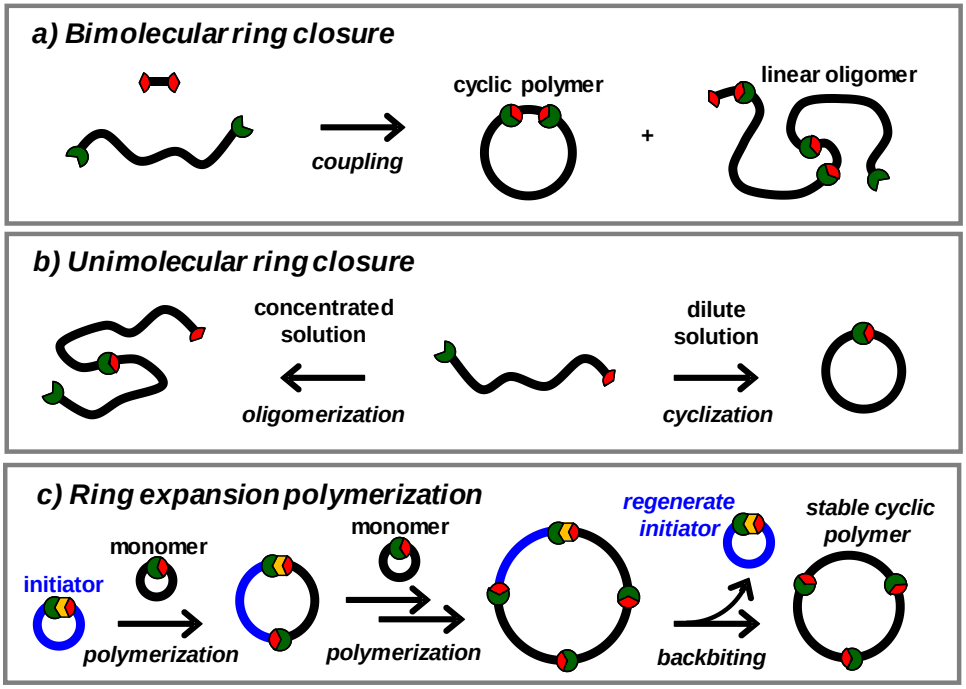

Figure 1.2. a) the bimolecular ring closure involves reaction between a bisfunctional polymer and a complementary bisfunctional linker and exhibits competing cyclization and oligomerization; b) the unimolecular ring closure utilizes complementary end groups on opposite ends of the same polymer, and therefore favors cyclization under dilute conditions; c) the ring expansion approach overcomes the entropic penalty associated with ring closure, but can exhibit less control over molecular weight and dispersity.

1.4.1 Bimolecular ring closure

The bimolecular ring closure was an alternative early cyclization approach in which a bisfunctional polymer undergoes a coupling reaction with a bisfunctional coupling agent (**Figure 1.2a**). This method frequently utilized anionic polymerization of vinyl monomers from a telechelic initiator, followed by an *in situ* quenching with a bisfunctional coupling agent.[23, 24] Like the ring-chain equilibrium approach, the bimolecular ring closure involves the competition between forming cyclic polymers and extended linear polymers that can result in non-cyclic impurities. Although the use of highly dilute conditions can favor

cyclization, this also slows the initial reaction between the telechelic polymer and the bisfunctional coupling agent. As a result, both early techniques typically yielded products that include linear impurities and therefore require tedious purification methods.

Tezuka and coworkers developed an elegant method to address the inefficient cyclization in the bimolecular ring-closure approach. By incorporating a strained *N*-phenylpyrrolidinium cation onto each of the chain ends of poly(tetrahydrofuran), high-purity cyclic polymers could be prepared when reacted with an anionic dicarboxylate coupling agent in dilute solution. This approach, known as "electrostatic self-assembly and covalent fixation" (ESA-CF), makes use of the electrostatic attraction between the cationic polymer end groups and the dianionic coupling agent to enable cyclization. Upon heating, the preassembled salt-pairs can then generate a stable covalent bond.[25] This methodology overcomes one of the fundamental flaws of the bimolecular cyclization approach: typically dilution is used to favor cyclization over polymeric dimerization, yet dilution simultaneously slows the initial reaction with the coupling agent. However, the use of long-range electrostatic interactions to encourage the coupling reaction in dilute solution enables rapid coupling and cyclization, affording cyclic polymers in high purity and high yields. The utility of this approach has been further demonstrated by the generation of a wide range of complex, cyclic and multicyclic polymer topologies, including axially chiral cyclic polymers,[26] *spiro*-multicyclic polymers,[27] a δ-graph,[28] and a $K_{3,3}$ graph.[29] Furthermore, the elegant application of self-accelerating click reactions for the bimolecular ring closure can substantially increase the rate of the cyclization reaction,

and thereby minimize the generation of oligomers.[30, 31] This approach has also been employed for the generation of hyperbranched multicyclic polymers.[32]

1.4.2 Unimolecular ring closure

Unimolecular ring closure involves the cyclization of linear polymers by coupling the opposite ends of a polymer chain under dilute conditions (**Figure 1.2b**). However, as the molecular weight of the polymer increases, it becomes increasingly difficult for the polymer chain ends to find each other and react. Because of this entropic penalty, it can be difficult to cyclize extremely high molecular weight polymers. However, if controlled polymerization techniques are used to make linear precursors and efficient coupling reactions are then employed to achieve the cyclization, well-defined cyclic polymers can be synthesized with low dispersity.

Early work by Schappacher and Deffieux addressed the primary shortcoming of the bimolecular ring-closure approach by using a single polymeric reagent with complimentary reactive hetero-end groups. Because only one reagent was involved in this cyclization, at extremely low concentrations, the reaction of the polymer chain with another polymer chain could be suppressed while the rates of intramolecular cyclization would be unaltered, therefore favoring the generation of cyclic polymers.[33] They designed a linear poly(chloroethyl vinyl ether) with a styrenyl group on the initiator and an iodo terminal group that could undergo cyclization in the presence of $SnCl_4$, a Lewis acid catalyst. They also demonstrated that an efficient trans-acetalization reaction could be used to generate

cyclic polymers.[34]

Laurent and Grayson expanded on this unimolecular cyclization approach by taking advantage of a highly efficient click reaction for the cyclization, specifically copper(I)-catalyzed azide-alkyne cycloaddition (CuAAC) reaction (**Scheme 1.1**).[35] Because azide and alkyne end groups can be easily installed onto a variety of polymer backbones, and because this coupling chemistry is tolerant to a wide range of functional groups, this approach has seen broad application for the synthesis of cyclic polymers as well as more complex architectures like multicyclic functional polymers[36] and star cyclic polymers.[37]

Scheme 1.1 shows the synthesis of the popularized CuAAC "click" reaction to form macrocyclic polystyrene. This method of making cyclic polymers is particularly advantageous as it involves atom transfer radical polymerization, which is a facile way of polymerizing a wide array of vinyl monomers such as styrenics, methacrylates, and acrylates.[38] Furthermore, atom transfer radical polymerization (ATRP) allows the use of initiators with preinstalled functional groups, such as the alkyne-based initiator (1) shown in **Scheme 1.1**. The synthesis yields a linear polymer with a terminal bromide functional group (2) with high end group fidelity. Finally, for the purpose of the CuAAC "click" cyclization, the bromide end group can be converted to an azido group with ease using a substitution reaction, yielding the necessary difunctional linear polymer (3) needed for the synthesis of the cyclic macrocycle.

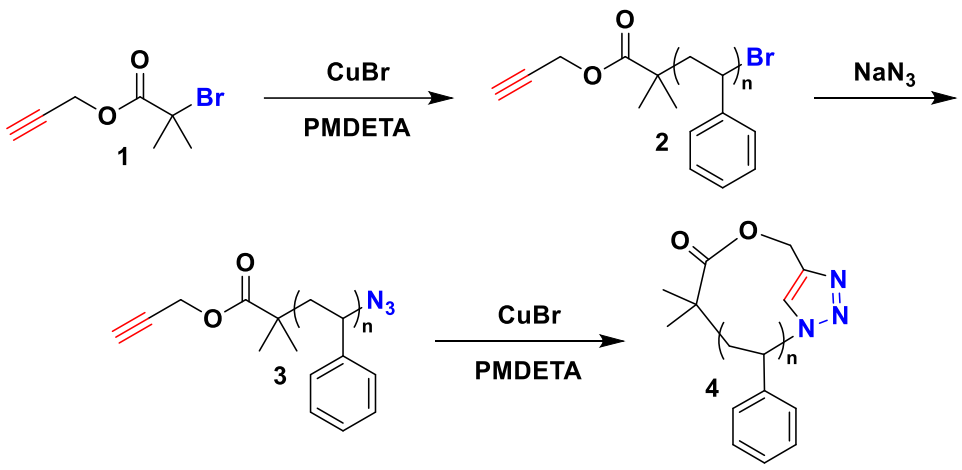

Scheme 1.1. Synthesis of cyclic polystyrene using ATRP, a controlled radical polymerization, to yield well defined linear polymers (2) and the CuAAC "click" reaction to undergo quantitative linear (3) to cyclic (4) architectural transformation[35, 39]

Because copper toxicity may be a concern for some biomedical applications, cyclization using alternative click chemistries have also been explored, including the strain-promoted azide-alkyne cycloadditions (SPAAC),[40] the coupling of maleimide and furan end groups,[41] and various photo-activated cycloaddition reactions.[42, 43]

1.4.3 Ring expansion polymerization

Ring-expansion is an alternative approach to forming cyclic polymers, utilizing a different mechanism which promises to avoid some of the complications with the ring-closure route. Instead of cyclizing a linear polymer via end-group coupling, it generates cyclic polymers by the repeated insertion of cyclic monomer into a cyclic catalyst/initiator (**Figure 1.2c**).[44] This technique is particularly useful for preparing extremely high molecular weight polymer macrocycles of high purity because the expansion of a pre-

existing cyclic structure effectively removes the entropic penalty associated with the ring-closure method. However, this method often presents synthetic challenges. Extremely high purity cyclic polymers can be difficult to form. In addition, unwanted chain transfer and termination events can occur during the polymerization and storage of the polymer. The primary disadvantage for the ring-expansion approach is that each initiator has a restricted monomer compatibility, and most initiators allow limited control over molecular weight and dispersity. Typical monomers include strained cyclic olefins or lactones, which provide an enthalpic driving force for polymerization.

Kricheldorf and coworkers carried out many of the early ring-expansion investigations, polymerizing lactone monomers with tin-based initiators.[44, 45] Initial work utilized 2,2-dibutyl-5,5-dimethyl-1,3-dioxa-2-stannane as the initiator with propagation involving the repeated insertion of strained lactones into the labile tin-alkoxide bond. Although this approach enabled the synthesis of a range of cyclic polyesters, the cyclic product was susceptible to bond cleavage resulting from the relatively weak tin-oxygen bonds present in the cyclic product. Recently, Kricheldorf *et al.* synthesized cyclic poly(L-lactide)s with 2,2-dibutyl-2-stanna-1,3-dithiolane as a polymerization catalyst. While the chosen catalyst has lower catalytic activity than previous catalysts, it results in a polymerization that forms exclusively cyclic polymer, and the use of tin sulfide instead of tin oxides results in a polymer with substantially higher stability.[46] However, one solution for removing these residual weak-linkages was the ring-expansion metathesis polymerization (REMP) developed by Grubbs and coworkers.[47, 48] Making use of a cyclic

ruthenium initiator/catalyst, ring-expansion polymerization was carried out on strained cyclic olefins, and a backbiting termination event removed the ruthenium catalyst, yielding a robust cyclic polyolefin product. Hedrick, Waymouth, and coworkers developed an alternative ring-expansion technique using metal-free organocatalytic N-heterocyclic carbene catalysts, termed zwitterionic ring-expansion polymerization (ZREP), to generate cyclic polyesters from lactone monomers.[49-51] With ZREP, however, it is often difficult to control the degree of polymerization as it is more greatly dependent on how readily the monomer terminates the polymerization rather than on the monomer to initiator ratio. This work has also been extended using similar catalysts to prepare cyclic polypeptides and polypeptoids.[52, 53]

Of the synthetic techniques described for generating cyclic polymers, there is no singular technique that surpasses the rest, but rather each technique exhibits a unique set of advantages and disadvantages. The ring-expansion technique is particularly powerful for generating polymers of high purity and high molecular weight (as high as 1,000,000 Da), though it can be very difficult to achieve tailored molecular weights and low dispersities. This technique has been optimized for a handful of specific monomers but lack the backbone diversity observed with other techniques. On the other hand, the ring-closure techniques have utility particularly when employing highly efficient coupling reactions, such as the CuACC click reaction. Because the coupling reaction is orthogonal to a diversity of polymerization chemistries, it exhibits an exceptional compatibility with a range of polymerization and backbone chemistries.[35, 54-60] With care, cyclization can be

carried out with high yields for lower molecular weight polymers (below 20,000 Da), however high-purity cyclization become increasingly difficult with larger molecular weights. Overall, the selection of the preferred synthetic route is dependent on the desired properties and function of the cyclic polymer product.

1.5 BASIC PHYSICAL PROPERTIES AND MATERIALS APPLICATIONS

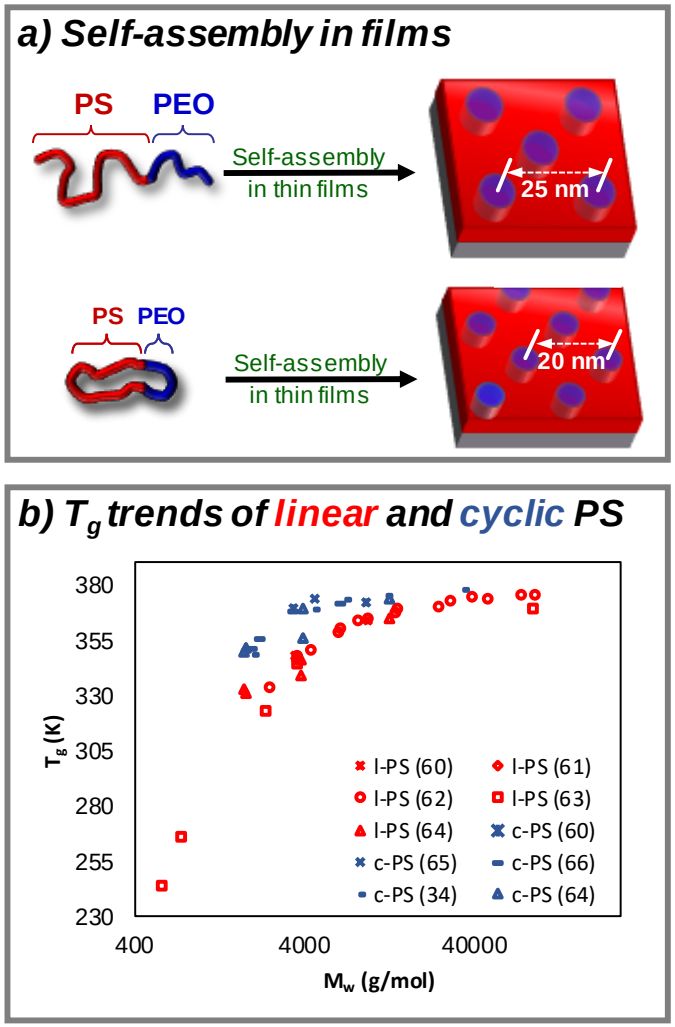

Figure 1.3. a) Cyclic diblock copolymer PS_{13K}-*b*-PEO_{5K} self-assembles in thin films, achieving significantly smaller domain spacings than its linear analog;[61] b) Displayed is the glass transition temperature of polystyrene as a function of molecular weight and linear or cyclic architecture. The cyclic architecture contributes to higher stability based on increased T_g of the polymer compared to the linear analogue, especially at lower molecular weights.[34, 62-68]

The efforts to develop efficient syntheses of cyclic polymers have been driven in part by the desire to understand and exploit the unique physical properties that are a result of the cyclic topology. A more comprehensive discussion of the physical properties of

cyclic polymers has been published by Kricheldorf.[69] In early studies, several unique properties were established, including the reduced hydrodynamic radii of cyclic polymers due to their constrained conformations relative to linear analogs (e.g. a ratio between 0.70 for PS M_n 22 kDa to 0.92 for PS of M_n 710 Da).[70, 71] This property can be used to distinguish cyclic polymers from linear analogs, as the cyclic polymers exhibit increased retention times and can even be used to purify them by preparative gel permeation chromatography (GPC).[72]

The cyclic topology results in a significant deviation of macromolecular thermal properties, as the lack of chain ends affects the mobility and interactions (inter and intra-chain) of a polymer segment within a given macromolecule. Generally, the glass transition temperature (T_g) for a given polymer family increases with molecular weight towards an asymptotic value that would correspond to a chain of infinite molecular weight (**Figure 1.3b**). Although cyclic polymers have been shown to exhibit a similar increasing trend with molecular weight, the T_g values observed for any given molecular weight are higher than those of linear analogs. Analogous and complementary behavior of increased crystallization temperature (T_c) has been observed for poly(ε-caprolactone) as demonstrated by the groups of Grayson and Müller,[73, 74] and Hedrick and Waymouth.[75] Similar trends have been observed for melting and crystallization temperatures T_g,[76, 77] T_c,[47] and T_m[47] for various polymer systems; however, a few studies have yielded an exact opposite effect.

The architecture of polymers can also influence how the glass transition temperature

changes when confined in thin films. It is well established that polymers in thin films can exhibit a significant change in T_g as the film thickness decreases (e.g. either an increase or decrease depending upon the nature of the interactions with the substrate or free surface).[78-82] In the case of polystyrene, this effect was found to relate strongly to both the identity (strength of interaction) and the mass fraction (polymer molecular weight) of the end groups. As predicted by this trend, Zhang *et al.* confirmed that while linear PS exhibited as much as a 10 degree reduction of the T_g (T_g mid relative to linear analog) in films as thin as 21 nm, the cyclic analogs exhibited insignificant change in T_g when confined in a film of the same thickness.[62, 83] This confinement behavior was seen in both hydrophilic and hydrophobic substrates, thereby suggesting this characteristic to be a result of the cyclic architecture rather than possible H-bonding from heterogeneous atoms in the initiator. This behavior also suggests that it arises from enhanced cyclic packing ability, likely related to the reduced viscosity and reduced entanglement of cyclic polymers. Given the importance of polymer thin films in industrial applications such as photolithography, the ability to control the glass transition temperature of cyclic polymers under confinement may prove to be useful.

Moreover, cyclic polymers are known to provide a stark difference in their rheological properties, allowing them to be potentially useful viscosity modifiers. Significant efforts have been pursued to understand cyclic rheological behavior and linear-cyclic mixing.[84-86] For example, cyclic polymers are shown to exhibit significantly reduced melt viscosities, likely a consequence of reduced chain entanglements.[86, 87] In the case of linear/cyclic

blends, however, it was found that the melt viscosities can increase by as much as 2.3 times those of linear polymers alone.[87] This unique example of increased viscosities for blends is thought to be a direct result of the threading of linear chains through the cyclic ones. The combination of higher T_g and lower viscosity may prove useful for polymer processing, as doping a high molecular weight polymer sample with low molecular weight cyclic polymers might reduce melt viscosity (provided the cyclic M_n is low enough to minimize threading by linear polymers), while minimizing the reduction of T_g typically seen with linear dopants.[69]

Additionally, cyclic polymers are known to crystallize faster and to a larger extent to form thermally stable crystalline domains,[73, 88] which may be useful for improving the robustness of a material without changing the repeat unit chemistry. This enhanced crystallization rate is believed to result from reduced viscosity and increased diffusion rates with respect to linear analogues. The removal of chain ends significantly reduces entanglement[84, 86, 89] thereby allowing crystalline domains to reach an equilibrium state faster. Moreover, crystallization studies of poly(ε-caprolactone) (M_n = 6000 Da) films are characterized with a greatly enhanced film stability as demonstrated by the polymer's resistance to dewetting unlike the linear analogue.[90] These studies provide additional evidence suggesting that the cyclic architecture greatly enhances polymer physical properties.

While linear block copolymers and their ability to self-assemble into structured nanodomains have been investigated in detail, the effect of cyclic topology on block

copolymer self-assembly has only recently been explored. In an early study, Marko calculated that the lamellar spacing for cyclic polymers could be reduced to 0.63 of that of the linear analog.[91] This concept was later demonstrated by Lecommandoux *et al*., where linear and cyclic PS_{290}-*b*-PI_{110} were found to have an experimental domain spacing ratio of 0.7, which was in close agreement with their mean field calculations of 0.67.[92] The concept of reducing domain size by using cyclic block copolymers was further demonstrated experimentally by Poelma *et al*., where they confirmed that cylindrical microdomain spacing of a PS_{13K}-*b*-PEO_{5K} cyclic diblock copolymer was 0.75 times that of the linear diblock copolymers of the same molecular weight and composition, enabling a domain spacing of a mere 19.5 nm (**Figure 1.3a**).[61] However, more importantly, this decreased domain size (relative to linear analogs) proved to be unobtainable with linear analogues of a shortened chain length, because linear block copolymers of this shorter size exhibit an insufficient thermodynamic driving force to phase separate. This confirms that the cyclic topology might be used to access smaller domain sizes, which are an important target in nanolithography in order to manufacture smaller and faster nanoelectronic devices than possible with traditional methods. Similar studies have been performed by looking at block copolymers' self-assembly in solution, providing analogous data, which will be discussed in the following section.

In order to make many nanoelectronic devices with polymers, several key properties are required for various applications, including specific fluorescence, electronic, and redox characteristics. To this end, Xu *et al*. synthesized linear and cyclic analogs of

poly[3′-ethynylphenyl[4-hexyl-(2-azido-2-methyl-propionate) phenyl] azobenzene] (PEHPA), which is the first example of the incorporation of azobenzene repeating unit chemistry in the polymer backbone.[76] The azobenzene functionality is known for its photoresponsive nature resulting from its ability to photoisomerize; this property is hoped to be exploited for potential optical data storage and liquid crystal display.[93]

Ring-opening metathesis polymerizations have been studied in some detail, leading to the stereoselective polymerization of many strained cyclic monomers.[94] Based on the work of Veige and coworkers, a Tungsten alkylidyne-mediated REMP technique has been developed to synthesize novel cyclic polyolefins. This work demonstrated the ability to polymerize norbornene to synthesize cyclic polynorbornene (PNB) with high stereoselectivity (>98% *cis*-syndiotactic by ^{1}H NMR).[95] Continued work has led to the polymerization of conjugated phenylacetylene, a useful material for electrically- and photo-conductive materials.[96] Moreover, the availability of olefins along the backbone provide a handle to make novel functional materials. With continued REMP developments, tunable cyclic polyolefins can be synthesized, which may be easily incorporated in the fabrication of electronic devices.

To take full advantage of the unique properties of cyclic polymers within a commercial environment, issues of scalability and purity must be addressed. However, it is possible that doping industrially optimized polymers with small amounts of cyclic polymers can result in a significant advantage by tuning the viscoelastic and thermal properties of the resultant homopolymer blends. Furthermore, cyclic polymer dopants

could improve the overall physical characteristics and processability of a commercial material while avoiding the common practices of doping with small-molecule additives, which are often subject to leaching that can result in shortened product lifetimes as well as the environmental and health risks associated with contamination.

1.6 BIOLOGICAL PROPERTIES AND BIOMEDICAL APPLICATIONS

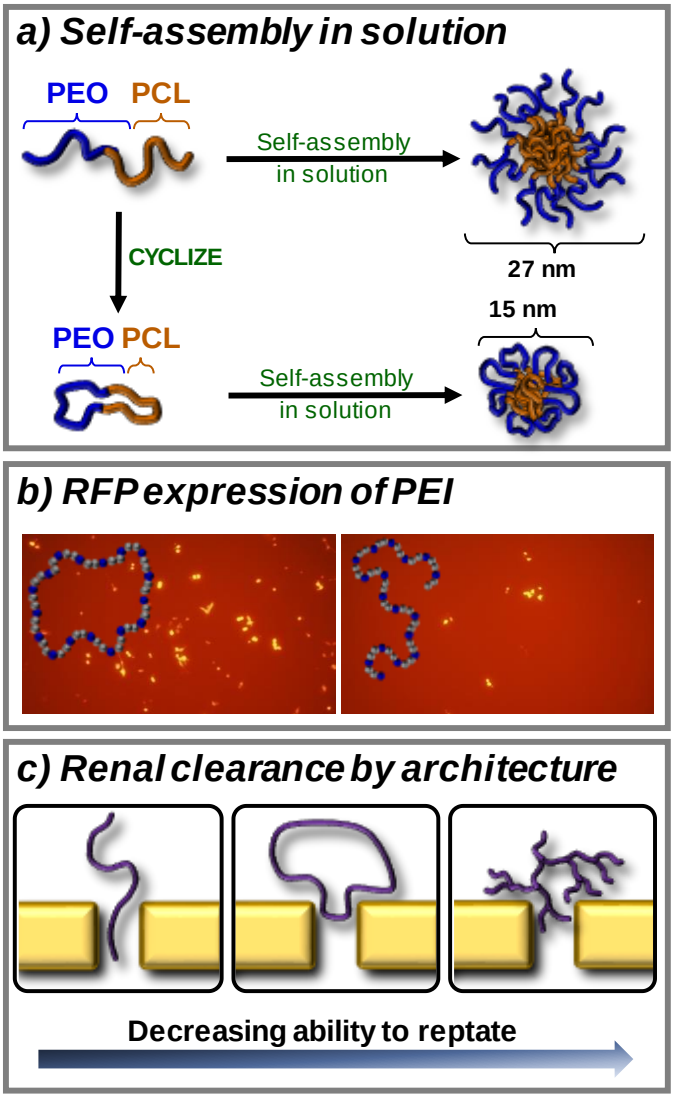

Figure 1.4. a) Direct comparisons of biocompatible block copolymers aggregates can be performed elucidating the more compact structure of the cyclic micelles;[97] b) When cyclic poly(ethylene imine) is used as gene transfection agent with a plasmid encoding a red fluorescence protein (RFP), the cyclic analog shows greatly increased fluorescence indicative of the utility of cyclic architecture in gene transfection;[55] c) Simply rigidifying the macromolecular structure through cyclizations or branching can limit their clearance via reptation in the nanoporous kidney. Synthetic control of architecture can directly lead to increased blood circulation time, offering a foundation for the construction of macromolecular drug targeting and delivery.[98]

Advancements in synthetic chemistry have granted scientists access to polymers

with a wide variation in size, dispersity, architecture, and composition to enable tailoring to specific biomedical applications. For example, the use of composition control among linear biocompatible amphiphilic block copolymers has enabled the optimization of self-assembling polymer micelles that can offer a viable means of administering poorly soluble drugs.[99-101] Despite the depth of research in this area, a number of challenges remain, especially in regards to preparing micelles of high loading capacity that remain stable upon loading and dilution, with appropriate targeting and unloading capabilities in a precise bodily location.[102, 103] Similar to the observed self-assembly of cyclic block-copolymers in bulk thin-films, they can also self-assemble into micelles with reduced aggregate sizes and an increased stability when compared to linear analogs.[104] The biological relevance of cyclic polymer micelles was foreshadowed in early work by Iatrou *et al*. exploring the solution behavior of cyclic polystyrene-*block*-polybutadiene. While these blocks are not ideal for biomedical applications, they did demonstrate the ability to assemble into smaller micelles (relative to linear analogs) in both DMF and *n*-decane, which are selective solvents for polystyrene and polybutadiene, respectively.[105] Similarly, when biocompatible and biodegradable amphiphilic blocks were utilized in the case of cyclic poly(ethylene glycol)-*block*-poly(ε-caprolactone) (c-PEG_{34}-*b*-PCL_{18}), the micelle diameters were again observed to be smaller for the cyclic (15 nm) than their exact linear precursors (27 nm) (**Figure 1.4a**).[97] In addition, self-assembled micelles with the cyclic topology are reported to have greatly enhanced stability, relative to both temperature and ionic strength, with respect to their linear analogs. These stabilities can be measured by observing the cloud

point temperature, the temperature at which micelles begin to form supramicellar agglomerations. The assembly behavior of a cyclic poly(butyl acrylate)-*block*-poly(ethylene oxide) (PBA_{11}-*b*-PEO_{64}), for example, was compared to a linear poly(butyl acrylate)-*block*-poly(ethylene oxide)-*block*-(butyl acrylate) (PBA_5-*b*-PEO_{64}-*b*-PBA_5) of identical composition. Because the triblock had to fold into a pseudo-cyclic conformation in order to form micelles, the size and critical micelle concentration observed for both the cyclic and linear polymers were nearly identical. However, the cyclic polymer did demonstrate a substantial increase in the cloud point temperature, from 24 ^{o}C for the linear triblock to 74 ^{o}C for the cyclic block copolymer, both at concentrations of 1 mg/mL.[106] For a similar polymer system, cloud point measurements also confirmed that the cyclic analog exhibited increased stabilities in the presence of different salts, as indicated by increased salting-out concentrations (C_s). In the case of linear PBA_5-*b*-PEO_{70}-*b*-PBA_5, C_s of 10 mg/mL and 130 mg/mL were exhibited in NaCl and $MgSO_4$, respectively, while the cyclic analog PBA_9-*b*-PEO_{70} exhibited a two-fold increase for NaCl and four-fold increase for $MgSO_4$.[107] The authors hypothesized this significant difference in stability was the result of the amphiphilic triblocks' ability to remove a non-polar terminal block from within the micelle core and reinsert it into a different micelle, acting as an effective bridge between two micelles and encouraging micelle agglomeration. The cyclic amphiphilic block copolymers, on the other hand, do not exhibit such flexibility of conformation and therefore cannot bridge two different micelles. Furthermore, the authors demonstrated that they could tailor the observed cloud points by making binary mixtures of the linear and cyclic

amphiphilic polymers. The ability to tune micelle size and stability through polymer composition and topology can be an invaluable tool for advancing micelle-based drug delivery.

Further investigations of cyclic polymer stability reveal a topology-dependent degradation profile. Hoskins and Grayson first provided evidence of this, when demonstrating cyclic poly(ε-caprolactone)'s significant lag in degradation under an acid catalyzed hydrolysis.[54] This behavior is believed to largely be a consequence of the fact that the first ester bond broken does not change molecular weight, but only changes the topology, from cyclic to linear. Perhaps most interesting, this first bond scission causes an increase in polymer size, as the linear polymer can exhibit more extended conformations than the cyclic precursor. Similarly, cyclic poly(ethylene glycol)-*block*-poly(ε-caprolactone) has been found to undergo an analogous phenomenon upon hydrolytic degradation.[97] Notably, self-assembled micelles of such cyclic amphiphiles would be expected to change their size in solution upon degradation from a cyclic to a linear topology. This initial increase in hydrodynamic volume upon degradation is a unique behavior allowing for the ability to tune polymer degradation profiles, possibly enhancing micelle-based drug delivery. This property could also be utilized in stimuli-responsive systems, for both biological and materials applications.

Other important consequences of molecular architecture for biomedical applications involve the structure-dependent behavior of the "enhanced permeability and retention" (EPR) effect. The EPR effect explains the more selective bioaccumulation of

macromolecules in tumor cells relative to healthy tissues due to rapid angiogenesis and larger gaps between endothelial cells in tumors. For an appropriately sized macromolecular therapeutic, they will largely be excluded from healthy tissue, because of their tighter junctions within the endothelial cell wall of the healthy vasculature. Early on, Matsumura and Maeda showed tumor's increased accumulation of a polymer conjugated to an anti-cancer protein compared to the protein on its own, suggesting the selective accumulation of polymer conjugates was based on their larger size.[108-111] Gillies and Fréchet have expanded on this EPR work through their comparative study of branched, dendritic, and linear analogues to be used as tumor-targeting agents; such work suggests that non-linear polymeric species more selectively target tumor cells as they are retained in the body longer while also not accumulating in non-targeted vital organs.[112, 113] Subsequent findings suggest the cyclic architecture can also assist in passive targeting, as seen by an enhanced EPR effect, due to their compact, non-linear topology. Specifically, Chen *et al.* found that in all cases, larger molecular weight PEGylated poly(acrylic acid) (PAA) comb polymers collected the most in tumors, but additionally the cyclic comb outperformed the linear comb in all respective cases. In one example, 66kDa cyclic PEGylated PAA was found to have 35% injected dose per gram (ID/g) at 48 hours in the tumor compared to linear which had about 28%.[114] It is also worth noting that larger molecular weights, in general, lead to bioaccumulation in a number of organs, such as the spleen, so the ability to reduce molecular weight needed to target tumors by using non-linear architectures provides a way to reduce the unnecessary bioaccumulation. This is evidence that the EPR effects play an

important role for enhancing the targeting effects of cyclic polymers in addition to the molecular weight.

Continued studies on the relationship of polymeric therapeutics in the bloodstream confirm that topology and conformation play a profound role in their blood circulation lifetimes. Blood circulation is largely controlled by a semi-permeable nanopourous barrier in the kidneys, which help remove foreign material from the bloodstream. Linear polymers (especially those in a random coil) are often characterized with shorter blood circulation times as they can reptate through kidney nanopores with significant ease as opposed to polymers with a rigid, globular conformation or cyclic polymers that lack chain ends, both of which must undergo a deformation process to pass through pores (**Figure 1.4c**).[98] In the case of cyclic polymers, threading through the pore would require two segments of the backbone to diffuse through simultaneously, making reptation significantly more difficult, thus increasing circulation time relative to linear analogs. Chen *et al.* demonstrated with linear and cyclic PEGylated PAA comb polymers that cyclic polymers in the molecular weight of 32-115 kDa had much longer renal clearance times (i.e. elimination half-lives of 25 ± 1.4 hours for 65 kDa linear and 35.4 ± 1.9 for 66 kDa cyclic).[114] Nasongkla *et al.* showed similar results when studying linear and cyclic PEGylated poly(ε-caprolactone) of molecular weights ranging from ~30-90 kDa, and specifically found in the case of the 90 kDa cyclic and linear pair that the cyclic had a 42% longer elimination time.[115] In both cases, the cyclic and linear polymers only had an appreciable difference in elimination time when the molecular weight was above that of the renal threshold molecular weight. The

increased circulation time resulting from reduced renal clearance in combination with the selective targeting by the EPR effect can contribute toward improved methods of passively targeting tumors.

More recently, polymeric composition and architecture have demonstrated an influential role in the development of macromolecules for gene transfection. Early findings suggested that degree of branching in poly(ethylene imine) can have a profound effect on both the transfection efficiency and cytotoxicity of DNA-polymer polyplexes, foreshadowing the importance of structure, topology, and end groups on gene transfection.[116] Using a monocyclic topology, Wei *et al*. prepared a number of different molecular weight cyclic and linear cationic poly((2-dimethylamino)ethylmethacrylate) (pDMAEMA) polymers for a nucleic acid delivery system. This study showed that the cyclic polymer maintained a reduced cytotoxicity compared to the linear polymer, which was attributed to less membrane disruption.[117] The DNA-polymer complex was notably smaller in the case of the cyclic topology, which is possibly why it showed less membrane disruption. A follow-up study was pursued comparing linear, comb, and "sunflower" pDMAEMA, and similarly the "sunflower" outperformed the other two polymers. An *in vitro* experiment using HeLa cells determined the increased inhibitory concentration (IC_{50}) of the "sunflower" polymer (9.1-13.4 mg/L),[118] which even outperformed the industry "gold standard" branched polyethyleneimine[119, 120] (PEI 25 kDa, IC_{50} = 4.6 mg/L).[121] More significantly, *in vivo* delivery of plasmid DNA to the brains of mice proved to be more successful with the "sunflower" pDMAEMA.[118] Cortez *et al*. prepared for the first time

cyclic poly(ethylene imine), which exhibited not only reduced toxicity relative to their exact linear analogues but also improved transfection efficiency (**Figure 1.4b**).[55] As reported for linear and branched systems, the transfection efficiency also improved with increasing molecular weight. Even when compared to the "gold standard" branched PEI of nearly 8 times the molecular weight, cyclic PEI proved to be able to transfect genes encoding a red fluorescent protein much better in the case of HAE cell lines and to an equal extent in the case of HFF-1 cell lines. Significantly, the cyclic PEI did exhibit substantially reduced cytotoxicity compared to the branched PEI "gold standard".

These biological studies collectively show the powerful influence of macromolecular architecture on *in vivo* polymer interactions. These preliminary results have left many unanswered questions regarding the exact mechanism for the improved biological properties but provide strong justification for continued research into the role of polymer topology for biomedical applications.

1.7 REMAINING CHALLENGES: PURITY AND SCALABILITY

Given the significant progress in the synthesis of cyclic polymers, demonstrated in recent academic research, it is reasonable to consider what challenges remain before these unique macromolecules can be integrated into commercial materials. From the industrial perspective, two significant and related challenges remain: the first is the discovery of efficient routes to access high purity samples, and the second is the development of synthetic routes for large batch production.

All routes for preparing cyclic polymers are inherently susceptible to generating linear impurities. In the case of ring-closure techniques, incomplete couplings and competing linear oligomerization reactions can result in non-cyclic byproducts. Furthermore, the cyclic purity can only be as high as the end group fidelity of the linear precursors, which becomes increasingly challenging at higher molecular weights.[122] While the ring-expansion approach ideally generates pure cyclic polymers, these techniques are also susceptible to linear byproducts. For example, REMP in the presence of trace linear alkene impurities can generate linear polymers,[123] while ZREP is susceptible to small molecule impurities, such as water, that can initiate or terminate the polymerization to generate linear byproducts.[124]

Regarding the evaluation and optimization of the purity of cyclic polymers, three concerns must be addressed: 1) quantification of the architectural purity, 2) confirmation of the structure of the non-cyclic impurities, and 3) the efficient removal of non-cyclic impurities.

First, traditional techniques like GPC and NMR can easily overlook trace amounts of linear impurities in cyclic polymer samples, however new liquid chromatography characterization techniques are being developed that can more accurately determine architectural purity. For example, liquid chromatography at the critical condition (LCCC) has been used to separate polymers not by length but based on their architecture. This technique, which balances the entropic effects of size exclusion chromatography and the enthalpic effects of interaction chromatography, has shown tremendous promise in

isolating cyclic polymers from non-cyclic byproducts.[125] Building off this, Elupula *et al.* pursued a detailed investigation of byproducts from the CuAAC ring-closure reactions of polystyrene. This study found no sign of cyclic impurities, though trace quantities of cyclic dimer impurities (0.4-2.8%) were isolated by HPLC. MALDI-TOF MS confirmed these dimers were exclusively cyclic, formed by the uncatalyzed dimerization of bisfunctional polymers that subsequently cyclized.[39] Alternatively, temperature gradient interaction chromatography (TGIC) has successfully isolated branched polymers based on their architecture, and also holds promise for characterization of cyclic polymers.[126-129] Josse *et al*. have demonstrated the use of ESI-tandem mass spectrometry to quantify cyclic polylactide purity based on the survival yield technique.[130] Despite these successes, sample-specific optimization is typically required for both techniques, and a general approach for quantifying architectural impurities remains elusive. Because of the sensitivity of rheology to the presence of trace architectural impurities, it offers an additional means of quantifying purity. Work by Kapnistos *et al.* confirms that rheology is very sensitive to linear impurities allowing for their quantification. Specifically, in cyclic samples with as little as 0.1% linear polymer, the stress-strain behavior exhibits a measurable deviation in the stress relaxation moduli.[84]

Secondly, improvements in the characterization of macromolecules by mass spectrometry has provided complimentary tools for differentiating polymers with contrasting end groups or architectures. For example, in the case of the CuAAC ring closure, the presence of azides in the linear precursor is confirmed by their unique

metastable behavior during MALDI-TOF MS characterization, while the cyclized polymer with a triazole linkage exhibits the loss of this unique fragmentation behavior.[131] Tandem mass spectrometry, which isolates specific ions and determines the masses of their subsequent fragmentations, has also been shown to exhibit unique fragmentation patterns based upon the linear or cyclic architecture of the parent ion.[130, 132] Ion mobility spectrometry (IMS) represents an additional technique which can differentiate polymers by architecture. IMS experiments are carried out similarly to a time-of-flight mass spectrometry experiment, but in the presence of a carrier gas rather than a vacuum. The collisions of the ions with this gas enable a measurement of "collisional cross section" (size/charge behavior) as the ions travel through the flight tube. When coupled with mass spectrometry, this technique can provide measurements of both compactness and mass with respect to charge, which has been used to differentiate cyclic polyesters from their linear analogs.[133, 134] However, while these modern MS techniques can clearly differentiate various polymer architectures, quantitative analysis using mass spectrometry is inherently challenging, complicating the accurate measurements of cyclic purity by MS.

Thirdly, while purification has been made possible in certain cases by fractionation or preparative GPC, high volume purification can be extremely demanding. However, recent advances by Haque *et al*. have allowed for a facile scalable "click" scavenging purification of cyclic poly(glycidyl phenyl ether)s synthesized by $B(C_6F_5)_3$-catalyzed ring-expansion polymerization. The hydroxy-functionalized non-cyclic impurities provided a functional handle that can undergo facile end group transformations. A selective,

quantitative propargylation, followed by a "click" reaction with azide-functionalized solid phase resin,[135, 136] should covalently bind all non-cyclic impurities (i.e. tadpoles and linear polymers) to the resin which can then be removed by a simple filtration.[137] The success of the click scavenging could be easily confirmed by GPC and MALDI-TOF MS.

The final issue remaining to be addressed is that of commercial scale-up. Ring-expansion techniques exhibit an inherent advantage for scale-up, as their synthesis does not require high dilution, and therefore is not dependent upon a large excess of solvent. The primary limitation for these techniques is the scarce availability of the catalysts and strained monomers, as well as the stringent conditions required to prevent non-cyclic byproducts. In this light, the ring expansion of lactide, ε-caprolactone, and other lactones with N-heterocyclic carbenes is particularly appealing for commercialization, although significant issues have to be addressed for industrial scaling of these polymerizations.

On the other hand, ring-closure techniques typically require dilution to yield high cyclic purity, and therefore scale-up is potentially expensive because of the required solvent volumes. Computational investigations by Monteiro and coworkers suggest that the judicious selection of solvents and rates of addition can increase reaction scales significantly, but that there is an inherent trade-off between purity and quantity of yield.[22, 138] In this context, the development of scalable, selective purification techniques, such as the "click" scavenging approach, provides a valid pathway forward for a synthetic method that may exhibit low percentages of linear impurities. In addition, the utilization of continuous flow reaction systems promises to further advance the scalability of the ring-

closure approach.[139] In just the last few years, rapid progress addressing the issues of purity and scalability has revealed great promise towards the goal of commercially viable cyclic polymer syntheses, making the commercial development of cyclic polymers, if justified by the application, plausible in the near future.

1.8 CONCLUSIONS

Within the last decade, progress in the field of cyclic polymers has rapidly advanced on both the synthetic and characterization fronts. Multiple synthetic routes have been developed, greatly broadening the scope and diversity of polymer backbones (monomer and composition versatility) that can be cyclized. Likewise, substantial progress has been made in addressing the challenges of purity and scalability using refined chemistry of increased efficiency in combination with advanced analytical techniques for characterization. Furthermore, complimentary experimental and computational studies have confirmed the many unique properties of cyclic polymers and have begun to elucidate the fundamental origin of their behavior. With much of the necessary foundation established, future research efforts will undoubtedly focus on the realization of many of the potential applications described above. These promising initial results foreshadow the use of cyclic polymers for applications ranging from drug delivery components with more robust micellar assemblies and nanolithography templating agents with reduced domain spacing to polymeric additives for tuning bulk viscoelastic properties. Cyclic polymers have at last matured from an academic curiosity, and they can now be considered a viable

material with unique and useful properties. Despite the substantial advances made in just the last decade, a substantial body of work remains to be done, and future research efforts will undoubtedly find additional utility for these fascinating materials.

1.9 REFERENCES

1. Kundukad, B.; Yan, J.; Doyle, P. S. Effect of YOYO-1 on the mechanical properties of DNA. *Soft Matter* **2014,** 10 (48), 9721-9728.

2. Sprott, G. D. Structures of archaebacterial membrane lipids. *Journal of Bioenergetics and Biomembranes* **1992,** 24 (6), 555-566.

3. Saether, O.; Craik, D. J.; Campbell, I. D.; Sletten, K.; Juul, J.; Norman, D. G. Elucidation of the primary and three-dimensional structure of the uterotonic polypeptide Kalata B1. *Biochemistry* **1995,** 34 (13), 4147-4158.

4. Jacob, F.; Wollman, E. L. Genetic and physical determinations of chromosomal segments in Escherichia coli. *Symposia of the Society for Experimental Biology* **1958,** 12, 75-92.

5. Freifelder, D.; Kleinschmidt, A. K.; Sinsheimer, R. L. Electron microscopy of single-stranded DNA: circularity of DNA of bacteriophage ϕX174. *Science* **1964,** 146 (3641), 254-255.

6. Wasserman, S. A.; Cozzarelli, N. R. Biochemical topology: applications to DNA recombination and replication. *Science* **1986,** 232 (4753), 951-60.

7. Vinograd, J.; Lebowitz, J. Physical and topological properties of circular DNA. *The Journal of General Physiology* **1966,** 49 (6), 103-125.

8. El-Sagheer, A.; Brown, T. Synthesis, serum stability and cell uptake of cyclic and hairpin decoy oligonucleotides for TCF/LEF and GLI transcription factors. *International Journal of Peptide Research and Therapeutics* **2008,** 14 (4), 367-372.

9. Sprott, G. D.; Meloche, M.; Richards, J. C. Proportions of diether, macrocyclic diether, and tetraether lipids in Methanococcus jannaschii grown at different temperatures. *Journal of Bacteriology* **1991,** 173 (12), 3907-3910.

10. Craik, D. J.; Daly, N. L.; Bond, T.; Waine, C. Plant cyclotides: a unique family of cyclic and knotted proteins that defines the cyclic cystine knot structural motif1. *Journal of Molecular Biology* **1999,** 294 (5), 1327-1336.

11. Conibear, A. C.; Craik, D. J. The chemistry and biology of theta defensins. *Angewandte Chemie International Edition* **2014,** 53 (40), 10612-10623.

12. Craik, D. J.; Daly, N. L.; Waine, C. The cystine knot motif in toxins and implications for drug design. *Toxicon* **2001,** 39 (1), 43-60.

13. Vlieghe, P.; Lisowski, V.; Martinez, J.; Khrestchatisky, M. Synthetic therapeutic peptides: science and market. *Drug Discovery Today* **2010,** 15 (1-2), 40-56.

14. Laimou, D.; Katsila, T.; Matsoukas, J.; Schally, A.; Gkountelias, K.; Liapakis, G.; Tamvakopoulos, C.; Tselios, T. Rationally designed cyclic analogues of luteinizing hormone-releasing hormone: Enhanced enzymatic stability and biological properties. *European Journal of Medicinal Chemistry* **2012,** 58 (0), 237-247.

15. Lazarova, T.; Chen, J. S.; Hamann, B.; Kang, J. M.; Homuth-Trombino, D.; Han, F.; Hoffmann, E.; McClure, C.; Eckstein, J.; Or, Y. S. Synthesis and biological evaluation of novel cyclosporin A analogues: potential soft drugs for the treatment of autoimmune diseases. *Journal of Medicinal Chemistry* **2003,** 46 (5), 674-676.

16. Eckstein, J. W.; Fung, J. A new class of cyclosporin analogues for the treatment of asthma. *Expert Opinion on Investigational Drugs* **2003,** 12 (4), 647-653.

17. Tapeinou, A.; Matsoukas, M.-T.; Simal, C.; Tselios, T. Review cyclic peptides on a merry-go-round; towards drug design. *Peptide Science* **2015,** 104 (5), 453-461.

18. Cheneval, O.; Schroeder, C. I.; Durek, T.; Walsh, P.; Huang, Y. H.; Liras, S.; Price, D. A.; Craik, D. J. FMOC-based synthesis of disulfide-rich cyclic peptides. *The Journal of Organic Chemistry* **2014,** 79 (12), 5538-44.

19. Colgrave, M. L.; Craik, D. J. Thermal, chemical, and enzymatic stability of the cyclotide Kalata B1: the importance of the cyclic cystine knot. *Biochemistry* **2004,** 43 (20), 5965-5975.

20. Clark, R. J.; Preza, G. C.; Tan, C. C.; van Dijk, J. W.; Fung, E.; Nemeth, E.; Ganz, T.; Craik, D. J. Design, synthesis, and characterization of cyclic analogues of the iron regulatory peptide hormone hepcidin. *Biopolymers* **2013,** 100 (5), 519-26.

21. Kricheldorf, H. R. Macrocycles. 21. role of ring−ring equilibria in thermodynamically controlled polycondensations. *Macromolecules* **2003,** 36 (7), 2302-2308.

22. Jia, Z.; Monteiro, M. J. Cyclic polymers: methods and strategies. *Journal of Polymer Science Part A: Polymer Chemistry* **2012,** 50 (11), 2085-2097.

23. Geiser, D.; Höcker, H. Synthesis and investigation of macrocyclic polystyrene. *Macromolecules* **1980,** 13 (3), 653-656.

24. Hild, G.; Kohler, A.; Rempp, P. Synthesis of ring-shaped macromolecules. *European Polymer Journal* **1980,** 16 (6), 525-527.

25. Oike, H.; Imaizumi, H.; Mouri, T.; Yoshioka, Y.; Uchibori, A.; Tezuka, Y. Designing unusual polymer topologies by electrostatic self-assembly and covalent fixation. *Journal of the American Chemical Society* **2000,** 122 (40), 9592-9599.

26. Honda, S.; Adachi, K.; Yamamoto, T.; Tezuka, Y. A twisting ring polymer: synthesis and thermally induced chiroptical responses of a cyclic poly(tetrahydrofuran) having axially chiral units. *Macromolecules* **2017,** 50 (14), 5323-5331.

27. Sugai, N.; Heguri, H.; Ohta, K.; Meng, Q.; Yamamoto, T.; Tezuka, Y. Effective click construction of bridged- and spiro-multicyclic polymer topologies with tailored cyclic prepolymers (kyklo-telechelics). *Journal of the American Chemical Society* **2010,** 132 (42), 14790-14802.

28. Tezuka, Y.; Fujiyama, K. Construction of polymeric δ-graph: a doubly fused tricyclic topology. *Journal of the American Chemical Society* **2005,** 127 (17), 6266-6270.

29. Suzuki, T.; Yamamoto, T.; Tezuka, Y. Constructing a macromolecular $K_{3,3}$ graph through electrostaticpself-assembly and covalent fixation with a dendritic polymer Precursor. *Journal of the American Chemical Society* **2014,** 136 (28), 10148-10155.

30. Sun, P.; Chen, J.; Liu, J. a.; Zhang, K. Self-accelerating click reaction for cyclic polymer. *Macromolecules* **2017,** 50 (4), 1463-1472.

31. Li, Z.; Qu, L.; Zhu, W.; Liu, J. a.; Chen, J.-Q.; Sun, P.; Wu, Y.; Liu, Z.; Zhang, K. Self-accelerating click reaction for preparing cyclic polymers from unconjugated vinyl monomers. *Polymer* **2018,** 137, 54-62.

32. Liu, C.; Fei, Y.-y.; Zhang, H.-l.; Pan, C.-y.; Hong, C.-y. Effective construction of hyperbranched multicyclic Polymer by combination of ATRP, UV-induced cyclization, and self-accelerating click reaction. *Macromolecules* **2019,** 52 (1), 176-184.

33. Schappacher, M.; Deffieux, A. Synthesis of macrocyclic poly(2-chloroethyl vinyl ether)s. *Die Makromolekulare Chemie, Rapid Communications* **1991,** 12 (7), 447-453.

34. Schappacher, M.; Deffieux, A. α-Acetal-ω-bis(hydroxymethyl) heterodifunctional polystyrene: synthesis, characterization, and investigation of intramolecular end-to-end ring closure. *Macromolecules* **2001,** 34 (17), 5827-5832.

35. Laurent, B. A.; Grayson, S. M. An efficient route to well-defined macrocyclic polymers via “click” cyclization. *Journal of the American Chemical Society* **2006,** 128 (13), 4238-4239.

36. Hossain, M. D.; Jia, Z.; Monteiro, M. J. Complex polymer topologies built from tailored multifunctional cyclic polymers. *Macromolecules* **2014,** 47 (15), 4955-4970.

37. Jia, Z.; Lonsdale, D. E.; Kulis, J.; Monteiro, M. J. Construction of a 3-miktoarm star from cyclic polymers. *ACS Macro Letters* **2012,** 1 (6), 780-783.

38. Matyjaszewski, K.; Xia, J. Atom Transfer Radical Polymerization. *Chemical Reviews* **2001,** 101 (9), 2921-2990.

39. Elupula, R.; Oh, J.; Haque, F. M.; Chang, T.; Grayson, S. M. Determining the origins of impurities during azide–alkyne click cyclization of polystyrene. *Macromolecules* **2016,** 49 (11), 4369-4372.

40. Sun, P.; Tang, Q.; Wang, Z.; Zhao, Y.; Zhang, K. Cyclic polymers based on UV-induced strain promoted azide–alkyne cycloaddition reaction. *Polymer Chemistry* **2015,** 6 (22), 4096-4101.

41. Glassner, M.; Blinco, J. P.; Barner-Kowollik, C. Diels–Alder reactions as an efficient route to high purity cyclic polymers. *Macromolecular Rapid Communications* **2011,** 32 (9-10), 724-728.

42. Josse, T.; Altintas, O.; Oehlenschlaeger, K. K.; Dubois, P.; Gerbaux, P.; Coulembier, O.; Barner-Kowollik, C. Ambient temperature catalyst-free light-induced preparation of macrocyclic aliphatic polyesters. *Chemical Communications* **2014,** 50 (16), 2024-2026.

43. Tang, Q.; Wu, Y.; Sun, P.; Chen, Y.; Zhang, K. Powerful ring-closure method for preparing varied cyclic polymers. *Macromolecules* **2014,** 47 (12), 3775-3781.

44. Kricheldorf, H. R.; Lee, S.-R. Polylactones. 35. macrocyclic and stereoselective polymerization of β-D,L-butyrolactone with cyclic dibutyltin initiators. *Macromolecules* **1995,** 28 (20), 6718-6725.

45. Kricheldorf, H. R.; Eggerstedt, S. Macrocycles 2. living macrocyclic polymerization of ε-caprolactone with 2,2-dibutyl-2-stanna-1,3-dioxepane as initiator. *Macromolecular Chemistry and Physics* **1998,** 199 (2), 283-290.

46. Kricheldorf, H. R.; Weidner, S. M.; Scheliga, F. Cyclic poly(l-lactide)s via ring-

expansion polymerizations catalysed by 2,2-dibutyl-2-stanna-1,3-dithiolane. *Polymer Chemistry* **2017,** 8 (9), 1589-1596.

47. Bielawski, C. W.; Benitez, D.; Grubbs, R. H. An "endless" route to cyclic polymers. *Science* **2002,** 297 (5589), 2041-2044.

48. Boydston, A. J.; Xia, Y.; Kornfield, J. A.; Gorodetskaya, I. A.; Grubbs, R. H. Cyclic ruthenium-alkylidene catalysts for ring-expansion metathesis polymerization. *Journal of the American Chemical Society* **2008,** 130 (38), 12775-12782.

49. Jeong, W.; Hedrick, J. L.; Waymouth, R. M. Organic spirocyclic initiators for the ring-expansion polymerization of β-lactones. *Journal of the American Chemical Society* **2007,** 129 (27), 8414-8415.

50. Kamber, N. E.; Jeong, W.; Gonzalez, S.; Hedrick, J. L.; Waymouth, R. M. N-Heterocyclic carbenes for the organocatalytic ring-opening polymerization of ε-caprolactone. *Macromolecules* **2009,** 42 (5), 1634-1639.

51. Culkin, D. A.; Jeong, W.; Csihony, S.; Gomez, E. D.; Balsara, N. P.; Hedrick, J. L.; Waymouth, R. M. Zwitterionic polymerization of lactide to cyclic poly(lactide) by using N-heterocyclic carbene organocatalysts. *Angewandte Chemie* **2007,** 46 (15), 2627-2630.

52. Guo, L.; Zhang, D. Cyclic poly(α-peptoid)s and their block copolymers from N-heterocyclic carbene-mediated ring-opening polymerizations of N-substituted N-carboxylanhydrides. *Journal of the American Chemical Society* **2009,** 131 (50), 18072-18074.

53. Zhang, Y.; Liu, R.; Jin, H.; Song, W.; Augustine, R.; Kim, I. Straightforward access to linear and cyclic polypeptides. *Communications Chemistry* **2018,** 1 (1), 40.

54. Hoskins, J. N.; Grayson, S. M. Synthesis and degradation behavior of cyclic poly(ε-caprolactone). *Macromolecules* **2009,** 42 (17), 6406-6413.

55. Cortez, M. A.; Godbey, W. T.; Fang, Y.; Payne, M. E.; Cafferty, B. J.; Kosakowska, K. A.; Grayson, S. M. The synthesis of cyclic poly(ethylene imine) and exact linear analogues: an evaluation of gene delivery comparing polymer architectures. *Journal of the American Chemical Society* **2015,** 137 (20), 6541-6549.

56. Xu, J.; Ye, J.; Liu, S. Synthesis of well-defined cyclic poly(N-isopropylacrylamide) via click chemistry and its unique thermal phase transition behavior. *Macromolecules* **2007,** 40 (25), 9103-9110.

57. Xie, M.; Shi, J.; Ding, L.; Li, J.; Han, H.; Zhang, Y. Cyclic poly(ε-caprolactone) synthesized by combination of ring-opening polymerization with ring-closing metathesis, ring closing enyne metathesis, or "click" reaction. *Journal of Polymer Science Part A: Polymer Chemistry* **2009,** 47 (12), 3022-3033.

58. Misaka, H.; Kakuchi, R.; Zhang, C.; Sakai, R.; Satoh, T.; Kakuchi, T. Synthesis of well-defined macrocyclic poly(δ-valerolactone) by "click cyclization". *Macromolecules* **2009,** 42 (14), 5091-5096.

59. Goldmann, A. S.; Quémener, D.; Millard, P.-E.; Davis, T. P.; Stenzel, M. H.; Barner-Kowollik, C.; Müller, A. H. E. Access to cyclic polystyrenes via a combination of reversible addition fragmentation chain transfer (RAFT) polymerization and click chemistry. *Polymer* **2008,** 49 (9), 2274-2281.

60. Qiu, X.-P.; Tanaka, F.; Winnik, F. M. Temperature-induced phase transition of well-defined cyclic poly(N-isopropylacrylamide)s in aqueous solution. *Macromolecules* **2007,** 40 (20), 7069-7071.

61. Poelma, J. E.; Ono, K.; Miyajima, D.; Aida, T.; Satoh, K.; Hawker, C. J. Cyclic block copolymers for controlling feature sizes in block copolymer lithography. *ACS Nano* **2012,** 6 (12), 10845-10854.

62. Zhang, L.; Elupula, R.; Grayson, S. M.; Torkelson, J. M. Major impact of cyclic chain topology on the T_g-confinement effect of supported thin films of polystyrene. *Macromolecules* **2016,** 49 (1), 257-268.

63. Lan, T.; Torkelson, J. M. Fragility-confinement effects: apparent universality as a function of scaled thickness in films of freely deposited, linear polymer and its absence in densely grafted brushes. *Macromolecules* **2016,** 49 (4), 1331-1343.

64. Zhang, L.; Marsiglio, J. A.; Lan, T.; Torkelson, J. M. Dramatic tunability of the glass transition temperature and fragility of low molecular weight polystyrene by initiator fragments located at chain ends. *Macromolecules* **2016,** 49 (6), 2387-2398.

65. Santangelo, P. G.; Roland, C. M. Molecular weight dependence of fragility in polystyrene. *Macromolecules* **1998,** 31 (14), 4581-4585.

66. Deffieux, A.; Schappacher, M.; Rique-Lurbet, L. New routes to macrocyclic polymers of controlled dimensions. **1994,** 35 (21), 4562-4568.

67. Santangelo, P. G.; Roland, C. M.; Chang, T.; Cho, D.; Roovers, J. Dynamics near the glass temperature of low molecular weight cyclic polystyrene. *Macromolecules* **2001,** 34 (26), 9002-9005.

68. Rique-Lurbet, L.; Schappacher, M.; Deffieux, A. A new strategy for the synthesis of cyclic polystyrenes: principle and application. *Macromolecules* **1994,** 27 (22), 6318-6324.

69. Kricheldorf, H. R. Cyclic polymers: synthetic strategies and physical properties. *Journal of Polymer Science Part A: Polymer Chemistry* **2010,** 48 (2), 251-284.

70. Alberty, K. A.; Hogen-Esch, T. E.; Carlotti, S. Synthesis and characterization of macrocyclic vinyl-aromatic polymers. *Macromolecular Chemistry and Physics* **2005,** 206 (10), 1035-1042.

71. Hadziioannou, G.; Cotts, P. M.; ten Brinke, G.; Han, C. C.; Lutz, P.; Strazielle, C.; Rempp, P.; Kovacs, A. J. Thermodynamic and hydrodynamic properties of dilute solutions of cyclic and linear polystyrenes. *Macromolecules* **1987,** 20 (3), 493-497.

72. Dodgson, K.; Sympson, D.; Semlyen, J. A. Studies of cyclic and linear poly(dimethyl siloxanes): 2. preparative gel permeation chromatography. **1978,** 19 (11), 1285-1289.

73. Lorenzo, A. T.; Cordova, M. E.; Grayson, S. M.; Müller, A. J.; Hoskins, J. N. A comparative study of crystallization behavior of analogous linear and cyclic poly(ε-caprolactones). **2011,** 44 (7).

74. Wang, J.; Li, Z.; Pérez, R. A.; Müller, A. J.; Zhang, B.; Grayson, S. M.; Hu, W. Comparing crystallization rates between linear and cyclic poly(ε-caprolactones) via fast-scan chip-calorimeter measurements. **2015,** 63 (0), 34-40.

75. Shin, E. J.; Jeong, W.; Brown, H. A.; Koo, B. J.; Hedrick, J. L.; Waymouth, R. M. Crystallization of cyclic polymers: synthesis and crystallization behavior of high molecular weight cyclic poly(ε-caprolactone)s. *Macromolecules* **2011,** 44 (8), 2773-2779.

76. Xu, X.; Zhou, N.; Zhu, J.; Tu, Y.; Zhang, Z.; Cheng, Z.; Zhu, X. The first example of main-chain cyclic azobenzene polymers. *Macromolecular Rapid Communications* **2010,** 31 (20), 1791-1797.

77. Kammiyada, H.; Ouchi, M.; Sawamoto, M. A study on physical properties of cyclic poly(vinyl ether)s synthesized via ring-expansion cationic polymerization. *Macromolecules* **2017,** 50 (3), 841-848.

78. Zhang, L.; Torkelson, J. M. Influence of initiator fragments as chain ends on the T_g-confinement effect and dewetting of thin films of ultralow molecular weight polymer. *Polymer* **2015,** 65, 105-114.

79. Fakhraai, Z.; Forrest, J. A. Probing slow dynamics in supported thin polymer films. *Physical Review Letters* **2005,** 95 (2), 025701.

80. Tsui, O. K. C.; Russell, T. P.; Hawker, C. J. Effect of interfacial interactions on the glass transition of polymer thin films. *Macromolecules* **2001,** 34 (16), 5535-5539.

81. Ellison, C. J.; Mundra, M. K.; Torkelson, J. M. Impacts of polystyrene molecular weight and modification to the repeat unit structure on the glass transition−nanoconfinement effect and the cooperativity length scale. *Macromolecules* **2005,** 38 (5), 1767-1778.

82. Park, C. H.; Kim, J. H.; Ree, M.; Sohn, B.-H.; Jung, J. C.; Zin, W.-C. Thickness and composition dependence of the glass transition temperature in thin random copolymer films. *Polymer* **2004,** 45 (13), 4507-4513.

83. Zhang, L.; Elupula, R.; Grayson, S. M.; Torkelson, J. M. Suppression of the fragility-confinement effect via low molecular weight cyclic or ring polymer topology. *Macromolecules* **2017,** 50 (3), 1147-1154.

84. Kapnistos, M.; Lang, M.; Vlassopoulos, D.; Pyckhout-Hintzen, W.; Richter, D.; Cho, D.; Chang, T.; Rubinstein, M. Unexpected power-law stress relaxation of entangled ring polymers. *Nature Materials* **2008,** 7 (12), 997-1002.

85. Halverson, J. D.; Grest, G. S.; Grosberg, A. Y.; Kremer, K. Rheology of ring polymer melts: from linear contaminants to ring-linear blends. *Physical Review Letters* **2012,** 108 (3), 038301.

86. Pasquino, R.; Vasilakopoulos, T. C.; Jeong, Y. C.; Lee, H.; Rogers, S.; Sakellariou, G.; Allgaier, J.; Takano, A.; Brás, A. R.; Chang, T.; Gooßen, S.; Pyckhout-Hintzen, W.; Wischnewski, A.; Hadjichristidis, N.; Richter, D.; Rubinstein, M.; Vlassopoulos, D. Viscosity of ring polymer melts. *ACS Macro Letters* **2013,** 2 (10), 874-878.

87. Roovers, J. Viscoelastic properties of polybutadiene rings. *Macromolecules* **1988,** 21 (5), 1517-1521.

88. Zaldua, N.; Liénard, R.; Josse, T.; Zubitur, M.; Mugica, A.; Iturrospe, A.; Arbe, A.; De Winter, J.; Coulembier, O.; Müller, A. J. Influence of chain topology (cyclic versus linear) on the nucleation and isothermal crystallization of poly(l-lactide) and poly(d-lactide).

Macromolecules **2018,** 51 (5), 1718-1732.

89. Kawaguchi, D. Direct observation and mutual diffusion of cyclic polymers. *Polymer Journal* **2013,** 45 (8), 783-789.

90. Kelly, G. M.; Haque, F. M.; Grayson, S. M.; Albert, J. N. L. Suppression of melt-induced dewetting in cyclic poly(ε-caprolactone) thin films. *Macromolecules* **2017,** 50 (24), 9852-9856.

91. Marko, J. F. Microphase separation of block copolymer rings. *Macromolecules* **1993,** 26 (6), 1442-1444.

92. Lecommandoux, S.; Borsali, R.; Schappacher, M.; Deffieux, A.; Narayanan, T.; Rochas, C. Microphase separation of linear and cyclic block copolymers poly(styrene-*b*-isoprene): SAXS experiments. *Macromolecules* **2004,** 37 (5), 1843-1848.

93. Natansohn, A.; Rochon, P. Photoinduced motions in azo-containing polymers. *Chemical Reviews* **2002,** 102 (11), 4139-4176.

94. Coates, G. W. Precise control of polyolefin stereochemistry using single-site metal catalysts. *Chemical Reviews* **2000,** 100 (4), 1223-1252.

95. Gonsales, S. A.; Kubo, T.; Flint, M. K.; Abboud, K. A.; Sumerlin, B. S.; Veige, A. S. Highly tactic cyclic polynorbornene: stereoselective ring expansion metathesis polymerization of norbornene catalyzed by a new tethered tungsten-alkylidene catalyst. *Journal of the American Chemical Society* **2016,** 138 (15), 4996-4999.

96. Roland, C. D.; Li, H.; Abboud, K. A.; Wagener, K. B.; Veige, A. S. Cyclic polymers from alkynes. *Nat Chem* **2016,** 8 (8), 791-796.

97. Zhang, B.; Zhang, H.; Li, Y.; Hoskins, J. N.; Grayson, S. M. Exploring the effect of amphiphilic polymer architecture: synthesis, characterization, and self-assembly of both cyclic and linear poly(ethylene gylcol)-*b*-polycaprolactone. *ACS Macro Letters* **2013,** 2 (10), 845-848.

98. Fox, M. E.; Szoka, F. C.; Fréchet, J. M. J. Soluble polymer carriers for the treatment of cancer: the importance of molecular architecture. *Accounts of Chemical Research* **2009,** 42 (8), 1141-1151.

99. Torchilin, V. P.; Weissig, V., Polymeric micelles for the delivery of poorly soluble drugs. In *Controlled Drug Delivery*, American Chemical Society: 2000; Vol. 752, pp 297-313.

100. Torchilin, V. P.; Lukyanov, A. N.; Gao, Z.; Papahadjopoulos-Sternberg, B. Immunomicelles: targeted pharmaceutical carriers for poorly soluble drugs. *Proceedings of the National Academy of Sciences of the United States of America* **2003,** 100 (10), 6039-6044.

101. Movassaghian, S.; Merkel, O. M.; Torchilin, V. P. Applications of polymer micelles for imaging and drug delivery. *Wiley Interdisciplinary Reviews: Nanomedicine and Nanobiotechnology* **2015,** 7 (5), 691-707.

102. Tyrrell, Z. L.; Shen, Y.; Radosz, M. Fabrication of micellar nanoparticles for drug delivery through the self-assembly of block copolymers. *Progress in Polymer Science* **2010,** 35 (9), 1128-1143.

103. Torchilin, V. P. Targeted polymeric micelles for delivery of poorly soluble drugs. *Cellular and Molecular Life Sciences CMLS* **2004,** 61 (19), 2549-2559.

104. Ree, B. J.; Satoh, T.; Yamamoto, T. Micelle structure details and stabilities of cyclic block copolymer amphiphile and its linear analogues. *Polymers* **2019,** 11 (1), 163.

105. Iatrou, H.; Hadjichristidis, N.; Meier, G.; Frielinghaus, H.; Monkenbusch, M. Synthesis and characterization of model cyclic block copolymers of styrene and butadiene. comparison of the aggregation phenomena in selective solvents with linear diblock and triblock analogues. *Macromolecules* **2002,** 35 (14), 5426-5437.

106. Honda, S.; Yamamoto, T.; Tezuka, Y. Topology-directed control on thermal stability: micelles formed from linear and cyclized amphiphilic block copolymers. *Journal of the American Chemical Society* **2010,** 132 (30), 10251-10253.

107. Honda, S.; Yamamoto, T.; Tezuka, Y. Tuneable enhancement of the salt and thermal stability of polymeric micelles by cyclized amphiphiles. *Nature Communications* **2013,** 4, 1574.

108. Maeda, H. Macromolecular therapeutics in cancer treatment: the EPR effect and beyond. *Drug Delivery and Cancer: Today's Challenges, Tomorrow's Directions.* **2012,** 164 (2), 138-144.

109. Maeda, H.; Nakamura, H.; Fang, J. The EPR effect for macromolecular drug delivery to solid tumors: improvement of tumor uptake, lowering of systemic toxicity, and distinct tumor imaging in vivo. **2013,** 65 (1), 71-79.

110. Maeda, H.; Wu, J.; Sawa, T.; Matsumura, Y.; Hori, K. Tumor vascular permeability and the EPR effect in macromolecular therapeutics: a review. **2000,** 65, 271-284.

111. Matsumura, Y.; Maeda, H. A new concept for macromolecular therapeutics in cancer chemotherapy: mechanism of tumoritropic accumulation of proteins and the antitumor agent smancs. *Cancer Research* **1986,** 46 (12 Part 1), 6387-6392.

112. Gillies, E. R.; Dy, E.; Fréchet, J. M. J.; Szoka, F. C. Biological evaluation of polyester dendrimer: poly(ethylene oxide) "bow-tie" hybrids with tunable molecular weight and architecture. *Molecular Pharmaceutics* **2005,** 2 (2), 129-138.

113. Gillies, E.; Frechet, J. Dendrimers and dendritic polymers in drug delivery. *Drug Discovery Today* **2005,** 10 (1), 35-43.

114. Chen, B.; Jerger, K.; Frechet, J. M.; Szoka, F. C., Jr. The influence of polymer topology on pharmacokinetics: differences between cyclic and linear PEGylated poly(acrylic acid) comb polymers. *Journal of Controlled Release* **2009,** 140 (3), 203-209.

115. Nasongkla, N.; Chen, B.; Macaraeg, N.; Fox, M. E.; Fréchet, J. M. J.; Szoka, F. C. Dependence of pharmacokinetics and biodistribution on polymer architecture: effect of cyclic versus linear polymers. *Journal of the American Chemical Society* **2009,** 131 (11), 3842-3843.

116. Seib, F. P.; Jones, A. T.; Duncan, R. Comparison of the endocytic properties of linear and branched PEIs, and cationic PAMAM dendrimers in B16f10 melanoma cells. *Journal of Controlled Release* **2007,** 117 (3), 291-300.

117. Wei, H.; Chu, D. S. H.; Zhao, J.; Pahang, J. A.; Pun, S. H. Synthesis and evaluation of cyclic cationic polymers for nucleic acid delivery. *ACS Macro Letters* **2013,** 2 (12), 1047-1050.

118. Cheng, Y.; Wei, H.; Tan, J.-K. Y.; Peeler, D. J.; Maris, D. O.; Sellers, D. L.; Horner, P. J.; Pun, S. H. Nano-sized sunflower polycations as effective gene transfer vehicles. *Small* **2016,** 12 (20), 2750-2758.

119. Klibanov, A. M.; Thomas, M. Enhancing polyethylenimine's delivery of plasmid DNA into mammalian cells. *Proceedings of the National Academy of Sciences* 99 (23), 14640-14645.

120. Benoist, C.; Goula, D.; Behr, J. P.; Demeneix, B. A.; Hassan, A.; Abdallah, B. A powerful nonviral vector for in vivo gene transfer into the adult mammalian brain:

polyethylenimine. **2008**.

121. Johnson, R. N.; Chu, D. S. H.; Shi, J.; Schellinger, J. G.; Carlson, P. M.; Pun, S. H. HPMA-oligolysine copolymers for gene delivery: optimization of peptide length and polymer molecular weight. *Journal of Controlled Release* **2011,** 155 (2), 303-311.

122. Jakubowski, W.; Kirci-Denizli, B.; Gil, R. R.; Matyjaszewski, K. Polystyrene with improved chain-end functionality and higher molecular weight by ARGET ATRP. *Macromolecular Chemistry and Physics* **2008,** 209 (1), 32-39.

123. Bielawski, C. W.; Benitez, D.; Grubbs, R. H. Synthesis of cyclic polybutadiene via ring-opening metathesis polymerization: the importance of removing trace linear contaminants. *Journal of the American Chemical Society* **2003,** 125 (28), 8424-8425.

124. Asenjo-Sanz, I.; Veloso, A.; Miranda, J. I.; Pomposo, J. A.; Barroso-Bujans, F. Zwitterionic polymerization of glycidyl monomers to cyclic polyethers with $B(C_6F_5)_3$. *Polymer Chemistry* **2014,** 5 (24), 6905-6908.

125. Takano, A.; Kushida, Y.; Aoki, K.; Masuoka, K.; Hayashida, K.; Cho, D.; Kawaguchi, D.; Matsushita, Y. HPLC characterization of cyclization reaction product obtained by end-to-end ring closure reaction of a telechelic polystyrene. *Macromolecules* **2007,** 40 (3), 679-681.

126. Chang, T. Polymer characterization by interaction chromatography. *Journal of Polymer Science Part B: Polymer Physics* **2005,** 43 (13), 1591-1607.

127. Lee, H. C.; Chang, T. Polymer molecular weight characterization by temperature gradient high performance liquid chromatography. *Polymer* **1996,** 37 (25), 5747-5749.

128. Berek, D. Coupled liquid chromatographic techniques for the separation of complex polymers. *Progress in Polymer Science* **2000,** 25 (7), 873-908.

129. Li, S. W.; Park, H. E.; Dealy, J. M.; Maric, M.; Lee, H.; Im, K.; Choi, H.; Chang, T.; Rahman, M. S.; Mays, J. Detecting structural polydispersity in branched polybutadienes. *Macromolecules* **2011,** 44 (2), 208-214.

130. Josse, T.; De Winter, J.; Dubois, P.; Coulembier, O.; Gerbaux, P.; Memboeuf, A. A tandem mass spectrometry-based method to assess the architectural purity of synthetic polymers: a case of a cyclic polylactide obtained by click chemistry. *Polymer Chemistry* **2015,** 6 (1), 64-69.

131. Li, Y.; Hoskins, J. N.; Sreerama, S. G.; Grayson, S. M. MALDI−TOF mass spectral characterization of polymers containing an azide group: evidence of metastable ions. *Macromolecules* **2010,** 43 (14), 6225-6228.

132. Yol, A.; Dabney, D.; Wang, S.-F.; Laurent, B.; Foster, M.; Quirk, R.; Grayson, S.; Wesdemiotis, C. Differentiation of linear and cyclic polymer architectures by MALDI tandem mass spectrometry (MALDI-MS^2). *Journal of The American Society for Mass Spectrometry* **2013,** 24 (1), 74-82.

133. Hoskins, J. N.; Trimpin, S.; Grayson, S. M. Architectural differentiation of linear and cyclic polymeric isomers by ion mobility spectrometry-mass spectrometry. *Macromolecules* **2011,** 44 (17), 6915-6918.

134. Li, X.; Guo, L.; Casiano-Maldonado, M.; Zhang, D.; Wesdemiotis, C. Top-down multidimensional mass spectrometry methods for synthetic polymer analysis. *Macromolecules* **2011,** 44 (12), 4555-4564.

135. Urbani, C. N.; Bell, C. A.; Lonsdale, D. E.; Whittaker, M. R.; Monteiro, M. J. Reactive alkyne and azide solid supports to increase purity of novel polymeric stars and dendrimers via the "click" reaction. *Macromolecules* **2007,** 40 (19), 7056-7059.

136. Zhang, B.; Zhang, H.; Elupula, R.; Alb, A. M.; Grayson, S. M. Efficient synthesis of high purity homo-arm and mikto-arm poly(ethylene glycol) stars using epoxide and azide–alkyne coupling chemistry. *Macromolecular Rapid Communications* **2014,** 35 (2), 146-151.

137. Haque, F. M.; Alegria, A.; Grayson, S. M.; Barroso-Bujans, F. Detection, quantification, and "click-scavenging" of impurities in cyclic poly(glycidyl phenyl ether) obtained by zwitterionic ring-expansion polymerization with $B(C_6F_5)_3$. *Macromolecules* **2017,** 50 (5), 1870-1881.

138. Lonsdale, D. E.; Bell, C. A.; Monteiro, M. J. Strategy for rapid and high-purity monocyclic polymers by CuAAC "click" reactions. *Macromolecules* **2010,** 43 (7), 3331-3339.

139. Sun, P.; Liu, J. a.; Zhang, Z.; Zhang, K. Scalable preparation of cyclic polymers by the ring-closure method assisted by the continuous-flow technique. *Polymer Chemistry* **2016,** 7 (12), 2239-2244.

CHAPTER 2

CHARACTERIZATION OF CYCLIC POLYSTYRENE*

2.1 ABSTRACT

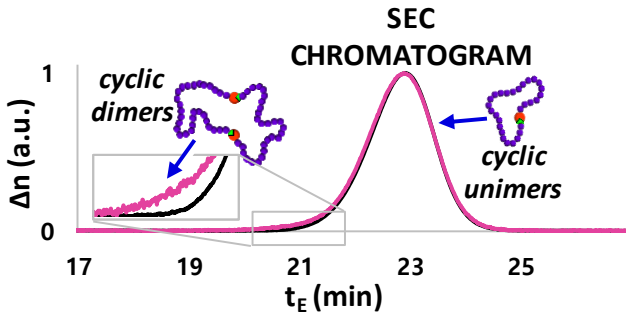

The CuAAC cyclization of linear polymers has proved to be a versatile technique for the preparation of cyclic polymers with diverse functionality. However, these products often exhibited trace amounts of impurities. These potential impurities are cause for concern when studying their thermal, rheological, and physical properties. The study herein attempts to quantify and characterize trace impurities formed during the CuAAC cyclization by the following analytical techniques: HPLC, SEC, and MALDI-ToF MS. Through this study, it was determined that the only known source of impurities arises from the uncatalyzed azide alkyne cycloaddition reaction during the storage of the α-alkynyl-ω-azido-polystyrene linear precursor. It was also determined that linear dimers are formed

* Portion of this work has been published in Elupula, R.; Oh, J.; Haque, F. M.; Chang, T.; Grayson, S. M. Determining the Origins of Impurities during Azide–Alkyne Click Cyclization of Polystyrene. *Macromolecules* **2016**, *49*, 4369-4372 and Gartner, T. E.; Haque, F. M.; Gomi, A. M.; Grayson, S. M.; Hore, M. J. A., Jayraman, A. Scaling exponent and effective interactions in linear and cyclic polymer solutions: theory, simulations, and experiments. *Macromolecules* **2019**, *52*, 4579-4589.

in less than 6% quantity over the course of 10 days. It was ascertained that during the CuAAC cyclization, the major product (i.e. unimer) and the minor "impurity" (i.e. dimer) quantitatively convert from a linear to cyclic architecture. While there is a slight broadening in the molecular weight distribution, the polymer still maintains a high architectural purity. For the future syntheses of cyclic polymers, it is now understood that storage time of the linear precursor should be minimized to reduce the content of linear dimers.

2.2 INTRODUCTION

Cyclic polymers are of significant interest in a variety of natural and synthetic systems. For example, plasmid and mitochondrial DNA are often cyclic.[1] Cyclic polymers' inability to reptate makes them promising candidates as rheology modifiers[2-4] and alters their biodistribution and blood circulation.[5] Additionally, cyclic block copolymers have been explored as next-generation nanolithographic templates due to their smaller domain spacing compared to linear polymers.[6, 7] These often preferred and unique properties of cyclic polymers over analogous linear polymer systems stem from their topological differences (i.e., lack of chain ends), which result in vast changes in chain size, *inter*-chain interactions, packing, thermal properties, and dynamics in both melts and solutions.[2, 3, 8-21] In particular, in solutions and/or during solvent processing approaches, understanding solvent-cyclic polymer interactions and contrasting them to established trends of linear polymers is vital to capitalize on the unique properties that cyclic polymers may offer for biological and industrially-relevant materials applications such as polymer synthesis, separation/purification, drug delivery, etc.

For synthetic chemists, the copper-catalyzed azide-alkyne cycloaddition (CuAAC) "click" reaction[22] has been popularly used for polymer conjugation and has proved to be particularly versatile in preparing cyclic polymers.[23] Specifically, the CuAAC cyclization technique has been applied to generate cyclic homopolymers prepared by ATRP,[24] ROP,[25-27] RAFT,[28, 29] and cationic polymerizations.[30] The technique is also amenable to preparing cyclic block copolymers,[31-33] figure-eight-shaped polymers,[34, 35] cyclic dendronized polymers,[36] and more complex structures.[37] However, the presence of linear impurities in a cyclic polymer sample, even in trace amounts, can result in an imprecise measurement of its physical properties.[2, 38] Therefore the critical analysis of cyclic polymer purity and identification of likely sources of impurities is imperative for broadening the scope of the CuAAC cyclization route. Traditional polymer characterization techniques, such as SEC and NMR can often fail in accurately identifying trace impurities due to their low sensitivity. Unlike SEC, HPLC can effectively resolve byproducts based on functionality[38] and polymer architecture.[39] Once the trace impurities are fractionated from the desired product, MALDI-TOF MS is useful to identify the polymer structure especially when limited sample quantities are available for minor impurities.[40] Therefore a detailed quantitative study on cyclic polystyrene synthesized through the CuAAC reaction, combining HPLC and MALDI-TOF MS with SEC has been pursued.

As originally reported by Laurent and Grayson,[2] the CuAAC cyclization route (Scheme 2.1) toward making cyclic polystyrene (PS) involves three distinct steps: 1) the polymerization of styrene from an alkyne functionalized initiator forming **1**, 2) nucleophilic displacement of the terminal bromide group with an azide to yield **2**, and 3) the CuAAC cyclization of the polymer chain under high dilution to favor the desired cyclic

product, **3**. The presence of trace amounts of a lower SEC retention time impurity have been commonly reported, and is the subject of this study.

Scheme 2.1. Synthesis of cyclic polystyrene and origin of impurities.

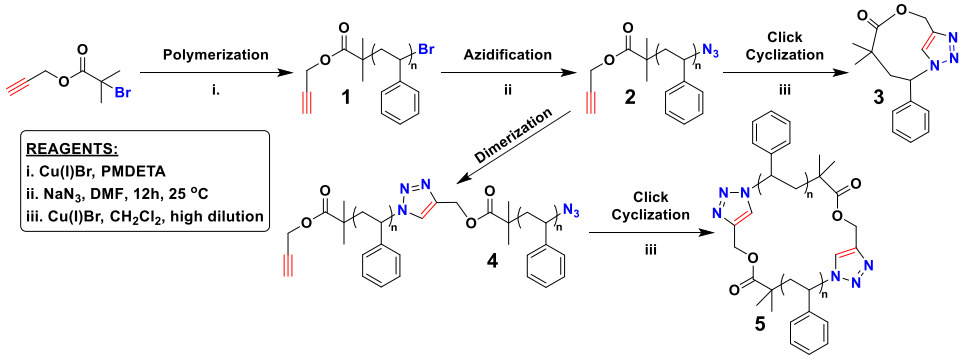

2.3 EXPERIMENTAL

2.3.1 Synthetic Protocols

α-Alkynyl-ω-bromo-polystyrene (1). To synthesize the α-alkynyl-ω-bromo-polystyrene precursor, a round bottomed flask was charged with PMDETA (43.6 mg, 0.252 mmol, 1.05 eq.), styrene (2.50 g, 24.0 mmol, 100 eq.), and the initiator propargyl 2-bromoisobutyrate (49.2 mg, 0.240, 1.00 eq). Upon two freeze/pump/thaw cycles, the flask is frozen, CuBr (34.0 mg, 0.240 mmol, 1.00 eq.) is added, and then further degassed by a final pump/thaw cycle. After warming to room temperature, the reaction mixture is placed into a preheated 100 °C oil bath and stirred under nitrogen for 30 min, 45 min, 5 h, and 6 h to synthesize *l*-PS_{2800}, *l*-$PS_{3700,}$ *l*-PS_{10k}, and *l*-$PS_{14k,}$ respectively. Upon completion of the designated reaction time, the reaction mixture is cooled to room temperature and purified by extraction from water into dichloromethane, followed by three additional washes with a saturated aqueous ammonium chloride solution. The organic layer is collected and dried

with sodium sulfate, followed by precipitation into methanol to yield the polymer as a white solid.

α-Alkynyl-ω-azido-polystyrene (2). In a typical reaction, α-alkynyl-ω-bromo-polystyrene **1** (2.46 g, 0.164 mmol, 1 eq.) is dissolved in dimethylformamide (10 mL). Sodium azide (1.07 g, 16.4 mmol, 100 eq.) is added to the reaction mixture and stirred under ambient conditions for 24 h, using a blast shield due to the reactive nature of azides. Finally, the reaction solution is diluted with dichloromethane (20 mL), followed by washing with deionized water (3 × 10 mL). The organic layer is collected and dried over anhydrous magnesium sulfate. After filtration, the solvent is removed *in vacuo* resulting in a ~90% yield.

Cyclic polystyrene (3). A solution of α-alkynyl-ω-azido-polystyrene **2** (39.7 mg, 0.004 mmol, 0.001 eq.) in 100 mL of dichloromethane is added to a 2-neck round bottom flask. In a second 2-neck round bottom flask, a solution of PMDETA (0.415 g, 2.4 mmol, 0.66 eq.) in DCM (150 mL) is added. Two freeze/pump/thaw cycles are separately performed on the flasks containing the linear polymer and PMDETA solutions. Upon an additional freeze of the PMDETA solution, CuBr (0.315 g, 2.2 mmol, 0.61 eq.) is added to the frozen solution. The flask is resealed, refilled with N_2, degassed through vacuum, and thawed. Upon both flasks reaching room temperature, a N_2 purged gastight syringe is filled with the polymer solution and added to the CuBr/PMDETA solution via a syringe pump at a rate 2.0 mL/min. Once the polymer is completely added to the CuBr/PMDETA solution, the reaction mixture is stirred an additional two hours to ensure complete cyclization. After completion of the reaction time, the reaction mixture is opened to air and washed with several portions of saturated aqueous ammonium chloride until the organic and aqueous

layer are colorless. The organic layer is collected and dried over anhydrous magnesium sulfate. After filtration, the solvent is removed *in vacuo* to yield a white powder with a yield of 90%.

2.3.2 Analytical Protocols

Size-Exclusion Chromatography (SEC) data were acquired using two different setups. Data from Figure 2.1, Table 2.1, Figure 2.3, Figure A6, and Figure A7 are from a Bishoff HPLC compact pump with THF as the mobile phase with a 0.7 mL/min flow rate with columns heated at a constant 40 °C by a column oven. This system was operated with a set of two PLgel Mixed-E columns (Agilent 300 × 7.5 mm) in series. Viscotek TDA 302 detector was used as refractive index detector. The instrument was calibrated with a set of polystyrene standards. Data from Figure 2.4, Figure 2.6, and Table A1 are from a Waters model 1515 isocratic pump (Milford, MA) with THF as the mobile phase with a 1 mL/min flow rate with columns heated at a constant 30 °C by a column oven. This system was operated with a set of two columns in series from Polymer Laboratories Inc. consisting of PSS SDV analytical linear M (8 mm × 300 mm) and PSS SDV analytical 100Å (8 × 300 mm) columns. A Model 2487 differential refractometer detector was used as a refractive index detector. The instrument was calibrated with Polystyrene ReadyCal Standards from Waters.

For the normal phase liquid chromatography (NPLC) separation, a bare silica column (Nucleosil. 5 μm, 50 Å, 250 × 4.6 mm) was used. Mobile phase was a THF/n-hexane mixture (37/63, v/v) delivered by an HPLC pump (Shimadzu LC-20AD) at a flow of 0.5 mL/min. The column temperature was kept at 20 °C using a homemade column jacket and a water bath circulator (Julabo F25). Chromatograms were recorded with a

UV/Vis absorption detector (YounlinUV730D). All samples for NPLC analysis were dissolved in the eluent at a concentration of 1 mg/mL and the injection volume was 100 µL.

Mass spectral data were collected using two different instruments. Data in Table 2.1, Table A1, Figures 2.5, 2.7, 2.8, A3, and A5 were collected from a Bruker-Daltonics Matrix Assisted Laser Desorption Ionization Time-of-Flight (MALDI-TOF) Autoflex III mass spectrometer in reflector mode with positive ion detection. Typical sample preparation for MALDI-TOF MS data was performed by making stock solutions in THF of matrix (20 mg/ml), polymer analyte (2 mg/ml), and an appropriate cation source (2 mg/ml). The stock solutions were mixed in a 20/5/2 ratio (matrix/analyte/cation), deposited onto the MALDI target plate and allowed to evaporate via the dried droplet method. For polystyrene derivatives, dithranol was found to be an appropriate matrix and sodium trifluoroacetate (NaTFA) was used as the cation source to generate sodium adduct of the polystyrene. MALDI-TOF MS data were calibrated against SpheriCal dendritic calibrants from Polymer Factory (Stockholm, Sweden). Mn and Đ of the resultant spectra were calculated using Polytools software. Data in Figure 2.2 and Figure A4 were collected from Bruker-Daltonics MALDI-TOF Autoflex Speed mass spectrometer in linear mode with positive ion detection. DCTB was used as MALDI matrix and NaTFA was used as cationization agent. Mass calibration was performed using homemade polystyrene standards. Typical sample preparation was performed by making stock solutions in THF of matrix (20 mg/ml), polymer analyte (1 mg/ml), and NaTFA (2 mg/ml). The stock solutions were mixed in a 100/1/1 ratio (matrix/analyte/cation), and deposited onto the MALDI target plate.

2.4 RESULTS

In order to identify and quantify the impurities formed during the CuAAC cyclization, two different molecular weights of PS (M_n = 2800 and 3700) (Table 2.1) were prepared and cyclized as previously described.[2] The resultant SEC chromatograms of cyclic polystyrene (*c*-PS), and its linear polystyrene (*l*-PS) precursor exhibited no apparent shoulder of a larger hydrodynamic radius byproduct when immediately analyzed by SEC (Figure 2.1). However, HPLC could be used to effectively isolate trace higher molecular weight impurities (Figures A1 and A2) and enabled their quantification: 2.8% in the case of *c*-PS_{2800}, and 0.4% in the case of *c*-PS_{3700} (Table 2.2) after 10 days. Contrary to the observed results, the Jacobson-Stockmayer equation[41] predicts that intramolecular coupling that occurs during the cyclization process would decrease for higher M_n polymers because the larger end-to-end distance would inhibit intramolecular cyclization, therefore intermolecular coupling might be more competitive. This model was reinforced by Lonsdale and Monteiro, who demonstrated in kinetic simulations a decreasing yield of monocyclic polymers with increasing molecular weight of polystyrene.[42] Because the opposite was observed in this study, alternative explanations for the oligomeric byproducts were investigated.

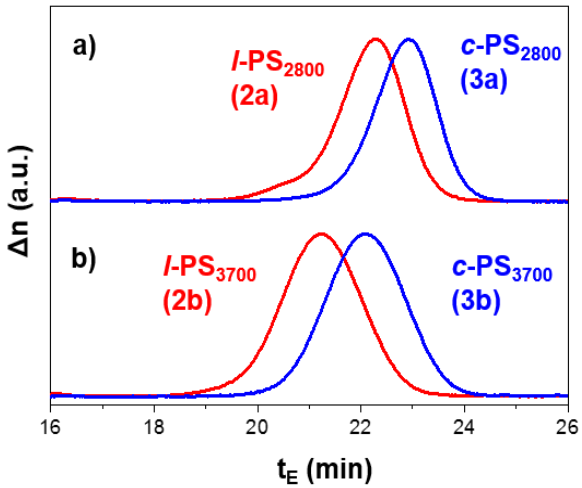

Figure 2.1. SEC chromatograms of a) *l*-PS_{2800} (**2a**) and *c*-PS_{2800} (**3a**) 10 days after click cyclization, b) *l*-PS_{3700} (**2b**) and *c*-PS_{3700} (**3b**) 10 days after click cyclization.

Table 2.1: Mass determination of *l*-PS (2) and *c*-PS (3) by SEC and MALDI-TOF MS *cyclic M_n values based on retention time and ratios of $M_{n\ c\text{-PS}}/M_{n\ l\text{-PS}}$ reported by Alberty et al.[43] as 0.80 for PS_{3000} and 0.78 for PS_{3800}

	MALDI-TOF MS		**SEC**	
Polymer	**M_n**	**Đ**	**M_n**	**Đ**
2a	2850	1.05	2500	1.12
3a	2700	1.01	2250*	1.09
2b	3600	1.01	3800	1.14
3b	3600	1.02	3200*	1.12

Table 2.2: The percentage of oligomeric impurities observed in samples *l*-PS, **2a**, *c*-PS, **3a**, *l*-PS, **2b**, and *c*-PS, **3b**.

M_n	**2800**		**3700**	
Polymer	***l*-PS 2a**	***c*-PS 3a**	***l*-PS 2b**	***c*-PS 3b**
10 days	5.50%	2.80%	2.00%	0.40%
20 days	7.70%	2.80%	3.50%	0.40%
30 days	10.00%	2.90%	5.50%	0.50%
50 days	12.20%	2.90%	7.30%	0.50%

Potential sources of higher molecular weight impurities include CuAAC oligomerization rather than cyclization resulting from either a missing azide end group (due to incomplete azidization or loss of the functional end group during polymerization), or a

missing alkyne end group (due to Glaser coupling during polymerization, storage, or cyclization). In addition, premature coupling of the azide and alkyne end groups might occur during the azidization reaction, storage, or cyclization. Structural determination of the impurity by MALDI-TOF MS will be critical to confirming which of these pathways is responsible for the observed impurities.

The MALDI-TOF mass spectra of the **2** and **3** before HPLC purification confirm qualitatively that the major component of these materials are the expected unimers (Figures 2.2a and 2.2d). For unpurified *l*-PS (**2a** + **4a**), the spectrum acquired in linear mode appears to be dominated by unimer (**2a**), with a trace amount of dimer (**4a**). MS analysis of purified **2a** (Figure 2.2b) exhibits the expected *l*-PS sodium adduct (25-mer m/z_{obs} = 2793.8, m/z_{theo} = 2794.0). However, characterization of the HPLC isolated impurity fraction (Figure 2.2c) enables confirmation of its assignment as linear dimer (*ld*-PS), **4a**, with a single triazole linkage as well as alkyne and azide end groups (46-mer m/z_{obs} = 5148.2, m/z_{theo} = 5148.3). Furthermore, when these samples are analyzed in reflector mode, both **2a** and **4a** show a strong metastable signal, confirming the presence of a single azide functionality (Figure A3).[44] Upon cyclization, the product again exhibits a major unimer distribution with a trace amount of dimer (Figure 2.2d). The mass spectrum of the major HPLC fraction, **3a**, (Figure 2.2e) shows only the sodium adduct of the expected cyclic product (25-mer m/z_{obs} = 2793.9, m/z_{theo} = 2794.0) while the fractionated cyclic dimer (*cd*-PS), **5a**, (Figure 2.2f) showed a mass distribution corresponding to sodium (and potassium) adducts of macrocycles with two triazole linkages (46-mer m/z_{obs} = 5148.3, m/z_{theo} = 5148.3) in agreement with previous MS characterization.[45] Examination of **3a** and **5a** in reflector mode confirmed the disappearance of the metastable azide signal, as expected for the

triazole products (Figure A3). Identical trends were observed for the higher molecular weight PS samples **2b**-**5b** (Figures A4 and A5). These data confirm that the predominant impurities in all samples are dimers, with the side reaction in question involving an intermolecular CuAAC coupling.

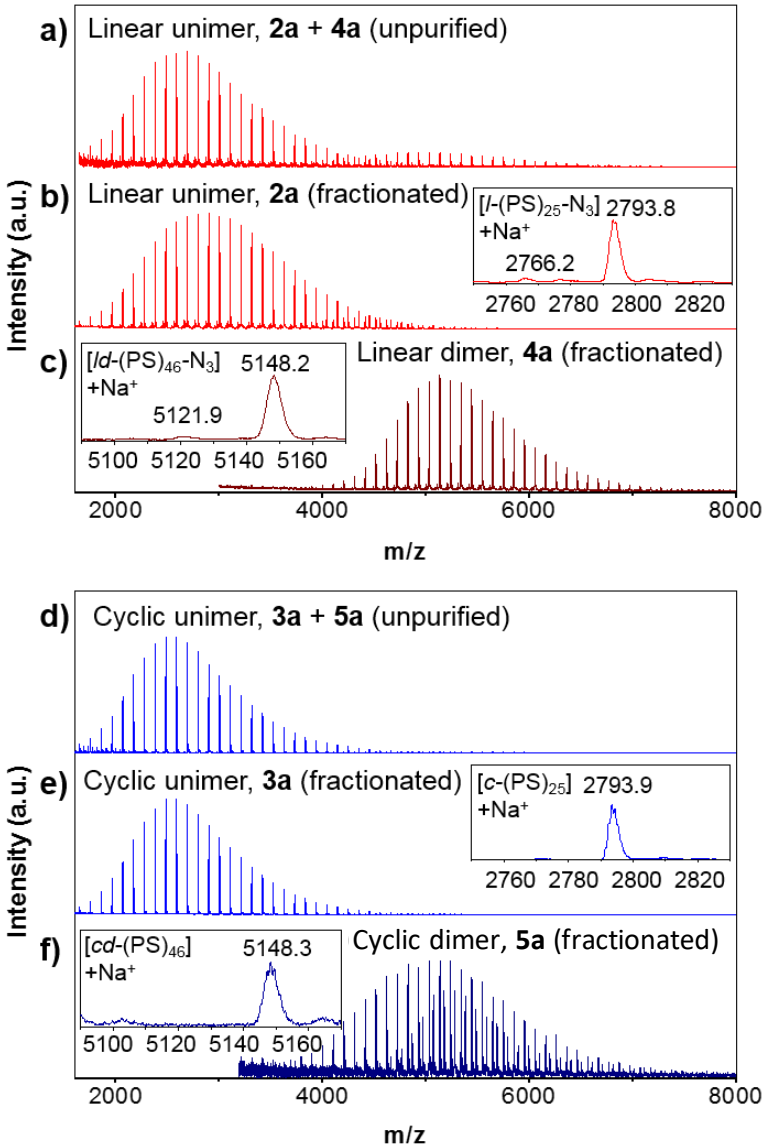

Figure 2.2. MALDI TOF mass spectra of samples in linear mode before and after fractionation: a) unpurified *l*-PS$_{2800}$, **2a + 4a**, b) purified *l*-PS$_{2800}$, **2a**, c) purified *ld*-PS$_{2800}$, **4a**, and d) unpurified *c*-PS$_{2800}$, **3a** + **5a**, e) purified *c*-PS$_{2800}$, **3a**, and f) purified *cd*-PS$_{2800}$, **5a**

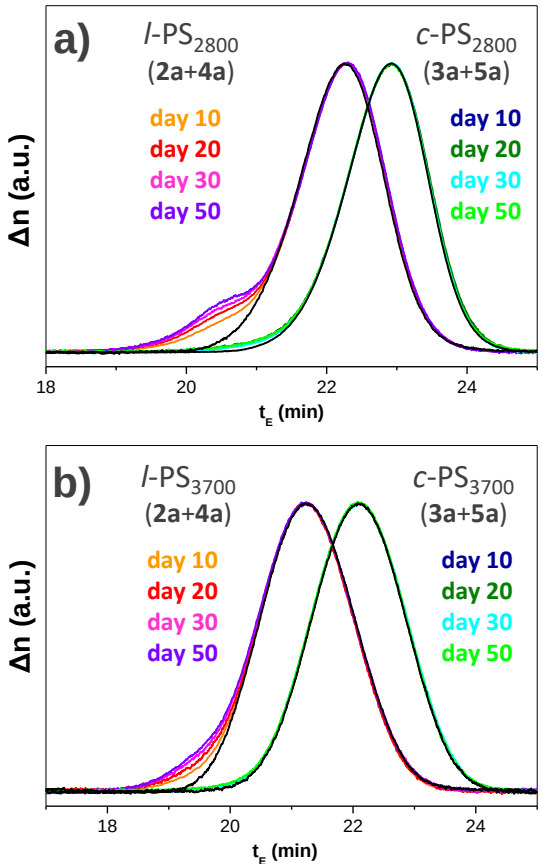

Figure 2.3: SEC chromatograms of *l*-PS and *c*-PS at days 10, 20, 30, and 50, (post-synthesis). Black traces are for the HPLC fractionated unimers.

The chemical stability of both the *l*-PS and *c*-PS could offer further insight into the origin of the observed dimers, and therefore the impurities were isolated and quantified by HPLC at 10, 20, 30 and 50 days post synthesis (Figures A6 and A7). First of all, if the higher molecular weight impurities in the *c*-PS samples were in fact *cd*-PS, both cyclics should be inert and therefore the sample should exhibit no change in relative proportions over time. HPLC analysis for 50 days post-cyclization confirmed the lack of reactivity of the cyclic samples (Table 2.1, Figure 2.3). The linear precursors, on the other hand, did exhibit a susceptibility to dimerization during this same time frame (when stored at ambient temperature in powder state). Specifically, the dimer fraction of PS_{2800} increased from 5.5% to 12.2% between 10 and 50 days, while the dimer fraction of PS_{3700} increased from

2.0 % to 7.3%. These results provide conclusive evidence that the linear precursors are subject to slow dimerization during storage, even in the absence of the copper catalyst.

Finally, in order to determine whether the azidization step was partially responsible for the generation of the PS dimers, MALDI-TOF MS and SEC were utilized to examine samples at various time points during the azidization. During the typical 12-24 h reaction time, *l*-PS samples did not exhibit an apparently higher molecular weight shoulder by SEC (Figure 2.4). Furthermore, by MALDI-ToF MS analysis (Figure 2.5), a secondary distribution corresponding to dimers did not arise, suggesting the azidization step was likely not a major source of byproducts.

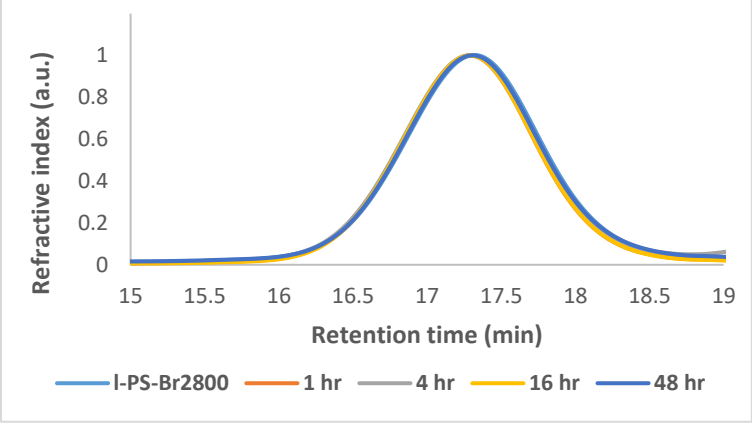

Figure 2.4: SEC chromatograms of azidization reaction of **1a** to generate **2a** at 1h, 4 h 16 h and 48h show no sign of click oligomerization.

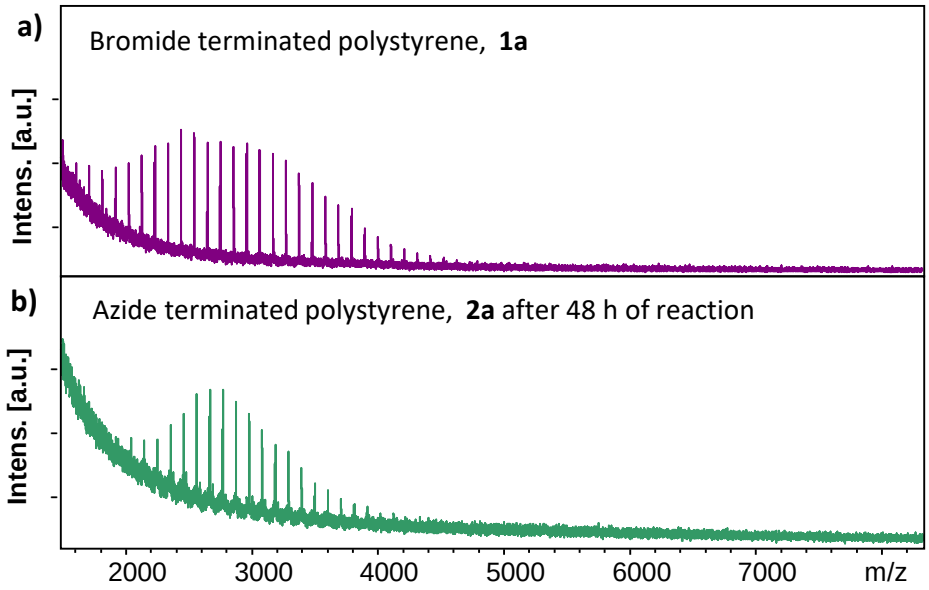

Figure 2.5: MALDI-TOF mass spectra of azidization reaction of **1a** to generate **2a** at a) 0h, and b) at 48 h exhibits no sign of "click" oligomerization.

Based on the findings of this study, two additional higher molecular weight cyclic polystyrene samples, PS_{11000} and PS_{15000}, were synthesized for additional characterization by small-angle neutron scattering. The polymers used in this study underwent the azidization directly prior to cyclization to minimize the chance of uncatalyzed azide-alkyne dimerization reactions. Illustrated below, in Figure 2.6, are chromatograms of *l*-PS before azidization and *c*-PS after cyclization. The increased retention time post-cyclization is indicative of minimal dimerization. See Table A1 for molecular weight data by SEC and MALDI-ToF MS.

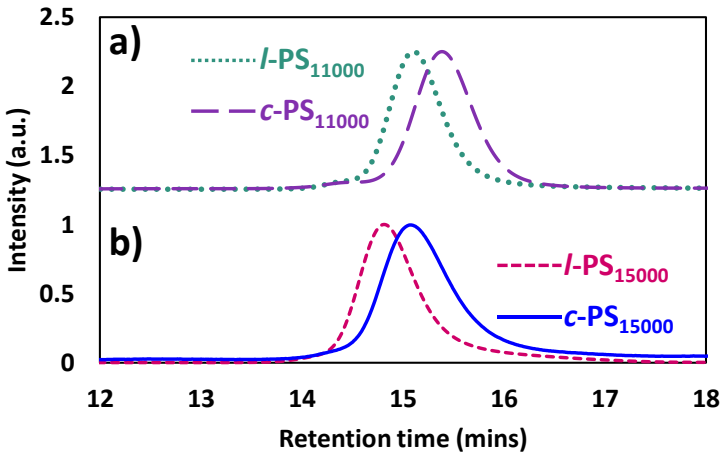

Figure 2.6. GPC chromatograms of (a) *l*- and *c*-PS_{10k} and (b) *l*- and *c*-PS_{14k}. Both sets of chromatograms illustrate a longer retention time for the cyclic analog due to reduced hydrodynamic volume.

Further analysis of the *l*-PS and *c*-PS polymers by MALDI-ToF MS is shown below in Figure 2.7 and 2.8. The polymers maintain the same molecular weight distribution before and after cyclization, with no visual secondary dimer distribution. This data suggests that if these polymers contain cyclic dimers, it is a very minimal quantity.

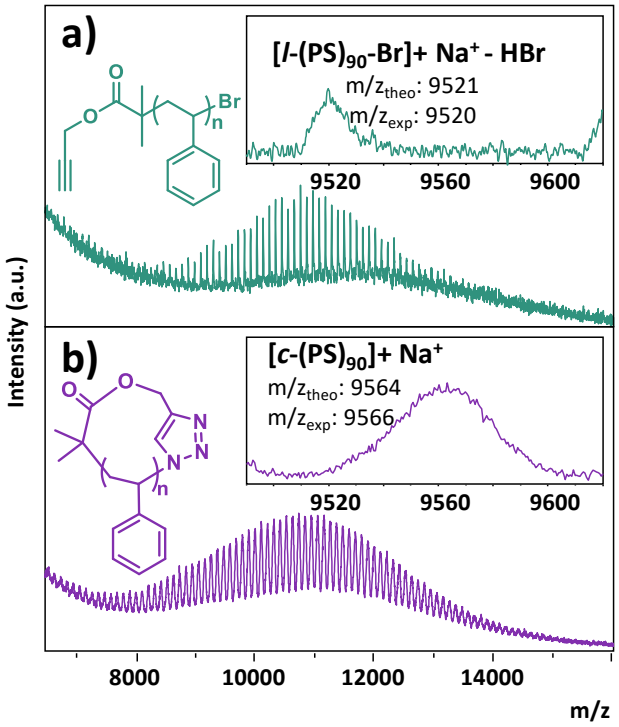

Figure 2.7. MALDI-TOF MS spectra of *l*- and *c*-PS_{10k} with expanded spectra from m/z = 9490 to 9620 confirm quantitative end group and architectural transformation.

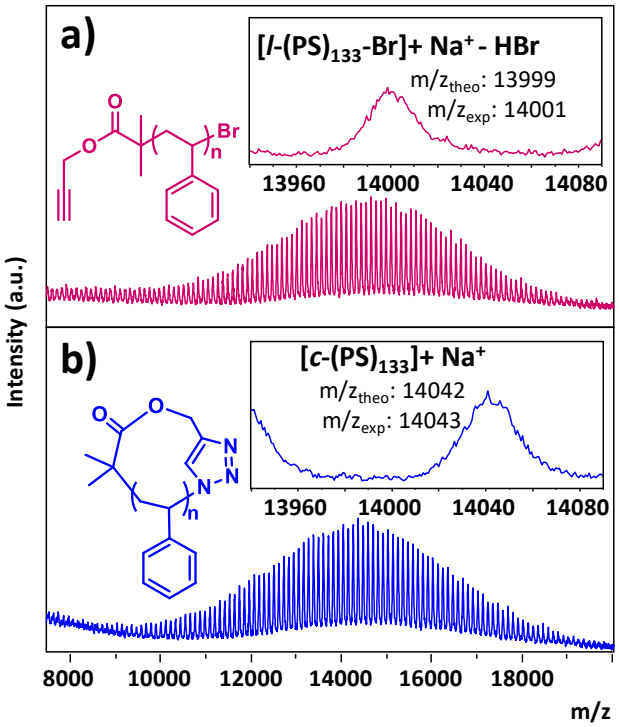

Figure 2.8. MALDI-TOF MS spectra of l- and c-PS_{14k} with expanded spectra from m/z = 13940 to 14090 confirm quantitative end group and architectural transformation.

2.5 CONCLUSIONS

With the growing importance of the CuAAC cyclization to enable the investigation of cyclic polymer properties, critical assessment of cyclic purity remains an important issue. Towards that goal, a detailed analysis was carried out to identify and quantify the impurities generated during the CuAAC cyclization of polystyrene. Although some generation of cyclic dimers appears to occur during cyclization (and this process may follow the traditional Jacobson-Stockmayer model), monitoring the stability of the α-alkynyl, ω-azido linear precursors confirmed that the predominant sensitivity during the reported reaction pathway is the uncatalyzed dimerization of the activated linear precursor ***before*** the cyclization step. Therefore reduced storage times of the linear precursor at low temperature are recommended to optimize product purity. While this dimerization reaction led to the generation of cyclic dimers upon cyclization, MALDI-TOF MS analysis of the isolated impurities after cyclization provided no appreciable evidence for alternative byproduct pathways, including incomplete terminal group azidization, or Glaser dimerization of alkyne initiating groups. Most importantly, no evidence was found for the presence of any linear impurities after cyclization, confirming the efficiency of CuAAC cyclization and the high topological purity of the cyclic PS product.

The above results confirm that cyclic polymers with high topological purity can be prepared as long as the coupling reaction utilized is extremely rapid, as reported for a number of alternative "click" reactions. This study also highlights a critical problem with such highly activated coupling reactions: their highly exothermic nature makes them prone to premature reactivity. Therefore, alternative conjugation reactions that are explored as candidates for this ring-closure methodology should ideally exhibit highly efficient coupling when exposed to cyclization conditions (e.g. the copper catalyst for CuAAC

cyclization) but also demonstrate negligible reactivity during their pre-cyclization dormant conditions. Furthermore, the analysis described above is suggested as a starting point to more rigorously analyze and compare the cyclic purity of the numerous reported cyclization techniques.

2.6 REFERENCES

1. Helinski, D. R.; Clewell, D. B. Circular DNA. *Annual Review of Biochemistry* **1971,** 40, 899-942.

2. Kapnistos, M.; Lang, M.; Vlassopoulos, D.; Pyckhout-Hintzen, W.; Richter, D.; Cho, D.; Chang, T.; Rubinstein, M. Unexpected power-law stress relaxation of entangled ring polymers. *Nature Materials* **2008,** 7 (12), 997-1002.

3. Halverson, J. D.; Grest, G. S.; Grosberg, A. Y.; Kremer, K. Rheology of ring polymer melts: from linear contaminants to ring-linear blends. *Physical Review Letters* **2012,** 108 (3), 038301.

4. Pasquino, R.; Vasilakopoulos, T. C.; Jeong, Y. C.; Lee, H.; Rogers, S.; Sakellariou, G.; Allgaier, J.; Takano, A.; Brás, A. R.; Chang, T.; Gooßen, S.; Pyckhout-Hintzen, W.; Wischnewski, A.; Hadjichristidis, N.; Richter, D.; Rubinstein, M.; Vlassopoulos, D. Viscosity of ring polymer melts. *ACS Macro Letters* **2013,** 2 (10), 874-878.

5. Nasongkla, N.; Chen, B.; Macaraeg, N.; Fox, M. E.; Fréchet, J. M. J.; Szoka, F. C. Dependence of pharmacokinetics and biodistribution on polymer architecture: effect of cyclic versus linear polymers. *Journal of the American Chemical Society* **2009,** 131 (11), 3842-3843.

6. Poelma, J. E.; Ono, K.; Miyajima, D.; Aida, T.; Satoh, K.; Hawker, C. J. Cyclic block copolymers for controlling feature sizes in block copolymer lithography. *ACS Nano* **2012,** 6 (12), 10845-10854.

7. Gartner, T. E.; Kubo, T.; Seo, Y.; Tansky, M.; Hall, L. M.; Sumerlin, B. S.; Epps, T. H. Domain spacing and composition profile behavior in salt-doped cyclic vs linear block polymer thin films: a joint experimental and simulation study. *Macromolecules* **2017,** 50 (18), 7169-7176.

8. Semlyen, J. A., *Cyclic Polymers*. 2nd ed.; Kluwer Academic Publishers: The Netherlands, 2000.

9. Wang, Z.-G. 50th anniversary perspective: polymer conformation—a pedagogical review. *Macromolecules* **2017,** 50 (23), 9073-9114.

10. Narros, A.; Moreno, A. J.; Likos, C. N. Influence of topology on effective potentials: coarse-graining ring polymers. *Soft Matter* **2010,** 6 (11), 2435-2441.

11. Narros, A.; Moreno, A. J.; Likos, C. N. Architecture-induced size asymmetry and effective interactions of ring polymers: simulation and theory. *Macromolecules* **2013,** 46 (23), 9437-9445.

12. Halverson, J. D.; Lee, W. B.; Grest, G. S.; Grosberg, A. Y.; Kremer, K. Molecular dynamics simulation study of nonconcatenated ring polymers in a melt. I. statics. *The Journal of Chemical Physics* **2011,** 134 (20), 204904.

13. Halverson, J. D.; Lee, W. B.; Grest, G. S.; Grosberg, A. Y.; Kremer, K. Molecular dynamics simulation study of nonconcatenated ring polymers in a melt. II. dynamics. *The Journal of Chemical Physics* **2011,** 134 (20), 204905.

14. Ge, T.; Panyukov, S.; Rubinstein, M. Self-similar conformations and dynamics in entangled melts and solutions of nonconcatenated ring polymers. *Macromolecules* **2016,** 49 (2), 708-722.

15. Sakaue, T. Ring polymers in melts and solutions: scaling and crossover. *Physical Review Letters* **2011,** 106 (16), 167802.

16. Moore, N. T.; Lua, R. C.; Grosberg, A. Y. Topologically driven swelling of a polymer loop. *Proceedings of the National Academy of Sciences of the United States of America* **2004,** 101 (37), 13431-13435.

17. Reigh, S. Y.; Yoon, D. Y. Concentration dependence of ring polymer conformations from Monte Carlo simulations. *ACS Macro Letters* **2013,** 2 (4), 296-300.

18. Iwamoto, T.; Doi, Y.; Kinoshita, K.; Takano, A.; Takahashi, Y.; Kim, E.; Kim, T.-H.; Takata, S.-i.; Nagao, M.; Matsushita, Y. Conformations of ring polystyrenes in semidilute solutions and in linear polymer matrices studied by SANS. *Macromolecules* **2018,** 51 (17), 6836-6847.

19. Zhang, L.; Elupula, R.; Grayson, S. M.; Torkelson, J. M. Major impact of cyclic chain topology on the T_g-confinement effect of supported thin films of polystyrene. *Macromolecules* **2016,** 49 (1), 257-268.

20. Lorenzo, A. T.; Cordova, M. E.; Grayson, S. M.; Müller, A. J.; Hoskins, J. N. A comparative study of crystallization behavior of analogous linear and cyclic poly(ε-caprolactones). **2011,** 44 (7).

21. Shin, E. J.; Jeong, W.; Brown, H. A.; Koo, B. J.; Hedrick, J. L.; Waymouth, R. M. Crystallization of cyclic polymers: synthesis and crystallization behavior of high molecular weight cyclic poly(ε-caprolactone)s. *Macromolecules* **2011,** 44 (8), 2773-2779.

22. Kolb, H. C.; Finn, M. G.; Sharpless, K. B. Click chemistry: diverse chemical function from a few good reactions. *Angewandte Chemie International Edition* **2001,** 40 (11), 2004-2021.

23. Laurent, B. A.; Grayson, S. M. An efficient route to well-defined macrocyclic polymers via “click” cyclization. *Journal of the American Chemical Society* **2006,** 128 (13), 4238-4239.

24. Xu, J.; Ye, J.; Liu, S. Synthesis of well-defined cyclic poly(N-isopropylacrylamide) via click chemistry and its unique thermal phase transition behavior. *Macromolecules* **2007,** 40 (25), 9103-9110.

25. Hoskins, J. N.; Grayson, S. M. Synthesis and degradation behavior of cyclic poly(ε-caprolactone). *Macromolecules* **2009,** 42 (17), 6406-6413.

26. Xie, M.; Shi, J.; Ding, L.; Li, J.; Han, H.; Zhang, Y. Cyclic poly(ε-caprolactone) synthesized by combination of ring-opening polymerization with ring-closing metathesis, ring closing enyne metathesis, or "click" reaction. *Journal of Polymer Science Part A: Polymer Chemistry* **2009,** 47 (12), 3022-3033.

27. Misaka, H.; Kakuchi, R.; Zhang, C.; Sakai, R.; Satoh, T.; Kakuchi, T. Synthesis of well-defined macrocyclic poly(δ-valerolactone) by "click cyclization". *Macromolecules* **2009,** 42 (14), 5091-5096.

28. Qiu, X.-P.; Tanaka, F.; Winnik, F. M. Temperature-induced phase transition of well-defined cyclic poly(N-isopropylacrylamide)s in aqueous solution. *Macromolecules* **2007,** 40 (20), 7069-7071.

29. Goldmann, A. S.; Quémener, D.; Millard, P.-E.; Davis, T. P.; Stenzel, M. H.; Barner-Kowollik, C.; Müller, A. H. E. Access to cyclic polystyrenes via a combination of reversible addition fragmentation chain transfer (RAFT) polymerization and click chemistry. *Polymer* **2008,** 49 (9), 2274-2281.

30. Cortez, M. A.; Godbey, W. T.; Fang, Y.; Payne, M. E.; Cafferty, B. J.; Kosakowska, K. A.; Grayson, S. M. The synthesis of cyclic poly(ethylene imine) and exact linear analogues: an evaluation of gene delivery comparing polymer architectures. *Journal of the American Chemical Society* **2015,** 137 (20), 6541-6549.

31. Eugene, D. M.; Grayson, S. M. Efficient preparation of cyclic poly(methyl acrylate)-*block*-poly(styrene) by combination of atom transfer radical polymerization and click cyclization. *Macromolecules* **2008,** 41 (14), 5082-5084.

32. Zhang, B.; Zhang, H.; Li, Y.; Hoskins, J. N.; Grayson, S. M. Exploring the effect of amphiphilic polymer architecture: synthesis, characterization, and self-assembly of both cyclic and linear poly(ethylene gylcol)-*b*-polycaprolactone. *ACS Macro Letters* **2013,** 2 (10), 845-848.

33. Ge, Z.; Zhou, Y.; Xu, J.; Liu, H.; Chen, D.; Liu, S. High-efficiency preparation of macrocyclic diblock copolymers via selective click reaction in micellar media. *Journal of the American Chemical Society* **2009,** 131 (5), 1628-1629.

34. Shi, G.-Y.; Pan, C.-Y. Synthesis of well-defined figure-of-eight-shaped polymers by a combination of ATRP and click chemistry. *Macromolecular Rapid Communications* **2008,** 29 (20), 1672-1678.

35. Shi, G.-Y.; Yang, L.-P.; Pan, C.-Y. Synthesis and characterization of well-defined polystyrene and poly(ε-caprolactone) hetero eight-shaped copolymers. *Journal of Polymer Science Part A: Polymer Chemistry* **2008,** 46 (19), 6496-6508.

36. Laurent, B. A.; Grayson, S. M. Synthesis of cyclic dendronized polymers via divergent "graft-from" and convergent click "graft-to" routes: preparation of modular toroidal macromolecules. *Journal of the American Chemical Society* **2011,** 133 (34), 13421-13429.

37. Jeong, J.; Kim, K.; Lee, R.; Lee, S.; Kim, H.; Jung, H.; Kadir, M. A.; Jang, Y.; Jeon, H. B.; Matyjaszewski, K.; Chang, T.; Paik, H.-j. Preparation and analysis of bicyclic polystyrene. *Macromolecules* **2014,** 47 (12), 3791-3796.

38. Im, K.; Kim, Y.; Chang, T.; Lee, K.; Choi, N. Separation of branched polystyrene by comprehensive two-dimensional liquid chromatography. *Journal of Chromatography A* **2006,** 1103 (2), 235-242.

39. Lee, H. C.; Lee, H.; Lee, W.; Chang, T.; Roovers, J. Fractionation of cyclic polystyrene from linear precursor by HPLC at the chromatographic critical condition. *Macromolecules* **2000,** 33 (22), 8119-8121.

40. Park, S.; Cho, D.; Ryu, J.; Kwon, K.; Chang, T.; Park, J. Temperature gradient interaction chromatography and matrix-assisted laser desorption/ionization time-of-flight mass spectrometry analysis of air terminated polystyryllithium. *Journal of Chromatography A* **2002,** 958 (1), 183-189.

41. Jacobson, H.; Stockmayer, W. H. Intramolecular reaction in polycondensations. I. the theory of linear systems. *The Journal of Chemical Physics* **1950,** 18 (12), 1600-1606.

42. Lonsdale, D. E.; Monteiro, M. J. Kinetic simulations for cyclization of α,ω-telechelic polymers. *Journal of Polymer Science Part A: Polymer Chemistry* **2010,** 48 (20), 4496-4503.

43. Alberty, K. A.; Hogen-Esch, T. E.; Carlotti, S. Synthesis and characterization of macrocyclic vinyl-aromatic polymers. *Macromolecular Chemistry and Physics* **2005,** 206 (10), 1035-1042.

44. Li, Y.; Hoskins, J. N.; Sreerama, S. G.; Grayson, S. M. MALDI−TOF mass spectral characterization of polymers containing an azide group: evidence of metastable ions. *Macromolecules* **2010,** 43 (14), 6225-6228.

45. Sreerama, S. G.; Elupula, R.; Laurent, B. A.; Zhang, B.; Grayson, S. M. Use of MALDI-ToF MS to elucidate the structure of oligomeric impurities formed during ‘click’ cyclization of polystyrene. *Reactive and Functional Polymers* **2014,** 80, 83-94.

CHAPTER 3

DETECTION, QUANTIFICATION AND "CLICK-SCAVENGING" OF IMPURITIES IN CYCLIC POLY(GLYCIDYL PHENYL ETHER) OBTAINED BY ZWITTERIONIONC RING-EXPANSION POLYMERIZATION WITH $B(C_6F_5)_3$*

3.1 ABSTRACT

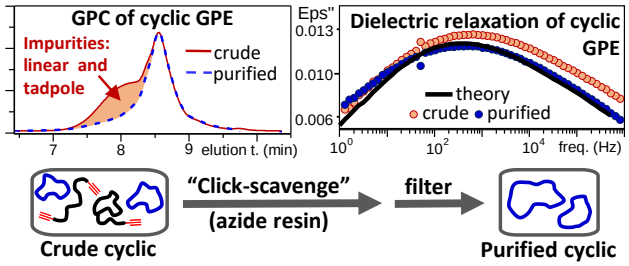

The physical properties of cyclic polymers can be perturbed by the presence of architectural impurities, even in trace amounts. As a result, it is important to develop techniques for quantifying and improving the purity of cyclic polymer samples. The zwitterionic ring-expansion polymerization (ZREP) of glycidyl phenyl ether (GPE) with $B(C_6F_5)_3$ is a convenient, one-step method to generate cyclic polyethers in large amounts. However, the obtained cyclic samples are inherently contaminated by architectural impurities, which in this study are detected, identified, quantified, and successfully removed by a "click-scavenging" approach. The analytical techniques employed

*A portion of this work has been published in Haque, F. M.; Alegria, A.; Grayson, S. M.; Barroso-Bujans, F. Detection, Quantification and "Click-Scavenging" of Impurities in Cyclic Poly(Glycidyl Phenyl Ether) Obtained by Zwitterionic Ring-Expansion Polymerization with $B(C_6F_5)_3$. *Macromolecules* **2017**, *50*, 1870-1881.

included matrix-assisted laser desorption/ionization time-of-flight mass spectrometry (MALDI–TOF MS), quantitative Fourier transform infrared spectroscopy (FTIR), and gel permeation chromatography/multiangle light scattering (GPC-MALS). The end group functionalization of the architectural impurities was a particularly useful method in the identification of tadpole and linear polymers in cyclic poly(glycidyl phenyl ether) samples of M_n = 1.1 and 11.7 kg/mol. Moreover, differential scanning calorimetry (DSC) measurements demonstrated that the presence of architectural impurities cause only a small reduction (1.4-2.0 °C) of the glass transition temperature (T_g) of the cyclic polyether; an effect that is corroborated in this investigation by means of dielectric spectroscopy. The segmental and local dynamics of cyclic samples are shown to be only slightly modified by the presence of a small percentage of architectural impurities.

3.2 INTRODUCTION

Cyclic polymers have been the subject of increasing investigations because their ring-like topology and lack of chain ends imparts upon them unique properties, both in bulk and in solution, relative to their linear analogues.[1-5] In solution, cyclic chains show reduced hydrodynamic volumes, radii of gyration, and intrinsic viscosities relative to their linear counterparts. In the melt, cyclic chains of low or medium molecular weight are characterized by showing higher glass transition temperatures (T_g) than their linear counterparts as a consequence of the absence of the plasticizing end groups. This effect disappears at high molecular weights, where the T_g becomes independent of both the molecular weight and the topology as the contribution of the end groups vanishes. Cyclic polymers also show lower melt viscosities than their linear analogues, and intriguing

rheological behavior: entangled pure cyclic polymers do not exhibit plateau modulus and exhibit faster terminal relaxation than the linear counterparts.

The presence of linear impurities and other contaminants in cyclic samples is a crucial consideration to take into account when reporting cyclic polymer properties. For example, it has been observed experimentally[6] and by simulations[7] that a small fraction of linear chains significantly influences the rheology of cyclic polymers in the terminal regime of the modulus. These unwanted contaminants are often formed as byproducts during the synthesis of macrocycles. The ring-expansion techniques used for the synthesis of cyclic polymers are less prone to generate linear contaminants than the ring-closure techniques for very high molecular weight polymers.[8] However, even though some examples of ring-expansion techniques generate very pure macrocycles, such as in the zwitterionic ring-expansion polymerization (ZREP) of lactide with N-heterocyclic carbenes[9] and in the ring-expansion metathesis polymerization (ROMP) of cyclic olefins with ruthenium catalysts,[10, 11] there are several examples where mixtures of linear and cyclic chains are cogenerated. For example, Grubbs et al. found that during the ROMP of 1,5-cyclooctadiene to generate cyclic polybutadiene, traces of an acyclic impurity in the monomer led to linear contaminants.[11] Likewise, Waymouth et al. found that the DBU-mediated ZREP of lactide to generate cyclic polylactides was accompanied by the cogeneration of linear impurities due to the formation of a ketene aminal intermediate.[12, 13]

Identification of architectural impurities in cyclic polymers is typically done by MALDI-TOF MS,[14] GPC-MALS,[15] GPC-MALS-viscometer analysis,[11] and HPLC under critical conditions.[16] Other techniques such as ion mobility spectrometry-mass

spectrometry have been used to differentiate cyclic chains from linear analogues with high sensitivity.[17] Since most synthetic techniques are susceptible to the generation of linear byproducts, a significant effort has been directed to identify the presence of linear impurities in cyclic polymer samples. However, as it will be demonstrated in the present work, other architectural impurities such as tadpole polymers (a cyclic head connected to a linear tail) can contaminate the cyclic polymers but their detection by traditional MS may be hindered if both compounds exhibit an identical molecular weight.

In a previous study, we found that ZREP of glycidyl ethers with $B(C_6F_5)_3$ generated cyclic polyethers but that they were contaminated with hydroxyl-terminated linear impurities (**Scheme 3.1**).[18] The generation of cyclic polyethers by ZREP has the significant advantage of producing large scales of the cyclic product in one-pot synthesis (several grams of sample in few hours). Such scales are difficult to achieve using the ring-closure technique because of the high dilution that is required to achieve the intramolecular cyclization.[19] Therefore, a way to exploit the scalable generation of cyclic polyethers by ZREP is to find an efficient method to remove the architectural impurities.

Scheme 3.1. ZREP of Glycidyl Ethers Producing Cyclic, Tadpole, and Linear Polyethers by a Backbiting Event, Dimerization, and the Addition of Water, respectively, where their respective functionality is shown based on the "click-scavenging" purification protocol. See **Scheme 3.3** for a proposed mechanism for the formation on the tadpole impurity.

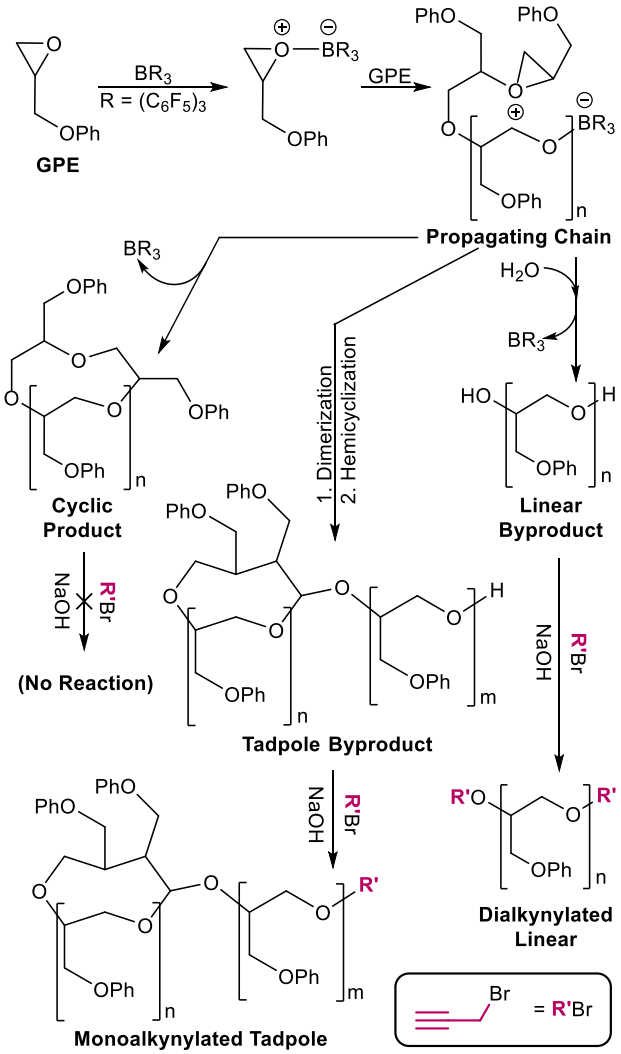

The present study assesses a simple one-pot "click-scavenging" protocol to effect the removal of unwanted byproducts. Herein, we perform an extensive study on the detection, quantification and removal of architectural contaminants in cyclic poly(glycidyl phenyl ether) [poly(GPE)] obtained by ZREP of GPE with $B(C_6F_5)_3$. The major architectural impurities in low molecular weight cyclic poly(GPE) were

determined to be tadpole structures with identical molecular formulas as cyclic chains rather than the previously reported linear polymer impurities.[18] Purification of cyclic chains was then achieved by a simple "click-scavenging" protocol involving the quantitative alkyne functionalization of hydroxyl-containing impurities and "click" coupling of the functionalized impurities onto an azide-functionalized solid resin. Filtration then enabled the efficient isolation of soluble cyclic polymers from the resin-bound impurities. The effectiveness of this purification method was confirmed for samples of low (M_n = 1.1 kg/mol) and medium (M_n = 11.7 kg/mol) molecular weights. DSC and dielectric relaxation experiments confirmed the increased architectural purity of the "click-scavenged" samples.

3.3 EXPERIMENTAL

Synthesis of Cyclic Poly(glycidyl phenyl ether). Reagents were manipulated and transferred either by distillation or under argon in a vacuum line. Glycidyl phenyl ether (GPE) and dichloromethane (Aldrich) were dried over CaH_2, degassed and distilled. $B(C_6F_5)_3$ (Aldrich) was sublimed in vacuo at 50 °C and transferred to the reaction flask in a glovebox. Low molecular weight poly(GPE) (M_n = 1.0 kg/mol, Đ = 1.3, hereafter poly(GPE)$_{1K}$) was synthesized as follows: $B(C_6F_5)_3$ (16 mg, 31 μmol), CH_2Cl_2 (40 mL) and GPE (4.4 g, 29.5 mmol) were placed in this order in a Schlenk-flask. The reaction was stirred for 48 h at room temperature under argon. To terminate the reaction, 0.3 mL of dry methanol was added to the flask. Before precipitation, the solution was concentrated in the vacuum line to a final volume of about 10 mL. Then, the polymer was precipitated in 50 mL of methanol and subsequently dried in a vacuum oven at 80 °C

until the sample weight remained constant (56 wt% yield). Higher molecular weight poly(GPE) (M_n = 11.7 kg/mol, Đ = 1.9, hereafter poly(GPE)$_{11K}$) was synthesized as follows: GPE (1.1 g, 7.4 mmol) was placed in an argon-filled Schlenk-flask and submerged in an ice bath. Then, $B(C_6F_5)_3$ (3.9 mg, 7.6 μmol) was carefully added. After complete mixing, the flask was stored in a refrigerator at -15 °C for 24 h. The flask was submerged again in an ice bath, and 1 mL of dry CH_2Cl_2 was added to dissolve the viscous product. To terminate the reaction, 0.1 mL of dry methanol was added to the flask. To isolate the polymer, the product was precipitated in 20 mL of methanol and dried in a vacuum oven at 80 °C until the sample weight remained constant (88 wt% yield). The polymers were stored under reduced pressure at room temperature until being used.

Synthesis of Linear Poly(glycidyl phenyl ether) Standards. Linear poly(GPE) samples were synthesized following the method of Endo et al.[20] All reagents were manipulated and transferred either by distillation or under inert gas in a vacuum line. GPE was dried over CaH_2, degassed and distilled. Tetrabutylammonium fluoride (TBAF) (0.7 mL), purchased from Aldrich (1 M in THF solution), was added to a Schlenk-flask. THF was evaporated under vacuum, and then 2 mL of GPE were added. To prepare samples of different molecular weights, the polymerization reactions were conducted at 60 °C for 10 min, 15 min, 30 min, 1 h, and 6 h. To increase the molecular weight, a postpolymerization reaction was conducted by further addition of 2 mL of GPE after 6 h. The reactions were terminated by the addition of methanol. The resulting polymers were precipitated twice from THF into methanol and dried in a vacuum oven at 80 °C until the sample weight remained constant (the polymerization yields varied from 25 to 85 wt%

going from lower to higher reaction times). Polymers were stored under reduced pressure at room temperature until being used.

End Group Modification of Impurities. End group modifications were developed based on modifications of the protocol reported by Zhang et al.[21] and used in conjunction with MALDI-TOF MS to elucidate the number of reactive end groups for all species present in the samples.

Formation of the Terminal Acetate Ester of Poly(GPE). Poly(GPE) (25 mg, 0.017 mmol, 1 eq.) was dissolved in dry THF (5 mL). Acetic anhydride (7.1 mg, 0.070 mmol, 4.1 eq.) and 4-(dimethylamino)pyridine (DMAP) (0.41 mg, 0.0034 mmol, 0.2 eq.) were added to the reaction mixture, which was then stirred overnight. The crude reaction mixture was concentrated *in vacuo* and then redissolved in dichloromethane. The solution was washed with saturated sodium bicarbonate (1 × 5 mL), water (2 × 5 mL), and 1 M HCl (1 × 5 mL). The organic layer was collected and dried with sodium sulfate. Finally, the organic solvent was removed *in vacuo* yielding the acetylated product for MALDI-TOF MS analysis.

Formation of the Terminal Benzyl Ether of Poly(GPE). Poly(GPE) (25 mg, 0.017 mmol, 1 eq.) was dissolved in dry THF (5 mL) and placed under N_2. Benzyl bromide (4.1 mg, 0.035 mmol, 2.1 eq.) and sodium hydride (2.6 mg, 0.067 mmol, 4 eq.) were added to the reaction mixture, which was then stirred overnight. The crude reaction mixture was concentrated *in vacuo* and then redissolved in dichloromethane. The solution was washed with water (3 x 5 mL) and dried with sodium sulfate. Finally, the organic solvent was removed *in vacuo* yielding the benzylated product for MALDI-TOF MS analysis.

Formation of the Terminal Pent-4-ynoate Ester of Poly(GPE). Poly(GPE) (25 mg, 0.017 mmol, 1 eq.) was dissolved in dry THF (5 mL) and placed under N_2. 4-Pentynoic acid (3.3 mg, 0.034 mmol, 2.0 eq.), N-(3-Dimethylaminopropyl)-N′-ethylcarbodiimide hydrochloride (EDC) (6.5 mg, 0.034 mmol, 2.0 eq.) and DMAP (0.41 mg, 0.0034 mmol, 0.2 eq.) were added to the reaction mixture. The reaction was stirred overnight. The crude reaction mixture was concentrated *in vacuo* and then redissolved in dichloromethane. The solution was washed with water (2 × 5 mL), 1 M HCl (1 × 5 mL), and saturated sodium bicarbonate solution. The organic layer was collected and dried with sodium sulfate. Finally, the organic solvent was removed *in vacuo* yielding the pentynoate ester product for MALDI-TOF MS analysis.

"Click-Scavenging" of Impurities. *Formation of the Terminal Propargyl Ether of Poly(GPE).* Poly(GPE) (60 mg, 0.040 mmol, 1 eq.) was dissolved in dry THF (5 mL) and placed under N_2. NaOH (15 mg, 0.38 mmol, 10 eq.) and propargyl bromide (24 mg, 0.20 mmol, 4 eq.) were added to the reaction mixture. The reaction stirred over night at 50 °C. The crude reaction mixture was concentrated *in vacuo* and then redissolved in dichloromethane. The solution was washed with water (3 × 5 mL) and dried with sodium sulfate. Finally, the organic solvent was removed *in vacuo* yielding the propargylated product (90% yield, 54 mg, 0.036 mmol) to evaluate the solid-phase "click-scavenging" technique.

Purification of Poly(GPE) by "Click-Scavenging" Architectural Impurities. First, an azide functionalized resin was prepared by exhaustive azidification of 1% cross-linked Merrifield resin with a chlorine loading of 3.5-4.5 mmol/g (from incorporation of *p*-chloromethylstyrene). The propargylated product (68.6 mg, 0.046 mmol, 1 eq.) was

dissolved in dichloromethane and placed under N_2. The azide functionalized Merrifield resin[22] (686 mg) and PMDETA (0.594 mg, 3.43 mmol, 75 eq.) were added to the reaction mixture. After undergoing 2 freeze-pump-thaw cycles, CuBr (492 mg, 3.43 mmol, 75 eq.) was added to the flask, followed by an additional pump-thaw cycle. The reaction flask was stirred at room temperature for 48 hours to ensure coupling between the propargylated impurities and the azido resin. The solid phase resin was then removed by filtration. The filtrate was collected, washed with ammonium chloride until the organic layer was transparent, and then the organic layer was dried with sodium sulfate. The product (80% yield, 54 mg, 0.037 mmol) was collected by removing solvent *in vacuo*, and later analyzed with MALDI-TOF MS. Alternatively, the pent-4-ynoate ester of poly(GPE) can be purified using analogous conditions, providing similar results.

Characterization. GPC-MALS measurements were performed at the University of the Basque Country, Spain. THF (1.0 mL/min) was used as an eluent in an Agilent G-1310A HPLC connected to miniDAWN MALS and Optilab rEX dRI detectors from Wyatt. PLgel 5µm 500Å and PLgel 5 µm Mixed-C columns were used for separation, both kept in a column heater at 30 °C. ASTRA software (Wyatt, version 6.1.2.84) was used for data collection and processing. Differential refractive index (dn/dc) of poly(GPE) was calculated from offline batch mode GPC-Refractive Index detection operating at 690 nm. Five THF solutions of a linear poly(GPE) standard (M_n = 2.8 kg/mol) obtained by Endo's method[20] were used at concentrations of 2-10 × 10^{-4} g/mL. A dn/dc value of 0.137 mL/g was obtained.

MALDI-TOF MS measurements were performed using two different mass spectrometers, the first located at the University of the Basque Country, Spain, and

second at Tulane University, USA. The first one is a Bruker Autoflex Speed system (Bruker, Germany) equipped with a 355 nm NdYAG laser, which was used to collect **Figure 3.1**. Data were acquired using reflector-positive ion mode, an acceleration voltage of 20 kV, and delayed extraction. Data acquisition was performed using Bruker Daltonics FlexControl 3.0 software, and data analysis was carried out with Bruker Daltonics FlexAnalysis 3.0 software. To optimize the accuracy of the mass determinations, the mass scale for the MALDI-TOF MS was calibrated using SpheriCal mass standards (Polymer Factory, Sweden). *trans*-2-[3-(4-*tert*-Butylphenyl)-2-methyl-2-propenylidene] malonitrile (DCTB, Fluka) was used as a matrix. Potassium trifluoroacetate (KTFA) (Aldrich) was added as the cationic ionization agent (~10 mg/mL dissolved in THF). The matrix was also dissolved in THF at a concentration of 20 mg/mL. Poly(GPE) samples were dissolved in THF at a concentration of ~10 mg/mL. In a typical MALDI experiment, the matrix, salt and polymer solutions were premixed at a 20:1:3 ratio, respectively. Approximately 0.5 µL of the obtained mixture were spotted by hand on the ground steel target plate. For each spectrum 1000 laser shots were accumulated.

The second mass spectrometer is a Bruker Autoflex III MALDI-TOF mass spectrometer (Bruker Daltonics, Billerica, MA), which was used to collect **Figures 3.2-3.5** and **Figures B1-B13**. Mass spectra data were collected in both linear and reflector mode with positive ion detection. Typical sample preparation for MALDI-TOF MS data was performed by making stock solutions in THF of matrix (20 mg/mL), polymer analyte (2 mg/mL), and an appropriate cation source (2 mg/mL). The stock solutions were mixed in a 10/2/1 ratio (matrix/analyte/cation), deposited onto the MALDI target plate and

allowed to evaporate via the dried droplet method. For poly(GPE) derivatives, DCTB was found to be an appropriate matrix and sodium trifluoroacetate was used as the cation source to generate sodium adducts of the polymer. MALDI-TOF MS data were calibrated against SpheriCal dendritic calibrants (Polymer Factory, Sweden).

Quantitative FTIR measurements were performed at 25 °C in a Jasco 6300 FTIR. Spectra were registered in transmission mode under nitrogen atmosphere. The polymer samples were spread on ZnSe windows with a spatula to form films of about 0.2 mm. All samples were dried at 100 °C in a vacuum oven before measurements and stored under reduced pressure at room temperature until being used. The samples were rapidly transferred to the ZnSe window and immediately introduced into the nitrogen-filled FTIR chamber. The calibration curve was done with the linear poly(GPE) standards synthesized by Endo's method, as described above. Baselines of FTIR spectra were not corrected.

DSC measurements were carried out on ~3 mg specimens using a Q2000 TA Instruments in standard mode. A helium flow rate of 25 mL/min was used throughout. Measurements were performed by placing the samples in sealed aluminum pans, heating to 150 °C and remaining at this temperature for 1 h (to ensure removal of low molecular weight molecules), cooling to -100 °C at 20 °C/min and heating to 100 °C at 20 °C/min. This procedure was repeated twice at the same cooling and heating rates.

Broadband dielectric spectroscopy (BDS) measurements were registered in a Novocontrol high-resolution dielectric analyzer (Alpha-S analyzer). The complex dielectric permittivity [$\varepsilon(\omega)^* = \varepsilon'(\omega)-i\varepsilon''(\omega)$] was measured isothermally over a frequency ($f = \omega/2\pi$) and temperature range of 10^{-2}-10^{7} Hz and 130-370 K, respectively.

Samples were placed between parallel gold-plated electrodes with a diameter of 20 mm and a thickness of 0.1 mm. The separation between both electrodes was maintained by using a cross-shaped Teflon spacer of small area. Samples were first dried for one hour at 420 K within the equipment. Then, isothermal frequency scans were performed every 5 K over the mentioned temperature range. The temperature was controlled within ±0.1 K using a Novocontrol Quatro cryostat that uses a continuous nitrogen jet flow.

3.4 RESULTS AND DISCUSSIONS

Initially, in order to determine which polyether architectures may be present in the sample, more traditional characterization techniques such as NMR were explored. However, the presence of multiple architectural species in the sample combined with stereocenters in each repeat unit along the backbone[23] resulted in complicated NMR spectra with broad, overlapping resonances. Likewise the overlapping distributions of multiple architectures made chromatographic purification of the cyclic polymers unreasonable. Consequently, MALDI-TOF was explored as an alternative means of identifying the major architectural byproducts present in the cyclic sample based on their unique mass shifts with respect to the main cyclic product. Furthermore resin-based scavenging techniques were then explored as a means of purifying the desired cyclic product.

3.4.1 MALDI-TOF MS Analysis of Architectural Impurities in Cyclic Poly(GPE)

The MALDI-TOF MS spectrum of the crude cyclic poly(GPE)$_{1K}$ sample is shown in **Figure 3.1**. The data reveal high intensity signals of potassium-complexed cyclic poly(GPE) separated by 150.07 Da, the expected repeat unit mass of poly(GPE). In addition, a series of signals with much lower intensities were observed that exhibited mass shifts of -16.01, +18.01, +56.02, +74.05, and +94.03 Da with respect to those of major cyclic distribution. The signal at -16.01 Da could be attributed to sodium-complexed cyclic chains. The signal at +18.01 Da was attributed to the linear chains terminated in two OH groups as described in our previous work.[18] Assignment of the remainder of the signals required a more detailed analysis that is described in the next section.

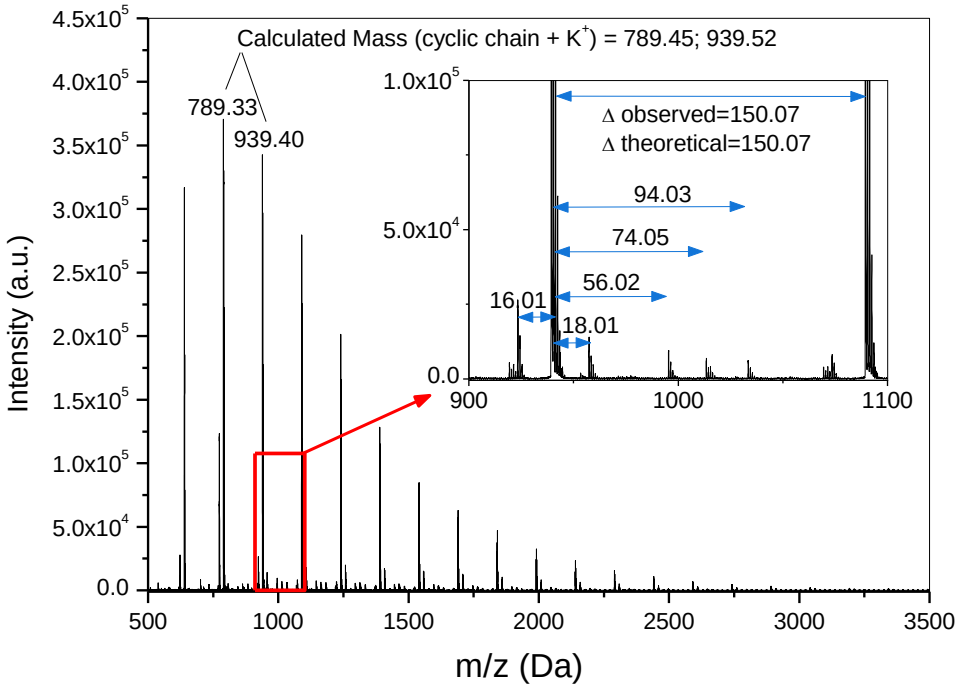

Figure 3.1. MALDI-TOF MS spectrum of cyclic poly(GPE)$_{1K}$ synthesized by ZREP. Inset: expanded m/z = 900-1120 region showing low intensity signals. Spectra were acquired using KTFA to provide a cation and DCTB as matrix.

To help elucidate the structure of impurities present in the cyclic poly(GPE) samples, a series of end group modification reactions were carried out with acetic anhydride, benzyl bromide, and 4-pentynoic acid. Larger, more detailed figures of MALDI-TOF mass spectra can be found in the Supporting Information (**Figures B1-B12**).

These functionalization studies were initially explored using the lower molecular weight poly(GPE)$_{1K}$ sample. For the acetylation reaction, a 4-fold excess of acetic anhydride was used such that any hydroxyl functionalities that are present should be esterified to the corresponding acetyl ester. The resulting mass spectra should exhibit a 42.01 mass increase for each end group that undergoes esterification. Although a number of minor signals exhibited shifts in the product mass spectrum, the most significant

change relative to the starting material is a large new signal offset by exact 1 acetylation reaction from the cyclic distribution (**Figure 3.2b**). Similar results were observed for the benzylation reaction, where a 90.05 mass increase was expected per benzylation (**Figure 3.2c**), and the most significant new signal corresponded to the addition of a single benzyl ether relative to the primary cyclic distribution. Further confirmation of the reactivity of this impurity could be achieved by a third functionalization reaction with 4-pentynoic acid. Pentynoate esterification using EDC and DMAP yielded a product that exhibited an 80.03 mass shift relative to the dominant cyclic distribution in starting material (**Figure 3.2d**). Because the cyclic polymer, by definition, cannot have end groups this new peak must correspond to some alternative architecture with the same mass but a single, reactive end group.

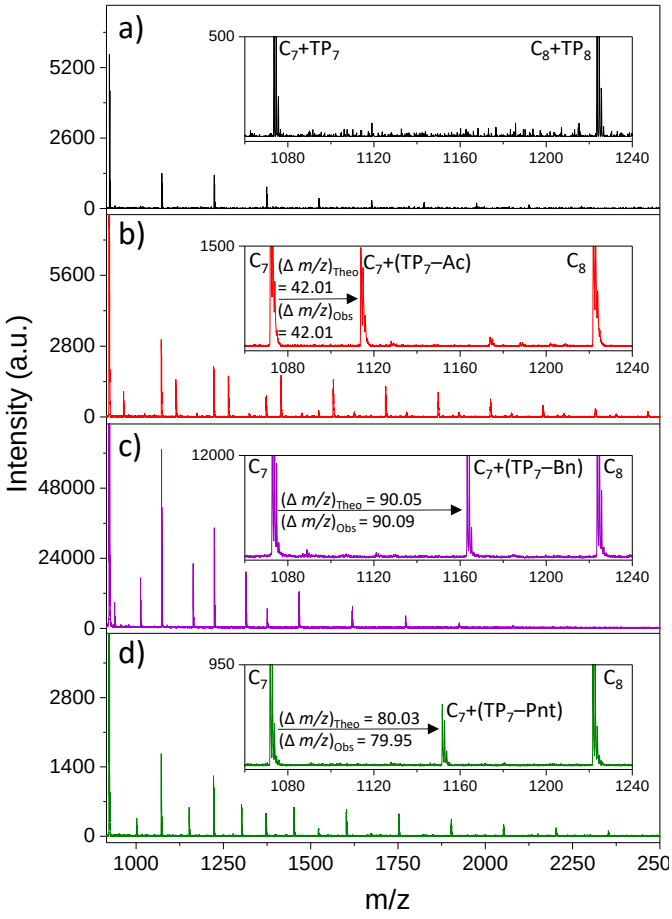

Figure 3.2. MALDI-TOF mass spectra of (a) crude poly(GPE)$_{1K}$ sample, (b) acetylated poly(GPE)$_{1K}$, (c) benzylated poly(GPE)$_{1K}$, and (d) the pentynoate ester of poly(GPE)$_{1K}$, respectively, with expanded spectra from *m/z* = 1060 to 1240 in each inset. The spectra were taken in positive reflector mode, and all labeled signals represent the sodiated adducts.

The data in **Figure 3.2** suggest that the samples are predominantly cyclic poly(GPE) (abbreviated "C") with the major impurity being a GPE-based polymer that has an identical mass distribution before functionalization but exhibits a single reactive alcohol group. The presence of a single functional group during a ring-expansion polymerization might be explained by the formation of a tadpole-shaped polymer (abbreviated "TP"). Because of the demonstrated ease with which this impurity can be functionalized via alkylation and esterification reactions, a similar functionalization route

has been investigated to enable purification of the cyclic poly(GPE). By forming the propargylated ethers of the crude poly(GPE)$_{1K}$ sample, using sodium hydroxide as a base and propargyl bromide as the electrophile, polymer impurities that bear any alcohol groups will be functionalized with a pendant alkyne group. The alkyne functionality can subsequently be coupled to an azido-functionalized resin via the copper-catalyzed azide-alkyne cycloaddition (CuAAC) reaction to affect the removal of architectural impurities. The detailed procedure for the purification of cyclic poly(GPE)$_{1K}$ will be described in a later section.

Preliminary analysis of the propargylated product further confirmed the presence of a major tadpole impurity, "TP", which exhibited a signal offset of +38 with respect to the major cyclic distribution, "C", confirming the functionalization of a single reactive group. Close examination of the mass spectra after propargylation also enabled the identification of a number of additional minor impurities, because the number of added propargyl groups allowed the number of reactive end groups to be determined (**Figure 3.3b and B2**). For example, the known linear impurity, L, with a +18 mass shift in the unfunctionalized, crude poly(GPE)$_{1K}$ sample shows the expected addition of two propargyl ethers (+76) upon reaction with propargyl bromide, and therefore is observed at an offset of +94 (18 + 76), with respect to the C distribution in the product mass spectrum. The impurity with an offset of +94 in the unfunctionalized starting material was hypothesized to be a linear poly(GPE) with one phenyl ether end group and one free hydroxyl end group, L'. Again, the expected product upon propargylation was observed bearing one additional propargyl ether in the product mass spectrum and an overall +132 mass shift (94 + 38) relative to the C distribution. Finally, it was proposed that two of the

impurities contain epoxide end groups. The first is an alternative linear impurity L" with a +74 offset in the crude, unfunctionalized cyclic sample, and upon propargylation it exhibited a mass increase of +38 for an overall offset of +112 with respect to the C distribution. L" is suspected to be a linear polymer like L with the addition of a terminal epoxide group. An alternative tadpole TP' is the second of these epoxide terminated impurities with a +56 offset in the unfunctionalized starting material, and exhibits no mass shift upon propargylation. It is therefore presumed to have no reactive alcohol end groups. **Table 3.1** lists the abbreviations, proposed structures, and number of reactive alcohol groups present for each of the identified impurities.

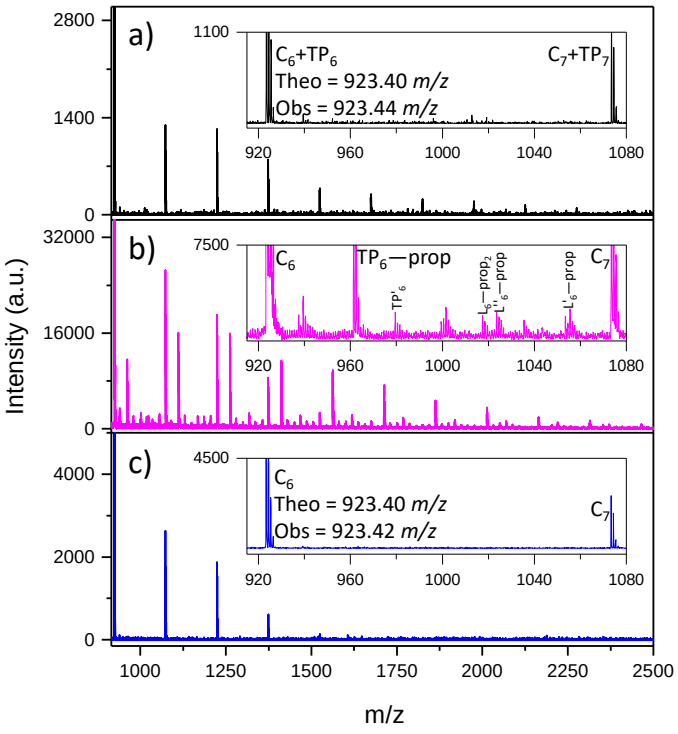

Figure 3.3. MALDI-TOF mass spectra of (a) crude poly(GPE)$_{1K}$ sample, (b) propargylated poly(GPE)$_{1K}$, and (c) "click-scavenged" poly(GPE)$_{1K}$, with expanded spectra from *m/z* = 915 to 1080 in each inset. The spectra were taken in positive reflector mode, and all labeled signals represent the sodiated adducts.

Table 3.1. Structures Assigned to MALDI-TOF MS Signals within a Crude Cyclic Poly(GPE) sample observed in **Figure 3.1**.

Name	Topology	Structure	Mass	Number of Hydroxyls
C		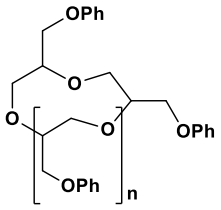	(n+2) x150	0
TP		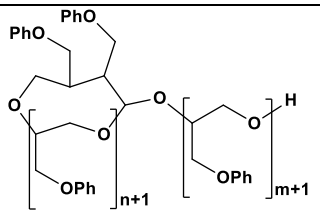	(n+m+2) x150	1
TP'		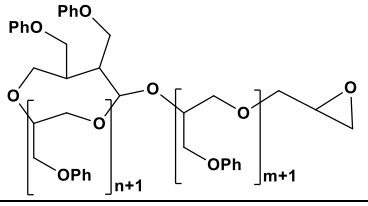	[(n+m+1) x150] + 56	0
L		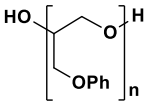	(nx150) + 18	2
L'		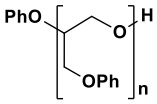	(nx150) + 94	1
L"		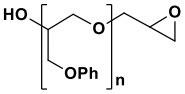	[(n+m+1)x 150] + 74	1

To confirm the generality of the byproduct formation for the zwitterionic ring-expansion polymerization, a larger ZREP polymer sample, poly(GPE)$_{11K}$ was also prepared, functionalized and analyzed by MALDI-TOF MS (**Figure 3.4**). In the case of the reaction with 4-pentynoic acid, again two major distributions are observed in the reflector mode mass spectra: the unreacted cyclic polymer, C, and a single esterification product, TP (or C + 80) (**Figure 3.4b**). Because the signals observed in MALDI-TOF mass spectra are biased to the lower mass range, especially for samples with dispersity

(Đ) > 1.3, the signals seen in the reflector mode mass spectra are of much lower mass than the GPC average molecular weight (11.7 kg/mol, Đ = 1.9). A broader mass range of this sample can be observed if mass spectra are collected in linear mode instead of reflector mode (**Figure 3.5**). In addition to enhancing the signals at much higher masses, linear mode also enables a number of the minor esterified impurities to be more easily visualized. Because the addition of the pentynoate ester increased the product mass by 80 mass units per hydroxyl functionalized, these same byproducts were observed as: L = C + 178 (or C + 18 + 2 x 80), L' = C + 174 (or C + 94 + 80) and L'' = C+ 154 (or C + 74 + 80) (**Table B1**). In order to determine the structure of the higher molecular weight materials (whose MS signals are suppressed with respect to the lower molecular weight components) preparative GPC was used to isolate a purified 10-20 kg/mol fraction of poly(GPE)$_{11K}$ for further analysis. This fraction was propargylated and its MALDI-TOF mass spectra before and after this reaction were compared. Analysis verified that the same components observed in the lower molecular weight ranges were also observed in this higher molecular weight fraction (See Appendix A, **Figure B13 and Table B2**).

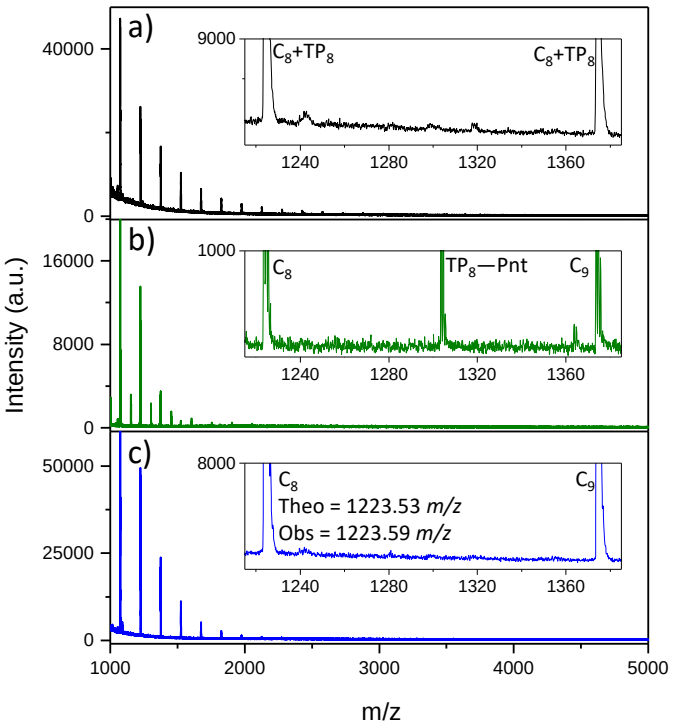

Figure 3.4. MALDI-TOF mass spectra of (a) crude poly(GPE)$_{11K}$ sample, (b) poly(GPE)$_{11K}$ product after esterification with 4-pentynoic acid, and (c) "click-scavenged" poly(GPE)$_{11K}$, with expanded spectra from *m/z* = 1215 to 1385 *m/z* in each inset. The spectra were taken in positive reflector mode, and all labeled peaks represent the sodiated adducts.

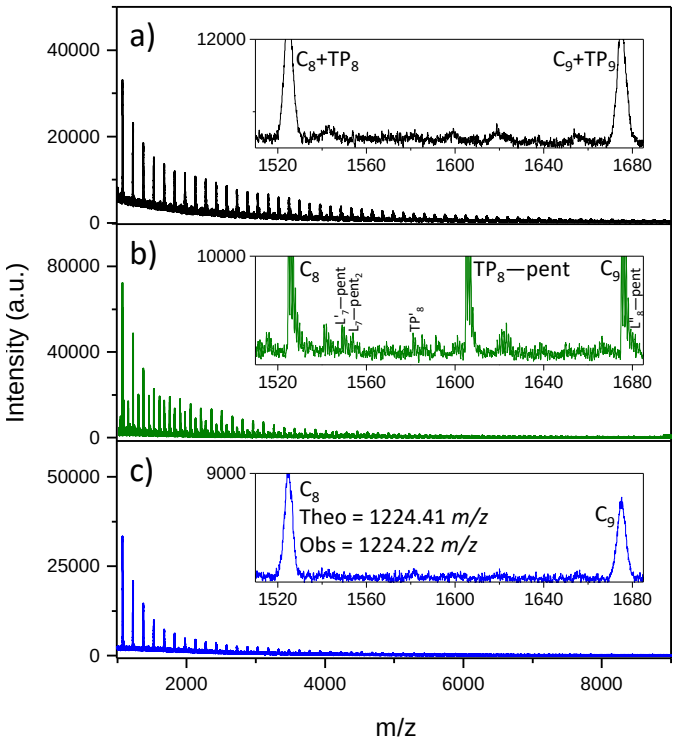

Figure 3.5. MALDI-TOF mass spectra of (a) crude poly(GPE)$_{11K}$ sample, (b) poly(GPE)$_{11K}$ product after esterification with 4-pentynoic acid, and (c) "click-scavenged" poly(GPE)$_{11K}$, with expanded spectra from *m/z* = 1210 to 1385 *m/z* in each inset. The spectra were taken in positive linear mode, and all labeled peaks represent the sodiated adducts.

3.4.2 "Click-Scavenging" of Impurities

Considering that the majority of the architectural impurities identified in the cyclic sample contain hydroxyl end groups (e.g. L, L', L'', TP), we applied a scavenging protocol based on the ability to attach an alkyne functional group onto these undesired impurities. A similar procedure has already been demonstrated for the removal of azide or alkyne functionalized impurities generated during the CuAAC-based synthesis of star polymers.[22, 24] By use of the highly efficient CuAAC "click" coupling reaction the alkyne-functionalized impurities in the cyclic poly(GPE) samples can be attached to an azide-functionalized cross-linked resin to remove them from solution. As long as the coupling is quantitative, the desired purified cyclic poly(GPE) may then be isolated by a

simple filtration. This purification route is depicted in **Scheme 3.2**. This method is modular, however, in that other functionalities can be attached the resin and utilize other quantitative, "click" reactions, depending on the functionality of the byproduct which is to be removed. This protocol also appears to be scalable; for example, if a true 10 molar excess of resin to polymer is desired, only 5.8 mg resin/10 mg polymer is required for the 1K and 0.52mg resin/10 mg for the 11K (where all the polymer is assumed to be difunctional). In the case of this paper, the amount of resin was largely used in considerable excess (10 mg polymer/100 mg resin) to ensure high purity samples for physical characterization.

First, the smaller crude cyclic sample, poly(GPE)$_{1K}$, was reacted with propargyl bromide and sodium hydroxide to generate a propargyl ether on the impurities. Second, the product was mixed with an azide-functionalized, cross-linked Merrifield resin and a Cu(I) catalyst to scavenge the architectural impurities from the solution. Third, the solution was filtered to isolate the cyclic chains from the modified impurities now bound to the resin. Finally, the purified polymer was dried *in vacuo* and characterized.

Scheme 3.2. Purification Protocol via "Click-Scavenging" of Cyclic Poly(GPE) Synthesized by ZREP.

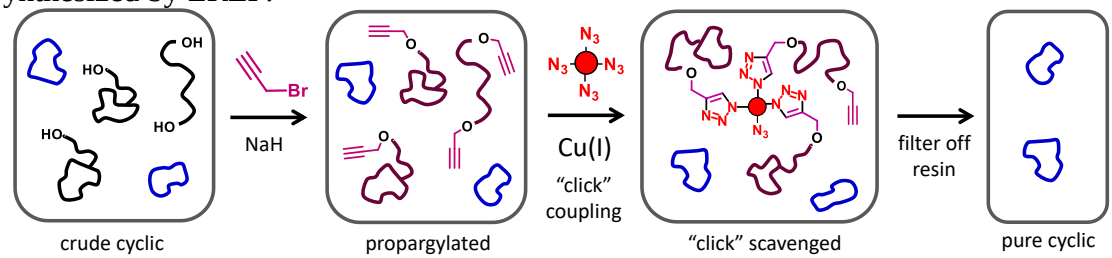

Confirmation of the effectiveness of the "click-scavenging" technique could be obtained from the MALDI-TOF mass spectra of the purified product, which exhibits a

much cleaner spectra than the propargylated sample (**Figure 3.3c**). The major TP impurities appear to be removed, as well as the majority of the trace impurities. Before "click-scavenging", the relative proportions of architectures in the propargylated spectra can be quantified by means of integrating the signals of the cyclic polymer and the major tadpole impurity, yielding a value of 71% cyclic by MALDI-TOF MS. After "click-scavenging", integration of the same regions suggests a cyclic purity of 99.5%. It is important to note that these MALDI-TOF MS integration determinations are limited by inherent signal bias toward smaller molecular weights as well as the potential for differing ionization efficiencies for species of differing architecture or functionality. However, the contrast between the spectra before and after "click-scavenging" confirm a significant improvement in cyclic purity. While this quantification method seemed appropriate for poly(GPE)$_{1K}$, the discrepancy in ionization efficiency of low vs. high molecular weight is exponentially higher for poly(GPE)$_{11K,}$ and thus was not calculated. Likewise, the same "click-scavenging" technique could be applied to the larger poly(GPE)$_{11K}$ sample, using the pentynoate ester instead of the propargyl ether functionalization. Again, the MALDI-TOF mass spectra in both reflector mode (**Figure 3.4c**) and linear mode (**Figure 3.5c**) show a much cleaner spectra with the major TP impurity removed. It should be stated explicitly that any impurity from the ZREP that does not bear an alcohol group will not be removed using this technique; however, the vast majority of the impurities were shown to bear at least one hydroxyl group. Additional characterization and physical evaluation of the "click-scavenged" cyclic polymer samples were carried out to confirm the effectiveness of this purification.

Given the identification of the major impurity as a tadpole bearing one hydroxyl group, a mechanism (**Scheme 3.3**) is proposed to help explain the observed products.

Scheme 3.3. A) Hydrogen Abstraction Leading to the Formation of the Vinyl Ether B) Intermolecular Dimerization between Vinyl Ether and Propagating Polymer C) Hemicyclization via Backbiting to Form the Tadpole Byproduct.

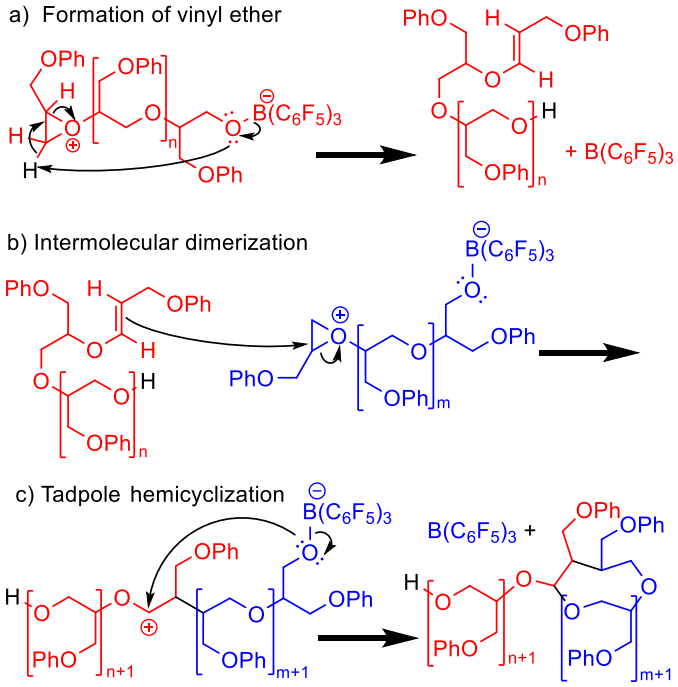

3.4.3 Quantification of Impurities on Cyclic Poly(GPE)

Given the complexity of NMR spectra to quantify the amounts of hydroxyl end groups in the samples, we selected FTIR for quantification of architectural impurities. **Figure 3.6a** shows the FTIR spectra of crude cyclic poly(GPE)$_{1K}$ sample obtained by ZREP, the purified cyclic product and a linear poly(GPE) synthesized by Endo's method bearing hydroxyl end groups.[20] The spectra show the bands associated with the stretching vibration of OH (ν_{OH}) and CH (ν_{CH}) groups, whose relative intensities depend on the polymer structure and the amounts of architectural impurities. As observed, FTIR

data of crude cyclic poly(GPE)$_{1K}$ sample confirm the presence of contaminants that contain OH groups, in agreement with the MALDI-TOF MS data in **Figures 3.1-3.5**. Upon purification of cyclic sample, the ν_{OH} band is noticeably reduced to values close to zero absorbance (the observed value being within the experimental limits). Similar results were obtained for purified poly(GPE)$_{11K}$ sample (See Appendix B, **Figure B14**).

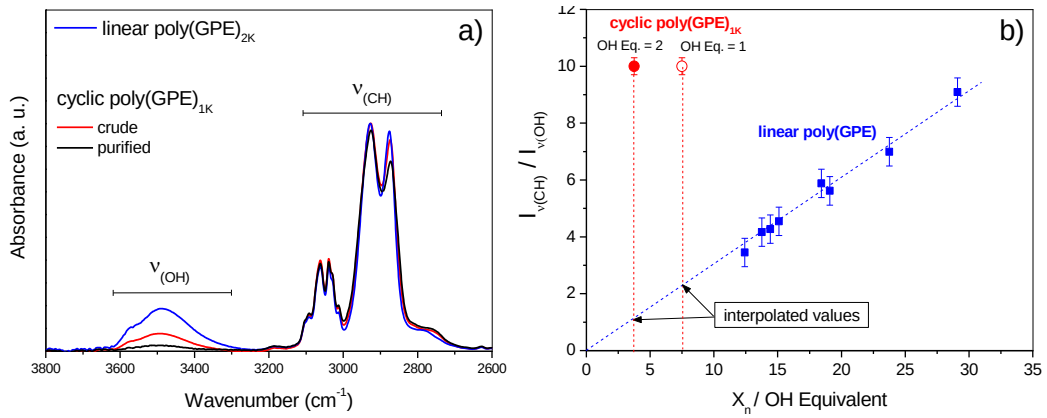

Figure 3.6. a) FTIR spectra of crude and purified cyclic poly(GPE)$_{1K}$ sample obtained by ZREP and a linear poly(GPE) standard (M_n = 2.2 kg/mol) synthesized by Endo's method.[20] b) Calibration curve obtained from linear poly(GPE) standards and FTIR data obtained for crude cyclic poly(GPE)$_{1K}$ considering OH Equivalent = 1 and 2.

To quantify the amount of impurities that contain OH groups we have implemented a quantitative FTIR method. Our method establishes that the ratio of the integrated areas of the stretching vibration signal of CH groups to that of OH groups ($I_{\nu(CH)}/I_{\nu(OH)}$) is proportional to the ratio of the degree of polymerization (X_n) to the OH equivalent number in the polymer chain (Equation 3.1).

$$\frac{I_{\nu(CH)}}{I_{\nu(OH)}} = K \cdot \frac{X_n}{OH\ \ Equivalent} \qquad \text{Equation 3.1}$$

K is a proportionality constant that can be determined by means of a calibration curve with low-molecular-weight linear poly(GPE) samples used as standards. With this aim, we synthesized a series of linear poly(GPE) with variable molecular weight in the range of 1900 to 4500 g/mol and Đ of 1.05, following Endo's method.[20] These linear standards are terminated with one OH group (OH Equivalent = 1) and one fluorine atom (see the calibration curve in **Figure 3.6b**). We noted that $I_{\nu(OH)}$ approached to zero values for $M_n \geq 12$ kg/mol, thus introducing large errors in $I_{\nu(CH)}/I_{\nu(OH)}$ (data not shown).

To determine the molar percentage of architectural contaminants containing OH groups (*AC* (mol%)) in cyclic samples, Equation 3.2 was used.

$$AC(mol\%) = \frac{\frac{I_{\nu(CH)}}{I_{\nu(OH)}}(sample)}{\frac{I_{\nu(CH)}}{I_{\nu(OH)}}(\text{int}erpolated)} \cdot 100\% \qquad \text{Equation 3.2}$$

where, $I_{\nu(CH)}/I_{\nu(OH)}$ (sample) is obtained from the FTIR data of the studied sample, and $I_{\nu(CH)}/I_{\nu(OH)}$ (interpolated) is obtained by interpolation of the calibration curve at the X_n/(OH Equivalent) value of the analyzed sample. For poly(GPE)$_{1K}$ sample we estimated a range of *AC* values within the limits where OH equivalents are 1 and 2 (the measured and interpolated $I_{\nu(CH)}/I_{\nu(OH)}$ values are indicated in **Figure 3.6b**) to quantify the amount of impurity based on assuming they exhibit exactly 1 and 2 alcohol end groups, respectively. As a result, we obtained *AC* values from 11 mol% (assuming 2 alcohols per chain, e.g. linear poly(GPE)) to 22 mol% (assuming 1 alcohol per chains, e.g. tadpole poly(GPE)).

To validate the *AC* values, we performed GPC experiments on the crude and purified cyclic poly(GPE)$_{1K}$ samples (**Figure 3.7**). The data revealed the loss of high molecular weight shoulder after "click-scavenging" that corresponds to a loss of 23 ± 2% of integrated area of the normalized differential refractive index (error calculated from three chromatograms registered with different GPC columns). This value is in agreement with the *AC* value obtained for an OH equivalent number of 1, suggesting that the majority of architectural impurities in cyclic poly(GPE)$_{1K}$ sample are terminated with a single OH group. This observation is consistent with the trends observed in the mass spectra, suggesting the major impurity is a tadpole-shape polyether, whose formation could be explained by the occurrence of intramolecular (back-biting) and intermolecular transfer reactions to polymer.

Calculation of the molar percentage of architectural contaminants containing OH groups in poly(GPE)$_{11K}$ by FTIR was rather inaccurate due to the larger molecular weight and larger dispersity of this sample. We observed in the GPC data of purified poly(GPE)$_{11K}$ (**Figure 3.7**) the disappearance of the shoulders at 5.9 and 7.5 min and the continuity of the peaks at 6.5 and 8.6 min when compared to that of crude compound. We then estimated that the major contribution to the stretching OH band in this sample (Supplementary Information) came from impurities with $M_n \leq 7$ kg/mol (GPC shoulder at 7.5 min) and that the reduction of the GPC area for the purified sample in comparison to that of the crude product is of about 40 ± 10% (error calculated from 3 independent purification experiments and several GPC experiments registered with different columns). Given the inaccuracy in the determination of *AC* values, it is not possible to

determine whether the major impurities come from linear or tadpole structures for this higher molecular weight sample.

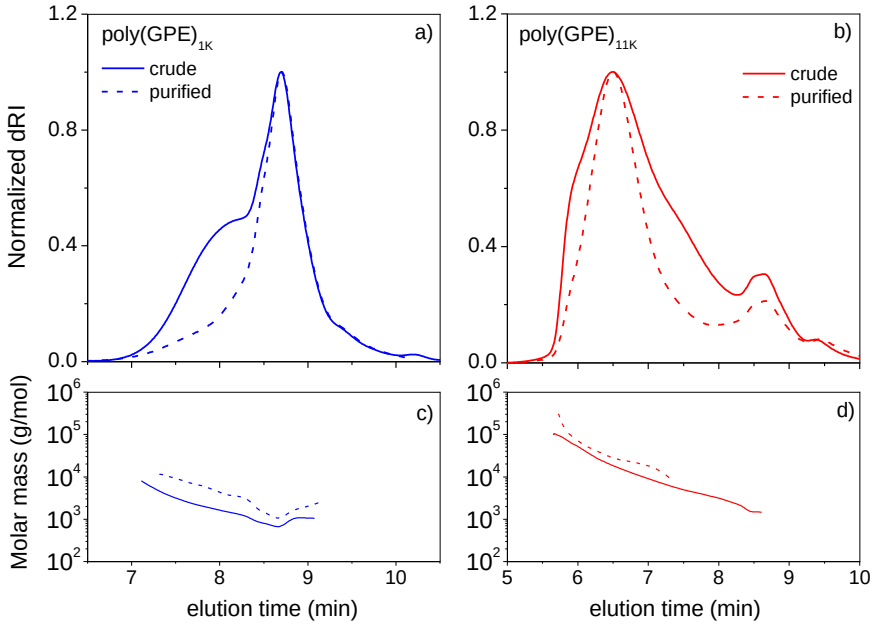

Figure 3.7. a, b) Refractive index chromatograms and c, d) molar mass of crude and purified poly(GPE)$_{1K}$ and poly(GPE)$_{11K}$ samples.

It is noteworthy that both M_n and M_w of poly(GPE)$_{1K}$ and poly(GPE)$_{11K}$ exhibit increased values, upon purification (**Table 3.2**). More importantly, this mass increase was observed along the whole elution time in both samples (**Figure 3.7**), thus revealing co-elution of cyclic chains and the previously detected architectural impurities. As expected from the lower hydrodynamic volume of cyclic chains in comparison with linear chains and tadpole structures of similar molecular weight, the architectural impurities would elute first followed by the more compact cyclic chains.[25] Because of the combined effects of topology and dispersity, cyclic chains would elute together with the architectural impurities of lower molecular weight, thus leading to an underestimation of the samples' average molecular weight. By analysis of the conformation plot (root

mean square, RMS, radius of gyration vs. molar mass)[26] of crude and purified poly(GPE)$_{11K}$ samples (**Figure 3.8**), the crude product exhibits a behavior without an apparent molecular-weight dependence, while the purified product reveals a consistent slope of about 0.5. Note that for the crude products, the RMS radius values are much lower (slightly above the detection limit of MALS detectors, 10 nm) than those of the purified product in the same molecular weight range, likely due to dispersity and the presence of multiple molecular architectures in the crude samples. On the other hand, the slope value of 0.5 indicates appropriate separation performance in the GPC column[26] in addition to confirming the successful purification of cyclic poly(GPE)$_{11K}$ sample.

Table 3.2. Molecular weight and glass transition characteristics of crude and purified poly(GPE)$_{1K}$ and poly(GPE)$_{11K}$.

	poly(GPE)$_{1K}$		**poly(GPE)$_{11K}$**	
	crude	purified	crude	purified
M_n (kg/mol)	1.0	1.7	11.7	24.6
M_w (kg/mol)	1.3	2.3	22.0	35.3
Đ	1.3	1.3	1.9	1.4
Onset T_g (K)[a]	281.4	282.8	282.4	284.4
T_g^{BDS} (K)	278.1	279.3	281.0	282.7
D[b]	6.20	6.35	6.40	7.35

[a]Obtained by DSC. [b]Dynamic fragility obtained by BDS.

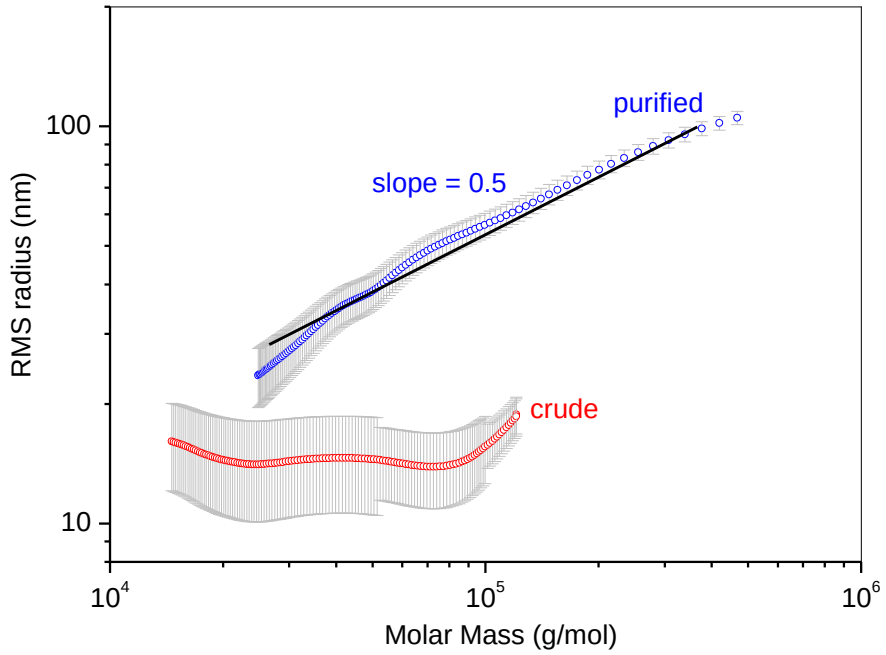

Figure 3.8. Conformation plot for crude and purified poly(GPE)$_{11K}$.

3.4.4 Effects of impurities on the physical properties of cyclic poly(GPE)

Physical properties of crude and purified cyclic polymer samples were investigated by DSC and broadband dielectric spectroscopy (BDS). DSC data revealed that cyclic poly(GPE) samples do not crystallize and that their glass transition temperature (T_g), is reduced by only 1.4 K and 2.0 K for poly(GPE)$_{1K}$ and poly(GPE)$_{11K}$, respectively, due to the presence of impurities (**Figure 3.9a-3.9b**, **Table 3.2**). The shape of the glass transition curve is also slightly modified after the removal of the impurities, becoming steeper but more extended after the glass transition step. Onset T_g values for purified samples are 282.8 K (poly(GPE)$_{1K}$) and 284.4 K (poly(GPE)$_{11K}$). Both values are higher than the high molecular weight limiting T_g, T_g^{∞} = 282 K, as previously obtained by using the Kanig-Ueberreiter equation[27] on linear poly(GPE) samples. The close T_g values for both pure cyclic samples of different molecular weights indicates

minor contribution of the molecular weight changes upon purification to the T_g variation between crude and purified cyclic samples. On the other hand, architectural impurities are expected to exert a plasticization effect on cyclic polymer, but this effect was found to be small in the present study probably because the majority of the impurities appears to be tadpole structures rather than purely linear structures. Because the tadpole polymers incorporate a cyclic portion, as well as a linear portion, the perturbation of the glass transition may be minimal if the linear tails are a minor component.

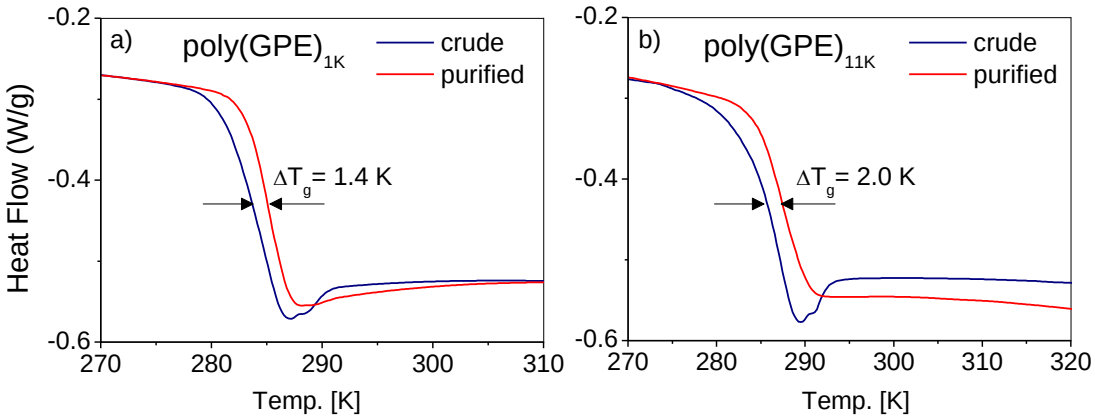

Figure 3.9. DSC data for crude and purified cyclic poly(GPE) samples. a) poly(GPE)$_{1K}$ and b) poly(GPE)$_{11K}$.

To gain further insight into the glass transition process, the segmental dynamics (responsible for the glass transition) of crude and pure cyclic poly(GPE) samples was studied by means of BDS. **Figure 3.10a** shows the permittivity loss, ε'', peaks detected for crude and purified poly(GPE)$_{1K}$ at four representative temperatures, just above the calorimetric T_g. At these temperatures, the dielectric α-relaxation is well distinguished as a peak, which is originating from segmental-scale motions giving rise to dipole moment fluctuations. The steep increase of the dielectric loss at lower frequencies in the spectra is originating from ionic conductivity contributions. The spectra show that the α-

relaxation peak of purified cyclic sample occurs at lower frequency than that in the crude sample. Analysis of the relaxation times of both samples is described as follows.

The relaxation times (τ) characterizing the segmental dynamics were obtained from the frequencies at the peak maximum (f_{max}) of the dielectric loss curves [ε''(*f*)] according to Equation 3.3. The temperature dependence of the α-relaxation times obtained for poly(GPE)$_{1K}$ and poly(GPE)$_{11K}$ samples is shown in **Figure 3.10b**. The data suggests that all samples show similar temperature dependence that can be described with the Vogel-Fulcher-Tammann (VFT) equation (Equation 3.4).

$$\tau = \frac{1}{2\pi f_{\max}} \qquad \text{Equation 3.3}$$

$$\tau(\mathrm{T}) = \tau_0 \exp\left(\frac{DT_0}{T - T_0}\right) \qquad \text{Equation 3.4}$$

where τ_0 is the typical vibrational time (fixed to $\tau_0 = 1\text{x}10^{-14}$ s), *D* is the parameter related to the so-called dynamic fragility (low D corresponds to high dynamic fragility and *vice-versa*) and T_0 is the so-called Vogel temperature, where the relaxation times would diverge.[28] We found that the so-called dynamic (dielectric) glass transition temperatures, T_g^{BDS} (the temperature at which the relaxation time value is 100 s), follow the same trend as the calorimetric T_g of crude and purified cyclic samples (**Table 3.2**). In addition, it is found that the dynamic fragilities for crude and purified poly(GPE) samples (**Table 3.2**) are higher than those obtained for linear poly(GPE) (D = 6.10), as previously reported.[23]

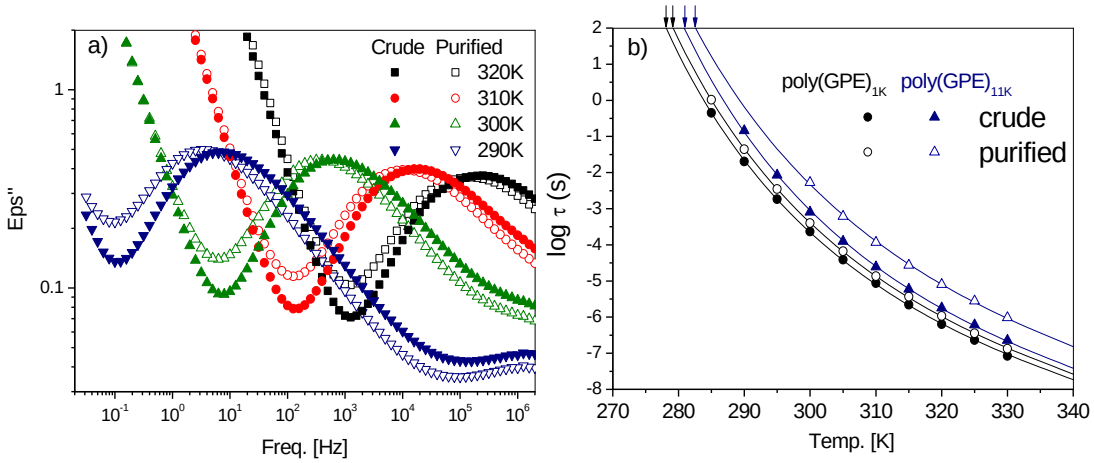

Figure 3.10. a) Dielectric relaxation for crude and purified poly(GPE)$_{1K}$ at temperatures above glass transition. b) Temperature dependence of the α-relaxation times for crude and purified cyclic poly(GPE) samples. Arrows indicate the dynamic (dielectric) glass transition temperatures, T_g^{BDS}.

BDS can also be used to probe more local molecular motions as those involving end groups and side chains. These molecular motions usually give rise to secondary relaxations which are detected well below T_g. **Figure 3.11** shows the permittivity loss peaks obtained for crude and purified cyclic sample at four representative temperatures below 200 K. At these temperatures, a secondary loss process (β-relaxation) is observed, which is originating from limited motions of side chains and end groups.[23] The spectra show peaks of slightly lower intensity for the purified poly(GPE)$_{1K}$ sample, as well as lower contributions to the losses at the high frequency side of the curves. These results indicate that impurities contribute with additional faster dynamics, which could be attributed to the extra mobility provided by the highly polar hydroxyl end groups. In a previous study on linear poly(GPE), we were able to separate the contributions of the end groups from those originating from the side chains.[23] The side group contribution for linear poly(GPE) at 170 K (shown in **Figure 3.11**) is in rather good agreement with the

data of purified cyclic poly(GPE)$_{1K}$, which corroborate the efficient removal of hydroxyl end groups in this sample.

This effect is not detected for poly(GPE)$_{11K}$, where both crude and purified samples show similar relaxation behavior due to the relatively low concentration of hydroxyl end groups expected for higher molecular weight polymer. Consistently, in this case, the calculated side group contribution is in good agreement with the experiments (See Appendix B, **Figure B15**).

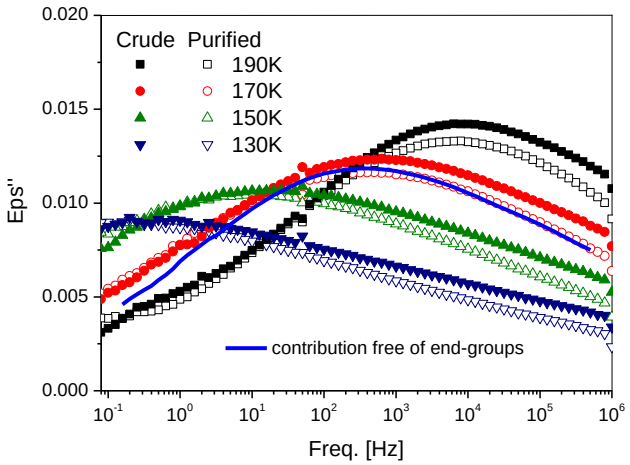

Figure 3.11. Dielectric relaxation for crude and purified poly(GPE)$_{1K}$ well-below T_g. Solid line shows the contribution to local dynamics of side groups (end groups are excluded) at 170 K, as previously obtained from linear poly(GPE) samples in reference.[23]

3.5 CONCLUSIONS

In this study, MALDI-TOF MS was utilized to identify the presence of architectural impurities within a sample of cyclic poly(GPE) prepared via ZREP, while a "click-scavenging" protocol was implemented to successfully and efficiently remove non-cyclic impurities. The quantity of the major impurity (tadpoles) could be calculated by FTIR, MALDI-TOF MS and GPC, and these values were in good agreement.

Furthermore, the purified samples were characterized by DSC and dielectric relaxation. Comparison of the dielectric relaxation before and after purification confirmed that the purified cyclic polyethers exhibited the expected trend for secondary relaxation assuming that cyclic polymer would behave akin to linear polymers, but with the contribution of the end groups removed. The techniques of "click-scavenging" and MALDI-TOF monitoring for architectural purification are presumed to be more generally applicable, as long as the impurities in question exhibit a functional handle that can be selectively addressed. By generating cyclic samples of high purity, it is hoped that the subsequent physical characterization will be more accurate and more informative about the potential applications for this fascinating class of polymers.

3.6 REFERENCES

1. Tezuka, Y., *Topological Polymer Chemistry. Progress of Cyclic Polymers in Syntheses, Properties and Functions*. Word Scientific Publishing Co. Pte. Ltd.: 2013.

2. Kricheldorf, H. R. Cyclic polymers: synthetic strategies and physical properties. *Journal of Polymer Science Part A: Polymer Chemistry* **2010,** 48 (2), 251-284.

3. Beckham, H. W., Ring Polymers: Effective Isolation and Unique Properties. In *Complex Macromolecular Architectures*, John Wiley & Sons (Asia) Pte Ltd: 2011; pp 791-821.

4. Williams, R. J.; Dove, A. P.; O'Reilly, R. K. Self-assembly of cyclic polymers. *Polym. Chem.* **2015,** 6 (16), 2998-3008.

5. Richter, D.; Goo; Wischnewski, A. Celebrating Soft Matter's 10th Anniversary: Topology matters: structure and dynamics of ring polymers. *Soft Matter* **2015,** 11 (44), 8535-8549.

6. Kapnistos, M.; Lang, M.; Vlassopoulos, D.; Pyckhout-Hintzen, W.; Richter, D.; Cho, D.; Chang, T.; Rubinstein, M. Unexpected power-law stress relaxation of entangled ring polymers. *Nat. Mater.* **2008,** 7 (12), 997-1002.

7. Halverson, J. D.; Grest, G. S.; Grosberg, A. Y.; Kremer, K. Rheology of Ring Polymer Melts: From Linear Contaminants to Ring-Linear Blends. *Phys. Rev. Lett.* **2012,** 108 (3), 038301.

8. Laurent, B. A.; Grayson, S. M. Synthetic approaches for the preparation of cyclic polymers. *Chem. Soc. Rev.* **2009,** 38 (8), 2202-2213.

9. Culkin, D. A.; Jeong, W.; Csihony, S.; Gomez, E. D.; Balsara, N. P.; Hedrick, J. L.; Waymouth, R. M. Zwitterionic Polymerization of Lactide to Cyclic Poly(Lactide) by Using N-Heterocyclic Carbene Organocatalysts. *Angew. Chem. Int. Ed.* **2007,** 46 (15), 2627-2630.

10. Bielawski, C. W.; Benitez, D.; Grubbs, R. H. An "endless" route to cyclic polymers. *Science* **2002,** 297 (5589), 2041-2044.

11. Bielawski, C. W.; Benitez, D.; Grubbs, R. H. Synthesis of Cyclic Polybutadiene via Ring-Opening Metathesis Polymerization: The Importance of Removing Trace Linear Contaminants. *J. Am. Chem. Soc.* **2003,** 125 (28), 8424-8425.

12. Brown, H. A.; De Crisci, A. G.; Hedrick, J. L.; Waymouth, R. M. Amidine-Mediated Zwitterionic Polymerization of Lactide. *ACS Macro Lett.* **2012,** 1 (9), 1113-1115.

13. Zhang, X.; Waymouth, R. M. Zwitterionic Ring Opening Polymerization with Isothioureas. *ACS Macro Lett.* **2014,** 3 (10), 1024-1028.

14. Sreerama, S. G.; Elupula, R.; Laurent, B. A.; Zhang, B.; Grayson, S. M. Use of MALDI-ToF MS to elucidate the structure of oligomeric impurities formed during 'click' cyclization of polystyrene. *React. Funct. Polym.* **2014,** 80, 83-94.

15. Narumi, A.; Hasegawa, S.; Yanagisawa, R.; Tomiyama, M.; Yamada, M.; Binder, W. H.; Kikuchi, M.; Kawaguchi, S. Ring expansion-controlled radical polymerization: Synthesis of cyclic polymers and ring component quantification based on SEC–MALS analysis. *React. Funct. Polym.* **2016,** 104, 1-8.

16. Chang, T., Liquid Chromatography / FTIR Microspectroscopy / Microwave Assisted Synthesis. In *Adv. Polym. Sci.* , Springer Berlin Heidelberg: Berlin, Heidelberg, 2003; Vol. 163, pp 1-60.

17. Hoskins, J. N.; Trimpin, S.; Grayson, S. M. Architectural differentiation of linear and cyclic polymeric isomers by ion mobility spectrometry-mass spectrometry. *Macromolecules* **2011,** 44 (17), 6915-6918.

18. Asenjo-Sanz, I.; Veloso, A.; Miranda, J. I.; Pomposo, J. A.; Barroso-Bujans, F. Zwitterionic polymerization of glycidyl monomers to cyclic polyethers with $B(C_6F_5)_3$. *Polym. Chem.* **2014,** 5 (24), 6905-6908.

19. Misaka, H.; Tamura, E.; Makiguchi, K.; Kamoshida, K.; Sakai, R.; Satoh, T.; Kakuchi, T. Synthesis of end-functionalized polyethers by phosphazene base-catalyzed ring-opening polymerization of 1,2-butylene oxide and glycidyl ether. *J. Polym. Sci., Part A: Polym. Chem.* **2012,** 50 (10), 1941-1952.

20. Morinaga, H.; Ochiai, B.; Endo, T. Metal-Free Ring-Opening Polymerization of Glycidyl Phenyl Ether by Tetrabutylammonium Fluoride. *Macromolecules* **2007,** 40 (16), 6014-6016.

21. Zhang, B.; Zhang, H.; Myers, B. K.; Elupula, R.; Jayawickramarajah, J.; Grayson, S. M. Determination of polyethylene glycol end group functionalities by combination of selective reactions and characterization by matrix assisted laser desorption/ionization time-of-flight mass spectrometry. *Anal. Chim. Acta* **2014,** 816, 28-40.

22. Zhang, B.; Zhang, H.; Elupula, R.; Alb, A. M.; Grayson, S. M. Efficient Synthesis of High Purity Homo-arm and Mikto-arm Poly(ethylene glycol) Stars Using Epoxide and Azide–Alkyne Coupling Chemistry. *Macromol. Rapid Commun.* **2014,** 35 (2), 146-151.

23. Gambino, T.; Martínez de Ilarduya, A.; Alegría, A.; Barroso-Bujans, F. Dielectric relaxations in poly(glycidyl phenyl ether): effects of microstructure and cyclic topology. *Macromolecules* **2016,** 49 (3), 1060-1069.

24. Urbani, C. N.; Bell, C. A.; Lonsdale, D. E.; Whittaker, M. R.; Monteiro, M. J. Reactive alkyne and azide solid supports to increase purity of novel polymeric stars and dendrimers via the "click" reaction. *Macromolecules* **2007,** 40 (19), 7056-7059.

25. Vakhrushev, A. V.; Gorbunov, A. A. Theory of chromatography of partially cyclic polymers: Tadpole-type and manacle-type macromolecules. *J. Chromatogr. A* **2016,** 1433, 56-65.

26. Podzimek, S., Combination of SEC and Light Scattering. In *Light Scattering, Size Exclusion Chromatography and Asymmetric Flow Field Flow Fractionation*, John Wiley & Sons, Inc.: 2011; pp 207-258.

27. Ueberreiter, K.; Kanig, G. Self-plasticization of polymers. *J. Colloid Sci.* **1952,** 7 (6), 569-583.

28. Kremer, F.; Schönhals, A., *Broadband Dielectric Spectroscopy*. Springer-Verlag Berlin Heidelberg: 2003.

CHAPTER 4

A MALDI-TOF MS STUDY OF MACROCYCLIC POLYETHERS GENERATE BY ELECTROPHILIC ZWITTERIONIC RING EXPANSION POLYMERIZATION OF MONOSUBSTITUTED EPOXIDES WITH $B(C_6F_5)_3$*

4.1 ABSTRACT

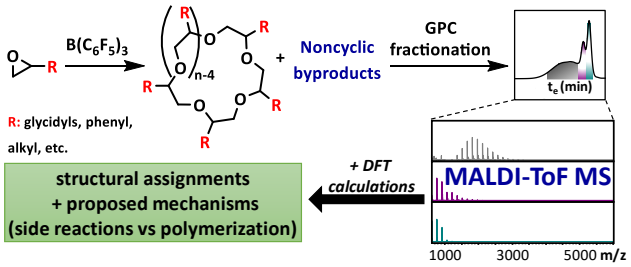

The electrophilic zwitterionic ring expansion polymerization (eZREP) of monosubstituted epoxides initiated by tris(pentafluorophenyl)borane [$B(C_6F_5)_3$] is investigated to reveal the effect of substituents on the generation of functional macrocyclic polyethers and to understand the formation of topological impurities for better control of architectural purity during polymerization. With this aim, different families of monofunctional epoxides were polymerized, and the products were analyzed by MALDI-ToF MS. The data revealed that side reactions coexist with the macrocyclization reaction,

*A portion of this work has been reproduced from Haque, F.; Schexnayder, C.; Matxain, J.; Barroso-Bujans, F.; Grayson, S. A MALDI-ToF MS study of macrocyclic polyethers generated by electrophilic zwitterionic ring expansion polymerization of monosubstituted epoxides with $B(C_6F_5)_3$. *Macromolecules,* **under review**.

including chain transfer reactions to the monomer. With detailed MALDI-ToF MS analysis, it was possible to ascertain structural assignments of major and minor products and propose corresponding reaction mechanisms. Substituents effects were also studied to probe the functional group tolerance of this polymerization. Finally, computational studies were performed to examine the chemical interaction between the monomer and $B(C_6F_5)_3$ catalyst, which corroborated the experimental results by providing insight into the likelihood of generating non-cyclic byproducts. By using both analytical and computational tools, the polymerization could be optimized to generate macrocyclic polyethers with substantially increased purity.

4.2 INTRODUCTION

Macrocyclic polymers offer an attractive architecture with potential biomedical and materials applications due to their interesting biological and physical properties. Macrocyclic block copolymers, for example, show potential for micelle-based drug delivery as demonstrated by enhanced stability in respect to varying thermal,[1] ionic,[2] and acidic environments,[3] when compared to linear analogues. Additionally, cyclic polymers are characterized with many unique physical properties such as reduced melt viscosity,[4, 5] reduced entanglement,[5-7] and decreased T_g.[8, 9]

Early on, inefficiencies in synthetic methods prevented the use of cyclic polymers for industrial applications. While methods of synthesis have recently been improved, purity remains an ongoing concern and especially for remaining linear polymer contaminants. Today, there are two primary methods for the synthesis of cyclic polymers: 1) ring closure cyclization and 2) ring expansion polymerization. The ring closure method,

most popularly performed via the CuAAC "click" reaction, involves the unimolecular cyclization of a linear precursor with complementary azide and alkyne end groups under dilute conditions.[10] Under optimized dilution, low- and mid-molecular weight polymers preferentially undergo intramolecular cyclization, yielding cyclic polymer in greater than 99% purity, although the success of this method for high-molecular weight material has yet to be determined.[11] The ring expansion method, however, does not require a linear polymer precursor and instead a cyclic polymer can be directly accessed via the ring opening polymerization of a strained cyclic monomer in the presence of a catalyst, namely either Grubbs' cyclic ruthenium-alkylidene catalyst[12, 13] or a metal-free N-heterocyclic carbene as developed by Hedrick, Waymouth, and coworkers.[14-16] This method involves the insertion of monomer into an activated cyclic chain that is maintained until the expulsion of the catalyst by a backbiting reaction, yielding a cyclic polymer product. If a well-controlled polymerization is utilized with highly pure starting materials, an architecturally well-defined material can be achieved but the cyclic product is also usually characterized with a broad dispersity.

The electrophilic zwitterionic ring expansion polymerization (eZREP), as described herein, provides a direct route of synthesizing cyclic polyethers from monofunctional epoxides initiated by $B(C_6F_5)_3$ in a facile one-pot procedure at room temperature.[17] Through a previous study on this system, the major product (~70%) was determined to be cyclic in architecture but the product also contained a diversity of noncyclic structures, and particularly a monohydroxylated tadpole (TP-OH).[18] The TP-OH is proposed to have an identical mass as the cyclic structure and to be formed through a dimerization event (**Scheme C1**), as supported by MALDI-ToF MS experiments and SEC data, both of which

suggested that the TP-OH exists more prominently in the higher molecular weight region of the polymer sample. Previously, it was also proposed that the competition between water and monomer for the active catalyst center led to the formation of hydroxy terminated linear chains.[17, 18] In this study, a rational explanation is proposed for the formation of other linear and tadpole impurities as detected by MALDI-ToF MS, which is based on an ether-cleavage mechanism of epoxide substituents upon the formation of oxonium ions by reaction with the $B(C_6F_5)_3$ catalyst. Additionally, some of these experimental findings are corroborated by computational data to help support the formation of certain polymeric species.

The proposed mechanism was confirmed by studying two series of monofunctional epoxides, one containing a glycidyl ether (GE) linkage in the alpha carbon (**Scheme 4.1A and 4.1C**), which is susceptible to oxonium ion formation, and others that do not contain such a linkage (**Scheme 4.1B, 4.1D and 4.1E**). Additionally, the monomers were evaluated to probe the electronic nature of the substituent in the GE and styrene oxide (SO) families on the occurrence of side reactions. In general, it was observed that the first series of GE monomers behave similarly, but the SO series presented different topological impurities, suggestive of a secondary mechanism of their formation. In particular, the polymerization of ETD and Cl-PGE was exempt of side reactions induced by the ether-cleavage mechanism, thus generating cyclic structures in high yield with much higher purity than those produced by PGE. On the contrary, the polymerization of the SO family yielded a very low monomer conversion and was plagued with side reactions. Herein, we describe the polymerization of many epoxides using $B(C_6F_5)_3$ and the impact of pendant functional groups on the formation of byproducts. We hope to demonstrate the power of mass

spectrometry to identify the vast majority of polymeric components of a polymerization while only needing a limited sample quantity for characterization.

Scheme 4.1. Chemical structures of the monomers investigated in this study

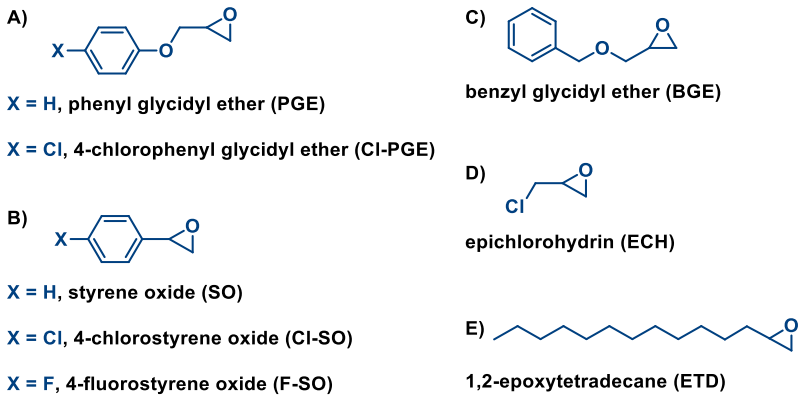

4.3 EXPERIMENTAL

Synthesis of cyclic polyethers. All reagents were manipulated and transferred either by distillation or under Argon in a vacuum line. BGE, PGE, Cl-PGE, SO, Cl-SO, F-SO, ETD, ECH, dichloromethane and methanol were dried over CaH_2, degassed and distilled under vacuum. $B(C_6F_5)_3$ (Aldrich) was sublimed at 50ºC under vacuum and transferred to the reaction flask in a glove box. All polymerization reactions were performed under argon at room temperature during 24 h. In a typical reaction, $B(C_6F_5)_3$ (2 mg, 3.9 μmol) was dissolved in 1 mL of dichloromethane, and then monomer was added by maintaining a monomer to catalyst molar ratio of 1100. In the case of PGE, a larger amount of solvent (5 mL) was used instead. To quench the reaction, a few drops of dry methanol were added. The polymers were then precipitated in cold methanol, separated by centrifugation and dried in a vacuum oven at 80 ºC until the sample weight remained constant. For all polymers synthesized, the corresponding yields are listed in Table 4.1

Table 4.1. Polymer molecular weight characteristics of synthesized polymers.

Entry	Monomer	$M_{n(SEC)}$ (Da)	Đ	Yield (wt%)[a]
1	PGE	900	1.3	70[b]
2	Cl-PGE	2100	2.6	85[b]
3	BGE	1900	1.8	75
4	ETD	2600	2.0	72
5	ECH	2100	2.3	50
6	SO	1600	1.5	2
7	F-SO	1400	1.3	2
8	Cl-SO	1600	1.5	6

[a]Determined gravimetrically after precipitation into methanol. [b]Determined to be greater than 90% by ^{1}H NMR

End group modification of impurities. *Formation of the terminal propargyl ether of polyether impurities.* Poly(BGE) (10.0 mg, 5.6 µmol, 1 eq.) was dissolved in dry THF (5 mL) and placed under N_2. NaH (1 mg, 60 µmol, 10 eq.) and propargyl bromide (3 mg, 20 µmol, 4 eq.) were added to the reaction mixture. The reaction stirred over night at 50 °C. The crude reaction mixture was concentrated *in vacuo* and then redissolved in dichloromethane. The solution was washed with water (3 x 5 mL) and dried with sodium sulfate. Finally, the organic solvent was removed *in vacuo* yielding the propargylated product for MALDI-TOF MS analysis. The same protocol was used for the propargylation of poly(ETD).

Formation of the terminal acetate ester of polyether impurities. Poly(SO) (1 mg, 0.6 µmol, 1 eq.) was dissolved in dry THF (5 mL). Acetic anhydride (5 mg, 50 µmol, 80 eq.) and 4-(dimethylamino)pyridine (DMAP) (1 mg, 8 µmol, 10 eq.) were added to the reaction mixture, which was then stirred overnight. The crude reaction mixture was concentrated *in vacuo* and then redissolved in dichloromethane. The solution was washed with saturated sodium bicarbonate (1 x 5 mL), water (2 x 5 mL), and 1M HCl (1 x 5 mL).

The organic layer was collected and dried with sodium sulfate. Finally, the organic solvent was removed *in vacuo* yielding the acetylated product for MALDI-TOF MS analysis.

Size exclusion chromatography. Molecular weight information and fractionation for poly(PGE), poly(BGE), and poly(ETD) was collected from a Waters model 1515 isocratic pump (Milford, MA). THF (1.0 mL/min) was used as the eluent with columns heated at a constant 30 °C by a column oven. This system was operated with a set of two columns in series from Polymer Laboratories Inc. consisting of PSS SDV analytical linear M (8 × 300 mm) and PSS SDV analytical 100Å (8 x 300 mm) columns. A Model 2487 differential refractometer detector was used as a refractive index detector. The instrument was calibrated with Waters Polystyrene ReadyCal Standards.

Molecular weight information and fractionation for poly(Cl-PGE), poly(ECH), poly(SO), poly(F-SO), and poly(Cl-SO) were collected on the same Waters system but were instead operated with three columns in series from Polymer Laboratories Inc. consisting of three PSS SDV analytical 5μm 500Å (8 x 300 mm) columns.

Mass spectrometry. MALDI-ToF MS measurements were collected on a Bruker Autoflex III MALDI-ToF mass spectrometer (Bruker Daltonics, Billerica, MA) in reflector mode with positive ion detection. Typical sample preparation for MALDI-ToF MS data was performed by making stock solutions in THF of matrix (20 mg/ml), polymer analyte (2 mg/ml), and an appropriate cation source (2 mg/ml). The stock solutions were mixed in a 10/2/1 ratio (matrix/analyte/cation), deposited onto the target plate and allowed to evaporate via the dried droplet method. For all polymers, DCTB was found to be an appropriate matrix. Both potassium and sodium trifluoroacetate were used as cation sources to generate potassium or sodium adducts, respectively, of the polymer. MALDI-

ToF MS data were calibrated against SpheriCal dendritic calibrants (Polymer Factory, Sweden).

Computational modeling. All geometry optimizations and vibrational frequency calculations were carried out within the Density Functional Theory (DFT),[19, 20] using the Gaussian16 program.[21] Specifically, geometries were optimized considering the solvent effect (chloroform) by means of the integral equation formalism of the polarized continuum model (IEFPCM),[22] using the TPSS exchange-correlation functional,[23] combined with the DEF2TZVP basis set.[24, 25] Dispersion interactions were considered using the empirical D3 version of Grimme's dispersion with Becke-Johnson damping.[27] This level of theory was proposed by Grimme and coworkers to be the most appropriate for weak acid-base interactions.[28] After geometry optimizations, harmonic vibrational frequencies were obtained by analytical differentiation of gradients, at the same level of theory, to identify whether the characterized structures were true minima. Such frequencies were then used to evaluate the zero-point vibrational energy (ZPVE) and the thermal (T = 298 K) vibrational corrections to the enthalpy. Finally, these enthalpy values were used to calculate the ΔH values of the studied processes.

4.4 RESULTS AND DISCUSSION

The monomers listed in **Scheme 4.1** and **Table 4.1** were polymerized via eZREP with $B(C_6F_5)_3$ in a concentrated solution (~2 g/mL) at room temperature for 24 h, except PGE which was polymerized in diluted conditions (~0.1 g/mL) for obtaining low-molecular weight polymer. The results exhibited high polymerization yield for the GE family and ETD monomer in agreement with previous results,[17] whereas very low yield for

the family of styrene oxide monomers. An intermediate case was observed for ECH. The results also demonstrated that in most cases, the molecular weights observed by SEC deviate from those predicted from the $[monomer]_0/[B(C_6F_5)_3]_0$ values. It has been suggested that termination in $B(C_6F_5)_3$-catalyzed eZREP occurs by backbiting to form the cyclic polymer and the subsequent regeneration of $B(C_6F_5)_3$, followed by reinitiation of new chains.[17] This type of termination was previously proposed by Hedrick, Waymouth and coworkers in the nucleophilic ZREP of lactide with N-heterocyclic carbenes.[26] It was also suggested that the narrow molecular weight distribution obtained in nucleophilic ZREP was due to a high rate of propagation relative to cyclization and chain transfer. In the case of eZREP with $B(C_6F_5)_3$, the varying and often high dispersity observed in most of the studied monomers and the low polymerization yield observed with some monomers already suggests that these systems are far from trivial. In order to provide mechanistic insight into the generation of polymeric species and the occurrence of side reactions during eZREP, which contributed to the deviations in molecular weight and varying monomer conversions, a detailed MALDI-ToF MS characterization study was performed.

4.4.1 Poly(phenyl glycidyl ether) and poly(4-chlorophenyl glycidyl ether).

Figure 4.1 presents the MALDI-ToF MS data corresponding to a SEC fractionated poly(PGE) sample prepared via eZREP. The data illustrates the complexity of the sample at increased molecular weight and hydrodynamic volume. As reported in a previous investigation,[18] the synthesis of poly(PGE) via eZREP is affected by side reactions leading to the formation of noncyclic structures as those identified in the MS data. At low-molecular weight, the sample contains primarily cyclic and TP-OH (**Figure 4.1D**). In the

mid-molecular weight fraction, the MS data (**Figure 4.1C**) also shows the presence of both cyclic and TP-OH, but an additional distribution arises that corresponds to HO-L-OH. In the high-molecular weight fraction (**Figure 4.1B**), the polymer has a significant contamination of linear and tadpole structures, especially when compared to the smaller molecular weight fractions. The formation of these additional structures is described below in detail.

In the same prior study, a secondary functionalization was performed on poly(PGE) via propargyl bromide to confirm the proposed structures in **Scheme 4.2**. Through the propargylation reaction, all species with one hydroxy group increased in nominal mass by +38 m/z, or +76 m/z in the case of structures with two hydroxy groups. Additionally, the confirmation of the cyclic structure is in part by the result of the cyclic polymer not reacting with propargyl bromide. Consequently, this study provided significant evidence for the identification of signals in **Figure 4.1**.

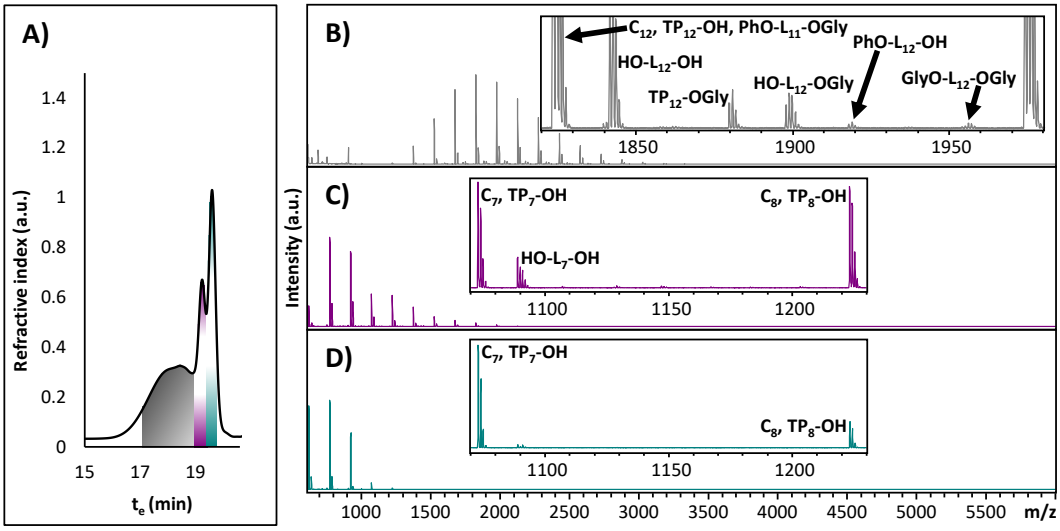

Figure 4.1. Poly(PGE) was fractionated by SEC (A), and the corresponding MALDI-ToF mass spectra of each SEC fraction is shown (B, C, and D). Identification of signals is based on the end group functionalization performed in a previous study.[18] The spectra were acquired in reflector mode, and all signals represent the sodiated adducts.

Figure 4.2 of poly(Cl-PGE), however, demonstrates that the simple addition of a chlorine moiety to PGE results in a substantially improved polymerization as evident by the MS data. Contrary to poly(PGE), poly(Cl-PGE) illustrates two peak distributions, the first being the distribution of cyclic and TP-OH structures and the second being the distribution of HO-L-OH. At both low- and mid-molecular weights (**Figure 4.2C-4.2D**), the polymer appears to be exclusively cyclic or TP-OH, and only at high-molecular weights does an additional peak arise corresponding to HO-L-OH. Furthermore, the HO-L-OH appears to exist in relatively low concentration. These results suggest that the weak electron withdrawing effect of chlorine helps to counteract side reactions as explained below.

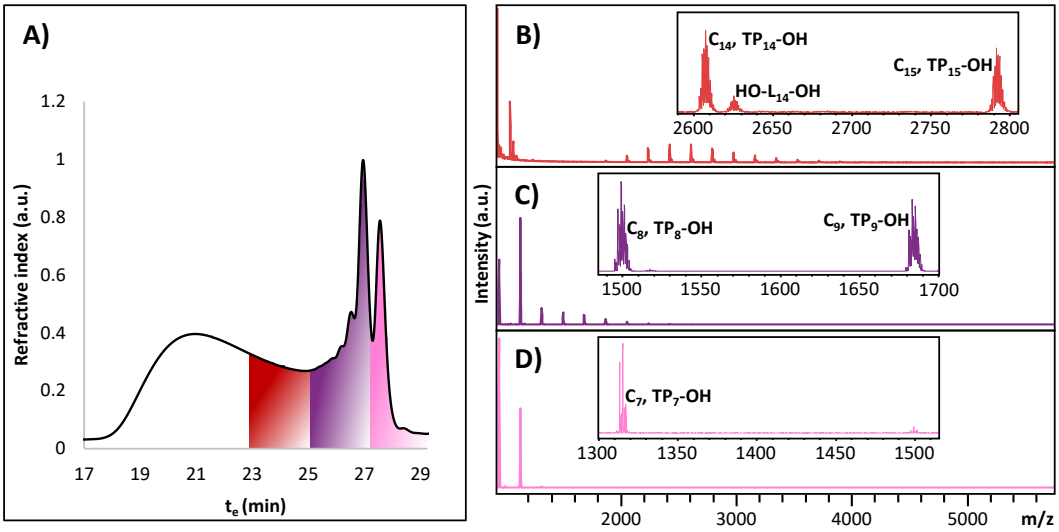

Figure 4.2. Poly(Cl-PGE) was fractionated by SEC (A), and the corresponding MALDI-ToF mass spectra of each SEC fraction is shown (B, C, and D). The spectra were acquired in reflector mode, and all signals represent the sodiated adducts.

To explain the formation of topological impurities in poly(PGE), several reaction mechanisms (**Scheme 4.2**) are provided to support the hypothesized structures, two of

which were proposed in a previous study. The tadpole TP-OH was explained to form through an intermolecular dimerization between a vinyl ether-functionalized structure and propagating polymer chain (**Scheme C1**).[18, 27, 28] Additionally, the presence of the larger hydrodynamic distribution in the SEC can be attributed to the occurrence of these tadpole dimers in addition to those of linear structures, which would have a larger hydrodynamic volume than the cyclic and thus elute at an earlier time. And, the dihydroxy-functionalized linear polymer (HO-L-OH) mechanism was characterized by the addition of water (**Scheme 4.2**) to either initiate a new propagating chain or react with an already existing propagating chain, both resulting in the same HO-L-OH structure.[17, 18] Here, a third mechanism is proposed that explains the formation of the remaining structures in the eZREP polymerization of phenyl glycidyl ether, based on the formation of an oxonium ion in the methoxyphenyl substituent via coordination with $B(C_6F_5)_3$ (illustrated in **Scheme 4.2**), as occurring in other Lewis acid-catalyzed systems.[29] Upon formation of the oxonium ion species, the adjacent carbon is susceptible to nucleophilic attack by reactive hydroxyl groups to generate terminal glycidyl ether (Gly) moieties and free phenol. For example, TP-OH can react with the oxonium ion to form TP-OGly. Similarly, HO-L-OH can react with the oxonium ion either once or twice to produce HO-L-OGly and GlyO-L-OGly, respectively. In such cases, phenol is released *in situ*, which can either react with the propagating zwitterionic chain or act as a nucleophilic initiator to form a new polymer; in both cases PhO-L-OH is formed, which can also be converted to PhO-L-OGly via the oxonium ion ether-cleavage mechanism. Unfortunately, this structure has the same molecular weight formula as the TP-OH and cyclic species, and consequently all three signals overlay. Additionally, the lack of a free hydroxyl group prevents it from being

distinguished via a functionalization reaction. It is worth noting, however, that an appreciable concentration of PhO-L-OH only appears in the large hydrodynamic volume fraction (**Figure 4.1B**). Due to its relatively low concentration compared to the other structures, it is assumed that PhO-L-OGly exists in even lower concentrations.

To verify the proposed mechanism leading to the formation of terminal glycidyl ethers, further MS analysis was performed on a previously purified poly(PGE) sample via our "click-scavenging" purification protocol.[18] To remove all hydroxy containing impurities, these functional groups were converted to an alkyne moiety via a propargylation reaction. The impurities were scavenged by undergoing a CuAAC "click" reaction with an azide functionalized solid phase resin, which could easily be filtered out to yield relatively pure cyclic material. SEC fractionation was performed on this sample, and two fractions were collected. MS data of the lower molecular weight fraction (**Figure C1C**) suggested it contained pure cyclic material, while the higher molecular weight fraction (**Figure C1B**) yielded a sample with mostly cyclic polymer and a minor contribution from TP-OGly and GlyO-L-OGly. These contaminant structures do not contain the necessary functionalizable handle (i.e., OH groups) and therefore cannot be removed by the "click-scavenging" protocol, and as such, provide the necessary evidence to support the oxonium ion mechanism. Analysis of MALDI-ToF MS and SEC data demonstrated that after the purification process much of the higher molecular weight and increased hydrodynamic volume species were removed from the polymer distribution. The distribution became significantly narrower post-purification, indicating that these non-cyclic impurities significantly impact the dispersity of the polymer sample.

Based on this previously purified poly(PGE) sample, the purity of the crude polymer was quantified using various techniques to determine overall purity and try to determine which non-cyclic structure contributed the most.[18] The reaction yield after "click-scavenging" was determined to be 80% (determined gravimetrically), which matched well with the purified sample having 77% of the integrated area as the crude polymer in the SEC chromatogram. Finally, when the crude sample was compared to linear poly(PGE) standards in FTIR, it had a purity of 89% if all impurities were dihydroxylated structures and a purity of 78% if all the impurities were monohydroxylated structures.[18] In this case, all results pointed to a polymer of ~80% purity with the majority of the impurities being the monohydroxy TP-OH. While purity can be gauged qualitatively by MALDI-ToF MS, it is important to recognize that varying structures and functionalities can affect the ionization efficiency. As such, MALDI-ToF MS provides structural insight into the polymer mixture, which is impossible with techniques like FTIR and SEC, but using it to quantitatively determine the concentration of polymer components can be very challenging.

Moreover, it appears that in the halogenated monomer (i.e., Cl-PGE), the ether-cleavage mechanism via the oxonium ion does not operate due to electronic effects of the chlorine atom on the phenyl ring making the *p*-chlorophenol an ineffective leaving group compared to phenol. Based on the SEC-fractionated MALDI-ToF MS data, minimal amounts of HO-L-OH are formed, which is only present in the high-molecular weight fraction (**Figure 4.2B**); more importantly, the mid- and low-molecular weight fractions appear to be exclusively cyclic. An end group functionalization was performed on the crude polymer (before fractionation), and a secondary distribution of TP-OH did not

appear, suggesting that this species does not exist in appreciable quantities in the polymer. Furthermore, the lack of impurities from this polymerization, especially from non-functionalizable structures makes eZREP a viable avenue to achieve extremely pure cyclic product. Finally, it appears that a simple modification in the PGE monomer used (to include a 4-chlorophenyl group) yields cyclic samples of substantially increased Cl-PGE purity.

Scheme 4.2. Schematic illustrating the formation of products during the polymerization of PGE including cyclic, tadpole, and linear architectures.

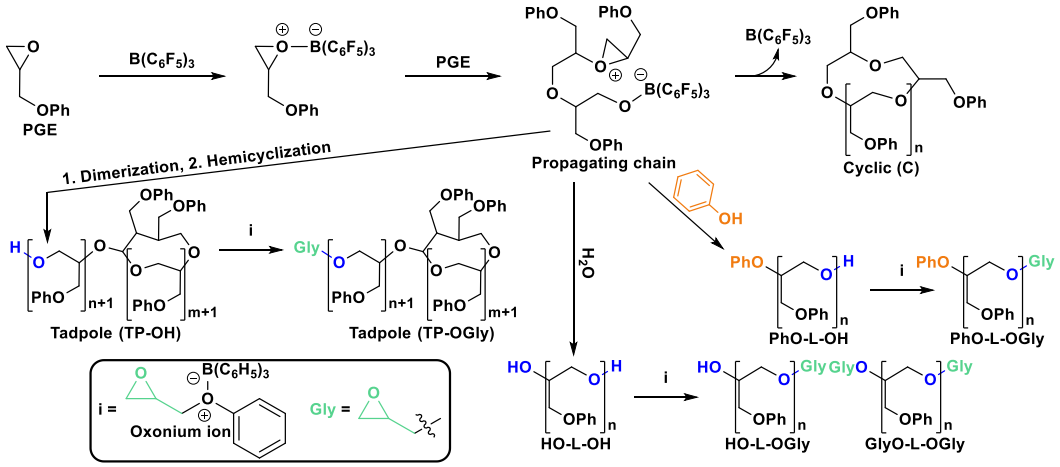

To obtain theoretical insight into the effect of the chlorine atom on the ether-cleavage mechanism via the oxonium ion formation in Cl-PGE, theoretical calculations were performed using density functional theory (DFT) to compare the chloride substituent effect to that of a strong electron donor, a strong electron acceptor, and finally to having a hydrogen substituent (i.e., PGE). It is well known that chlorine can act as both an electron donor through resonance and an electron acceptor through induction, especially when attached to a phenyl ring, and so this study was done to probe the electronic characteristics of the chloride moiety when added to the PGE monomer. Additional details on how the

computations were performed can be found in the experimental section. Based on these calculations, a reaction pathway is shown below in **Figure 4.3**. This describes the boron catalyst's affinity to coordinate with either the oxygen in the glycidyl ether moiety or the epoxide moiety, activating the PGE monomer for further reactivity, namely, polymerization or undesired side reactions, along with the formation of non-reactive species.

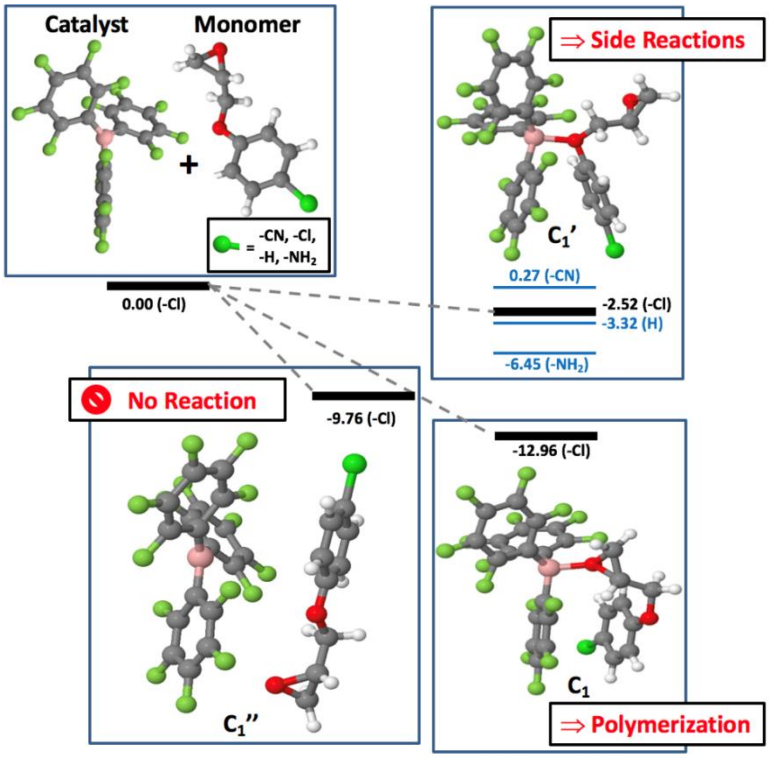

Figure 4.3. DFT calculations to compare the reaction of $B(C_6F_5)_3$ with the epoxide (C_1 complex) and ether oxygen of PGE (C_1' complex) with varying substituents (-CN, -Cl, -H, and $-NH_2$), and the formation of non-active complexes (C_1" complex). The values given are the calculated formation enthalpies, ΔH (kcal/mol), at the local minima. For the C_1' complex, the ΔH values obtained for other substituents in the phenyl ring (-CN, -H and $-NH_2$) are also given (**Table C1**).

The enthalpy reference is set to 0.0 for the separated reactant species, namely, Cl-PGE monomer and the boron catalyst. When both species approach each other, two activated complexes can form, C_1 or C_1', and a non-active complex, C_1". It is worth noting, however, that in the activated complexes the B-O bond lengths are in a range of 1.6 – 1.8

Å, while in the non-active complex this distance is much longer, up to 3.5 Å (see **Table C2**). The X-PGE monomer activation process will be explained below.

In the case of Cl-PGE, the formation of C_1 exhibited a negative enthalpy value of -12.96 kcal/mol, which is in agreement with previous calculations based on PGE.[17] Furthermore, C_1 is more stable than C_1' by around 10.0 kcal/mol indicating that the formation of the C_1 complex is more likely. This result supports the preference of the monomer to polymerize rather than undergo side reactions to form terminal glycidyl ether end groups via the ether-cleavage mechanism. While in the case of PGE, there is evidence of the ether cleavage mechanism but still this is relatively minimal and the polymerization of PGE to form macrocycles is preferred. As such when the polymerization of PGE is performed, there is a high monomer conversion.

Moreover, these calculations describe the formation of a second species (C_1') by complexation of $B(C_6F_5)_3$ to the glycidyl ether oxygen. The results suggest the stability of this complex is strongly dependent on the phenyl ring substituent. To understand the effect of para-substituents, two extreme situations were studied – the addition of a cyano group (i.e., -CN) and the addition of an amino group (i.e., $-NH_2$). The calculations performed for the strong electron acceptor substituent (i.e., -CN group) resulted in an enthalpy increase to a value of 0.27 kcal/mol, suggesting that this type of substituent could completely suppress the ether-cleavage mechanism and prevent the formation of terminal glycidyl ether end groups. On the contrary, with a strong electron donor group (i.e., $-NH_2$ group) the complexation energy is sharply decreased to a value of -6.45 kcal/mol, thus favoring side reactions. It is worth noting here that model does not take into account the nucleophilic character of amino groups and their ability to interact with epoxides (e.g., polymerization

initiation via the amino group). Additionally, all ΔH values for the formation of both C_1 and C_1' were calculated with all four substituents (i.e., -CN, -Cl, -H, and -NH_2) and can be found in **Table C1**.

The activation of these two C_1 and C_1' species occurs via the acid-base interaction between the B and O atoms. During the polymerization or side reaction of Cl-PGE, the coordination of the B with the O atom results in the weakening of the O-C bonds (where O is from either the epoxy or ether group). This is demonstrated by the elongation of their bond lengths (**Table C2 and Figure C2**). **Table C2** reveals that in the non-affiliated complex, when the monomer is separate from the Lewis acid, the O-C bonds of the monomer are 1.448 Å and 1.445 Å within the epoxy ring, and 1.441 Å and 1.371 Å for the ether oxygen. When the monomer is affiliated with the Lewis acid, these values are elongated to 1.472 Å and 1.495 Å for the epoxy ring in the C_1 complex, and to 1.493 Å and 1.433 Å in the ether oxygen in the C_1' complex. Because these bonds are weaker in the mentioned complexes, they become increasingly electrophilic and are possibly prone to attack by other nucleophilic species found in the reaction media, leading to either further polymerization or to side reactions.

In addition to these two active complexes, a final species C_1" can be formed in which the catalyst and monomer approach each other but instead form an inactive species. Contrary to the C_1 and C_1' cases, where the interaction between the catalyst and the monomer is electrostatic, the interaction resulting in the C_1" species is purely of van der Waals type forces. Consequently, their association results in a favorable interaction but it does not induce a chemical reaction (e.g., polymerization or side reactions). As seen in **Table C2**, X-PGE bond distances are not altered before and after complexation to lead to

C_1'' complex, indicating that the formation of this inactive species does not provide a major impact on the polymerization of GPE.

Finally, when comparing the two monomers studied experimentally herein, Cl-PGE and PGE, it was determined that Cl-PGE exhibited a complexation enthalpy of C_1' (-2.52 kcal/mol) slightly higher than that of GPE (-3.32 kcal/mol), implying that the ether-cleavage mechanism via oxonium ion is less probable to occur in Cl-PGE than in PGE. This is indicative of the chloro group providing some electron withdrawing character like –CN, helping to suppress the side reactions. This result also supports the experimental MALDI-ToF MS findings, where minor amounts of TP-OGly, HO-L-OGly, and GlyO-L-OGly were found in poly(PGE) (**Figure 4.1B**) but do not appear in poly(Cl-PGE) (**Figure 4.2**).

Since the interaction between the catalyst and the monomer through the ether oxygen is sterically hindered, this complex may be considered a frustrated Lewis pair. The accurate calculation of this weak interaction energy in such compounds is difficult, and although a sophisticated method has been used to probe this interaction, the calculated values should be considered in a qualitative manner. However, it is observed that electron donor substituents would stabilize this complex, leading to undesirable side products, while electron acceptor substituents act in an opposite way, helping to prevent the formation of side reactions during the polymerization of GPE-based monomers. The corresponding Cartesian coordinates for all calculated species can also be found in the Supporting Information (**Table C3-C4**).

4.4.2 Poly(benzyl glycidyl ether).

Poly(BGE) was the final polymer studied in the series of monomers containing glycidyl ether linkages. Unlike the previous two monomers studied, the benzyl moiety of this monomer increases the complexity of the polymerization as demonstrated by the MALDI-ToF mass spectrum data of the obtained polymer (**Figure 4.4B-4.4C**). However, many of the peaks were identified based on the previous ether-cleavage mechanism described in **Scheme 4.2** for poly(PGE). Analogous to **Scheme 4.2**, **Scheme 4.3** illustrates the formation of the cyclic, TP-OH, and HO-L-OH poly(BGE) products. The free hydroxyl groups can undergo a similar secondary termination via an oxonium ion of the BGE monomer to form terminal glycidyl ethers. However, after the oxonium ion is formed, the benzylic position is also susceptible to nucleophilic attack by free hydroxyl groups to form polymers with terminal benzyl ethers. In the case of TP-OH, for example, the reaction of this structure with the oxonium ion yields TP-OGly and TP-OBn, while also forming benzyl alcohol (BnOH) and glycidol, respectively, *in situ*. Consequently, both nucleophilic alcohols can either initiate a new polymerization or react with a propagating chain to form additional linear structures. After collecting MS data on a mid-molecular weight SEC-fraction of poly(BGE) sample, **Scheme 4.3** can be used to elucidate the majority of its components. It is worth noting, however, that the data on low- and high-molecular weight fractions (**Figure C3**) are equally complex and ridden with the same noncyclic impurities as **Figure 4.4** and **Scheme 4.3**. The scheme can be further validated through doing a secondary functionalization on poly(BGE) using propargyl bromide, confirming the number of hydroxyls per structure and validating the proposed structures (**Figure C4**).

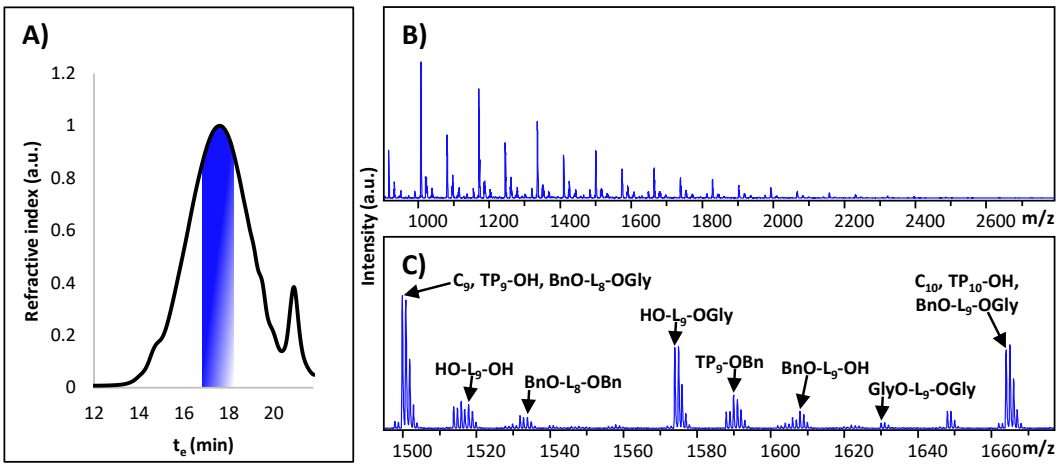

Figure 4.4. A mid-molecular weight fraction of poly(BGE) was collected by SEC (A) and further analyzed by MALDI-ToF MS (B). An inset identifying the structures formed during the polymerization is also shown (C). Due to the complexity of the polymerization, only the mid-molecular weight fraction is shown here, but the additional low- and high-molecular weight fractions can be found in **Figure C3**. Identification of signals is based on the end group functionalization (**Figure C4**). The spectra were acquired in reflector mode, and all signals represent the sodiated adducts.

Scheme 4.3. Schematic illustrating the formation of products during the polymerization of BGE including cyclic, tadpole, and linear architectures.

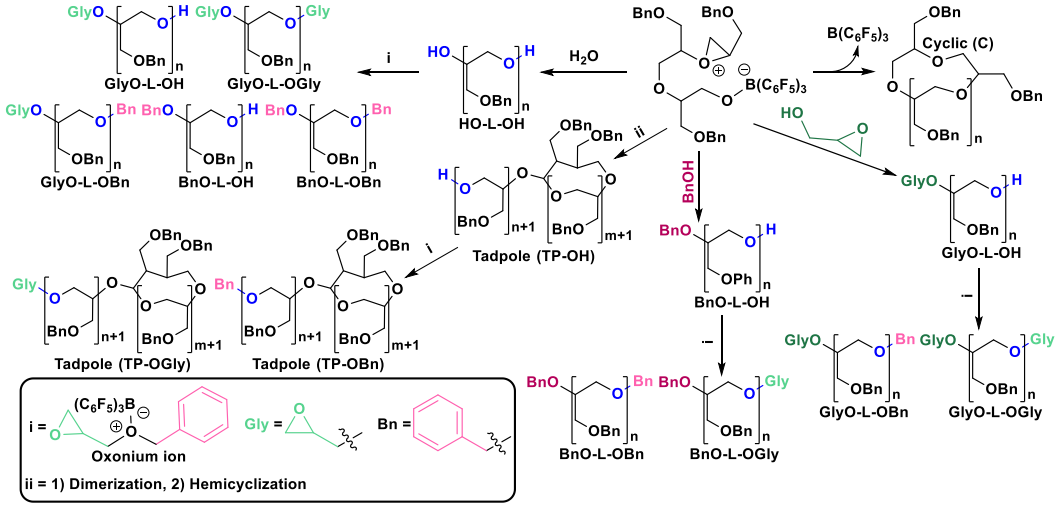

4.4.3 Poly(1,2-epoxytetradecane)

To validate the ether-cleavage mechanism proposed in **Scheme 4.2 and 4.3**, ETD was polymerized which does not contain the glycidyl ether linkage but a long aliphatic

chain instead. A schematic of the products formed during the ETD polymerization is shown below (**Scheme 4.4**). Like the previous samples, poly(ETD) was also fractionated by SEC, and MALDI-ToF MS data was collected on three corresponding fractions (**Figure 4.5**). The lower molecular weight fraction appears to be mostly cyclic, however TP-OH polymer as well as a small contribution from the HO-L-OH linear polymer also appear (**Figure 4.5D**). Moreover, there appears to be a minor secondary peak overlapping with the HO-L-OH with a molecular weight of -2 m/z in respect to the HO-L-OH (or +16 m/z from the cyclic); a larger figure of this fraction is provided in **Figure C5**, better illustrating the presence of this structure. The structure is proposed to be a polymer with one terminal hydroxy group and one aldehyde group and is referred to as CHO-L-OH. A proposed mechanism of CHO-L-OH is also provided below in **Scheme 4.7** with the discussion of the styrene oxide family. The formation of CHO-L-OH is based on polymer initiation with a tetradecanal carbocation, as illustrated in **Scheme 4.4**. The concentration of this polymeric species is assumed to be very low (and only seen in **Figure 4.5D**), because secondary carbocations are relatively unstable, especially if compared to benzylic carbocations as seen in the case of the styrene oxide family. Nonetheless, a propargylation reaction was performed on the crude poly(ETD) confirming the presence of cyclic, TP-OH, and HO-L-OH (**Figure C6**). The functionalization reaction also confirmed that only one propargyl group adds to what is proposed to be a linear structure with a terminal hydroxy and aldehyde group (i.e., CHO-L-OH), validating the proposed structure.

The mid-molecular weight fraction also contains cyclic, TP-OH, and HO-L-OH (**Figure 4.5C**). Based on signal intensity, there appears to be a higher concentration of

HO-L-OH than cyclic and TP-OH. Lastly, the highest molecular weight fraction has almost exclusively HO-L-OH linear polymer (**Figure 4.5B**).

Furthermore, the reaction of the crude polymer with propargyl bromide (**Figure C6**) elucidated that TP-OH is a minor impurity compared to the cyclic polymer, resulting in a polymer with a high cyclic polymer content. And while the sample is contaminated with some noncyclic structures, all of these impurities have a functionalizable handle (i.e. OH groups), and therefore poly(ETD) can be purified via the "click-scavenging" protocol. More importantly, however, there is absence of peaks associated with terminal glycidyl ethers, and therefore if a monomer without a glycidyl ether linkage is used, it prevents the additional impurities arising from the oxonium ether-cleavage mechanism, and results in a significantly purer sample.

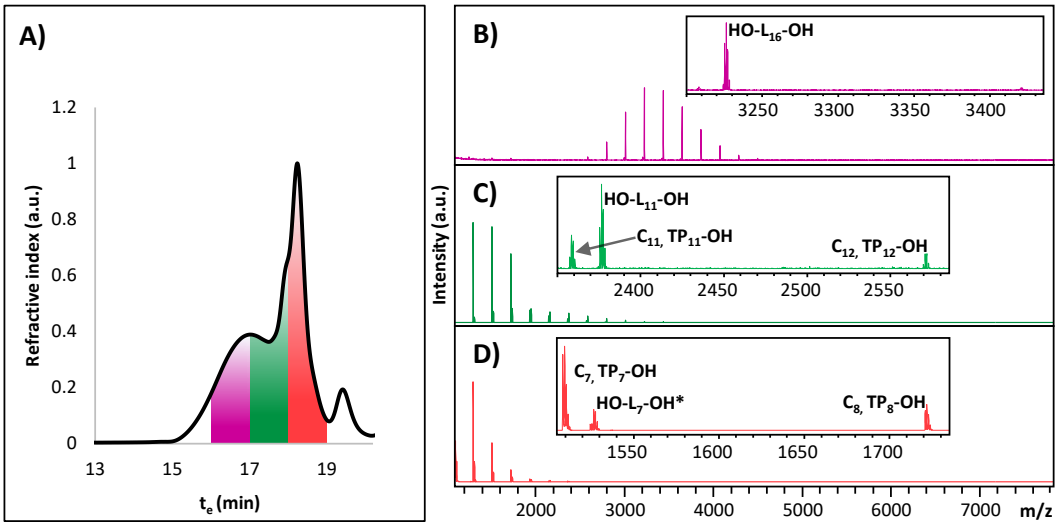

Figure 4.5. Poly(ETD) was fractionated by SEC (A), and the corresponding MALDI-ToF mass spectra of each SEC fraction is shown (B, C, and D). Identification of signals is based on the end group functionalization (**Figure C6**). Please note that the asterisk (*) adjacent to HO-L_7-OH is a result of two overlaying signals, which are further depicted in **Figure C5**. The spectra were acquired in reflector mode, and all signals represent the sodiated adducts.

Scheme 4.4. Schematic illustrating the formation of products during the polymerization of ETD including cyclic, tadpole, and linear architectures. The formation of the tetradecanal carbocation (ii) is further described in **Scheme 4.6 and 4.7**.

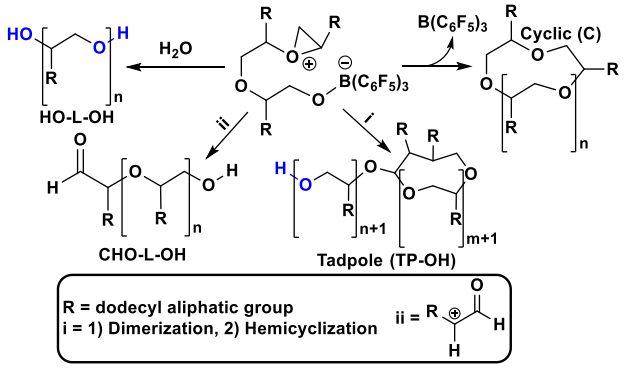

4.4.4 Poly(epichlorohydrin)

Epichlorohydrin (ECH) was an additional monomer polymerized, and like ETD, it does not contain the glycidyl ether linkage. ECH was polymerized to further investigate the role of the glycidyl ether linkage in the monomer. It was determined that that side reactions in addition to the intended cyclization occur through a mechanism not dissimilar to the GE family of monomers. The low-molecular weight fraction is especially pure, and the cyclic or TP-OH is the major distribution. In the mid-molecular weight fraction, there are several structures that arise, with the first three being the well understood cyclic, TP-OH, and HO-L-OH. Three additional structures appear, with the first of those arising from the hydroxy group of TP-OH undergoing a nucleophilic substitution with an additional monomer unit to form TP-OGly and Cl^- as a leaving group. Similarly, HO-L-OH undergoes an analogous reaction to form HO-L-OGly, but GlyO-L-OGly is not observed. In both side reactions, chloride is released as a byproduct, which can initiate a polymerization yielding Cl-L-OH, which is also observed in the mid-molecular weight fraction (**Figure 4.6C**). It is worth noting, however, that the major product is the cyclic

distribution and these additional structures exist in extremely minimal quantity based on the relative MS peak intensities. Finally, in the highest molecular weight fraction (**Figure 4.6B**), the cyclic polymer is still the major product, but the relative concentration of additional impurities is much higher than the mid-molecular weight fraction (**Figure 4.6C**), and the additional peaks appear through the same nucleophilic substitution of hydroxy groups with ECH to form terminal glycidyl ethers.

While the precursor, ECH, does not contain a glycidyl ether linkage, terminal glycidyl ethers are still formed during the polymerization due to the presence of chlorine and its ability to act as a good leaving group during nucleophilic substitution reactions (see **Scheme 4.5**). Similar to the GE monomers, the chlorine heteroatom also has electron lone pairs that can complex with the boron catalyst. However, it is hypothesized that in the previous GE monomers, the side reactions are increasingly favored due to the activated oxonium species. In the case of ECH, it is assumed that an activated species is less likely to form due to chlorine's propensity to act as an electron withdrawing group through induction. However, the lack of ether-based oxygen in ECH and the inability to form an activated species, likely disfavors these additional side reactions.

To further probe the validity of this hypothesis, DFT calculations were performed to study this monomer and its ability to undergo side reactions. In the case of the previously discussed DFT calculations for PGE and Cl-PGE, the likelihood of side reactions occurring was based on the complex stability and the elongation of several bond lengths resulting from their weakening. With the PGE monomers, the resultant coordination of boron in the catalyst with either of the oxygens (i.e., glycidyl ether or epoxide) resulted in very similar bond distances. In the case of ECH, complex stability calculations can be performed to

elucidate the stability of the coordination of boron with either the oxygen in the epoxide or the pendant chlorine. As seen previously, the polymerization is preferred (ΔH = -9.38 kcal/mol) as demonstrated by a negative enthalpy value. However, the complexation with the chlorine atom (ΔH = -4.33 kcal/mol) has a less negative enthalpy value than the enthalpy value of polymerization. While the difference between these numbers is smaller than the PGE values, what is seen is that the B-Cl has a much larger bond distance than B-O. And while chlorine may have a favorable interaction with the boron, this interaction is of van der Waals type forces, as previously mentioned for the non-active C_1" complex, rather than an electrostatic interaction. Therefore, this interaction is not strong enough to activate the monomer and to encourage the side reactions. Consequently, the side reactions do occur but in minimal quantity. See **Table C5-C6** for calculated bond lengths, ΔH values, and Cartesian coordinates used to describe the polymerization of ECH.

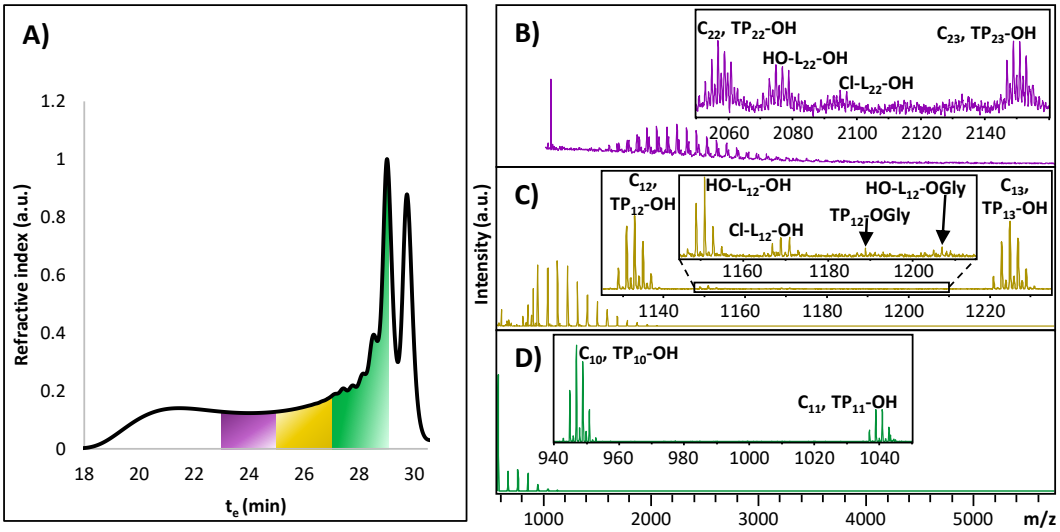

Figure 4.6. Poly(ECH) was fractionated by SEC (A), and the corresponding MALDI-ToF mass spectra of each SEC fraction is shown (B, C, and D). The spectra were acquired in reflector mode, and all signals represent the sodiated adducts.

Scheme 4.5. Schematic illustrating the formation of products during the polymerization of ECH including cyclic, tadpole, and linear architectures.

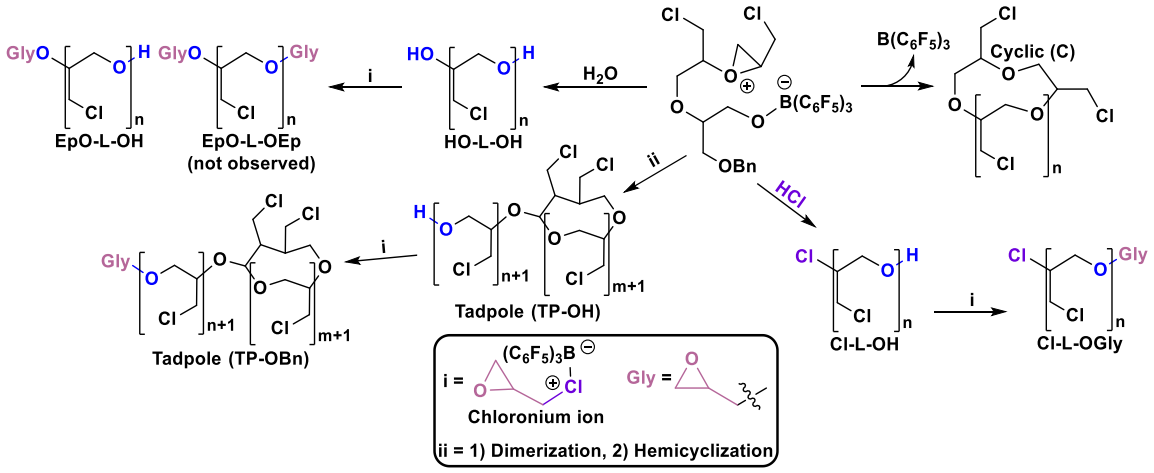

4.4.5 Poly(styrene oxide), poly(4-chlorostyrene oxide) and poly(4-fluorostyrene oxide)

The final attempt to investigate monomers without the glycidyl ether linkage led to the study of monofunctional styrene oxides. In the case of all three monomers used—styrene, 4-chlorostyrene and 4-fluorostyrene oxide —the monomer conversion was always very low (~5%). A likely explanation for the result was found in the literature - styrene oxide easily converts to phenylacetaldehyde in the presence of a Lewis acid, which would deactivate the borane catalyst for initiating the polymerization (**Scheme 4.6**).[30, 31]

Scheme 4.6. Deactivation of SO monomer via Lewis acid[30]

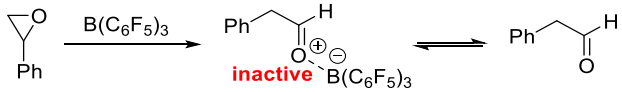

The reason for styrene oxide's inactivity during the polymerization was a very important finding for understanding the low conversion of monomer and low-molecular weights achieved. However, to ascertain a more complete picture of the eZREP polymerization, the family of poly(styrene oxide)s were still analyzed using MALDI-ToF

MS. Poly(SO) was also fractionated using SEC and notably the HO-L-OH exists as the major product in all three fractions (**Figure 4.7**) unlike all the previously discussed polymers. Additionally, poly(SO) forms six products during the polymerization, some of which appear to be unique to this family of polymers (**Table 4.2**).

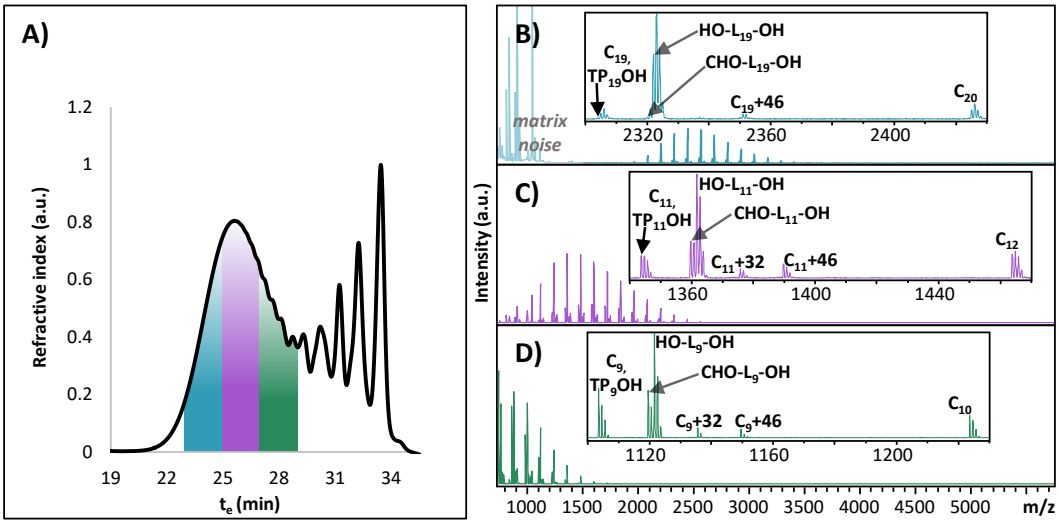

Figure 4.7. Poly(SO) was fractionated by SEC (A), and the corresponding MALDI-ToF mass spectra of each SEC fraction is shown (B, C, and D). Identification of signals is based on the end group functionalization (**Figure C7**). The spectra were acquired in reflector mode, and all signals represent the sodiated adducts.

In both low- and mid-molecular weight fractions (**Figure 4.7C-4.7D**), the concentration of all six products are very similar. Like the previous samples, poly(SO) also has the cyclic and TP-OH distribution, however, in this sample it is not the major product. Instead, the HO-L-OH is the major product. An additional CHO-L-OH linear structure appears to overlay with the linear HO-L-OH with a molecular weight formula - 2 m/z in respect to the HO-L-OH structure. Due to the ease of the monomer converting to phenylacetaldehyde, it is hypothesized that this linear polymer begins with the formation of a carbocation in the benzylic position on the phenylacetaldehyde through hydrogen abstraction. The carbocation acts as a Lewis acid to initiate a polymerization similar to $B(C_6F_5)_3$. The propagating linear chain is terminated with water to form the final structure,

as illustrated in **Scheme 4.7**. The observation of a carbonyl stretching peak at 1723 cm^{-1} in the FTIR data supports this mechanism and the incorporation of a carbonyl end group in the polymer chain (**Figure C8**).

Scheme 4.7. Mechanism for the formation of CHO-L-OH

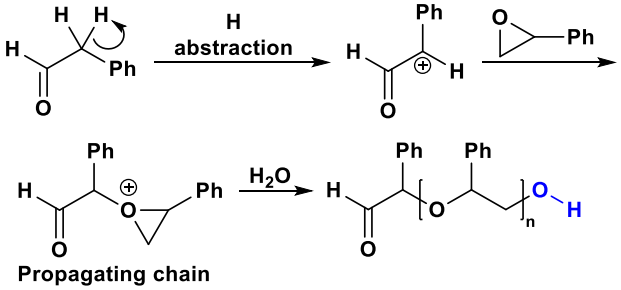

The final two structures that appear in this sample are two signals that are offset +32 and +46 m/z from the cyclic signal. The identity and origin of these two structures has yet to be determined. However, it is hypothesized that these two structures are possibly an artifact of the formation of phenylacetaldehyde as these components are unique to the styrene oxide polymer family. Finally, the highest molecular weight fraction (**Figure 4.7B**), has the cyclic, TP-OH, CHO-L-OH, HO-L-OH, and cyclic + 46 m/z structures. However, most of the fraction is HO-L-OH, like the other two fractions, and the rest of these structures are present in extremely minimal concentration.

The presence of several unknown and new structures led to two additional experiments, the first being a study with respect to two different cations. Shown in **Figure C9**, MALDI-ToF MS data is collected on the smallest molecular fraction (from **Figure 4.7D**) using both NaTFA and KTFA, independently, to confirm that all signals ionize with sodium and potassium, respectively, rather than trace amounts of other cation sources, possibly originating from the polymer sample. In both MS spectra, the polymer ionized

with the intended cation, and the two additional peaks (+32 and +46) also ionized with the intended cation. The second experiment involved the functionalization of the same fraction C using acetic anhydride (**Figure C7**). This experiment confirmed the presence of the cyclic and TP-OH structures, as there is still a cyclic peak post-functionalization without an acetyl group, and a second peak forms as a result of the TP-OH adding one acetyl group. Similarly, HO-L-OH is confirmed by the addition of two acetyl groups. In the case of CHO-L-OH, it adds only one acetyl group, supporting the hypothesis that this structure only has one free hydroxyl group. Moreover, the cyclic +32 and +46 m/z signals remain unknown, but the functionalization confirms that they both have exactly one free hydroxyl group each. It is worth noting, that while their structure is unknown, the MS data of the functionalized polymer provides some structural information regarding end groups.

Table 4.2. Structural assignments of poly(styrene oxide) based on MALDI-ToF MS data

Name	Structure	Mass	Number of Hydroxyls
C	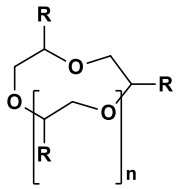	(n+2) x 120	0
TP-OH	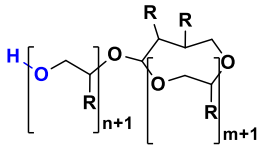	(n+m+2) x 120	1
CHO-L-OH	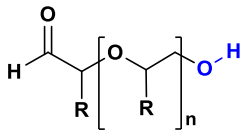	(nx120) + 16	1
HO-L-OH	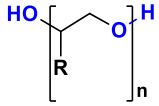	(nx120) + 18	2
C+32	**Unknown**	(nx120) + 32	1
C+46	**Unknown**	(nx120) + 46	1

As previously mentioned, 4-chlorostyrene oxide and 4-fluorostyrene oxide were also polymerized to probe the effect of substituents on the formation of side products. For 4-fluorostyrene oxide, 6 products form during the polymerization, the first four being the cyclic, TP-OH, CHO-L-OH, and HO-L-OH structures, and the additional unknown structures for cyclic +32 m/z and +46 m/z also form. In the case of 4-chlorostyrene, it appears that during the polymerization the same 6 structures also form. However, due to the complex nature of the isotopic distribution arising from the very high chlorine content, it is difficult to differentiate CHO-L-OH from HO-L-OH despite only having a difference in mass of 2 m/z, but it is assumed both exist as they existed in the cases of poly(SO) and poly(F-SO). The respective MS data for poly(F-SO) and poly(Cl-SO) can be found in **Figure C10 and C11**, respectively.

While a significant amount of information has been learned about the polymerization of styrene oxides via eZREP, these monomers are not viable for eZREP with $B(C_6F_5)_3$ due to the extremely low monomer conversion. While the monomers do not contain glycidyl ethers and the impurities do not appear to form terminal glycidyl ethers, many noncyclic structures arise due to the chemical structure of styrene oxides. If styrene oxides are used for polymerization, the reaction conditions ought to be optimized, and a different catalyst is likely required that does not favor the formation of phenylacetaldehyde and noncyclic polymeric structures.

4.5 CONCLUSIONS

In this study, many different monomers were polymerized via eZREP using the $B(C_6F_5)_3$ Lewis acid catalyst. To analyze the success of the polymerization, polymer samples were fractionated by SEC and analyzed by MALDI-ToF MS. The combination of using a chromatographic tool to separate the polymer by hydrodynamic volume and a secondary tool that provides structural insight as to the products formed during the polymerization yields a significant amount of information about the ring opening polymerization as well the presence of structures as a function of molecular weight and size. In addition, the use of DFT computations allowed for a better understanding of the polymerizations and helped to explain the proposed mechanisms.

However, among these polymerizations, poly(BGE) and the family of poly(styrene oxide)s were least successful via the eZREP protocol, and were severely contaminated with noncyclic impurities. Additionally, due to side reactions occurring during many of these polymerizations, (e.g., dimerizations to form tadpoles or formation of phenylacetaldehyde

during the SO polymerization), large deviations are seen in experimental molecular weight and monomer conversion compared to the theoretical results. Rather, the polymerization of ETD and Cl-PGE, yielded polymers of significantly more value. In the case of Cl-PGE, the simple addition of a chlorine moiety to PGE results in a polymer that appears to be almost exclusively cyclic and consequently, does not require post-polymerization purification. ETD, however, had a minor content of impurities, but all of which could be removed via the "click-scavenging" purification protocol. Importantly, the polymerization of ETD resulted in a much cleaner and simpler distribution of products by removing the possibility of forming terminal glycidyl ethers. Finally, in the case of ECH, the polymer appeared to contain minimal impurities. While some of these structures did contain terminal glycidyl ethers, their content was likely minimized because the monomer could not form an activated oxonium ion complex. For both the polymerization of Cl-PGE and ECH the minimal formation of side products can be validated and explained by DFT calculations by comparing the stability of reaction intermediates.

From this study alone, it is worth noting that highly pure cyclic polymers can be achieved in a 1-step polymerization of either Cl-PGE or ETD, especially if performed in ultra-dry conditions to minimize the presence of water. While much has been learned about eZREP polymerization via $B(C_6F_5)_3$ from this study, further studies must be done to fully understand the effect of different types of monomers with varying chemical linkages and substituents. More importantly, this study highlights the impact of using mass spectrometry as an analytical tool that gives structural insight into a polymerization that is otherwise not possible with many traditional techniques (e.g., ^{1}H NMR or SEC). Continued efforts to advance analytical and computational techniques will lead to a better

understanding of how polymerizations occur to ultimately optimize the synthesis, to make valuable cyclic materials with beneficial biological and materials properties.

4.6 REFERENCES

1. Honda, S.; Yamamoto, T.; Tezuka, Y. Topology-directed control on thermal stability: micelles formed from linear and cyclized amphiphilic block copolymers. *Journal of the American Chemical Society* **2010,** 132 (30), 10251-10253.

2. Honda, S.; Yamamoto, T.; Tezuka, Y. Tuneable enhancement of the salt and thermal stability of polymeric micelles by cyclized amphiphiles. *Nature Communications* **2013,** 4, 1574.

3. Hoskins, J. N.; Grayson, S. M. Synthesis and degradation behavior of cyclic poly(ε-caprolactone). *Macromolecules* **2009,** 42 (17), 6406-6413.

4. Roovers, J. Viscoelastic properties of polybutadiene rings. *Macromolecules* **1988,** 21 (5), 1517-1521.

5. Pasquino, R.; Vasilakopoulos, T. C.; Jeong, Y. C.; Lee, H.; Rogers, S.; Sakellariou, G.; Allgaier, J.; Takano, A.; Brás, A. R.; Chang, T.; Gooßen, S.; Pyckhout-Hintzen, W.; Wischnewski, A.; Hadjichristidis, N.; Richter, D.; Rubinstein, M.; Vlassopoulos, D. Viscosity of ring polymer melts. *ACS Macro Letters* **2013,** 2 (10), 874-878.

6. Kapnistos, M.; Lang, M.; Vlassopoulos, D.; Pyckhout-Hintzen, W.; Richter, D.; Cho, D.; Chang, T.; Rubinstein, M. Unexpected power-law stress relaxation of entangled ring polymers. *Nature Materials* **2008,** 7 (12), 997-1002.

7. Kawaguchi, D. Direct observation and mutual diffusion of cyclic polymers. *Polymer Journal* **2013,** 45 (8), 783-789.

8. Xu, X.; Zhou, N.; Zhu, J.; Tu, Y.; Zhang, Z.; Cheng, Z.; Zhu, X. The first example of main-chain cyclic azobenzene polymers. *Macromolecular Rapid Communications* **2010,** 31 (20), 1791-1797.

9. Zhang, L.; Elupula, R.; Grayson, S. M.; Torkelson, J. M. Major impact of cyclic chain topology on the T_g-confinement effect of supported thin films of polystyrene. *Macromolecules* **2016,** 49 (1), 257-268.

10. Laurent, B. A.; Grayson, S. M. An efficient route to well-defined macrocyclic polymers via “click” cyclization. *Journal of the American Chemical Society* **2006,** 128 (13), 4238-4239.

11. Elupula, R.; Oh, J.; Haque, F. M.; Chang, T.; Grayson, S. M. Determining the origins of impurities during azide–alkyne click cyclization of polystyrene. *Macromolecules* **2016,** 49 (11), 4369-4372.

12. Bielawski, C. W.; Benitez, D.; Grubbs, R. H. An "endless" route to cyclic polymers. *Science* **2002,** 297 (5589), 2041-2044.

13. Boydston, A. J.; Xia, Y.; Kornfield, J. A.; Gorodetskaya, I. A.; Grubbs, R. H. Cyclic ruthenium-alkylidene catalysts for ring-expansion metathesis polymerization. *Journal of the American Chemical Society* **2008,** 130 (38), 12775-12782.

14. Jeong, W.; Hedrick, J. L.; Waymouth, R. M. Organic spirocyclic initiators for the ring-expansion polymerization of β-lactones. *Journal of the American Chemical Society* **2007,** 129 (27), 8414-8415.

15. Kamber, N. E.; Jeong, W.; Gonzalez, S.; Hedrick, J. L.; Waymouth, R. M. N-Heterocyclic carbenes for the organocatalytic ring-opening polymerization of ε-caprolactone. *Macromolecules* **2009,** 42 (5), 1634-1639.

16. Culkin, D. A.; Jeong, W.; Csihony, S.; Gomez, E. D.; Balsara, N. P.; Hedrick, J. L.; Waymouth, R. M. Zwitterionic polymerization of lactide to cyclic poly(lactide) by using N-heterocyclic carbene organocatalysts. *Angewandte Chemie* **2007,** 46 (15), 2627-2630.

17. Asenjo-Sanz, I.; Veloso, A.; Miranda, J. I.; Pomposo, J. A.; Barroso-Bujans, F. Zwitterionic polymerization of glycidyl monomers to cyclic polyethers with $B(C_6F_5)_3$. *Polymer Chemistry* **2014,** 5 (24), 6905-6908.

18. Haque, F. M.; Alegria, A.; Grayson, S. M.; Barroso-Bujans, F. Detection, quantification, and "click-scavenging" of impurities in cyclic poly(glycidyl phenyl ether) obtained by zwitterionic ring-expansion polymerization with $B(C_6F_5)_3$. *Macromolecules* **2017,** 50 (5), 1870-1881.

19. Kohn, W.; Sham, L. J. Self-consistent equations including exchange and correlation effects. *Physical Review* **1965,** 140 (4A), A1133-A1138.

20. Hohenberg, P.; Kohn, W. Inhomogeneous electron gas. *Physical Review* **1964,** 136 (3B), B864-B871.

21. Frisch, M. J.; Trucks, G. W.; Schlegel, H. B.; Scuseria, G. E.; Robb, M. A.; Cheeseman, J. R.; Scalmani, G.; Barone, V.; Petersson, G. A.; Nakatsuji, H.; Li, X.; Caricato, M.; Marenich, A. V.; Bloino, J.; Janesko, B. G.; Gomperts, R.; Mennucci, B.; Hratchian, H. P.; Ortiz, J. V.; Izmaylov, A. F.; Sonnenberg, J. L.; Williams; Ding, F.; Lipparini, F.; Egidi, F.; Goings, J.; Peng, B.; Petrone, A.; Henderson, T.; Ranasinghe, D.; Zakrzewski, V. G.; Gao, J.; Rega, N.; Zheng, G.; Liang, W.; Hada, M.; Ehara, M.; Toyota, K.; Fukuda, R.; Hasegawa, J.; Ishida, M.; Nakajima, T.; Honda, Y.; Kitao, O.; Nakai, H.; Vreven, T.; Throssell, K.; Montgomery Jr., J. A.; Peralta, J. E.; Ogliaro, F.; Bearpark, M. J.; Heyd, J. J.; Brothers, E. N.; Kudin, K. N.; Staroverov, V. N.; Keith, T. A.; Kobayashi, R.; Normand, J.; Raghavachari, K.; Rendell, A. P.; Burant, J. C.; Iyengar, S. S.; Tomasi, J.; Cossi, M.; Millam, J. M.; Klene, M.; Adamo, C.; Cammi, R.; Ochterski, J. W.; Martin, R. L.; Morokuma, K.; Farkas, O.; Foresman, J. B.; Fox, D. J. *Gaussian 16 Rev. B.01*, Wallingford, CT, 2016.

22. Scalmani, G.; Frisch, M. J. Continuous surface charge polarizable continuum models of solvation. I. General formalism. *The Journal of Chemical Physics* **2010,** 132 (11), 114110.

23. Tao, J.; Perdew, J. P.; Staroverov, V. N.; Scuseria, G. E. Climbing the density functional ladder: nonempirical meta-generalized gradient approximation designed for molecules and solids. *Physical Review Letters* **2003,** 91 (14), 146401.

24. Weigend, F.; Ahlrichs, R. Balanced basis sets of split valence, triple zeta valence and quadruple zeta valence quality for H to Rn: Design and assessment of accuracy. *Physical Chemistry Chemical Physics* **2005,** 7 (18), 3297-3305.

25. Weigend, F. Accurate Coulomb-fitting basis sets for H to Rn. *Physical Chemistry Chemical Physics* **2006,** 8 (9), 1057-1065.

26. Jeong, W.; Shin, E. J.; Culkin, D. A.; Hedrick, J. L.; Waymouth, R. M. Zwitterionic polymerization: a kinetic strategy for the controlled synthesis of cyclic polylactide. *Journal of the American Chemical Society* **2009,** 131 (13), 4884-4891.

27. Kanazawa, A.; Kanaoka, S.; Aoshima, S. Rational design of oxirane monomers for efficient crossover reactions in concurrent cationic vinyl-addition and ring-opening copolymerization with vinyl ethers. *Macromolecules* **2014,** 47 (19), 6635-6644.

28. Kanazawa, A.; Kanaoka, S.; Aoshima, S. Concurrent cationic vinyl-addition and ring-opening copolymerization using $B(C_6F_5)_3$ as a catalyst: copolymerization of vinyl ethers and isobutylene oxide via crossover propagation reactions. *Journal of the American Chemical Society* **2013,** 135 (25), 9330-9333.

29. Clayden, J.; Greeves, N.; Warren, S.; Wothers, P., Nucleophilic substitution at saturated carbon. In *Organic Chemistry*, Oxford University Press: 2001; pp 407-445.

30. Nam, S. G. C. The mechanism of Lewis acid catalysed epoxide rearrangement to aldehyde. University of Canterbury, New Zealand, 2005.

31. Solid-acid catalysis: rearrangement and isomerization. In *Fine chemicals through heterogeneous catalysis*, pp 217-231.

CHAPTER 5

SUPPRESSION OF MELT-INDUCED DEWETTING IN CYCLIC POLY(ε-CAPROLACTONE) THIN FILMS[‡]

5.1 ABSTRACT

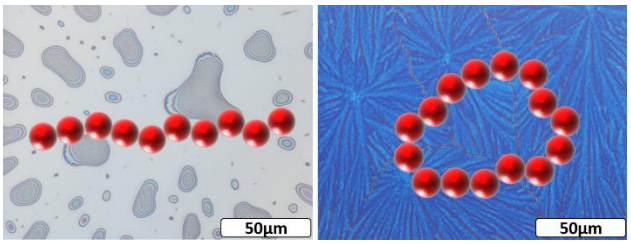

This work describes the discovery that cyclic poly(ε-caprolactone) (*c*-PCL_{6k}) exhibits enhanced film stability and resistance to dewetting compared to linear poly(ε-caprolactone) (*l*-PCL_{6k}). For comparison, a comprehensive study was conducted to examine how topology affects film stability. Linear PCLs containing triazole groups and terminated with hydroxy, propargyl, azide, and acetyl groups all exhibit varying amounts of dewetting despite significantly different end groups and substrate interactions. In contrast, *c*-PCL_{6k} retains thin film stability and does not dewet under the same conditions. The reason for enhanced stability of *c*-PCL_{6k} films remains unclear based on previous work exploring the physical properties of cyclic PCLs and the numerous efforts to understand dewetting phenomena in thin films. For example, because *c*-PCL_{6k} has a lower viscosity

[‡] A portion of this work has been published in Kelly, G.*; Haque, F.*; Grayson, S.; Albert, J. Suppression of melt-induced dewetting in cyclic poly(ε-caprolactone) thin films. *Macromolecules*, **2017**, *50* (24), 9852-9856 **authors made equal contribution to the manuscript*

than *l*-PCL$_{6k}$, one would expect *c*-PCL$_{6k}$ films to dewet more readily than *l*-PCL$_{6k}$ films. Herein the opposite behavior is reported. Furthermore, the ability to enhance film stability via the cyclic topology has powerful ramifications in the context of applications that require film stability in thin and ultrathin film geometries.

5.2 INTRODUCTION

In the last decade, the pace of research studying cyclic and other non-linear polymer architectures has increased dramatically due to the development of novel synthetic routes to control polymer architecture, size, dispersity, and composition while also maintaining the high purity necessary for phenomenological study. Specifically, advances in conjugation reactions have led to the use of the copper(I)-catalyzed azide-alkyne cycloaddition (CuAAC) "click" reactions to efficiently synthesize cyclic homopolymers,[1] cyclic block copolymers,[2] star polymers,[3] and multi-cyclic topologies.[4] It has been known for some time that very small amounts of linear impurities (0.1%) can significantly alter some cyclic polymer properties,[5] making their study challenging and some previously reported results difficult to reproduce. Due the quantitative and highly efficient nature of the CuAAC coupling chemistry, the presence of linear impurities can be nearly eliminated.[6] These advances have allowed researchers to begin to better understand the fundamental differences between the linear and cyclic topology.

Progress in the synthesis of cyclic polymers has taken place alongside significantly increased interest in studying polymers confined to thin and ultrathin films, which are relevant to applications in photolithography[7, 8] and nanoscale membranes.[9-13] However, thin film confinement often produces dramatic and sometimes deleterious effects on

physical properties, such as the depression or elevation of thermal transitions.[14-20] Additionally, poor substrate adhesion can lead to film dewetting.[21-35] By contrast, several groups have shown that the cyclic architecture exhibits unique and useful phenomena, such as a decrease in domain size in cyclic block copolymer thin films,[8, 36] and a lack of T_g depression in cyclic polystyrene thin films.[37] In this note, we describe our observation that low molecular weight cyclic poly(ε-caprolactone) (PCL) resists thin film dewetting in the melt state better than its linear analog, regardless of linear PCL end group chemistry. As research focuses more closely on polymers confined to thin and ultrathin films, the suppression of dewetting will become necessary as an unstable, discontinuous layer is impractical for most applications. Our results show that the cyclic topology may offer a practical solution to the problem of film dewetting.

5.3 EXPERIMENTAL

Nomenclature. The following nomenclature will be used throughout: *l*-PCL_{6k} and *c*-PCL_{6k} designate the linear and cyclic poly(ε-caprolactone), respectively (see **Figure 5.1**). Unless otherwise noted, *l*-PCL_{6k} refers to α-propagyl-ω-hydroxy-poly(ε-caprolactone). The subscript "6k" indicates the molecular weight (M_n = 6 kDa).

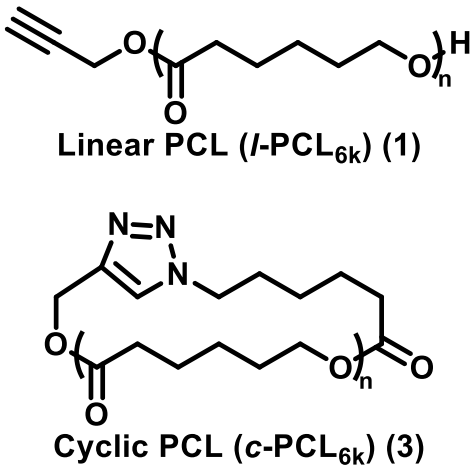

Figure 5.1. Structures of *l*-PCL_{6k} and *c*-PCL_{6k}. The numbers (1) and (3) correspond to the synthetic identification of these polymers in the "Synthetic Protocols" section of the Supporting Information.

5.3.1 Synthetic and analytical methods

In order to synthesize *l*-PCL_{6k}, distilled ε-caprolactone (CL) was polymerized in the presence of propargyl alcohol to install the necessary alkyne moiety. The terminating hydroxy-group allowed for end group functionalization with an azide-containing carboxylic acid using ethyl(dimethylaminopropyl) carbodiimide (EDC) based ester coupling chemistry. With the synthesized α-propargyl-ω-azide-polymer, the final CuAAC "click" cyclization coupling was performed to generate the desired *c*-PCL_{6k} (see **Scheme 5.1**).

Scheme 5.1. Synthesis of cyclic PCL.

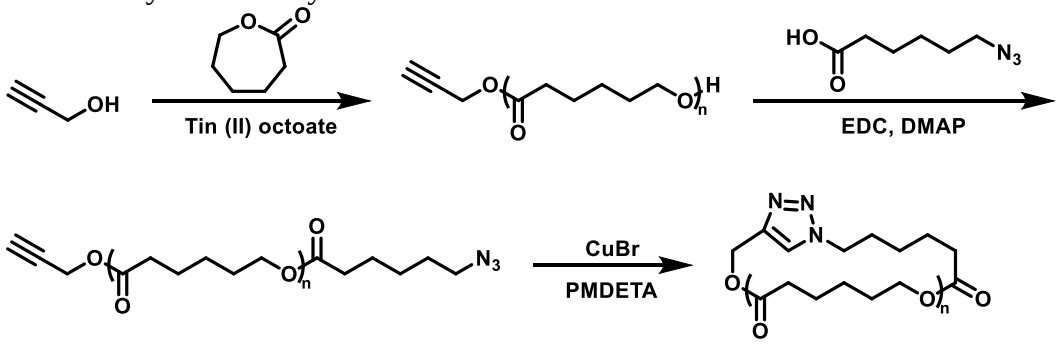

Gel permeation chromatography (GPC) was used to quantify relative molecular weights (M_n and M_w) and dispersity (Đ). GPC also was used to confirm cyclization based on the increased retention time of the cyclic polymer due to the decreased hydrodynamic volume.[38, 39] Matrix-assisted laser desorption/ionization time of flight (MALDI-TOF) mass spectrometry (MS) offered complementary results, providing precise molecular weight information, while simultaneously detailing exact molecular weight values of specific *n*-mers to confirm end group modifications.[40] A more extensive discussion of the analytical and synthetic methods can be found in the Supporting Information.

Gel permeation chromatography (GPC) data were acquired from a Waters model 1515 isocratic pump (Milford, MA) with THF as the mobile phase, a 1 mL/min flow rate, and columns heated at a constant 30 °C by a column oven. This system was operated with a set of two columns in series from Polymer Laboratories Inc. consisting of PSS SDV analytical linear M (8 × 300 mm) and PSS SDV analytical 100Å (8 x 300 mm) columns. A Model 2487 differential refractometer detector was used as a refractive index detector. The instrument was calibrated with Polystyrene ReadyCal Standards from Waters.

Mass spectral data were collected using a Bruker-Daltonics Matrix Assisted Laser Desorption Ionization Time-of-Flight (MALDI-TOF) Autoflex III mass spectrometer in

reflector mode with positive ion detection. Typical sample preparation for MALDI-TOF MS data was performed by making stock solutions in THF of matrix (20 mg/ml), polymer analyte (2 mg/ml), and an appropriate cation source (2 mg/ml). The stock solutions were mixed in a 10/2/1 ratio (matrix/analyte/cation), deposited onto the MALDI target plate and allowed to evaporate via the dried droplet method. *trans*-2-[3-(4-*tert*-Butylphenyl)-2-methyl-2-propenylidene]malononitrile (DCTB) and sodium trifluoroacetate were used as matrix and cation, respectively. MALDI-TOF MS data were calibrated against SpheriCal dendritic calibrants from Polymer Factory (Stockholm, Sweden). M_n and Đ of the resultant spectra were calculated using Polytools software.

Optical microscopy images were taken using an Olympus BX53 optical microscope operating in bright field mode. Atomic force microscopy images were taken using a Bruker Dimension ICON AFM operating in Peak Force Quantitative Nanomechanical Mapping (PFQNM) mode and using ScanAsyst-Air tips (k = 0.4 N/m; resonant frequency = 70 kHz).

Synthesis of α-propagyl-ω-hydroxy-PCL$_{6k}$ (*l*-PCL$_{6k}$) (1). Tin(II) ethylhexanoate ($Sn(Oct)_2$) was dried under vacuum overnight. The ε-caprolactone (εCL) was stirred overnight with calcium hydride, and freshly distilled prior to polymerization into a flask containing activated molecular sieves. Note that all flasks used in this synthesis of polymer (**1)** were flame dried and place under inert atmosphere to reduce water and air content. The propargyl alcohol was dried over $MgSO_4$ and activated molecular sieves directly prior to polymerization. In a representative polymerization, all reagents were dried as mentioned, followed by the syringe-addition of propargyl alcohol (12 mg, 0.21 mmol, 1.1 eq.) and εCL (4.4 g, 38 mmol, 200 eq.) to a flame dried 2-neck round bottom flask. The reaction mixture was inserted into an oil bath at 130 °C, followed by the immediate addition of tin(II)

ethylhexanoate ($Sn(Oct)_2$) (8 mg, 0.020 mmol, 0.1 eq.). Depending on the desired molecular weight, the polymerization could be stopped by exposure to air and dilution with dichloromethane. Alternatively, aliquots could be taken at various time points to have a series of different molecular weights. However, if at any point the stir bar slowed, due to increased solution viscosity, the polymerization would be stopped immediately in order to ensure control over dispersity. The crude solution of polymer in DCM was precipitated into diethyl ether, filtered, and dried *in vacuo* prior to characterization.

Synthesis of α-propargyl-ω-azide-PCL (2). Polymer **1** (100 mg, 16 mmol, 1 eq.) was dissolved in 10 mL of dichloromethane. 6-Azidohexanoic acid (5.1 mg, 32 mmol, 2 eq.), *N*-(3-(dimethylamino)propyl)-*N′*-ethylcarbodiimide hydrochloride (EDC) (5.0 mg, 32 mmol, 2.0 eq.), and 4-(dimethylamino)pyridine (0.10 mg, 0.81 mmol, 0.05 eq.) were added to the reaction flask. The reaction was stirred until MALDI-TOF monitoring indicated the reaction was complete (typically within 24 hours). The crude reaction mixture was washed with saturated aqueous $NaHSO_4$ (3 × 5 mL), saturated aqueous $NaHCO_3$ (3 × 5 mL), and brine (5 mL). The organic layer was dried over anhydrous $MgSO_4$, filtered, and dried *in vacuo*. The product was isolated in a 90% yield.

Synthesis of cyclic-PCL_{6k} (*c*-PCL_{6k}) (3). A 0.22 mM solution of the hetero-bisfunctional polymer **2** was prepared in 50 mL of DCM and placed under N_2, and underwent two freeze-pump-thaw cycles. In a separate flask, *N*,*N*,*N′*,*N″*,*N″*-pentamethyldiethylenetriamine (PMDETA) (100 mg, 16 mmol, 1 eq.) was dissolved in dichloromethane (100 mL) and degassed with two freeze-pump-thaw cycles. The PMDETA solution was refrozen, followed by the addition of CuBr (0.159 g, 1.1 mmol) and the final pump-thaw cycle. Upon thawing, a syringe and syringe pump were used to

transfer the polymer (**2**) solution to the stirring CuBr/PMDETA solution at a rate of 2 mL/hour. After the complete addition of the polymer **2** solution to the reaction mixture, the reaction continued to stir for an additional 2 h. The crude reaction mixture was then washed with saturated ammonium chloride several times, until the blue color was gone. The organic layer was then washed with saturated aqueous $NaHSO_4$ (3 × 10 mL). The organic layer was dried over anhydrous $MgSO_4$, filtered, and dried *in vacuo*. The product was isolated (80% yield) via filtration and dried *in vacuo*.

Synthesis of triazole-containing-α,ω-dihydroxy-PCL$_{6k}$ (4). Polymer **1** (100 mg, 16 mmol, 1 eq.) was dissolved in DCM (5 mL). 3-Azidopropanol (3.3 mg, 32 mmol, 2 eq.) and PMDETA (70 mg, 403 mmol, 25 eq.) were added to the reaction mixture. The reaction mixture underwent two freeze-pump-thaw cycles, followed by an additional freeze. CuBr (57 mg, 403 mmol, 25 eq.) was added followed by an additional pump-thaw cycle. The reaction was then stirred for 24 hours was then washed with saturated ammonium chloride several times, until the blue color was gone. The organic layer was then washed with saturated aqueous $NaHSO_4$ (3 × 10 mL). The organic layer was dried over anhydrous $MgSO_4$, filtered, and dried *in vacuo*. The product was isolated via filtration and dried in vacuo.

Synthesis of triazole-containing-α, ω-diacetyl-PCL$_{6k}$ (5). Polymer **4** (100 mg, 16 mmol, 1 eq.) was dissolved in DCM (5 mL). Acetic anhydride (7.1 mg, 0.070 mmol, 4.1 eq.) and DMAP (.10 mg, 0.81 mmol, 0.05 eq.) were added to the reaction mixture, which was then stirred overnight. The crude reaction mixture was concentrated *in vacuo* and then redissolved in dichloromethane. The solution was washed with saturated sodium bicarbonate (1 × 5 mL), water (2 × 5 mL), and 1 M HCl (1 × 5 mL). The organic layer was

collected and dried with sodium sulfate. Finally, the organic solvent was removed *in vacuo* yielding the acetylated product for MALDI–TOF MS analysis.

Synthesis of α-propargyl-ω-acetyl-PCL$_{6k}$ (6). Polymer **1** (100 mg, 16 mmol, 1 eq.) was dissolved in DCM (5 mL). Acetic anhydride (3.3 mg, 32 mmol, 2 eq.) and 4-(dimethylamino)pyridine (DMAP) (0.10 mg, .81 mmol, 0.05 eq.) were added to the reaction mixture, which was then stirred overnight. The crude reaction mixture was concentrated *in vacuo* and then redissolved in dichloromethane. The solution was washed with saturated sodium bicarbonate (1 × 5 mL), water (2 × 5 mL), and 1 M HCl (1 × 5 mL). The organic layer was collected and dried with sodium sulfate. Finally, the organic solvent was removed *in vacuo* yielding the acetylated product for MALDI–TOF MS analysis.

5.3.2 Film casting and characterization

Thin films were cast via spincoating from dilute solutions in toluene onto UV-ozone treated silicon wafers. Films were melted for 10 minutes at 100 °C and quenched to 25 °C, where they were left to crystallize for at least 24 hours. Although the melting temperature of cyclic PCL has been reported to be slightly higher than linear PCL ($T_m \approx$ 55 °C and 59 °C, respectively, for 7.5 kDa PCL)[41], the films were melted at 100 °C, which is significantly above both melting temperatures such that any differences in dynamics due to the slightly higher T_m of cyclic PCL are negligible. Films were subsequently studied via optical microscopy (Olympus BX53) to examine the global morphology as well as via atomic force microscopy (Bruker Dimension ICON) to examine local morphology and monitor dewetting. Film thicknesses ranged from 106 nm to 116 nm and were quantified using spectral reflectance (Filmetrics F20-UV). Static water contact angles (three drops per

film) were quantified using a Ramé-Hart goniometer to study surface energy differences between linear PCL and cyclic PCL.

5.4 RESULTS

Initial characterization by GPC revealed that the PCLs synthesized via the methods outlined above have low dispersity (see **Figure 5.2a**, **Table 5.1**). Successful cyclization was confirmed by the slightly longer polymer retention time due to decreased hydrodynamic volume of the cyclic architecture while exhibiting unchanged mass by MALDI-TOF MS. MALDI-TOF MS analysis also verified low dispersity and provided accurate molecular weights for all species (see **Figure 5.2b-5.2c**). Finally, several end group transformations were performed to provide a series of linear controls (see **Figure 5.4-5.5**) and were also confirmed by MALDI-TOF MS.

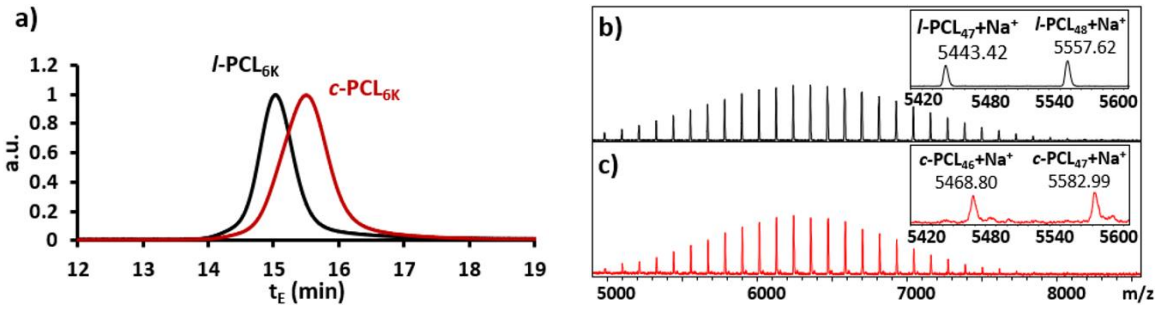

Figure 5.2. Molecular weight characterization data for *l*-PCL$_{6k}$ and *c*-PCL$_{6k}$. a) GPC chromatograms illustrate the longer elution time for the *c*-PCL$_{6k}$ due to its decreased hydrodynamic radius. b-c) MALDI-TOF MS spectra of *l*-PCL$_{6k}$ and *c*-PCL$_{6k}$ indicate exceptional uniformity in both species with respect to end group functionalities and architectural transformations.

Table 5.1. Mass determination of *l*-PCL_{6k} and *c*-PCL_{6k} by GPC and MALDI-TOF MS.

	M_n			Đ	
	GPC[a]	GPC[b]	MALDI	GPC	MALDI
***l*-PCL_{6k}**	**12400**	**6390**	**6360**	**1.08**	**1.01**
***c*-PCL_{6k}**	**12200***	**6270***	**6420**	**1.12**	**1.01**

[a]Calibrated based upon linear polystyrene standards
[b]Corrected value for PCL,[42] using $M_n(PCL) = 0.259M_n(PS)^{1.073}$
[*]Corrected cyclic M_n values based on retention time and ratios of $M_{n\ c\text{-}PS}/M_{n\ l\text{-}PS}$ reported by Alberty et al[39] as 0.70 for PS_{22000}

In order to explore the effect of chain topology on dewetting behavior, thin films (≈ 110 nm thickness) of 6 kDa PCLs were spincoated and subsequently melted and recrystallized to study their thermal stability in the melt state. A molecular weight of 6 kDa was chosen because polymers of this molecular weight can readily cyclize and because 6 kDa is sufficiently above the entanglement molecular weight of *l*-PCL (2-3 kDa) such that dewetting of *l*-PCL_{6k} cannot be attributed to lack of entanglements.[41] Furthermore, several groups have shown that the number of entanglements in cyclic polystyrene and polybutadiene is two to five times lower than their linear analogues.[43, 44] Thus, one would expect the *l*-PCL_{6k} film to be more resistant to dewetting than the *c*-PCL_{6k} film due to the greater presence of entanglements in *l*-PCL_{6k} and fewer entanglements in *c*-PCL_{6k}; however, the opposite result was observed herein. As seen by comparing **Figures 5.3a** and **Figure 5.3d**, *l*-PCL_{6k} has an as-cast morphology similar to that of the cyclic analog. After melting and recrystallization, dewetting of the *l*-PCL_{6k} film can be observed optically by substrate exposure (tan colored regions) and the raised edges of the dewet film (light blue) (**Figure 5.3b**). In contrast, the melted and recrystallized *c*-PCL_{6k} film (**Figure 5.3e**) showed no evidence of dewetting by optical microscopy. To verify the dewetting of the *l*-PCL_{6k} film, AFM height images were collected of both linear and cyclic species after melting and recrystallization, and height sections were taken across the regions of interest

(**Figure 5.3c, 5.3f**). The depression imaged in the *l*-PCL_{6k} film is broad in width (~10 μm), and its depth (104.6 ± 7.58 nm) is approximately equal to the film thickness, which is indicative of dewetting. In comparison, the width of the depression imaged in the *c*-PCL_{6k} film is narrow (~1 μm) and its depth (64.7 ± 6.46 nm) is much less than the film thickness, consistent with a crystal grain boundary.

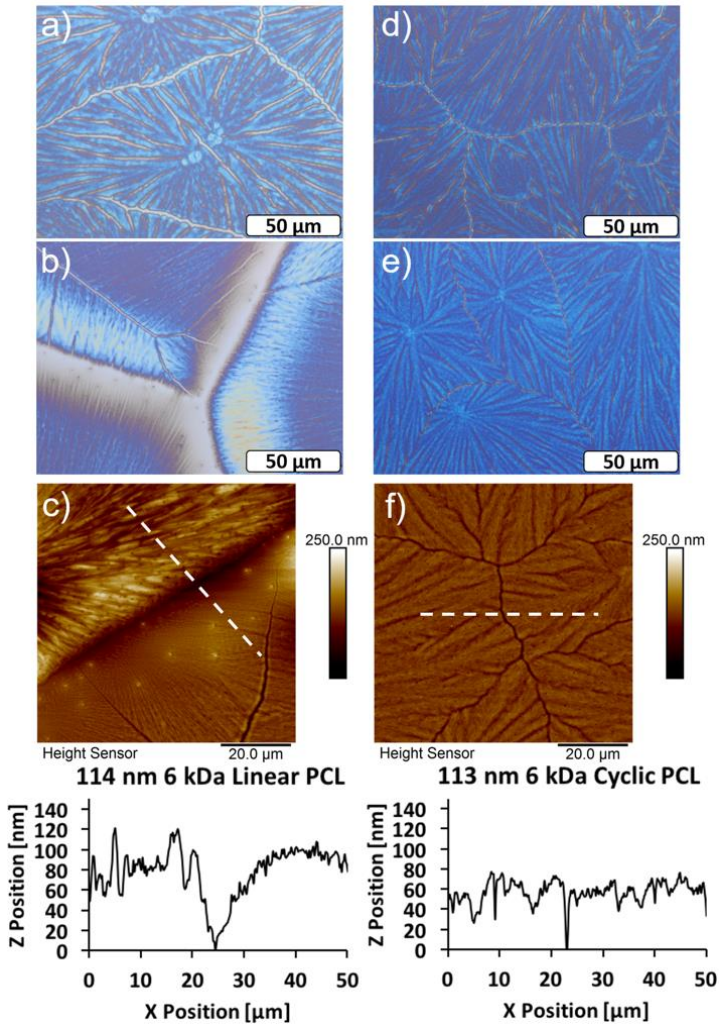

Figure 5.3. Comparison of *l*-PCL_{6k} and *c*-PCL_{6k} before and after melting and recrystallization: a) optical image of *l*-PCL_{6k} as cast; b) optical image of *l*-PCL_{6k} melted and recrystallized; c) AFM height image of *l*-PCL_{6k} melted and recrystallized showing a section taken across the dewet area (average depth: 104.6 ± 7.58 nm); d) optical image of *c*-PCL_{6k} as cast; e) optical image of *c*-PCL_{6k} melted and recrystallized; f) AFM height image of *c*-PCL_{6k} melted and recrystallized showing a section across a grain boundary (average depth: 64.7 ± 6.46 nm).

Static water contact angle measurements on as-cast films of *l*-PCL and *c*-PCL revealed water contact angles of 73.7° +/- 0.2° and 79.1° +/- 0.7°, respectively. These values are commensurate with advancing and receding contact angles reported previously for linear PCL (θ_A = 78.5° and θ_R = 71.6°, corresponding surface tension γ = 37.9 mN/m)[45] and show that the enhanced film stability of cyclic PCL is not due to a difference in surface tension. These data suggest that the cyclic topology of *c*-PCL_{6k} may inhibit thin film dewetting.

To support this assertion and to eliminate the competing hypothesis that chemical differences between *l*-PCL_{6k} and *c*-PCL_{6k} (*i.e.*, identity of the *l*-PCL_{6k} end groups, or the presence of the triazole linkage in *c*-PCL_{6k}) could account for the differences in film stability, several additional control *l*-PCLs were synthesized with varying end groups (see **Figure 5.4**). In the linear controls, both hydrophobic and hydrophilic end groups were chosen with and without the triazole linkage. And again, MALDI-TOF MS confirmed quantitative end group transformation, and the corresponding mass spectra of these controls can be seen in **Figure 5.5**.

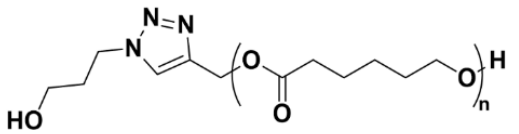

Triazole-containing α,ω-dihydroxy-PCL (4)

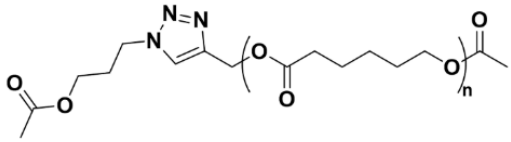

Triazole-containing α,ω-diacetyl-PCL (5)

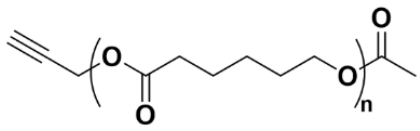

α-propargyl-ω-acetyl-PCL (6)

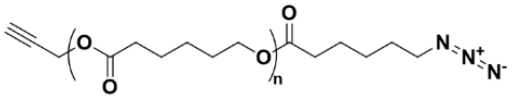

α-propargyl-ω-azide-PCL (2)

Figure 5.4. Chemical structures of the additional linear PCL controls. The numbers (2), (4), (5), and (6) correspond to the synthetic identification of these polymers in the "Synthetic Protocols" section of the Supporting Information.

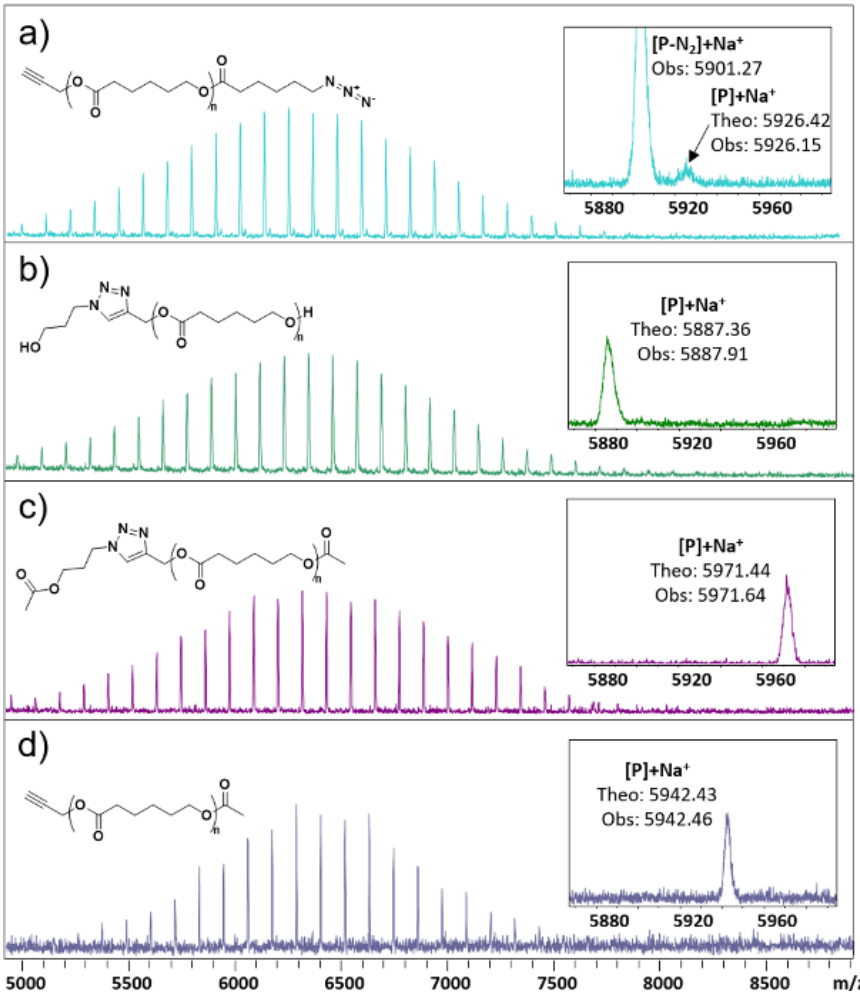

Figure 5.5. MALDI-TOF MS data illustrating the molecular weight distribution and purity of the four additional linear PCL controls: a) α-propargyl-ω-azide-PCL; b) triazole-containing-α,ω- dihydroxy-PCL; c) triazole-containing-α,ω- diacetyl-PCL; d) α-propargyl-ω-acetyl-PCL.

The same film stability experiments were performed (**Figure 5.6**). End groups were chosen to address the possible roles of end group polarity and presence of the triazole group on film stability. The triazole-containing-α,ω-dihydroxy-PCL_{6k} film exhibited partial dewetting during melting and recrystallization, much like the *l*-PCL_{6k} in **Figure 5.5b**, albeit with significantly wider dewet regions. Films of the triazole-containing-α,ω-diacetyl-PCL_{6k} and α-propargyl-ω-acetyl-PCL_{6k} dewet completely upon melting. Finally, the α-

propargyl-ω-azide-PCL$_{6k}$ film dewet upon casting. Unlike the cyclic polymer, all the linear controls exhibited various degrees of dewetting regardless of end group.

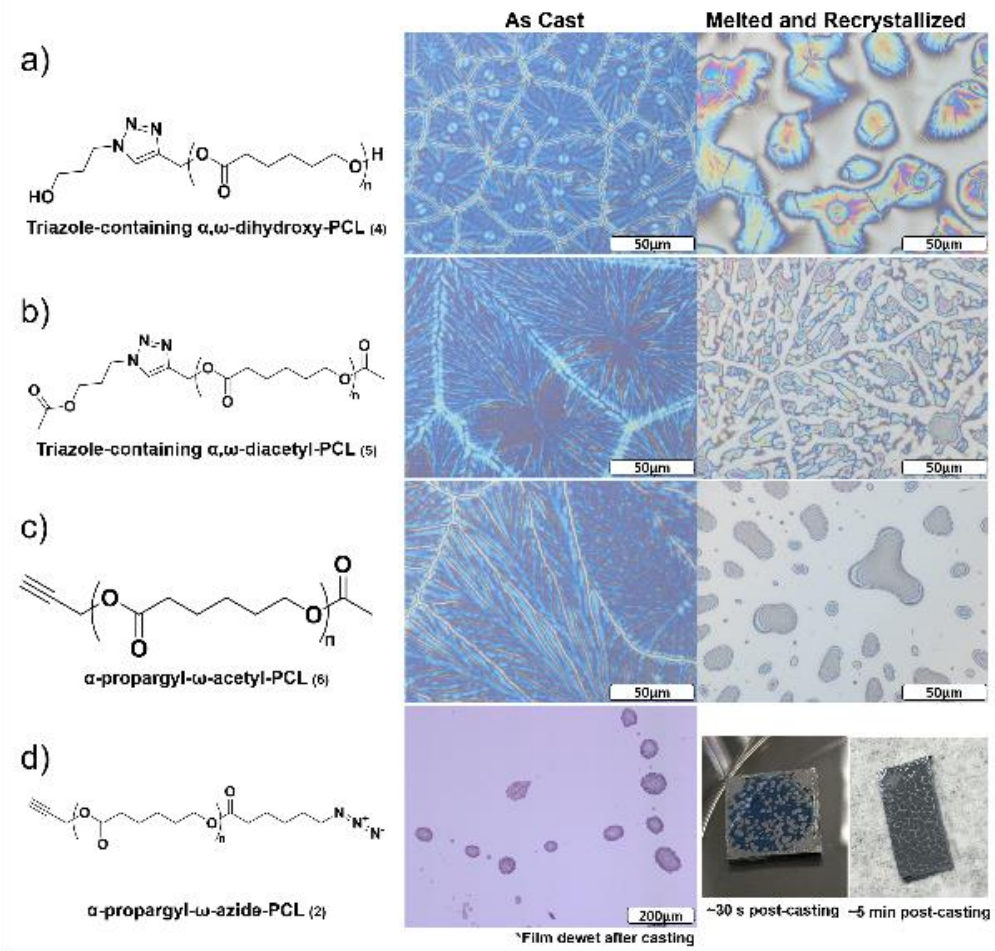

Figure 5.6. Optical microscopy of linear PCL control films before and after melting and recrystallization: a) triazole-containing-α,ω-dihydroxy-PCL$_{6k}$ exhibited a crystalline morphology as-cast but partially dewet during melting; b) triazole-containing-α, ω-diacetyl-PCL$_{6k}$ exhibited a crystalline morphology as cast but dewet completely upon melting. c) α-propargyl-ω-acetyl-PCL$_{6k}$ exhibited a crystalline morphology as cast but dewet completely upon melting; d) α-propargyl-ω-azide-PCL$_{6k}$ exhibited dewetting immediately after spin coating.

5.5 DISCUSSION

Dewetting is a complex and important phenomenon that can largely be attributed to a few important factors, namely, film thickness, polymer-substrate/polymer-polymer

interactions, temperature, and molecular weight.[21-25, 28, 31-35, 46] In sufficiently thick films (microns and above), molecular forces that drive film instability are overcome by gravity, which allows the polymer film to resist dewetting.[22, 46] Below a critical thickness, molecular forces become dominant, and the film may break up into droplets on the substrate through homogeneous or heterogeneous nucleation and propagation of dewetting holes.[21, 22, 24] A polymer also may be forced into an unstable or metastable state by casting onto a highly non-wettable substrate.[21, 47] Because of unfavorable polymer-substrate interactions, the film will spontaneously dewet upon casting, or if metastable, any perturbation, such as an increase in temperature above the thermal transition, will cause rupture of the film and dewetting from the substrate. Finally, the polymer molecular weight also plays a role in the dewetting rate due to the relationship between molecular weight and fluid viscosity; thus, a more highly-entangled polymer has significantly lower mobility and will resist dewetting.[22, 24, 48]

In this study, film thickness and molecular weight were held constant and the melting procedure was standardized so that topology (*l*-PCL_{6k} versus *c*-PCL_{6k}) and end group chemistry (of the control *l*-PCLs) were the only variables that could account for differences in film dewetting. The end group chemistries ranged from polar hydrophilic groups to non-polar hydrophobic groups. Although end groups can affect intermolecular interactions, all of the linear PCLs and *c*-PCL_{6k} exhibit crystallization upon film casting (see **Figure 5.6**) suggesting that the end groups minimally impact intermolecular interactions. However, the differences in dewetting behavior show that the end groups have a substantial impact on the interaction of the polymer chains with the substrate. For example, hydrophilic polymers and end groups can more easily interact with and wet polar

substrates than hydrophobic polymers, potentially improving film stability. This observation may explain the lesser extent of dewetting exhibited by *l*-PCLs containing polar hydroxy end groups compared to *l*-PCLs containing only hydrophobic end groups (see **Figure 5.3-5.6**). However, dewetting arises even in the presence of favorable end group interactions with the substrate. Reiter and others have described the phenomenon of "autophobic dewetting" which can occur when the confined polymer has "sticky ends" or end groups that are more inclined to complex with the substrate than the rest of the polymer chain.[23, 26, 27, 29, 30, 49] Repulsive interactions between the adsorbed polymer layer and the bulk polymer layer increase the likelihood of dewetting. Thus, films of *l*-PCLs containing polar hydroxy groups to facilitate favorable substrate interactions may still dewet by autophobic dewetting.

Although the dewetting behavior of the *l*-PCL_{6k} films can be explained based on analysis of interactions between the end groups and the substrate, this assessment provides an insufficient explanation for the dramatic increase in stability afforded by the cyclic topology. Furthermore, several research groups have shown that analogous cyclic polymers have significantly lower viscosities than their linear counterparts which should enhance their mobility in thin films.[38, 39, 50-52] Based on these facts, the cyclic polymer film would be expected to dewet more readily than films of exact linear analogues due to lack of end group stabilization and greater polymer mobility. Additionally, the presence of a triazole group, which has been suggested may affect PCL crystallization kinetics,[53] does not explain the stability of *c*-PCL_{6k} films, as triazole-containing linear controls readily dewet. Although there are many factors that dictate film stability, this initial investigation points

to the cyclic topology as the strongest contributing factor to the greatly enhanced thin film stability of *c*-PCL.

5.6 CONCLUSIONS

In this work, the enhanced thin film stability of low molecular weight cyclic poly(ε-caprolactone) compared to its linear analog is described. Linear poly(ε-caprolactone) with various end group functionalities was studied, and a stable *l*-PCL_{6k} was not observed. It is worth noting, however, that the dewetting behavior of the many *l*-PCL_{6k} polymers varied and to have a comprehensive understanding of the impact of end group functionality, further studies must be pursued. This finding that the cyclic architecture provides enhanced film stability is intriguing given that the physical characteristics of cyclic polymers compared to linear analogues (greater chain mobility, lower viscosity, and lower density of molecular entanglements) are all properties that are known to facilitate film dewetting processes rather than inhibit them. Although the underlying mechanism responsible for the enhanced stability of *c*-PCL_{6k} films over *l*-PCL_{6k} analogues has yet to be elucidated, this initial investigation provides compelling evidence that the cyclic topology is the strongest contributing factor. Finally, the ability to enhance film stability via the cyclic topology has the potential for far-reaching impacts on applications that require film stability in thin and ultrathin film geometries.

5.7 REFERENCES

1. Laurent, B. A.; Grayson, S. M. An Efficient Route To Well-Defined Macrocyclic Polymers Via "Click" Cyclization. *J. Am. Chem. Soc.* **2006,** 128 (13), 4238-4239.

2. Eugene, D. M.; Grayson, S. M. Efficient Preparation Of Cyclic Poly(Methyl Acrylate)-Block-Poly(Styrene) By Combination Of Atom Transfer Radical Polymerization And Click Cyclization. *Macromolecules* **2008,** 41 (14), 5082-5084.

3. Jia, Z. F.; Lonsdale, D. E.; Kulis, J.; Monteiro, M. J. Construction of a 3-Miktoarm Star from Cyclic Polymers. *Acs Macro Lett.* **2012,** 1 (6), 780-783.

4. Hossain, M. D.; Jia, Z. F.; Monteiro, M. J. Complex Polymer Topologies Built from Tailored Multifunctional Cyclic Polymers. *Macromolecules* **2014,** 47 (15), 4955-4970.

5. Kapnistos, M.; Lang, M.; Vlassopoulos, D.; Pyckhout-Hintzen, W.; Richter, D.; Cho, D.; Chang, T.; Rubinstein, M. Unexpected Power-Law Stress Relaxation Of Entangled Ring Polymers. *Nature Materials* **2008,** 7 (12), 997-1002.

6. Elupula, R.; Oh, J.; Haque, F. M.; Chang, T.; Grayson, S. M. Determining the Origins of Impurities during Azide-Alkyne Click Cyclization of Polystyrene. *Macromolecules* **2016,** 49 (11), 4369-4372.

7. Park, M.; Harrison, C.; Chaikin, P. M.; Register, R. A.; Adamson, D. H. Block Copolymer Lithography: Periodic Arrays Of Similar To 10(11) Holes In 1 Square Centimeter. *Science* **1997,** 276 (5317), 1401-1404.

8. Poelma, J. E.; Ono, K.; Miyajima, D.; Aida, T.; Satoh, K.; Hawker, C. J. Cyclic Block Copolymers For Controlling Feature Sizes In Block Copolymer Lithography. *ACS Nano* **2012,** 6 (12), 10845-10854.

9. Liu, F. Q.; Yi, B. L.; Xing, D. M.; Yu, J. R.; Zhang, H. M. Nafion/PTFE Composite Membranes For Fuel Cell Applications. *Journal of Membrane Science* **2003,** 212, 213-223.

10. Jeong, B. H.; Hoek, E. M. V.; Yan, Y. S.; Subramani, A.; Huang, X. F.; Hurwitz, G.; Ghosh, A. K.; Jawor, A. Interfacial Polymerization Of Thin Film Nanocomposites: A New Concept For Reverse Osmosis Membranes. *Journal of Membrane Science* **2007,** 294, 1-7.

11. Chakrabarty, B.; Ghoshal, A. K.; Purkait, M. K. Effect Of Molecular Weight Of PEG On Membrane Morphology And Transport Properties. *Journal of Membrane Science* **2008,** 309, 209-221.

12. Jackson, E. A.; Hillmyer, M. A. Nanoporous Membranes Derived From Block Copolymers: From Drug Delivery To Water Filtration. *ACS Nano* **2010,** 4 (7), 3548-3553.

13. Phillip, W. A.; O'Neill, B.; Rodwogin, M.; Hillmyer, M. A.; Cussler, E. Self-Assembled Block Copolymer Thin Films As Water Filtration Membranes. *ACS Applied Materials & Interfaces* **2010,** 2 (3), 847-853.

14. Keddie, J. L.; Jones, R. A. L.; Cory, R. A. Size-Dependent Depression of the Glass-Transition Temperature in Polymer-Films. *Europhysics Letters* **1994,** 27 (1), 59-64.

15. Richard, A. Interface And Surface Effects On The Glass-Transition Temperature In Thin Polymer Films. *Faraday Discussions* **1994,** 98, 219-230.

16. Forrest, J. A.; Dalnoki-Veress, K.; Stevens, J. R.; Dutcher, J. R. Effect of Free Surfaces on the Glass Transition Temperature of Thin Polymer Films. *Phys Rev Lett* **1996,** 77 (10), 2002-2005.

17. Forrest, J. A.; DalnokiVeress, K.; Dutcher, J. R. Interface And Chain Confinement Effects On The Glass Transition Temperature Of Thin Polymer Films. *Phys. Rev. E* **1997,** 56 (5), 5705-5716.

18. Ellison, C. J.; Ruszkowski, R. L.; Fredin, N. J.; Torkelson, J. M. Dramatic Reduction Of The Effect Of Nanoconfinement On The Glass Transition Of Polymer Films Via Addition Of Small-Molecule Diluent. *Physical Review Letters* **2004,** 92 (9), 095702.

19. Efremov, M. Y.; Kiyanova, A. V.; Last, J.; Soofi, S. S.; Thode, C.; Nealey, P. F. Glass Transition In Thin Supported Polystyrene Films Probed By Temperature-Modulated Ellipsometry In Vacuum. *Phys. Rev. E* **2012,** 86 (2 Pt 1), 021501.

20. Ediger, M. D.; Forrest, J. A. Dynamics near Free Surfaces and the Glass Transition in Thin Polymer Films: A View to the Future. *Macromolecules* **2014,** 47 (2), 471-478.

21. Reiter, G. Dewetting Of Thin Polymer Films. *Phys Rev Lett* **1992,** 68 (1), 75-78.

22. Reiter, G. Unstable Thin Polymer Films - Rupture and Dewetting Processes. *Langmuir* **1993,** 9 (5), 1344-1351.

23. Henn, G.; Bucknall, D. G.; Stamm, M.; Vanhoorne, P.; Jerome, R. Chain End Effects And Dewetting In Thin Polymer Films. *Macromolecules* **1996,** 29 (12), 4305-4313.

24. Xie, R.; Karim, A.; Douglas, J. F.; Han, C. C.; Weiss, R. A. Spinodal Dewetting Of Thin Polymer Films. *Physical Review Letters* **1998,** 81 (6), 1251-1254.

25. Meredith, J. C.; Smith, A. P.; Karim, A.; Amis, E. J. Combinatorial Materials Science For Polymer Thin-Film Dewetting. *Macromolecules* **2000,** 33 (26), 9747-9756.

26. Reiter, G.; Khanna, R. Kinetics Of Autophobic Dewetting Of Polymer Films. *Langmuir* **2000,** 16 (15), 6351-6357.

27. Matsen, M. W.; Gardiner, J. M. Autophobic Dewetting Of Homopolymer On A Brush And Entropic Attraction Between Opposing Brushes In A Homopolymer Matrix. *Journal of Chemical Physics* **2001,** 115 (6), 2794-2804.

28. Wang, C.; Krausch, G.; Geoghegan, M. Dewetting At A Polymer-Polymer Interface: Film Thickness Dependence. *Langmuir* **2001,** 17 (20), 6269-6274.

29. Edgecombe, S. R.; Gardiner, J. M.; Matsen, M. W. Suppressing Autophobic Dewetting By Using A Bimodal Brush. *Macromolecules* **2002,** 35 (16), 6475-6477.

30. Waltman, R. J.; Khurshudov, A.; Tyndall, G. W. Autophobic Dewetting Of Perfluoropolyether Films On Amorphous-Nitrogenated Carbon Surfaces. *Tribology Letters* **2002,** 12 (3), 163-169.

31. Suh, K. Y.; Park, J.; Lee, H. H. Controlled Polymer Dewetting By Physical Confinement. *Journal of Chemical Physics* **2002,** 116 (17), 7714-7718.

32. Reiter, G.; Hamieh, M.; Damman, P.; Sclavons, S.; Gabriele, S.; Vilmin, T.; Raphael, E. Residual Stresses In Thin Polymer Films Cause Rupture And Dominate Early Stages Of Dewetting. *Nat Mater* **2005,** 4 (10), 754-758.

33. Ma, M.; He, Z.; Yang, J.; Chen, F.; Wang, K.; Zhang, Q.; Deng, H.; Fu, Q. Effect Of Film Thickness On Morphological Evolution In Dewetting And Crystallization Of

Polystyrene/Poly(Epsilon-Caprolactone) Blend Films. *Langmuir* **2011,** 27 (21), 13072-13081.

34. Ma, M.; He, Z.; Yang, J.; Wang, Q.; Chen, F.; Wang, K.; Zhang, Q.; Deng, H.; Fu, Q. Vertical Phase Separation And Liquid-Liquid Dewetting Of Thin PS/PCL Blend Films During Spin Coating. *Langmuir* **2011,** 27 (3), 1056-1063.

35. Ma, M.; He, Z.; Li, Y.; Chen, F.; Wang, K.; Zhang, Q.; Deng, H.; Fu, Q. Surface Phase Separation, Dewetting Feature Size, And Crystal Morphology In Thin Films Of Polystyrene/Poly(Epsilon-Caprolactone) Blend. *J Colloid Interface Sci* **2012,** 387 (1), 262-269.

36. Lecommandoux, S.; Borsali, R.; Schappacher, M.; Deffieux, A.; Narayanan, T.; Rochas, C. Microphase separation of linear and cyclic block copolymers poly(styrene-*b*-isoprene): SAXS experiments. *Macromolecules* **2004,** 37 (5), 1843-1848.

37. Zhang, L.; Elupula, R.; Grayson, S. M.; Torkelson, J. M. Major Impact Of Cyclic Chain Topology On The Tg-Confinement Effect Of Supported Thin Films Of Polystyrene. *Macromolecules* **2015,** 49 (1), 257-268.

38. Hadziioannou, G.; Cotts, P. M.; Tenbrinke, G.; Han, C. C.; Lutz, P.; Strazielle, C.; Rempp, P.; Kovacs, A. J. Thermodynamic and Hydrodynamic Properties of Dilute-Solutions of Cyclic and Linear Polystyrenes. *Macromolecules* **1987,** 20 (3), 493-497.

39. Alberty, K. A.; Hogen-Esch, T. E.; Carlotti, S. Synthesis and Characterization of Macrocyclic Vinyl-Aromatic Polymers. *Macromolecular Chemistry and Physics* **2005,** 206 (10), 1035-1042.

40. Li, Y.; Hoskins, J. N.; Sreerama, S. G.; Grayson, S. M. MALDI-TOF Mass Spectral Characterization of Polymers Containing an Azide Group: Evidence of Metastable Ions. *Macromolecules* **2010,** 43 (14), 6225-6228.

41. Córdova, M. E.; Lorenzo, A. T.; Muller, A. J.; Hoskins, J. N.; Grayson, S. M. A Comparative Study On The Crystallization Behavior Of Analogous Linear And Cyclic Poly(caprolactones). *Macromolecules* **2011,** 44 (7), 1742-1746.

42. Dubois, P.; Barakat, I.; Jerome, R.; Teyssie, P. Macromolecular engineering of polyactones and polyactides. 12. Study of the depolymerization reactions of poly(ε-caprolactone) with functional aluminum alkoxide end groups. *Macromolecules* **1993,** 26 (17), 4407-4412.

43. Müller, M.; Wittmer, J.; Cates, M. Topological Effects In Ring Polymers: A Computer Simulation Study. *Physical Review E* **1996,** 53 (5), 5063.

44. Roovers, J. Viscoelastic properties of polybutadiene rings. *Macromolecules* **1988,** 21 (5), 1517-1521.

45. Khandwekar, A. P.; Patil, D. P.; Shouche, Y.; Doble, M. Surface Engineering Of Polycaprolactone By Biomacromolecules And Their Blood Compatibility. *Journal of Biomaterials Applications* **2011,** 26 (2), 227-252.

46. Xue, L. J.; Han, Y. C. Inhibition Of Dewetting Of Thin Polymer Films. *Progress in Materials Science* **2012,** 57 (6), 947-979.

47. Sharma, A.; Reiter, G. Instability Of Thin Polymer Films On Coated Substrates: Rupture, Dewetting, And Drop Formation. *Journal of Colloid and Interface Science* **1996,** 178 (2), 383-399.

48. Redon, C.; Brochard-Wyart, F.; Rondelez, F. Dynamics Of Dewetting. *Phys Rev Lett* **1991,** 66 (6), 715-718.

49. Reiter, G.; Khanna, R. Real-Time Determination Of The Slippage Length In Autophobic Polymer Dewetting. *Phys Rev Lett* **2000,** 85 (13), 2753-2756.

50. Schäler, K.; Ostas, E.; Schröter, K.; Thurn-Albrecht, T.; Binder, W. H.; Saalwächter, K. Influence of Chain Topology on Polymer Dynamics and Crystallization. Investigation of Linear and Cyclic Poly (ε-caprolactone) s by 1H Solid-State NMR Methods. *Macromolecules* **2011,** 44 (8), 2743-2754.

51. Su, H. H.; Chen, H. L.; Diaz, A.; Casas, M. T.; Puiggali, J.; Hoskins, J. N.; Grayson, S. M.; Perez, R. A.; Muller, A. J. New Insights On The Crystallization And Melting Of Cyclic PCL Chains On The Basis Of A Modified Thomson-Gibbs Equation. *Polymer* **2013,** 54 (2), 846-859.

52. Pérez, R.; Córdova, M.; López, J.; Hoskins, J.; Zhang, B.; Grayson, S.; Müller, A. Nucleation, Crystallization, Self-Nucleation And Thermal Fractionation Of Cyclic And Linear Poly (ε-caprolactone). *Reactive and Functional Polymers* **2014,** 80, 71-82.

53. Atanase, L. I.; Glaied, O.; Riess, G. Crystallization Kinetics of PCL Tagged With Well-Defined Positional Triazole Defects Generated By Click Chemistry. *Polymer* **2011,** 52 (14), 3074-3081.

CHAPTER 6

ONGOING RESEARCH PROJECTS

6.1 SYNTHESIS OF CYCLIC POLY(ETHYLENE GLYCOL)

Poly(ethylene glycol) (PEG) is a commonly used FDA-approved polymer in numerous biomedical applications due to its biocompatibility, water-solubility, and inexpensive cost.[1-4] Much of the work thus far is based on the study of linear PEG, which is why the scope of this research is based on looking into cyclic PEG to understand the impact of architecture on advanced biomedical applications.

Herein, the synthesis of cyclic PEG is described using two different routes. This work provides the proof of concept for the successful cyclization of PEG using the CuAAC "click" reaction. However, MALDI-TOF MS elucidated an unwanted linear PEG contaminant in the commercial linear PEG precursor used for the synthesis of the cyclic PEG. Described in Scheme 6.1 is the synthesis of cyclic PEG based on alkynylating α-azido-ω-hydroxy-PEG (from Polymer Source). Route A describes the addition of the alkyne via Williamson ether coupling reaction using propargyl bromide. Alternatively, an EDC catalyzed esterification reaction can be performed using 4-pentynoic acid. Depending on the substrate sensitivity to acid or base, it is useful to have both routes. However, the work herein focuses on Route A. These functionalizations are based on

previously reported post-polymerization modifications.[5] Finally, once the α-azido-ω-alkynyl-PEG is synthesized, it can be cyclized under high dilution in the presence of CuBr.[6]

Scheme 6.1. Synthesis of cyclic PEG

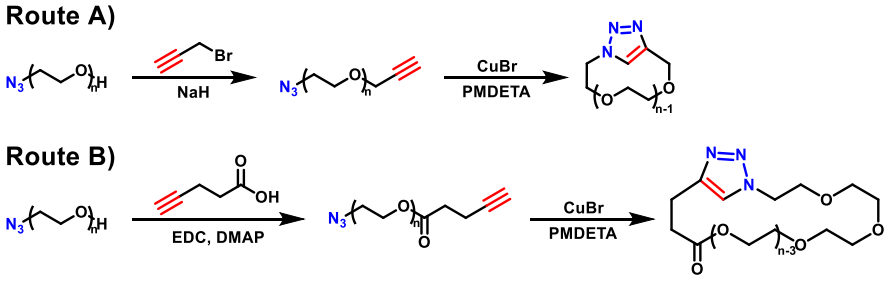

In the analysis of the linear PEG precursor (Figure 6.1) the sample was determined to have two components – the first and major component being the intended α-azido-ω-hydroxy-PEG and the second and very minor component being α-hydroxy-ω-hydroxy-PEG. The minor component was concluded based on its corresponding mass. When the polymer is analyzed by MALDI-TOF MS at increased laser power (Figure 6.1B), the sample exhibits 3 distinct signals. The polymer ionizes with the added cation (e.g. Na^+), and a second distribution corresponds to the polymer ionizing with residual K^+ coming from the storage of the sample. Finally, a third distribution corresponds to a metastable signal resulting from the loss of N_2. Instead of a loss of 28 m/z from the parent polymer, it has a partial mass (~23 m/z) loss due to fragmentation post-ionization. However, when less laser power is applied (Figure 6.1A), the sample demonstrates a clear major distribution from the parent polymer with Na^+ ionization. While the K^+ ionization also exists, it is extremely minimized thus elucidating the presence of α-hydroxy-ω-hydroxy-PEG.

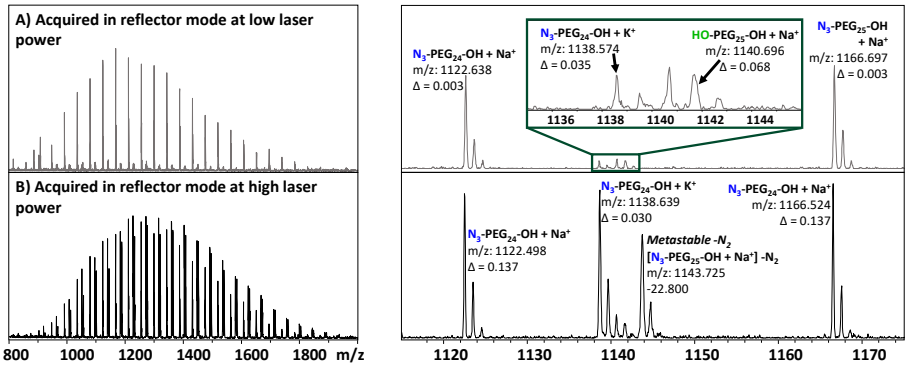

Figure 6.1. MALDI-TOF MS data of the α-azido-ω-hydroxy-PEG linear precursor

Figure 6.2 provides data confirming the successful propargylation of α-azido-ω-hydroxy-PEG. Mass spectrometry data is provided in both reflector and linear mode. A parent polymer distribution and metastable distribution is seen in reflector mode for the α-azido-ω-propargyl-PEG product. However, confirmation of the azide functionality is demonstrated by the loss of the metastable peak in linear mode. Finally, the α-hydroxy-ω-hydroxy-PEG is doubly functionalized with the propargyl group as expected, and this minor signal is seen in both reflector and linear modes.

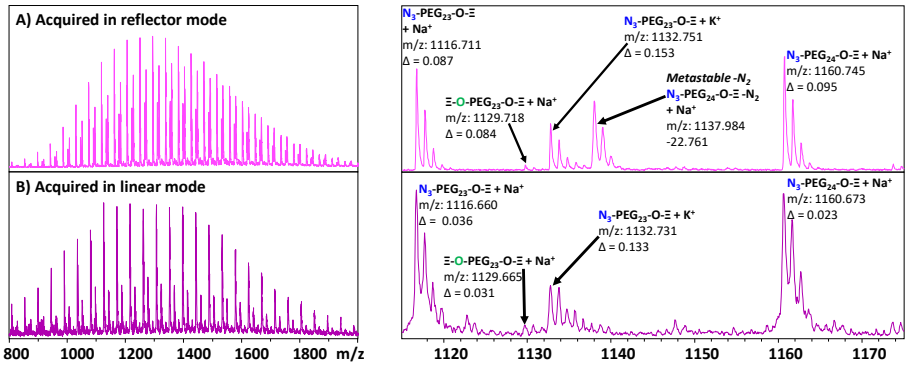

Figure 6.2. MALDI-TOF MS data of the α-azido-ω-propargyl-PEG

Lastly the MALDI-TOF MS data of the polymer post-cyclization is shown below. The major distribution is the cyclic polymer ionizing with Na^+ and a second very minor

distribution corresponds to the unreacted dialkyne functionalized α-hydroxy-ω-hydroxy-PEG impurity. Due to the low resolution and signal intensity for this minor distribution, it is difficult to pick the M^+ peak with confidence. It is presumed additionally that the cyclic polymer ionizes much more efficiently than this minor distribution contributing in the difficulty of assessing the minor impurity signal. Furthermore, the loss of the metastable signal in this final spectra (Figure 6.3) is further evidence of the successful cyclization.

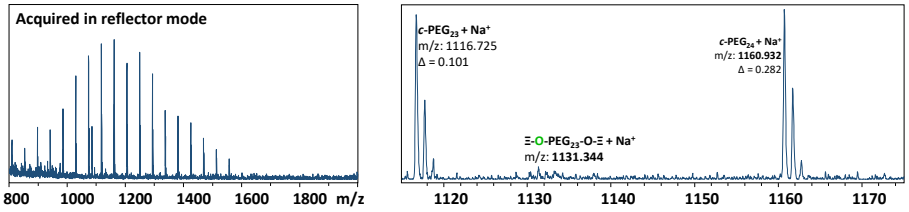

Figure 6.3. MALDI-TOF MS data of the cyclic PEG

For this work all evidence suggests the successful cyclization of the linear PEG polymer albeit a slight minor contamination in the linear precursor. This study was completed on a small scale (~20 mg), allowing for fairly comprehensive MALDI-TOF MS analysis. However, to ensure the reproducibility of this work, this work must be redone on a larger scale (> 100 mg). For the final immediate scope of this work, it is necessary to provide evidence of the ability to produce cyclic PEG cleanly. Towards this endeavor, a "click" scavenging purification protocol can be applied as depicted in Scheme 6.2.[5] If cyclic PEG is synthesized using the method above under optimized dilution, all the intended linear product will cyclize leaving behind the dialkynylated linear product. The product mixture can undergo a "click" reaction with an azide functionalized Merrifield resin. The cyclic product ought to remain unchanged, while the impurity will couple to the

resin. Due the insoluble nature of the solid phase resin, it can be removed via a facile filtration.

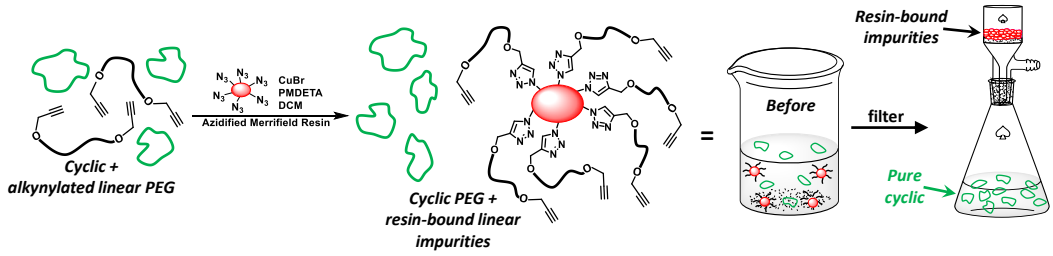

Scheme 6.2. "Click" scavenging purification protocol to remove unwanted linear impurities

6.2 SYNTHESIS OF TRIIODO-FUNCTIONALIZED POLYMER

The goal of the work here is to synthesize a triiodinated polymer for the purpose of mass spectrometry calibration. Mass spectrometry is an analytical tool used for the mass characterization of synthetic polymers and biological molecules alike. The scope of this work is to design mass calibrants that have masses offset from peptides by considering all the combinations of amino acids. Figure 6.4 maps out these possible combinations of amino acids, elucidating the regions known as Averagine and Scarcine Valley.[7] Averagine is the most densely populated portion of the map, where most peptides reside, while Scarcine Valley is the ideal location of mass calibrants due to this mass region being unpopulated with peptides.

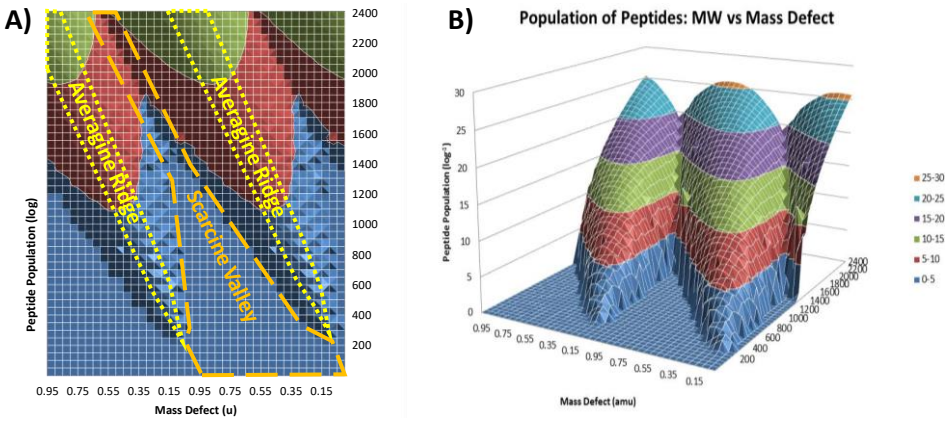

Figure 6.4. Population of peptides indicating Averagine (highest population of peptides) and Scarcine Valley (unpopulated with peptides)

The following synthetic pathway (Scheme 6.3) was designed as a mass spectrometry calibrant, which falls within the aforementioned Scarcine Valley due to the combination of having a monomer with the molecular formula $C_{10}H_{12}O_2$ and the addition of the three iodines. The monomer has the precise molecular formula to fall perfectly within Averagine and by adding the three iodines it moves it to fall perfectly within the line of Scarcine Valley.

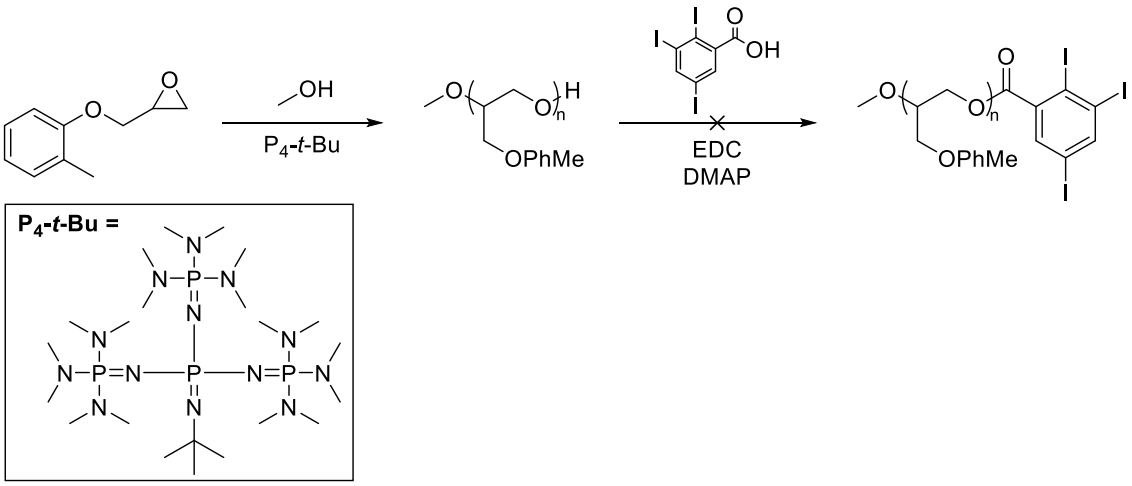

Scheme 6.3. Synthesis of triiodinated polymer

This polymerization was performed based on a previously described protocol,[8] using the monomer glycidyl 2-methylphenyl ether in the presence of P_4-*t*-Bu as a base/catalyst and methanol as an initiator. The following mass spectra was collected of the resultant product confirming the clean initiation with methanol.

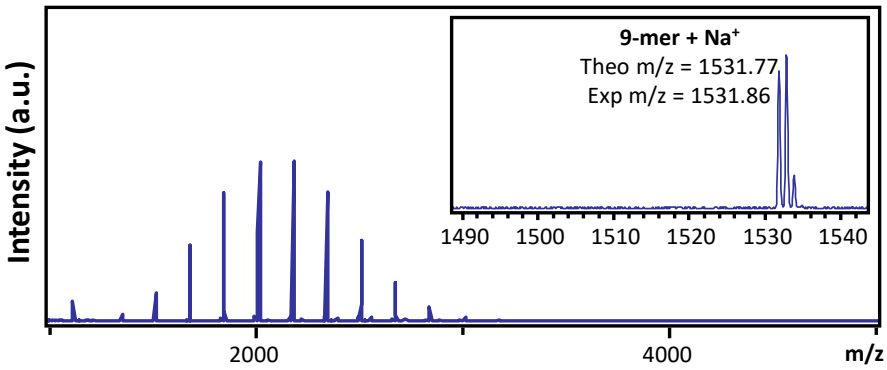

Figure 6.5. MALDI-TOF of methanol initiated poly(glycidyl 2-methylphenyl ether)

While this polymer was successfully synthesized, the terminal hydroxy group was unable to be coupled to triiodobenzoic acid via EDC coupling. This is possibly suggestive of the reaction being inhibited due to the steric bulk of three iodines. One future direction of incorporating three iodines to the polymer is by considering triiodophenol as an initiator. Due to the increased acidity of a phenolic group (compared to an alcohol like methanol) it is thought that this group might be able to initiate the polymerization well. If this polymerization is successful it will yield a 1-step process for generating a mass spectrometry calibrant.

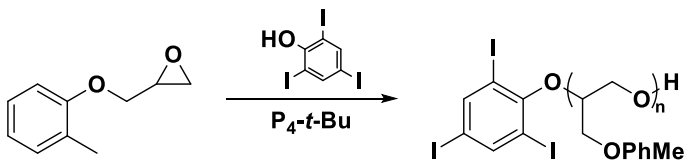

Scheme 6.4. Synthesis of triiodophenol initiated poly(glycidyl 2-methylphenyl ether)

6.3 REFERENCES

1. Bailon, P.; Berthold, W. Polyethylene glycol-conjugated pharmaceutical proteins. *Pharmaceutical Science & Technology Today* **1998,** 1 (8), 352-356.

2. Xu, Z.; Li, Y.; Zhang, B.; Purkait, T.; Alb, A.; Mitchell, B.; Grayson, S.; Fink, M. Water-soluble PEGylated silicon nanoparticles and their assembly into swellable nanoparticle aggregates. *Journal of Nanoparticle Research* **2015,** 17 (1), 1-16.

3. Chen, B.; Jerger, K.; Frechet, J. M.; Szoka, F. C., Jr. The influence of polymer topology on pharmacokinetics: differences between cyclic and linear PEGylated poly(acrylic acid) comb polymers. *Journal of Controlled Release* **2009,** 140 (3), 203-209.

4. Pasut, G.; Sergi, M.; Veronese, F. M. Anti-cancer PEG-enzymes: 30 years old, but still a current approach. *Advanced Drug Delivery Reviews* **2008,** 60 (1), 69-78.

5. Haque, F. M.; Alegria, A.; Grayson, S. M.; Barroso-Bujans, F. Detection, quantification, and "click-scavenging" of impurities in cyclic poly(glycidyl phenyl ether) obtained by zwitterionic ring-expansion polymerization with $B(C_6F_5)_3$. *Macromolecules* **2017,** 50 (5), 1870-1881.

6. Elupula, R.; Oh, J.; Haque, F. M.; Chang, T.; Grayson, S. M. Determining the origins of impurities during azide–alkyne click cyclization of polystyrene. *Macromolecules* **2016,** 49 (11), 4369-4372.

7. Giesen, J. A.; Diament, B. J.; Grayson, S. M. Iodine-containing mass-defect-tuned dendrimers for use as internal mass spectrometry calibrants. *Journal of The American Society for Mass Spectrometry* **2018,** 29 (3), 490-500.

8. Ochs, J.; Martínez-Tong, D. E.; Alegria, A.; Barroso-Bujans, F. Dielectric relaxation as a probe to verify the symmetrical growth of two-arm poly(glycidyl phenyl ether) initiated by t-BuP_4/ethylene glycol. *Macromolecules* **2019,** 52 (5), 2083-2092.

CHAPTER 7

CONCLUSIONS

Towards the advancement of polymer chemistry, significant utility lies in the ability to successfully synthesize and effectively characterize well-defined cyclic polymers. Towards this endeavor, two primary methods of synthesizing cyclic polymers have been made available, the ring closure and the ring expansion methods, both of which have their advantages and shortcomings. As described previously, the ring closure method proves to be effective and quantitative when cyclizing well-defined linear polymers with high end group fidelity. However, it is paramount that rapid high efficiency cyclization chemistry be utilized under high dilution to make high purity samples. In most cases, this method is beneficial for cyclizing lower and mid molecular weight linear polymers, but challenges arise in successfully cyclizing higher molecular polymers due to the difficulty in ensuring high end group fidelity of the linear precursors. To the contrary, the ring expansion method involves direct access to cyclic materials via the ring expansion polymerization of strained monomers, making it an enthalpically favorable process, while also avoiding the entropic penalties of cyclizing a linear polymer. Unfortunately, this method can be prone to impurities in the presence of minor contaminants (e.g. H_2O) and broad molecular weight distributions due to an uncontrolled chain cyclization process.

To synthesize cyclic polymers, our group has predominantly focused on utilizing the ring closure method via the CuAAC "click" cyclization. This chemistry was chosen for cyclization as it happens rapidly and quantitatively, and it is thought to only occur in the presence of the copper catalyst. This method has proven to be particularly versatile and amenable to an array of functional groups as demonstrated by its wide use in the polymer chemistry community. However, through a detailed study of cyclic polystyrene synthesized using this method, it was determined that minor amounts of unwanted dimers can form during the storage of the linear polystyrene precursor. Specifically, HPLC, an analytical technique, was able to separate the components of the linear precursor, which included the unimer (i.e. the linear precursor) and the dimer (i.e. minor impurity), and enough sample was able to be collected (μg quantities) to perform MALDI-ToF MS experiments. Analogous separations were also performed on the cyclic product. From the combination of these experiments, it was realized that during the storage of the linear precursor, the free end groups could react and undergo unintended and uncatalyzed azide alkyne cycloaddition reactions. However, importantly, during the cyclization reaction both the unimer and dimer components all cyclize as they both have the complimentary end groups needed for cyclization. While there is a minor broadening in the molecular weight distribution as a result of this unintended dimerization process, the polymer remains architecturally well-defined. This is further noted by the lack of reactivity within the cyclic polymer product. Finally, it is suggested for future work, that the end groups only be converted to the necessary azide or alkyne group directly prior to synthesis of the cyclic polymer to minimize potential dimerization. Furthermore, storage of linear precursors at colder temperatures can also help to minimize these impurities. A major concern among polymer physicists when studying cyclic polymers is the potential for linear contaminants within cyclic products, as they are known to severely alter the physical properties,

even when contained in small quantities (<5%). The work herein helps to validate the results of studies performed on cyclic polymers synthesized via the CuAAC method as any potential impurities are most likely cyclic in architecture.

Using this same cyclization protocol, cyclic polycaprolactone (*c*-PCL) was generated using an optimized synthesis of the linear precursor (*l*-PCL). The synthesis of the linear precursor is based on the ring opening polymerization of caprolactone with a propargyl alcohol initiator to install an alkyne moiety and tin(II) 2-ethylhexanoate as a catalyst. Previous methods alternatively used an azide initiator (i.e. 3-azidopropanol), possibly suggestive that azide group influences the initiation process during the polymerization. With this protocol, *l*-PCL and *c*-PCL were synthesized with a molecular weight of 6000 Da to study their properties as thin films. Both polymers yielded successful and stable as-cast films, but only the cyclic polymer was able to maintain a stable film after recrystallization. End group considerations were also a possibility for the instability within the linear film. However, regardless of the *l*-PCL end groups (e.g. hydrophobic, hydrophilic, containing triazole, without triazole), it always dewet upon recrystallization, suggesting the predominant factor contributing to the cyclic polymer's stability is its architecture. Furthermore, this work demonstrates the ability of the cyclic architecture to produce more durable materials for industrially relevant processes and applications.

In addition to the work studying the synthesis and characterization of cyclic polymers via the CuAAC ring closure, the ring expansion method was also studied in thorough detail on the electrophilic zwitterionic ring expansion polymerization (eZREP) of various monosubstituted epoxides. The original study began with the polymerization of phenyl glycidyl ether with $B(C_6F_5)_3$ to generate functional cyclic polyethers. While the major product (~70%) appeared to be cyclic, there was a substantial contribution from other non-cyclic products, including a monohydroxy

tadpole formed through a dimerization event and a dihydroxy linear polyether formed by the presence of minor amounts of water. Through strategic analysis of the crude cyclic polyether by MALDI-ToF MS the components of the mixture were identified. Further confirmation of the proposed structures was performed by doing a functionalization reaction on the crude polymer, and the structures added the respective number of functional groups based on the proposed number of hydroxy groups. This was further validation of the proposed mechanisms. Based on this concept of the impurities' ability to undergo functionalization while the cyclic structure remains inert, the polymer was reacted with propargyl bromide to alkynylate all impurities. The resultant mixture was reacted with an azide-modified solid phase resin using the CuAAC "click" reaction; consequently, the impurities were bound to the insoluble resin while the pure cyclic polymer remained in solution. This allowed for a facile purification process that merely required filtration of the resin from the filtrate and the product collected *in vacuo*. The benefit of the eZREP process is that it can be performed on a larger multigram scale, unlike the ring closure approach. While some impurities are formed they can largely be removed by the "click" scavenging purification technique described. This purification process takes advantage of the highly rapid and quantitative "click" reaction but is limited to only removing impurities that have a functionizable handle (e.g. OH groups).

One of the disadvantages of eZREP is that it is prone to making polymers of broad molecular weight dispersity, which is a common feature of cyclic polymers generated via a ring expansion method. This is particularly troublesome when analyzing these samples by MALDI-ToF MS, as this technique has an ionization bias towards small molecular weight structures. To overcome this issue, the cyclic poly(phenyl glycidyl ether) was fractionated by size exclusion chromatography to generate fractions of varying molecular weight and narrow dispersities,

consequently making them much easier to study via MALDI-ToF MS. It also made it clear that the majority of these impurity structures are abundant in the highest molecular weight portion of the crude polymer sample. Additionally, it was proposed that many of these side products form as a consequence of the boron catalyst coordinating and activating the glycidyl ether oxygen, making it receptive to nucleophilic attack. To further expand on the eZREP research, many other monofunctional epoxides were chosen including chlorophenyl glycidyl ether and benzyl glycidyl ether. It was determined that the addition of the chloro group to phenyl glycidyl ether greatly reduced the formation of side products by allowing it act as an electron withdrawing group, so the boron catalyst preferentially coordinates with the epoxide oxygen to exclusively polymerize. To further validate these results, DFT calculations were performed, which also pointed to the chloro group acting in an electron withdrawing fashion. On the other hand, the incorporation of the benzyl moiety in the monomer greatly enhanced the formation of side products due to the electrophilicity of the benzylic group, greatly complicating the MALDI-ToF MS results. However, with this chemical understanding, very complex MS data was able to be digested and the majority of the structures to be identified. While there are many aspects of the polymerization to consider during eZREP (e.g. monomer or catalyst), this research has greatly expanded upon some of those aspects, namely the type of monomer. Moreover, this work truly highlights the importance of MALDI-ToF MS and how it can be used to characterize complex polymerization systems, especially when used alongside other analytical techniques like size exclusion chromatography.

It has become well known within the polymer science community that cyclic polymers provide fascinating and unique properties that are advantageous to biomedical and industrial applications. One of the biggest questions to date remains the purity of these polymers and methods of determining purity both quantitatively and qualitatively. The work herein truly

demonstrates that no singular technique is able to provide all the answers, rather several techniques must be used together to provide a more complete story. There are many ways to synthesize cyclic polymers and all methods have their unique advantages and disadvantages. However, a fundamental understanding of the polymerization or cyclization chemistry can provide unique insight into ways of determining the successful synthesis. Based upon the methods described in this thesis, cyclic polymers of greatly enhanced purity can be generated for the purpose of studying their fundamental thermal, mechanical, and materials' properties to exploit these unique properties for new applications (e.g., drug delivery, nanolithography). With continued efforts in synthetic optimization, analytical methodology development, and characterization of physical properties, cyclic polymers will see the light in many polymer applications.

APPENDIX A

SUPPORTING INFORMATION FOR CHARACTERIZATION OF CYCLIC POLYSTYRENE*

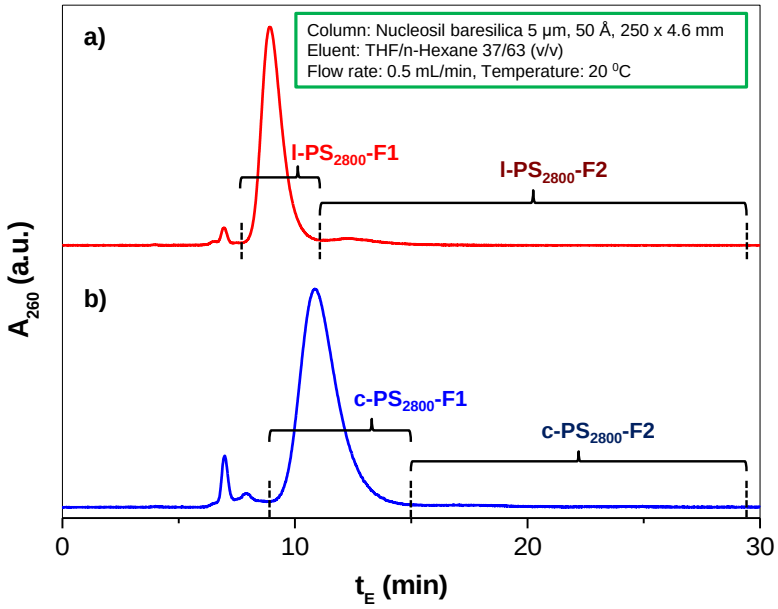

Figure A1. HPLC chromatograms during the separation and isolation of the unimer fraction 10 days after azidization and cyclization for a) *l*-PS_{2800} and b) *c*-PS_{2800}

* Portion of this work has been published in Elupula, R.; Oh, J.; Haque, F. M.; Chang, T.; Grayson, S. M. Determining the Origins of Impurities during Azide–Alkyne Click Cyclization of Polystyrene. *Macromolecules* **2016**, *49*, 4369-4372 and Gartner, T. E.; Haque, F. M.; Gomi, A. M.; Grayson, S. M.; Hore, M. J. A., Jayraman, A. Scaling exponent and effective interactions in linear and cyclic polymer solutions: theory, simulations, and experiments. *Macromolecules* **2019**, *52*, 4579-4589.

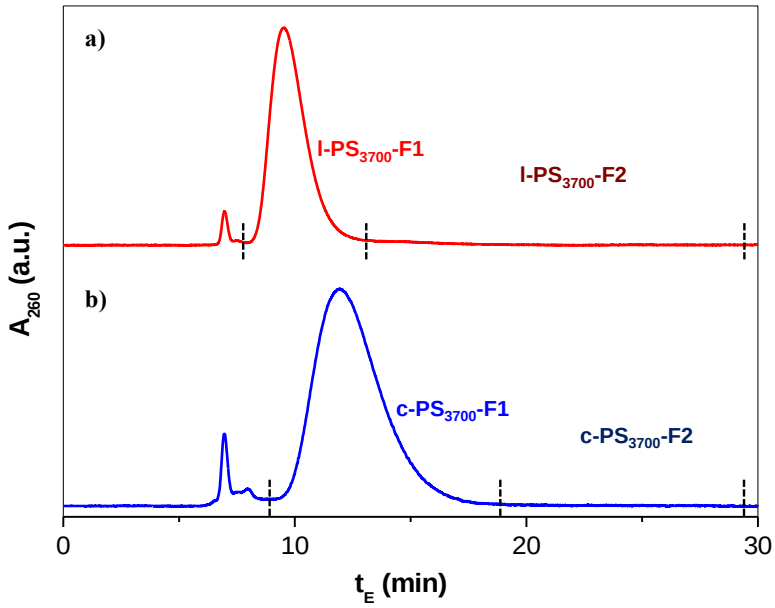

Figure A2. HPLC chromatograms during the separation and isolation of the unimer fraction 10 days after azidization and cyclization for a) *l*-PS$_{3700}$ and b) *c*-PS$_{3700}$

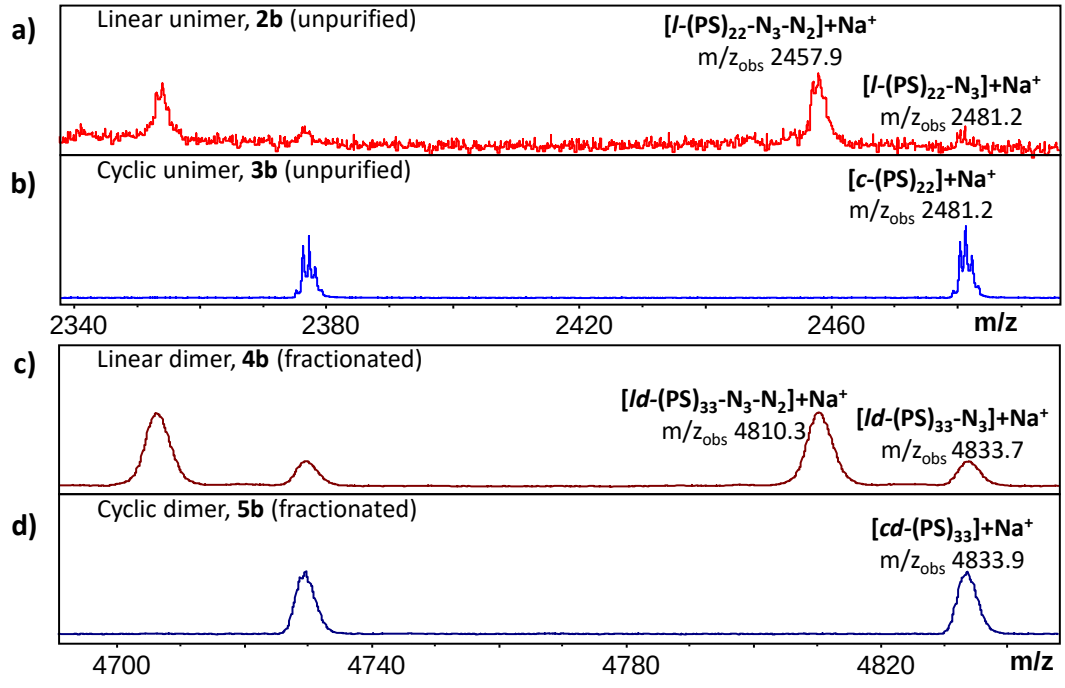

Figure A3. MALDI-TOF mass spectra in reflector mode of a) *l*-PS$_{2800}$, b) *c*-PS$_{2800}$, c) *ld*-PS$_{2800}$, d) *cd*-PS$_{2800}$ confirming the loss of the predominant metastable azide signal upon CuAAC cyclization to form the triazole linkage in the cyclic products.

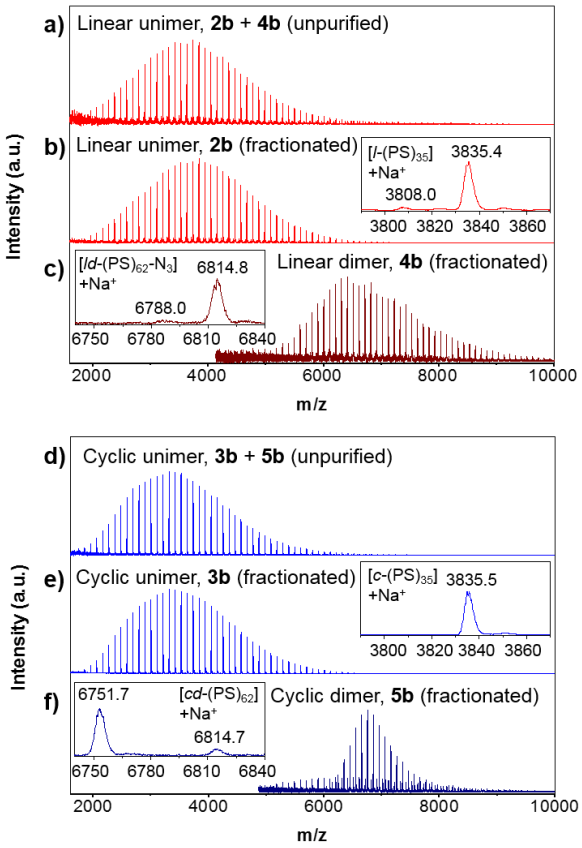

Figure A4. MALDI TOF mass spectra of a) *l*-PS_{2800}, **2b**+ **4b**, b) *l*-PS_{2800}, **2b**, c) *ld*-PS_{2800}, **4b**, and d) *c*-PS_{2800}, **3b**+ **5b**, e) *c*-PS_{2800}, **3b**, f) *cd*-PS_{2800}, **5b** The theoretical *m/z* for the *l*- and *c*-PS 35-mer was 3835.5, the theoretical *m/z* for the metastable *ld*- and *cd*-PS 62-mer was 6814.8. 6751.7 peak in f) is cyclic unimer, *c*-PS 63-mer.

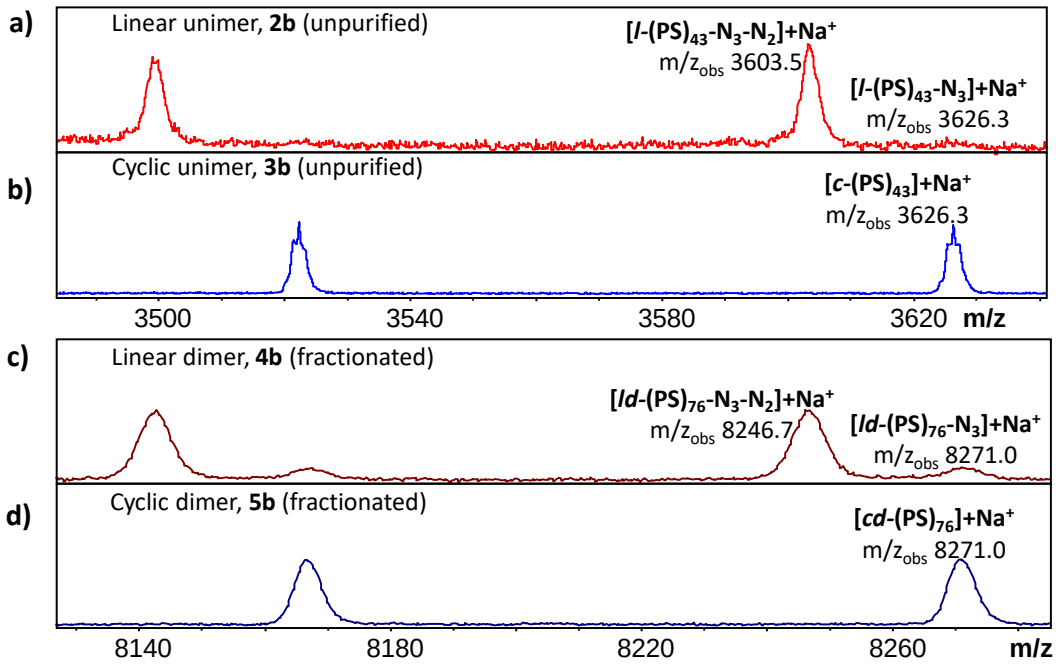

Figure A5. MALDI-TOF mass spectra in reflector mode of a) *l*-PS$_{3700}$, b) *c*-PS$_{3700}$, c) *ld*-PS$_{3700}$, d) *cd*-PS$_{3700}$ confirming the loss of the predominant metastable azide signal upon CuAAC cyclization to form the triazole linkage in the cyclic products.

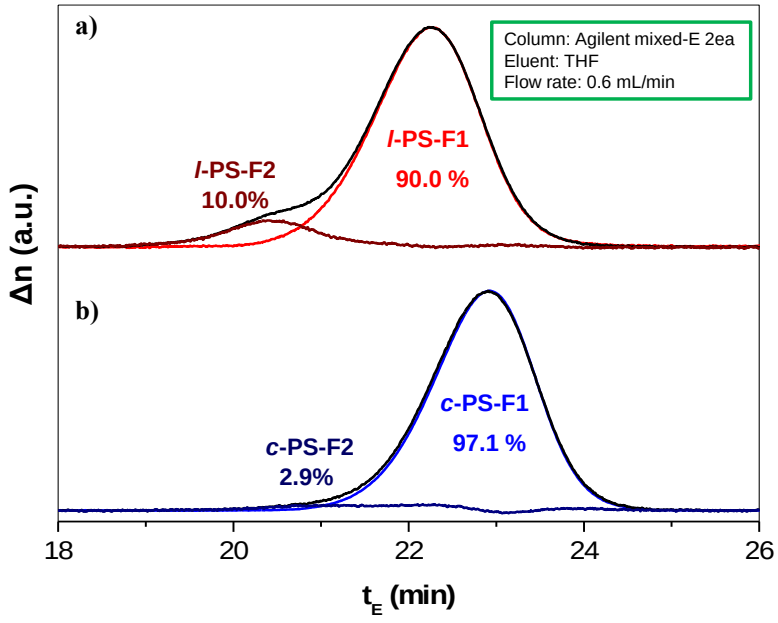

Figure A6. Representative SEC chromatograms of HPLC fractions 30 days after azidization and cyclization for a) *l*-PS$_{2800}$ and b) *c*-PS$_{2800}$. Fraction 1 corresponds to the isolated unimer fraction, while fraction 2 corresponds to the dimer fraction.

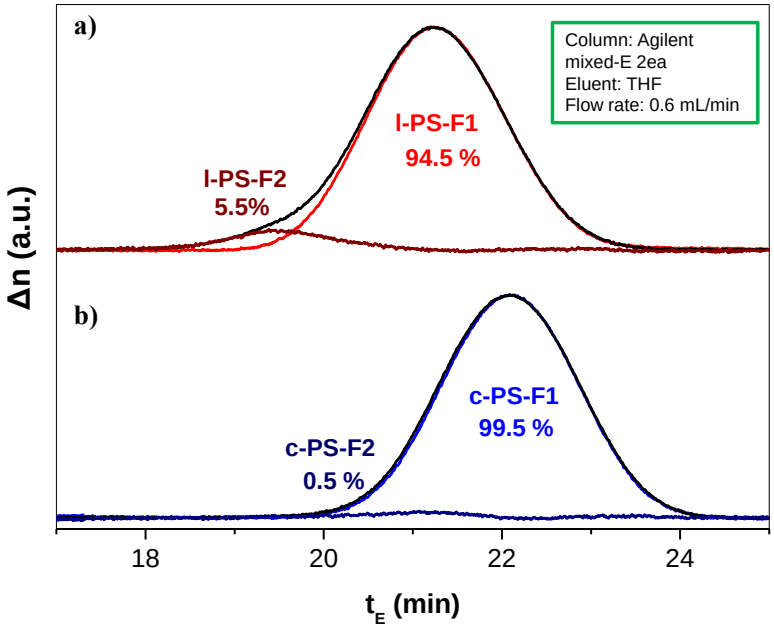

Figure A7. Representative SEC chromatograms of HPLC fractions 30 days after azidization and cyclization for a) *l*-PS$_{3700}$ and b) *c*-PS$_{3700}$. Fraction 1 corresponds to the isolated unimer fraction, while fraction 2 corresponds to the dimer fraction.

Table A1. Molecular weight determination of linear and cyclic polystyrene samples by GPC and MALDI-TOF MS based on Figures 2.6-2.8.

	SEC			**MALDI**[b]		
	M_n	M_w	$Đ$	M_n	M_w	$Đ$
l-PS$_{10k}$	12.0	13.1	1.10	10.8	11.0	1.02
c-PS$_{10k}$	9.70	10.8	1.12	10.7	10.9	1.02
l-PS$_{14k}$	13.2	15.9	1.20	14.3	14.6	1.02
c-PS$_{14k}$	11.2	12.9	1.15	14.4	14.7	1.02

APPENDIX B

SUPPORTING INFORMATION FOR DETECTION, QUANTIFICATION AND "CLICK-SCAVENGING" OF IMPURITIES IN CYCLIC POLY(GLYCIDYL PHENYL ETHER) OBTAINED BY ZWITTERIONIONC RING-EXPANSION POLYMERIZATION WITH $B(C_6F_5)_3$[1]

Table B1. Structures assigned to MALDI-TOF MS signals within crude cyclic poly(GPE) sample observed in Figure 3.1.

Name	Topology	Mass	Mass after Functionalizations			
			Propargylated	Acetylated	Benzylated	Pent-4-ynoated
C		nx150	(nx150)+ (0x38)	(nx150)+ (0x42)	(nx150)+ (0x90)	(nx150)+ (0x80)
TP		nx150	(nx150)+ (1x38)	(nx150)+ (1x42)	(nx150)+ (1x90)	(nx150)+ (1x80)
TP'	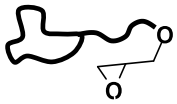	(nx150)+56	(nx150)+56+ (0x38)	(nx150)+56+ (0x42)	(nx150)+56+ (0x90)	(nx150)+56+ (0x80)
L		(nx150)+18	(nx150)+18+ (2x38)	(nx150)+18+ (2x42)	(nx150)+18+ (2x90)	(nx150)+18+ (2x80)
L'		(nx150)+94	(nx150)+94+ (1x38)	(nx150)+94+ (1x42)	(nx150)+94+ (1x90)	(nx150)+94+ (1x80)
L"	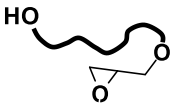	(nx150)+74	(nx150)+74+ (1x38)	(nx150)+74+ (1x42)	(nx150)+74+ (1x90)	(nx150)+74+ (1x80)

[1]A portion of this work has been published in Haque, F. M.; Alegria, A.; Grayson, S. M.; Barroso-Bujans, F. Detection, Quantification and "Click-Scavenging" of Impurities in Cyclic Poly(Glycidyl Phenyl Ether) Obtained by Zwitterionic Ring-Expansion Polymerization with $B(C_6F_5)_3$. *Macromolecules* **2017**, *50*, 1870-1881.

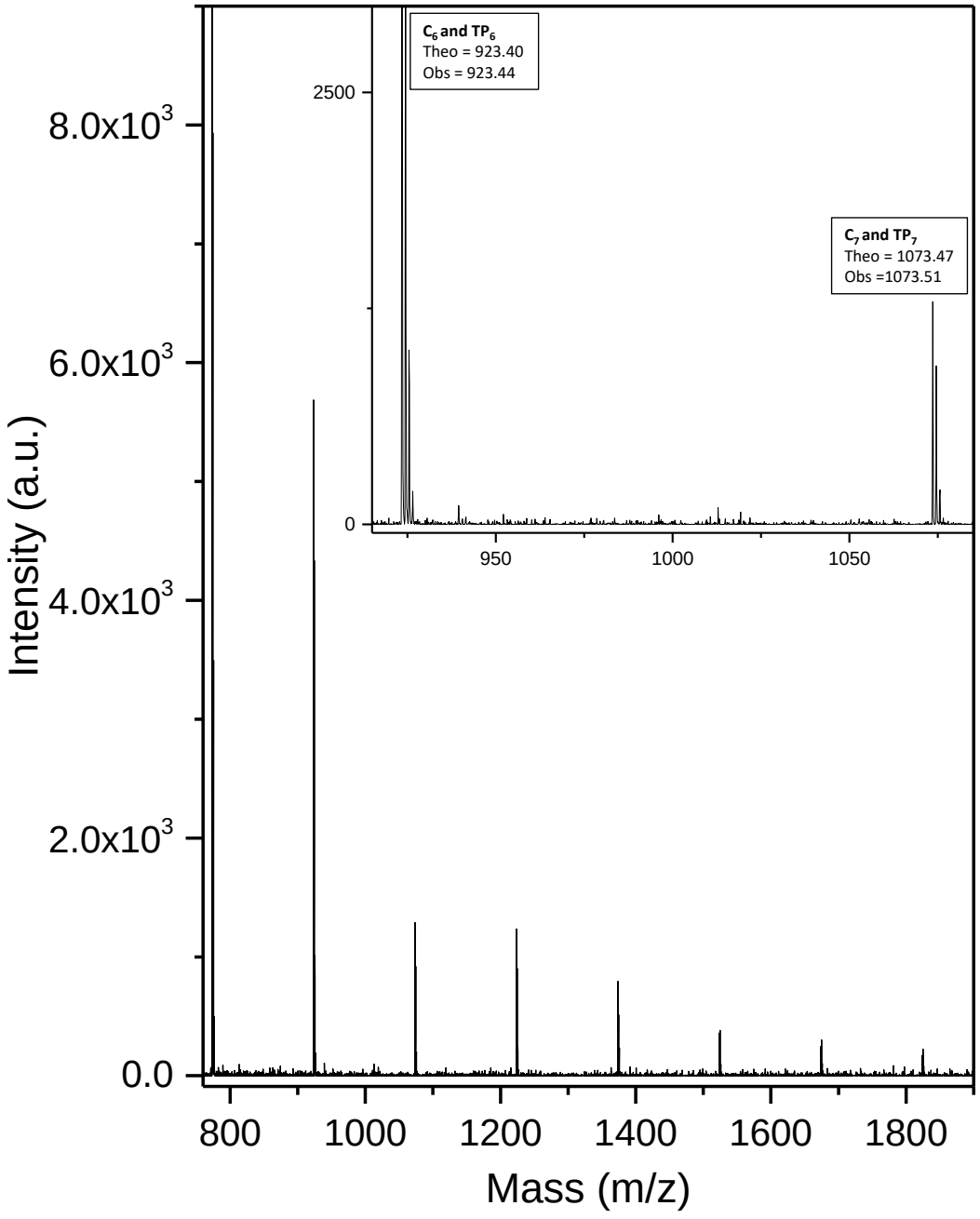

Figure B1. MALDI-ToF mass spectrum of crude poly(GPE)$_{1K}$ sample was taken in positive reflector mode, and all labeled signals represent the sodiated adducts.

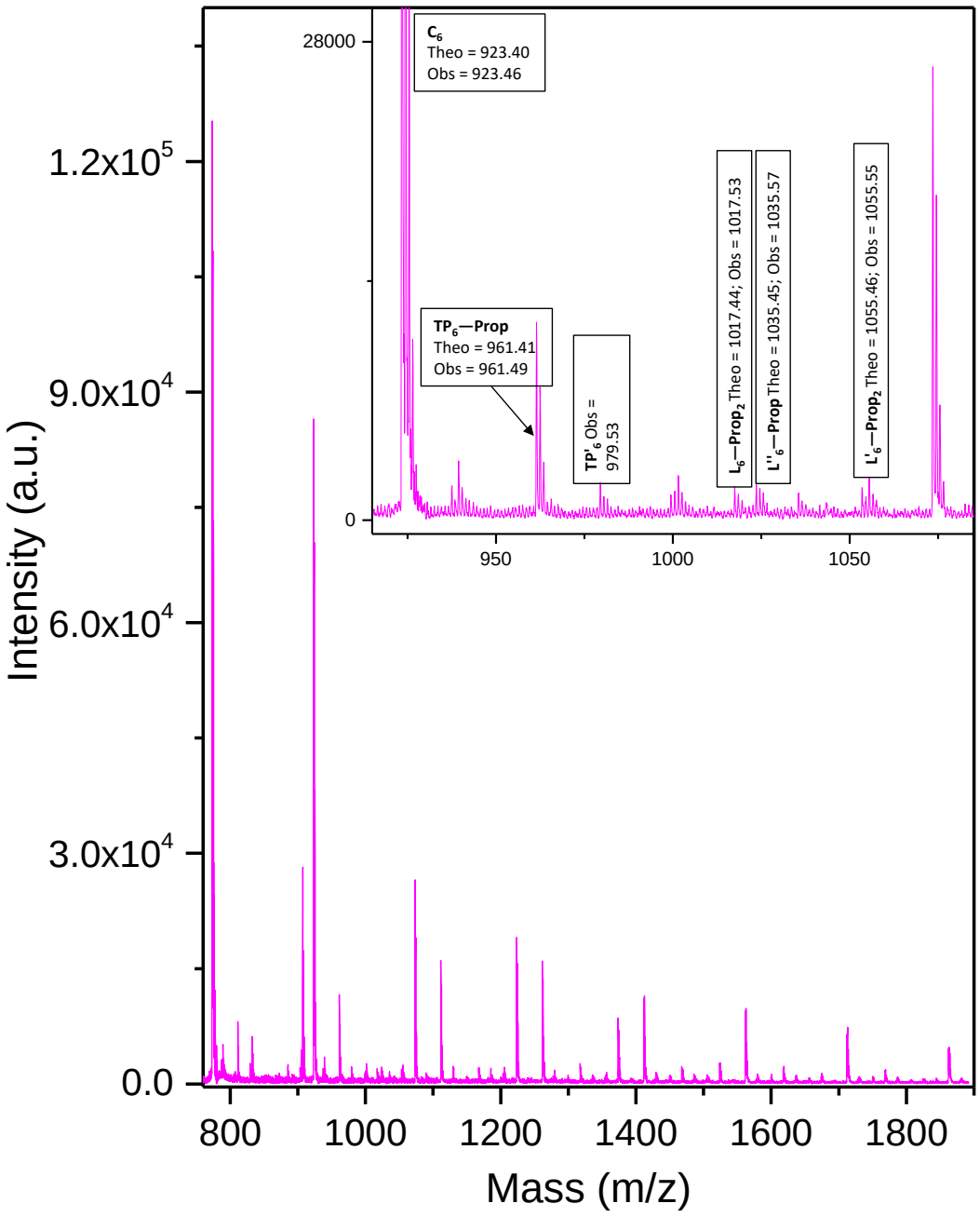

Figure B2. MALDI-ToF mass spectrum of propargylated poly(GPE)$_{1K}$ sample was taken in positive reflector mode, and all labeled signals represent the sodiated adducts.

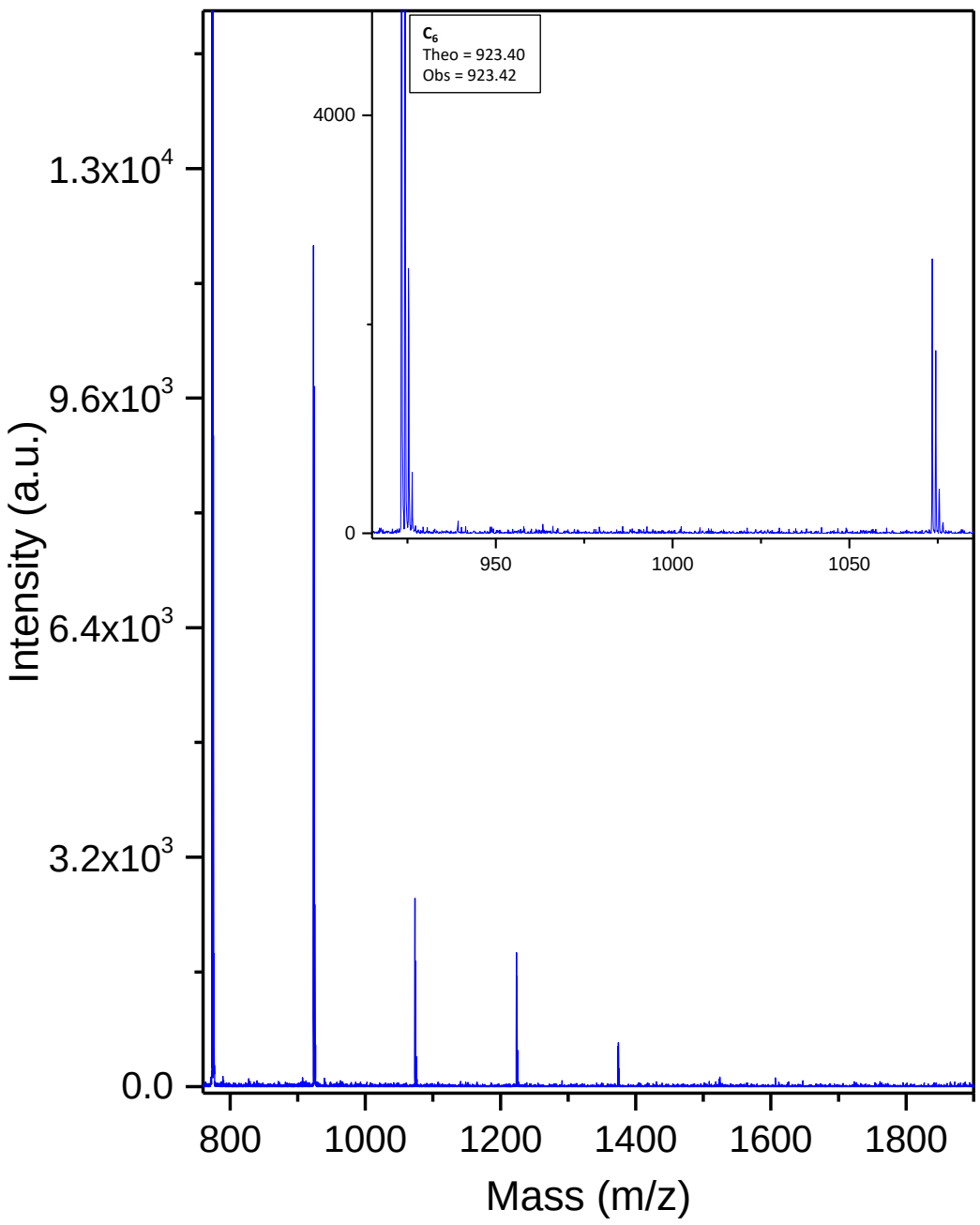

Figure B3. MALDI-ToF mass spectrum of "click-scavenged" poly(GPE)$_{1K}$ sample was taken in positive reflector mode, and all labeled signals represent the sodiated adducts.

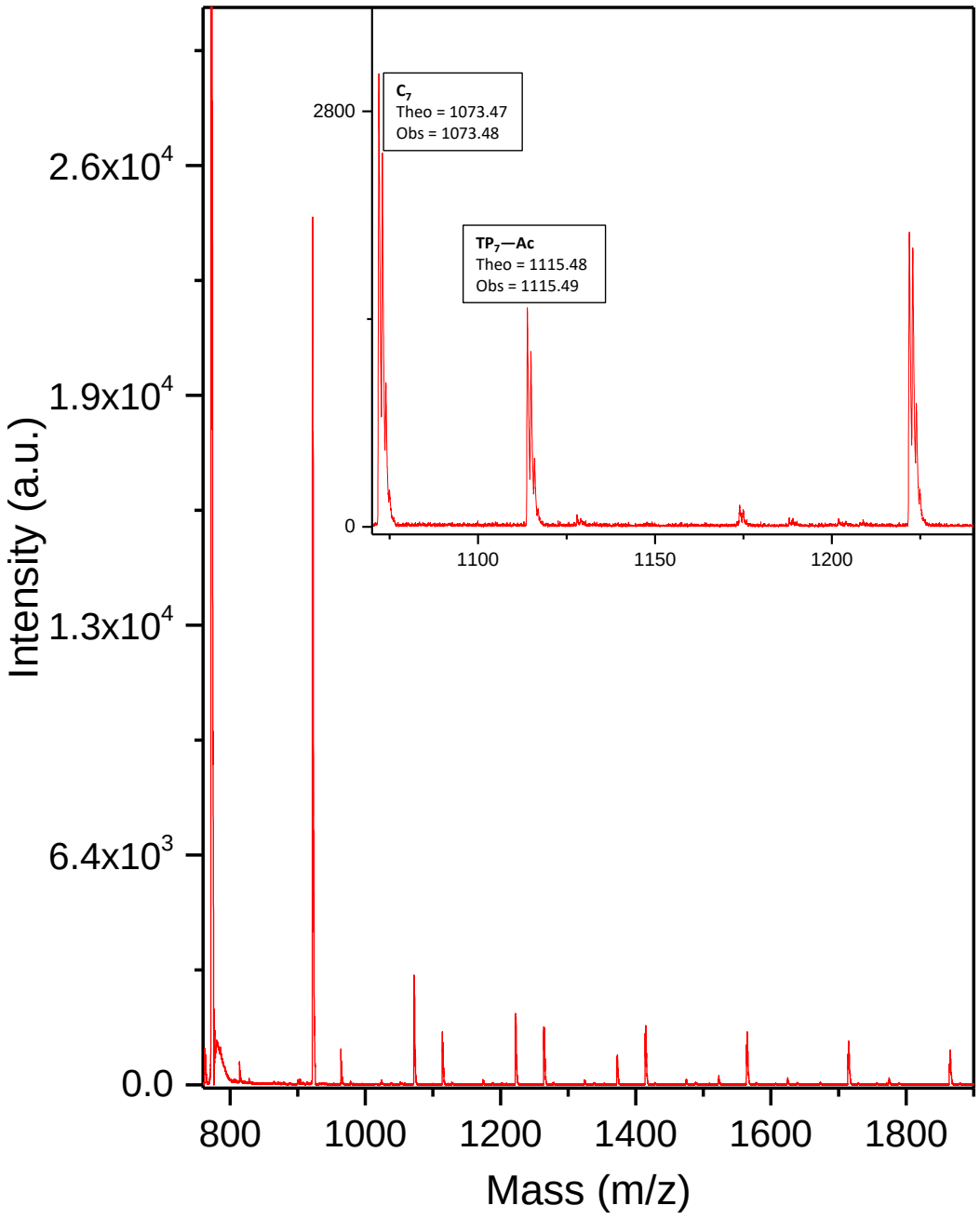

Figure B4. MALDI-ToF mass spectrum of acetylated poly(GPE)$_{1K}$ sample was taken in positive reflector mode, and all labeled signals represent the sodiated adducts.

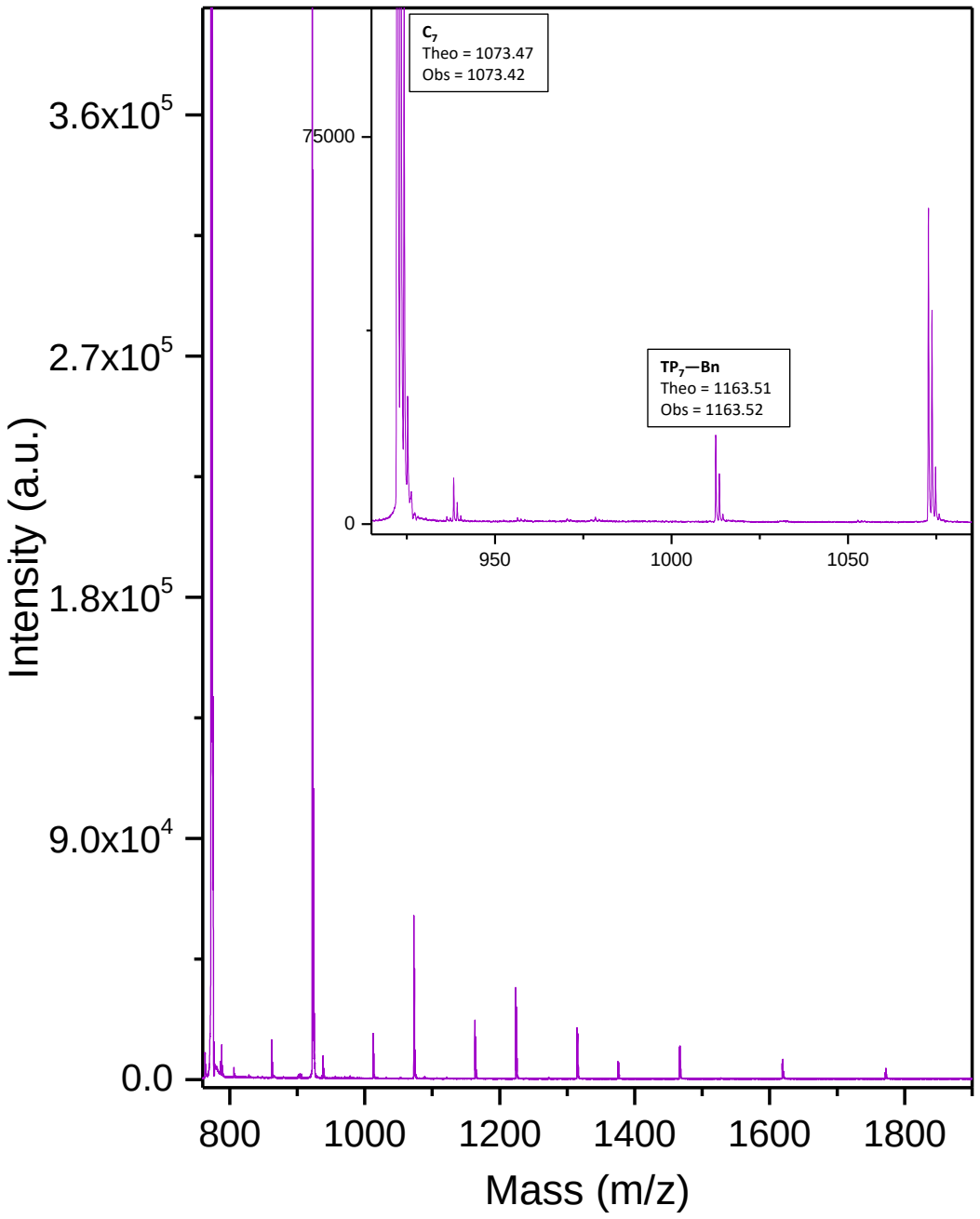

Figure B5. MALDI-ToF mass spectrum of benzylated poly(GPE)$_{1K}$ sample was taken in positive reflector mode, and all labeled signals represent the sodiated adducts.

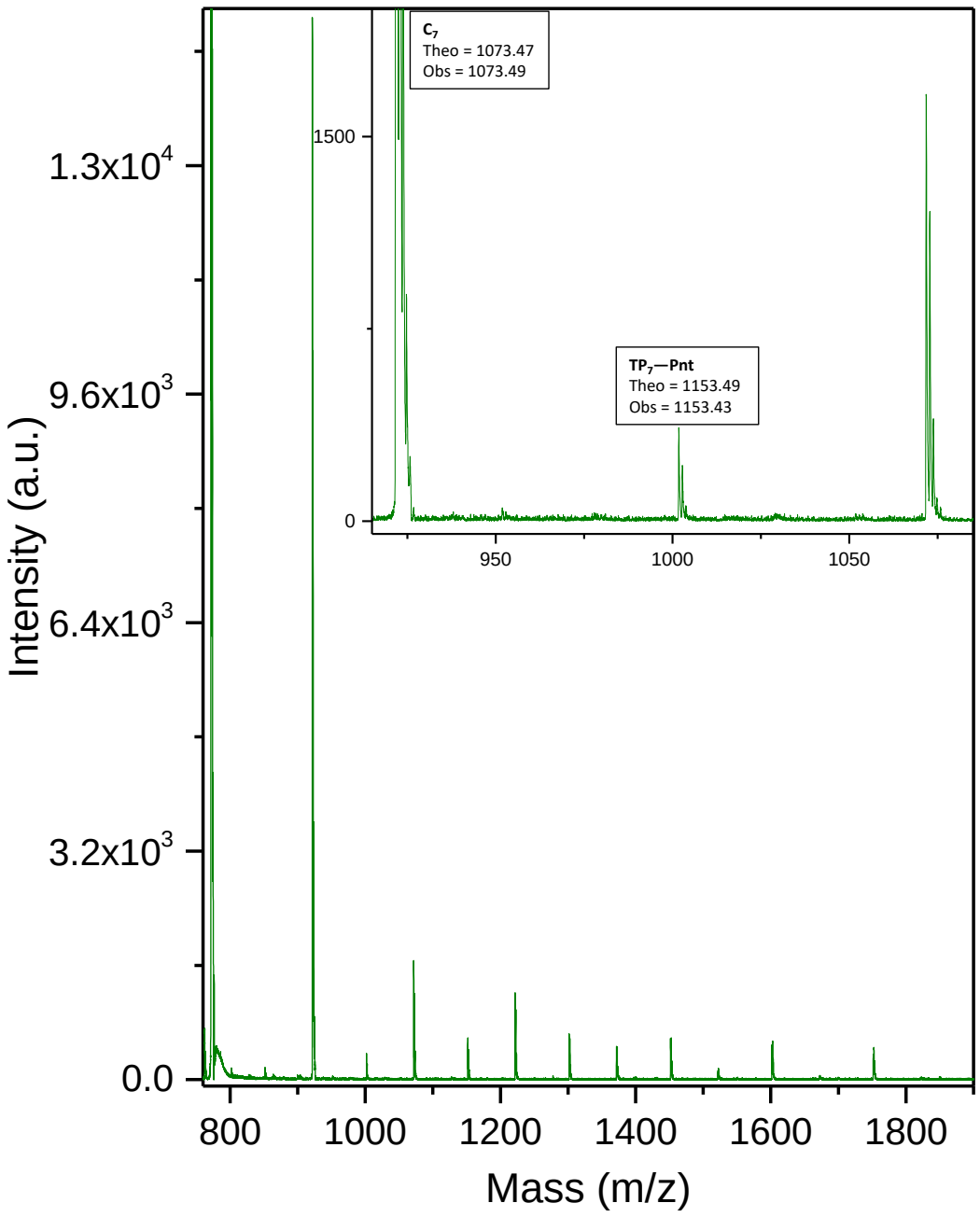

Figure B6. MALDI-ToF mass spectrum of pent-4-ynoated poly(GPE)$_{1K}$ sample was taken in positive reflector mode, and all labeled signals represent the sodiated adducts.

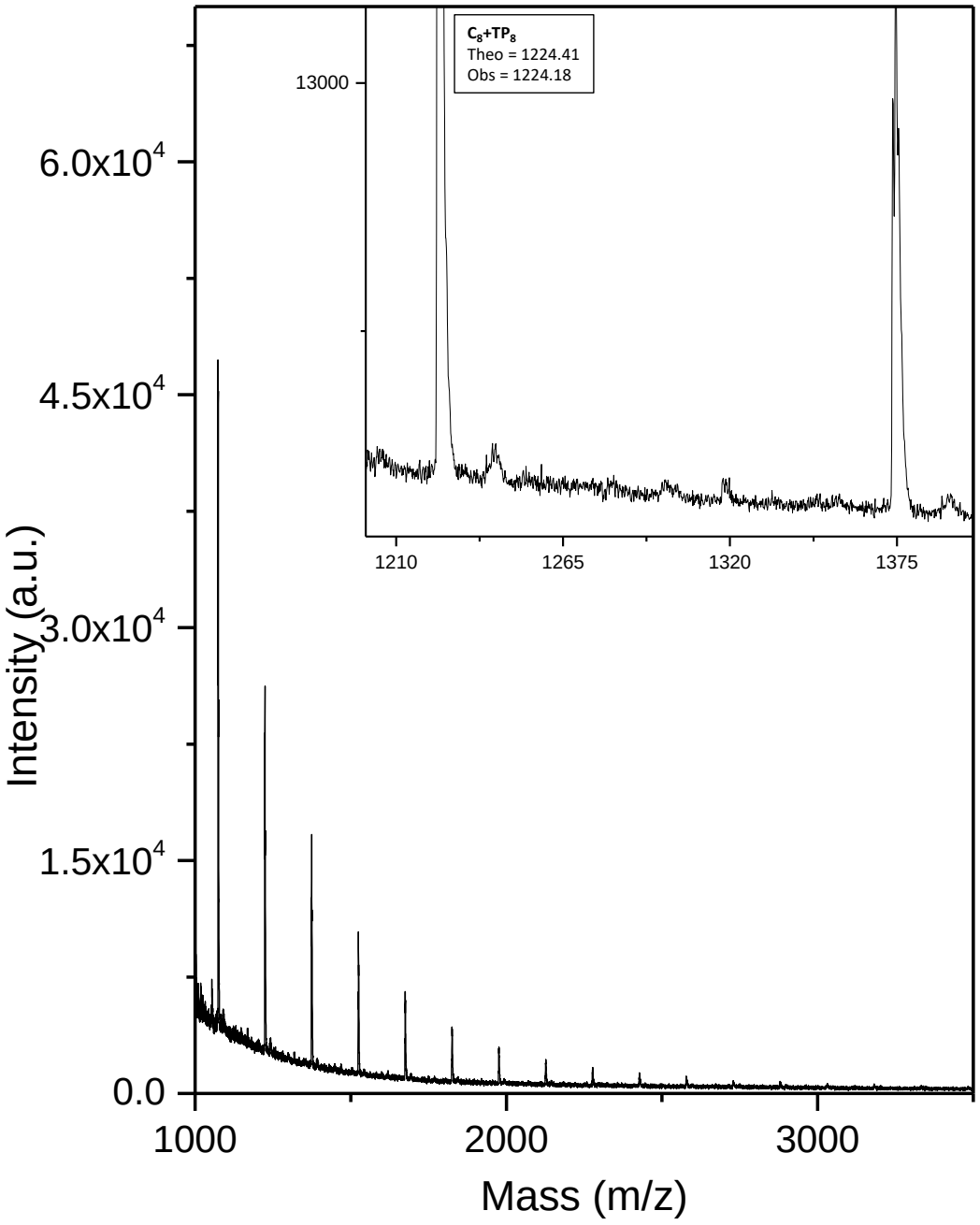

Figure B7. MALDI-ToF mass spectrum of crude poly(GPE)$_{11K}$ sample was taken in positive reflector mode, and all labeled signals represent the sodiated adducts.

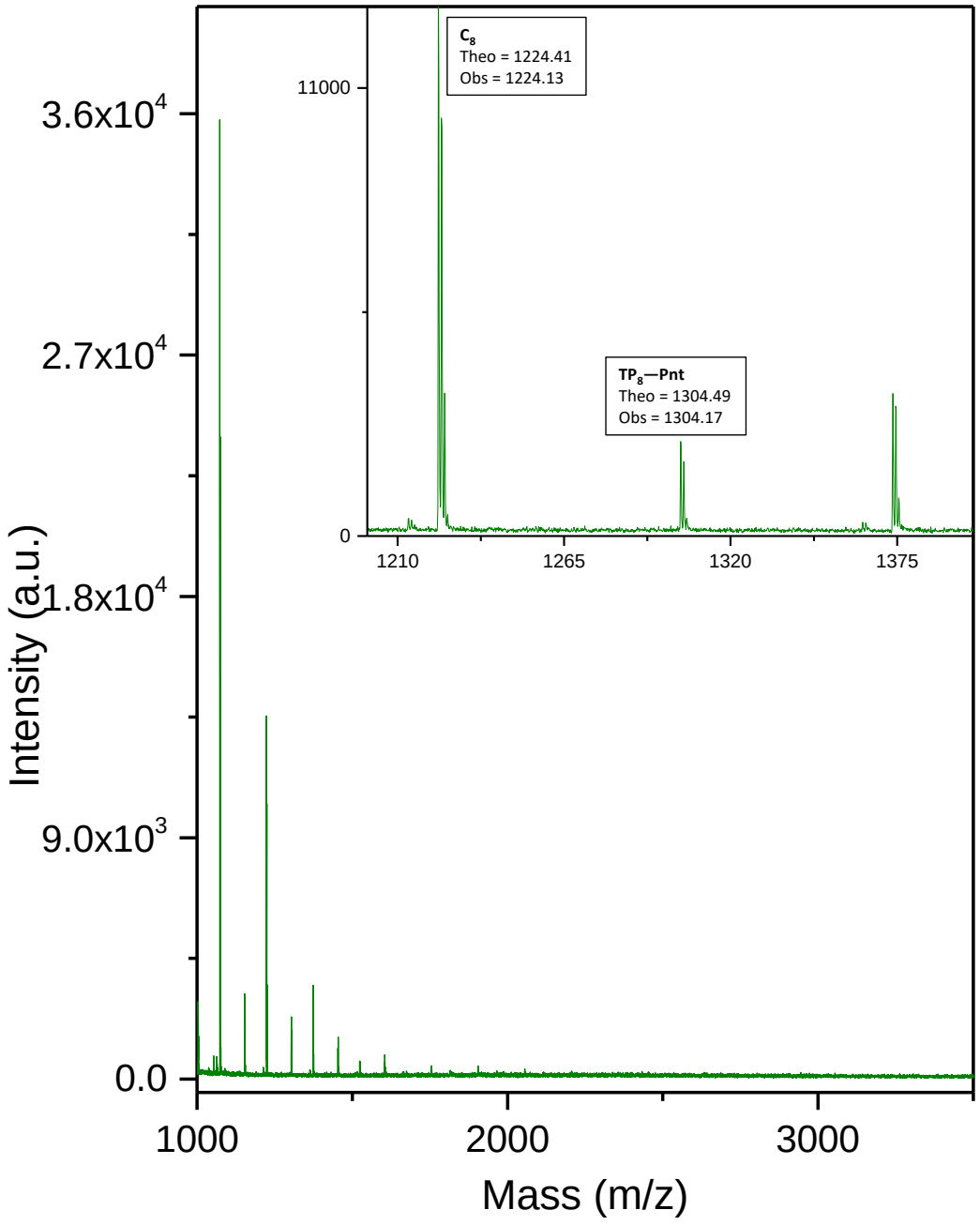

Figure B8. MALDI-ToF mass spectrum of pent-4-ynoated poly(GPE)$_{11K}$ sample was taken in positive reflector mode, and all labeled signals represent the sodiated adducts.

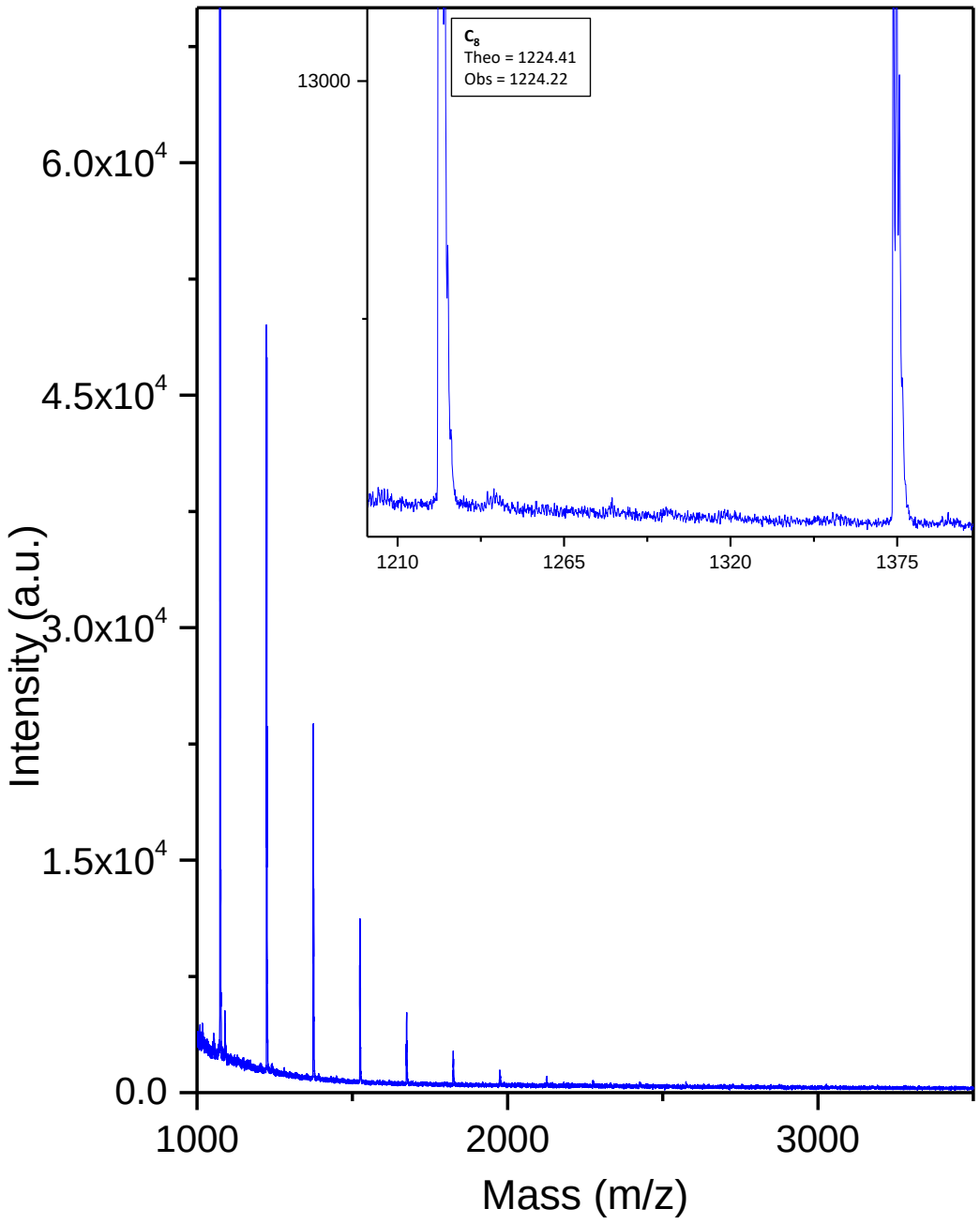

Figure B9. MALDI-ToF mass spectrum of "click-scavenged" poly(GPE)$_{11K}$ sample was taken in positive reflector mode, and all labeled signals represent the sodiated adducts.

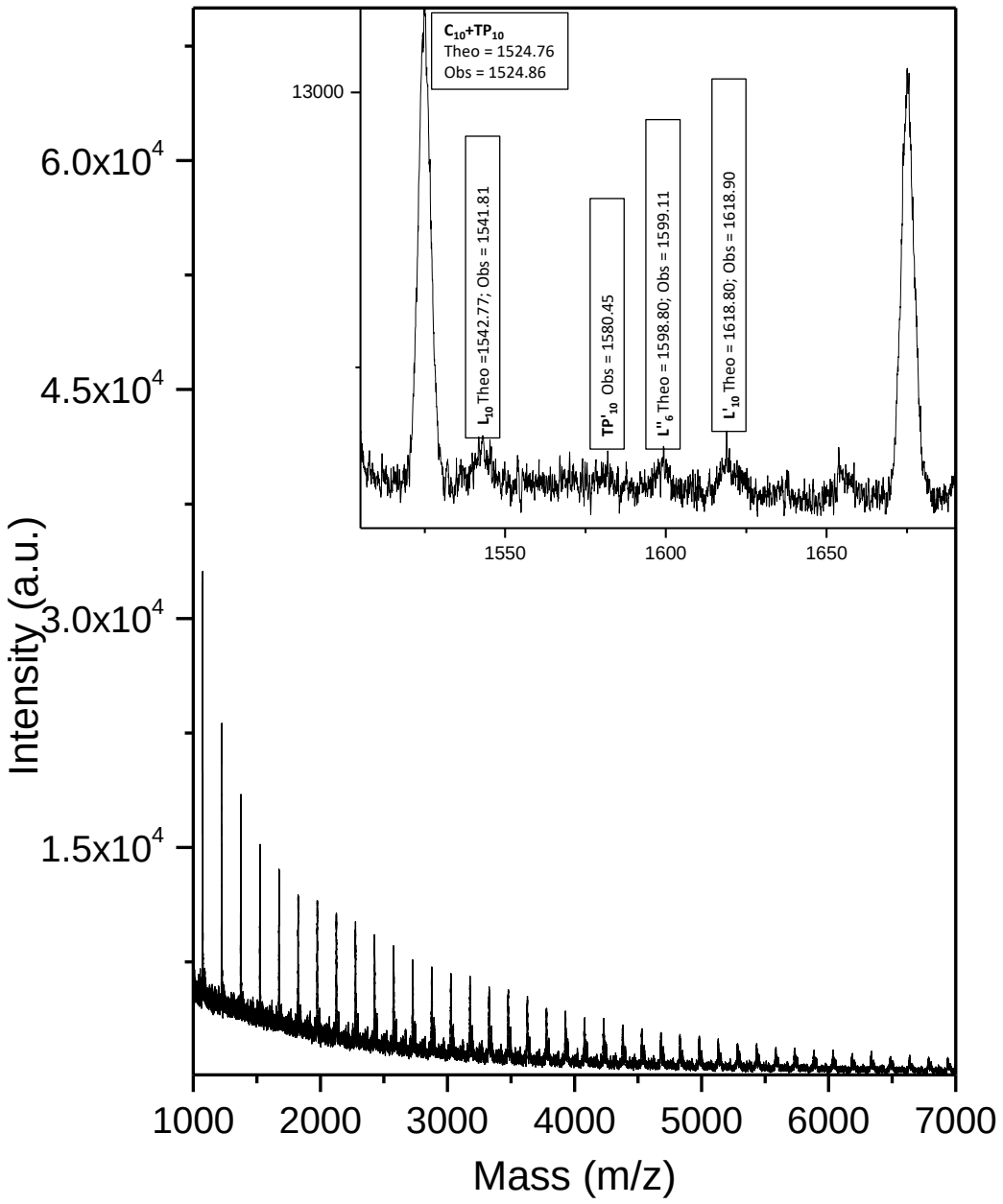

Figure B10. MALDI-ToF mass spectrum of crude poly(GPE)$_{11K}$ sample was taken in linear mode, and all labeled signals represent the sodiated adducts.

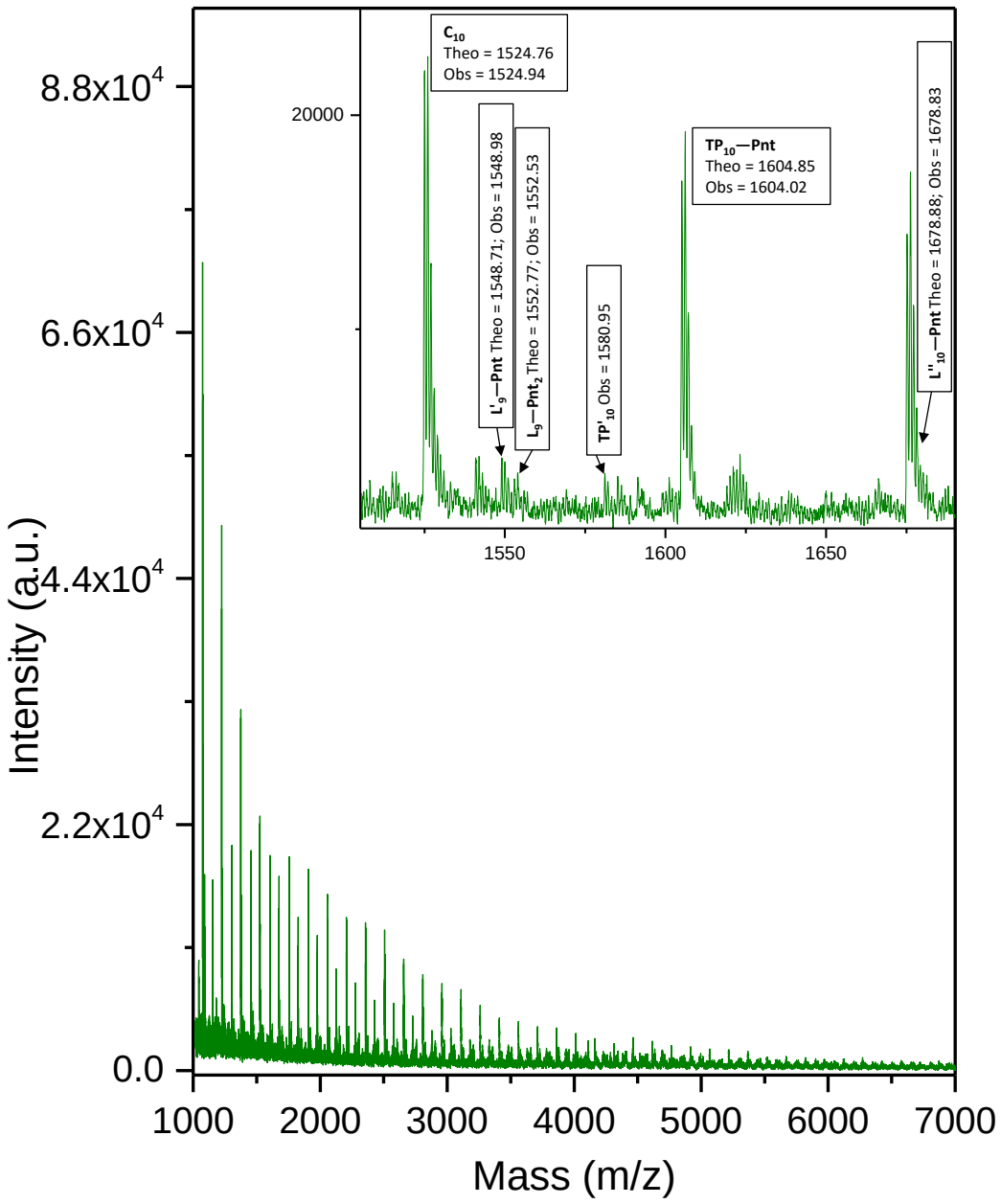

Figure B11. MALDI-ToF mass spectrum of pent-4-ynoated poly(GPE)$_{11K}$ sample was taken in linear mode, and all labeled signals represent the sodiated adducts.

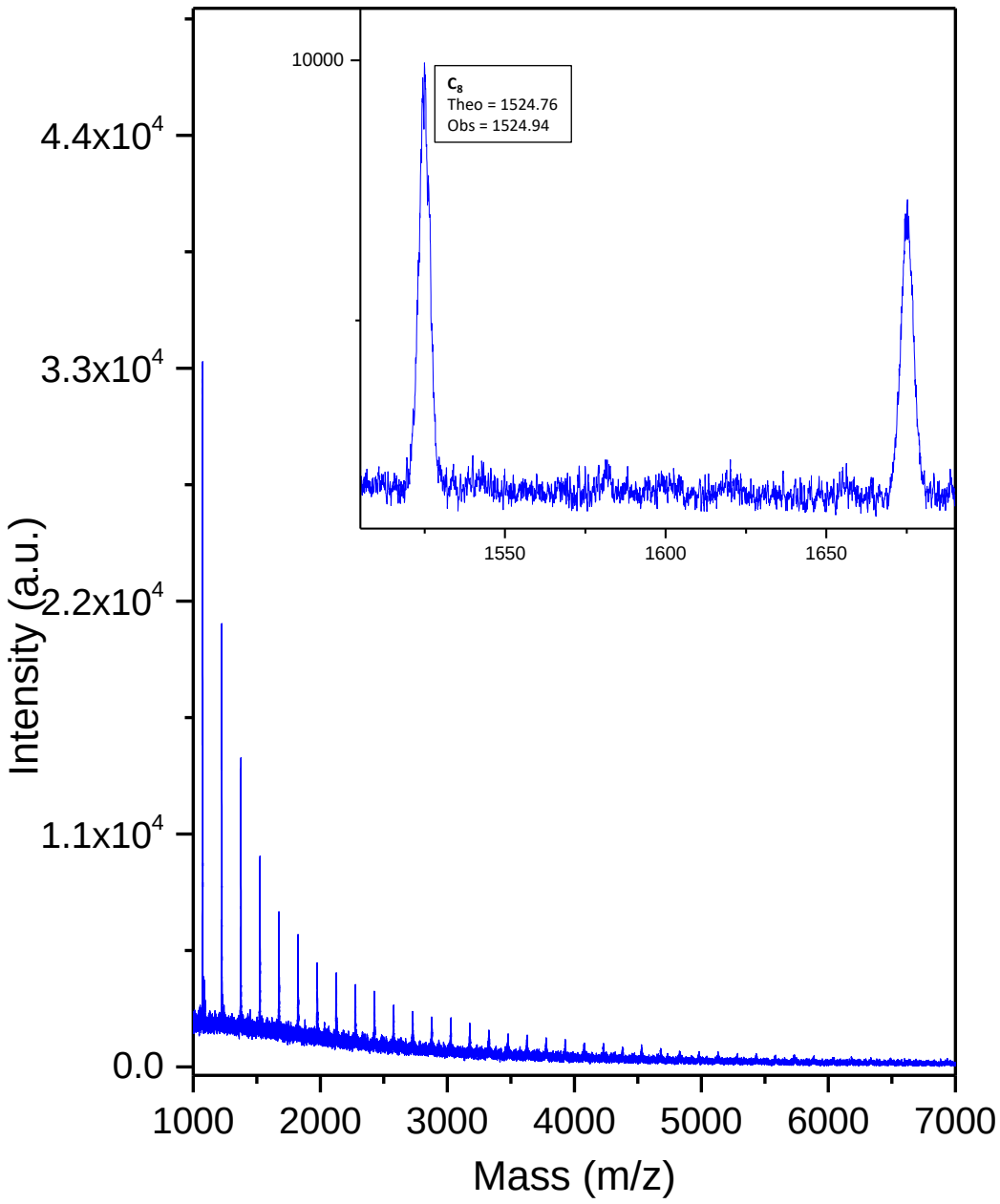

Figure B12. MALDI-ToF mass spectrum of "click-scavenged" poly(GPE)$_{11K}$ sample was taken in linear mode, and all labeled signals represent the sodiated adducts.

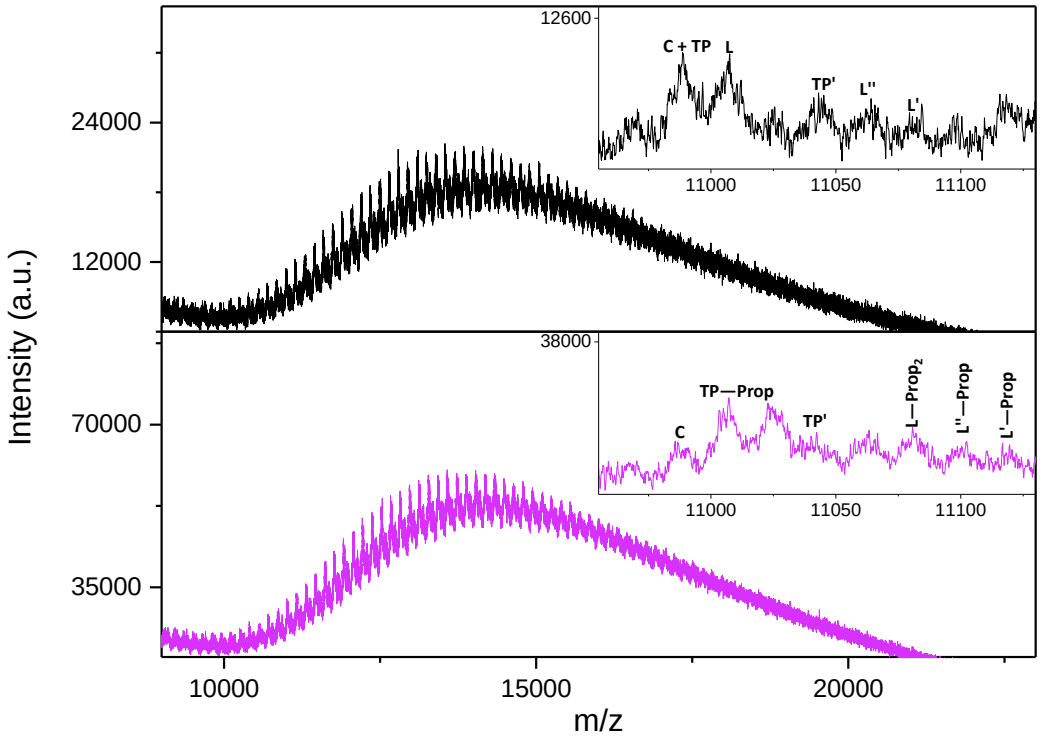

Figure B13. MALDI-ToF mass spectrum of crude (top) and propargylated (bottom) poly(GPE)$_{11K}$ samples were taken in linear mode, and all labeled signals represent the sodiated adducts.

Table B2. MALDI-ToF mass spectrum assignments of crude and propargylated poly(GPE)$_{11K}$ samples as shown in Figure B13.

Crude		Post-propargylation	
Species	m/z	Species	m/z
C$_{73}$	Theo = 10986; Obs = 10989	**C$_{73}$**	Theo = 10986; Obs = 10988
TP$_{73}$		**TP$_{73}$—Prop**	Theo = 11024; Obs = 11025
TP'$_{73}$	Theo = 11042; Obs = 11043	**TP'$_{73}$**	Theo = 11042; Obs = 11041
L$_{73}$	Theo = 11004; Obs = 11006	**L$_{73}$—Prop$_2$**	Theo = 11080; Obs = 11081
L'$_{73}$	Theo = 11080; Obs = 11082	**L'$_{73}$—Prop$_2$**	Theo = 11118; Obs = 11119
L''$_{73}$	Theo = 11060; Obs = 11062	**L''$_{73}$—Prop**	Theo = 11098; Obs = 11099

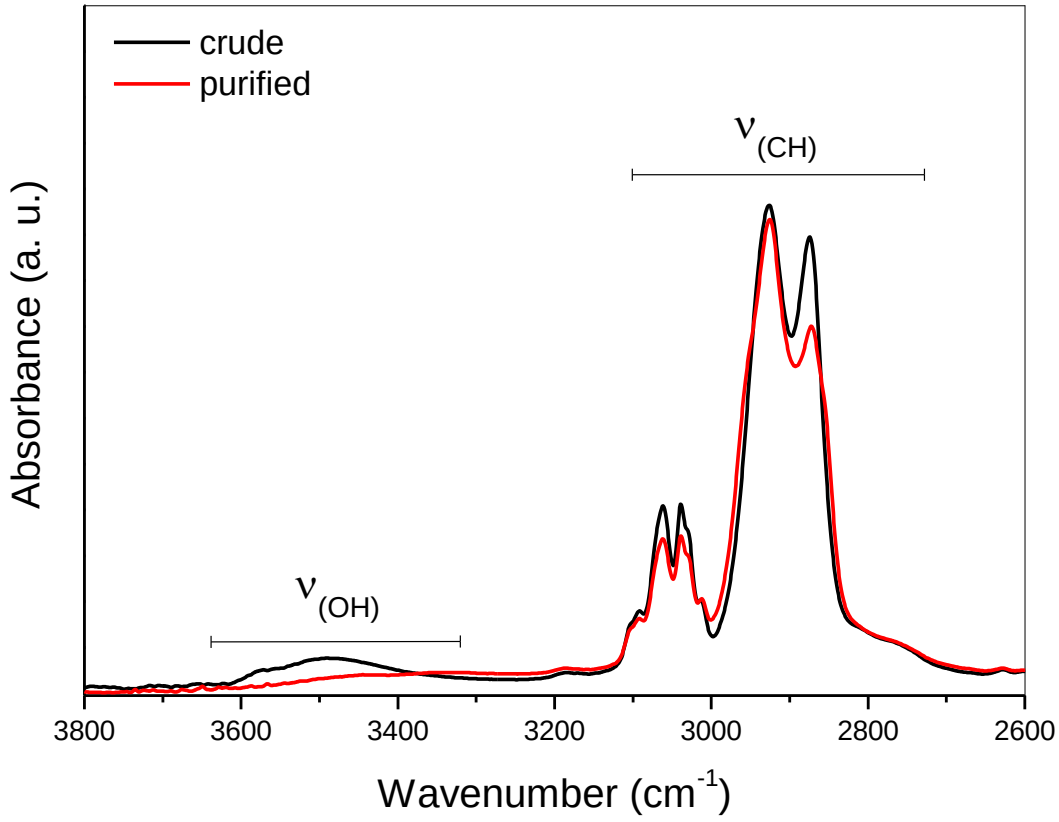

Figure B14. FTIR spectra of crude and purified cyclic poly(GPE)$_{11K}$.

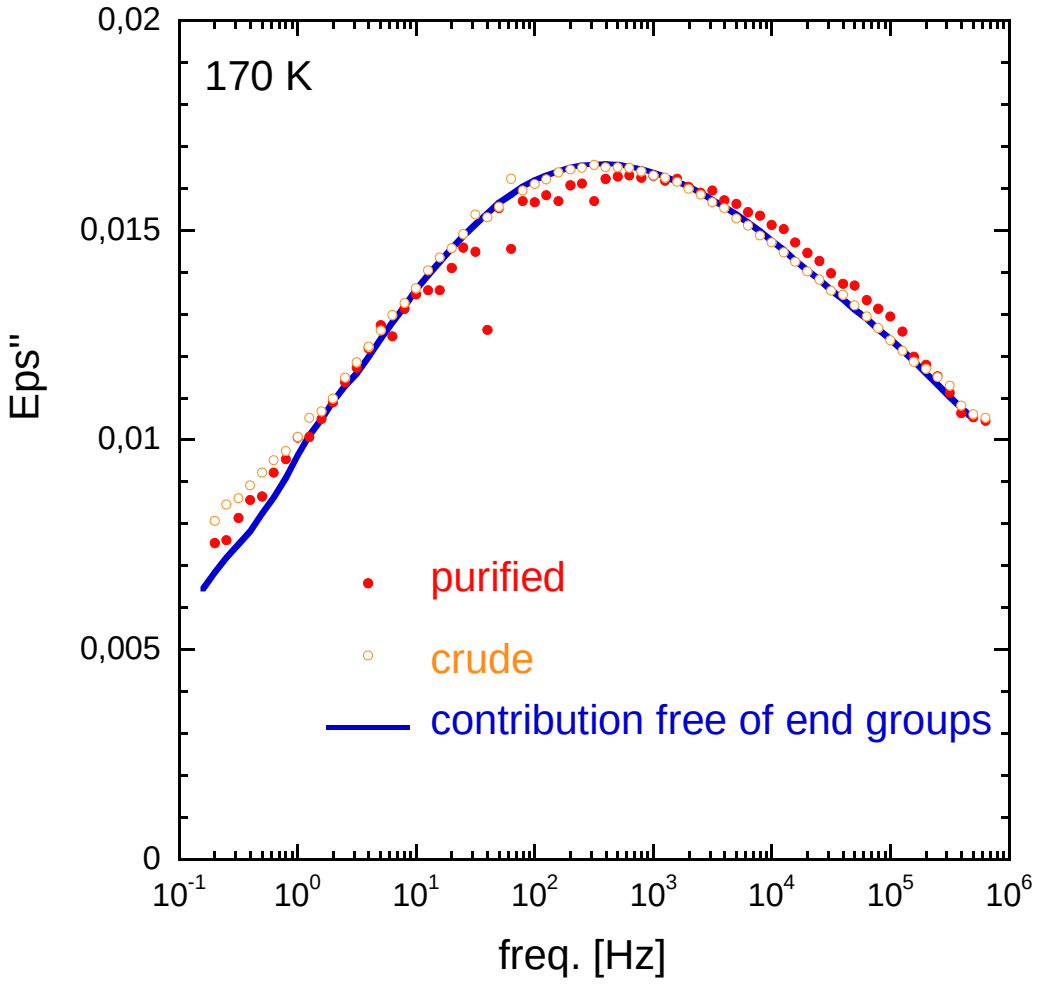

Figure B15. Frequency dependence of the ε'' for the β-relaxation of crude and purified poly(GPE)$_{11K}$ sample at 170K. Solid line shows the contribution to local dynamics of side groups (end groups are excluded), as previously obtained from linear poly(GPE) samples in reference S[1].

REFERENCES

1. Gambino, T.; Martínez de Ilarduya, A.; Alegría, A.; Barroso-Bujans, F., Dielectric relaxations in poly(glycidyl phenyl ether): effects of microstructure and cyclic topology. *Macromolecules* **2016,** *49* (3), 1060-1069.

APPENDIX C

SUPPORTING INFORMATION FOR A MALDI-TOF MS STUDY OF MACROCYCLIC POLYETHERS GENERATE BY ELECTROPHILIC ZWITTERIONIC RING EXPANSION POLYMERIZATION OF MONOSUBSTITUTED EPOXIDES WITH $B(C_6F_5)_3$[*]

[*]A portion of this work has been reproduced from Haque, F.; Schexnayder, C.; Matxain, J.; Barroso-Bujans, F.; Grayson, S. A MALDI-ToF MS study of macrocyclic polyethers generated by electrophilic zwitterionic ring expansion polymerization of monosubstituted epoxides with $B(C_6F_5)_3$. *Macromolecules,* **under review**.

Scheme C1. The proposed mechanism of the TP-OH tadpole formation is based on a dimerization event occurring during the polymerization. The work of Aoshima and coworkers describes the ability of vinyl ethers to react with epoxides in the presence of B(C6F5)3 providing additional support of the proposed intermolecular dimerization presented here.[1, 2]

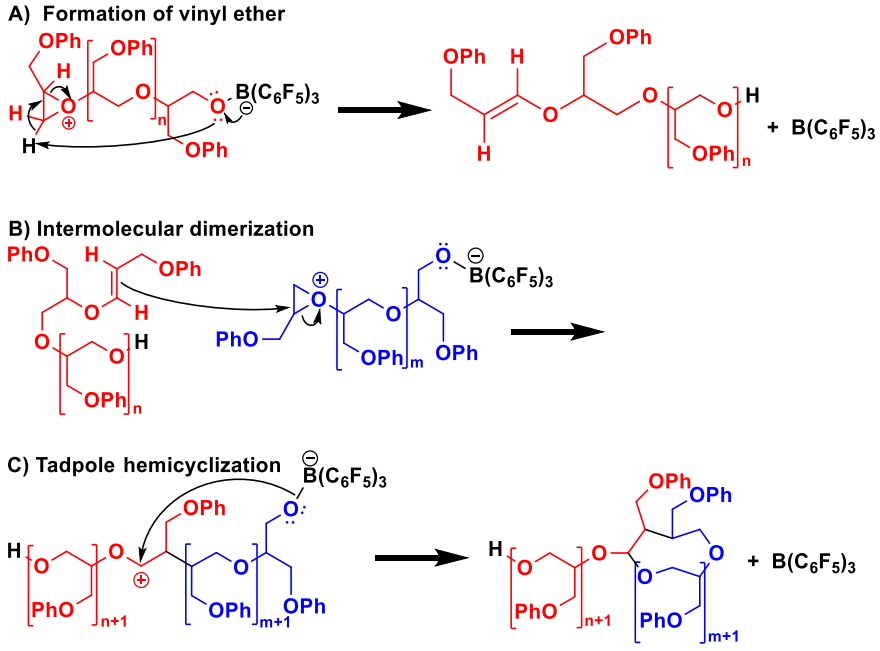

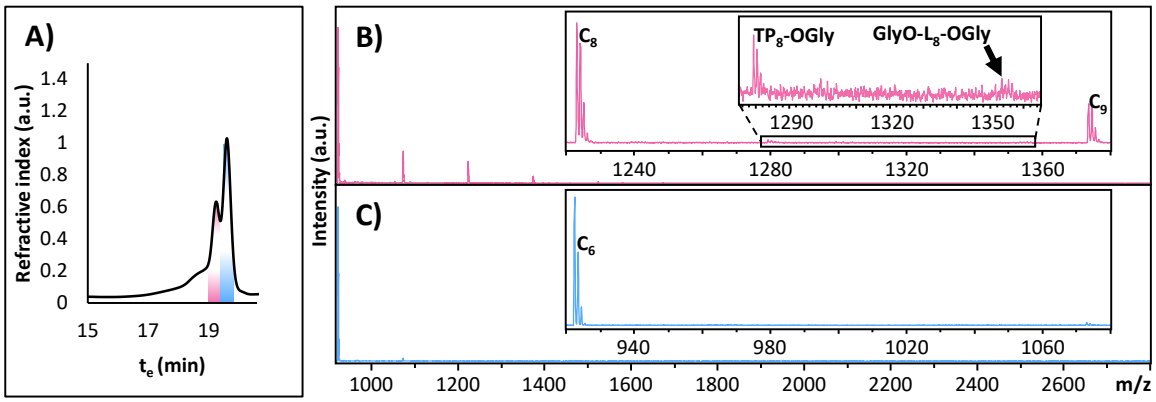

Figure C1. Poly(PGE) was purified via "click-scavenging" and fractionated by SEC (A), and the corresponding MALDI-ToF mass spectra of each SEC fraction is shown (B and C). Identification of signals is based on the end group functionalization performed in a previous study.[3] The spectra were acquired in reflector mode, and all signals represent the sodiated adducts.

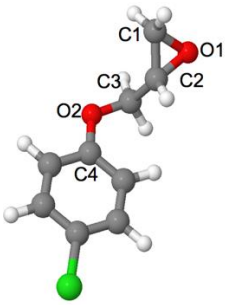

Figure C2. Atomic labeling within the X-PGE monomers, where X = H, Cl, NH2, and CN.

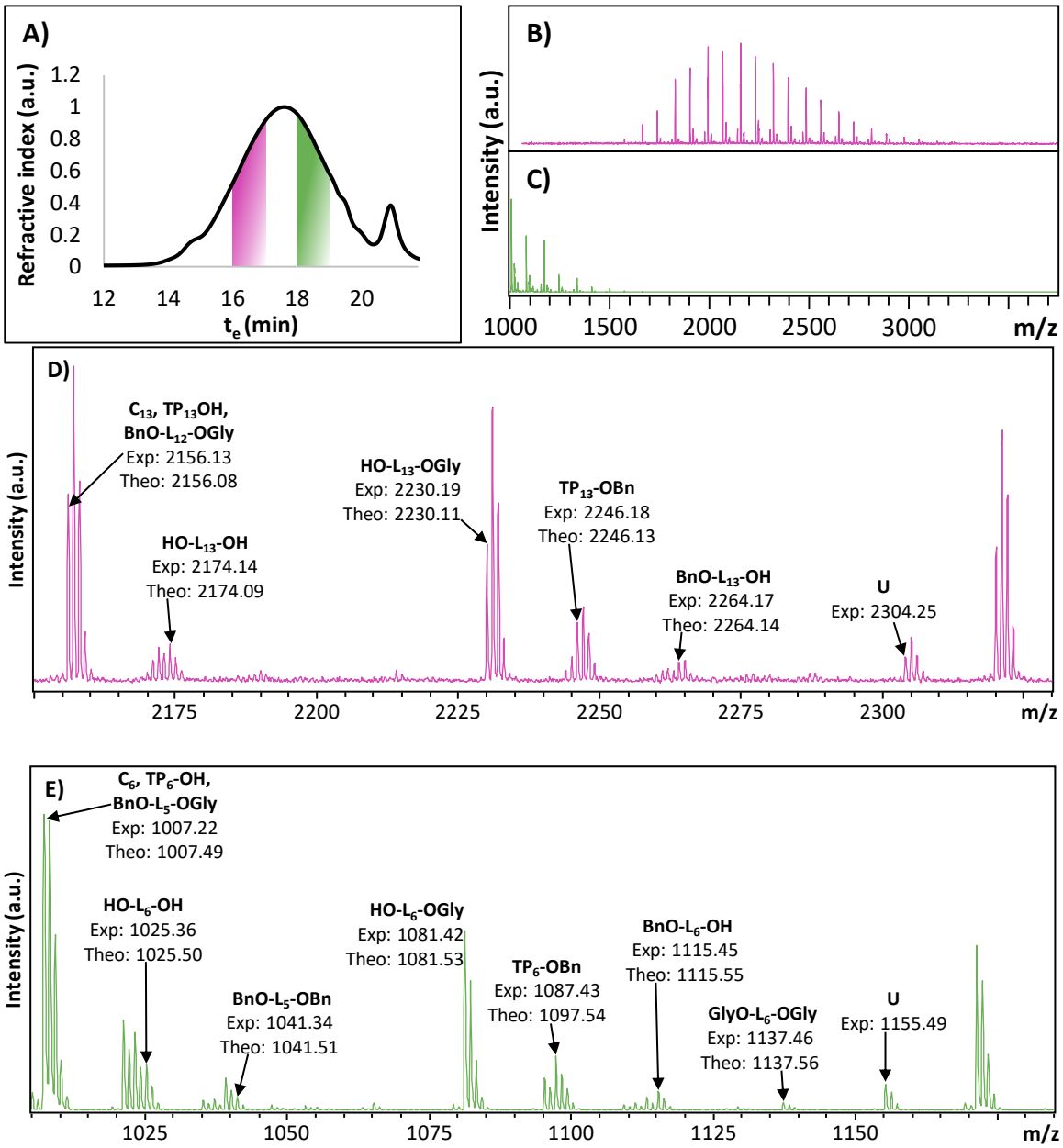

Figure C3. Poly(BGE) was fractionated by SEC (A), and the corresponding MALDI-ToF mass spectra of each SEC fraction is shown with full spectra (B and C) and corresponding insets (D and E).

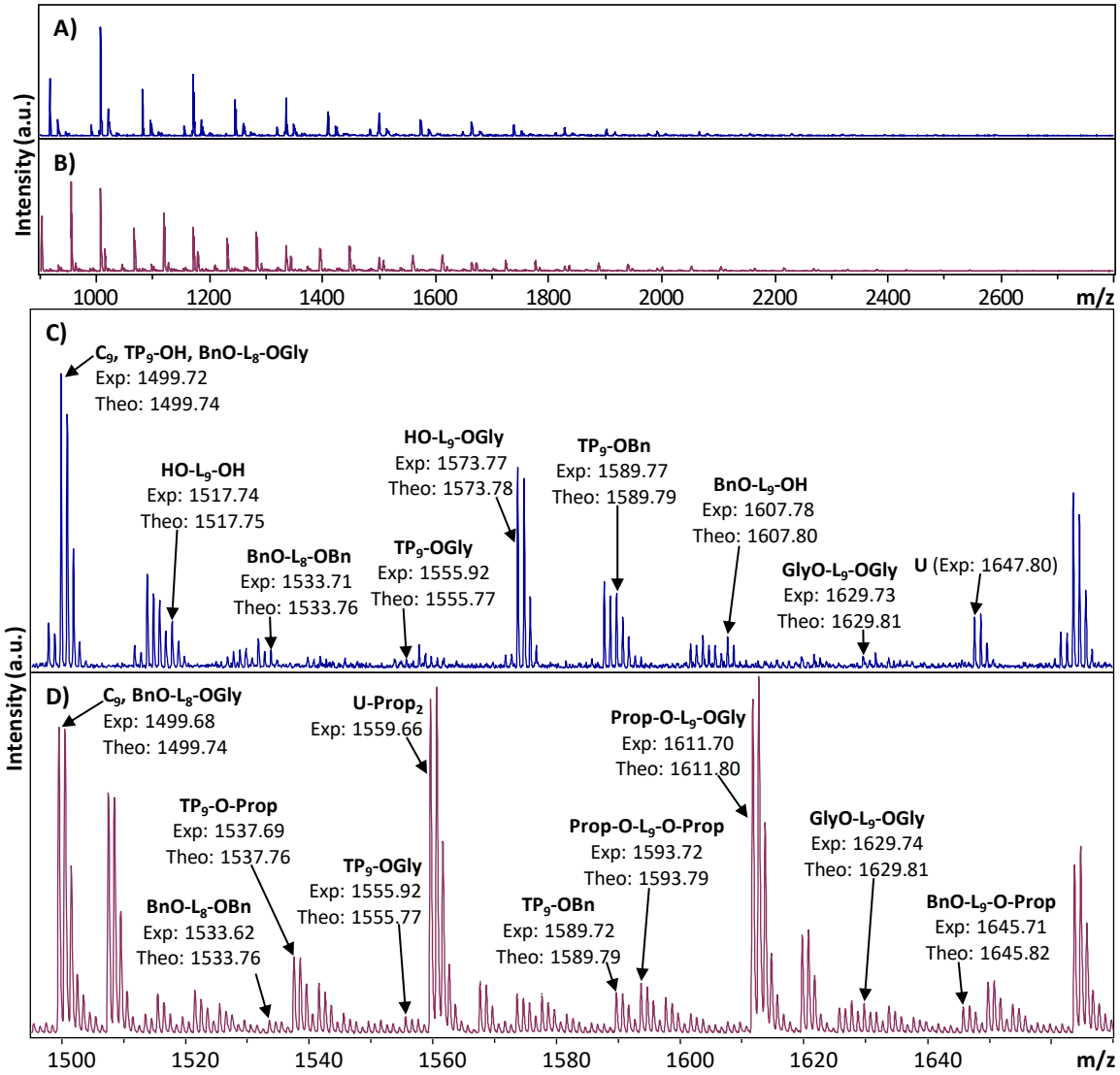

Figure C4. MALDI-ToF mass spectra of crude poly(BGE) (A,C) and propargylated poly(BGE) (B, D). Identification of signals is based on the end group functionalization. The spectra were acquired in positive reflector mode, and all signals represent the sodiated adducts.

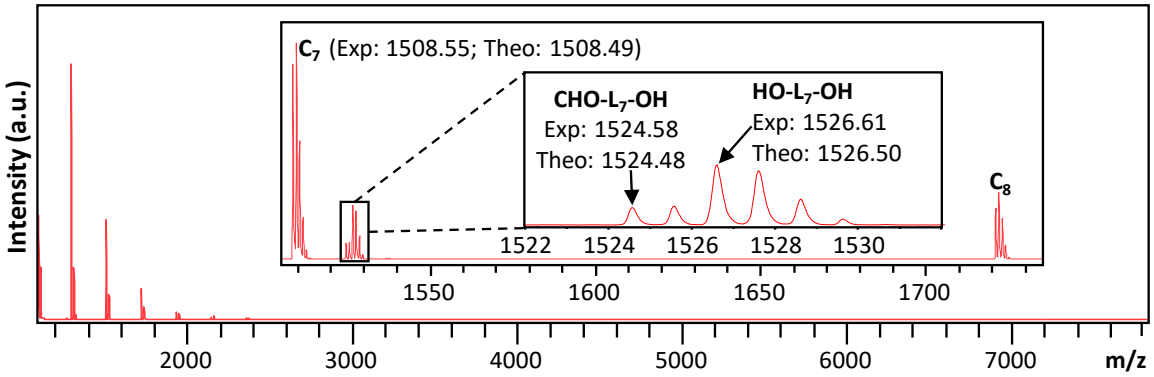

Figure C5. MALDI-ToF mass spectra of the mid-molecular weight fraction of poly(ETD) collected via SEC. Identification of signals is based on the end group functionalization (Figure C5). The expanded spectra illustrates that there are two overlapping signals, CHO-L7-OH and HO-L7-OH. The spectrum was acquired in positive reflector mode, and all signals represent the sodiated adducts.

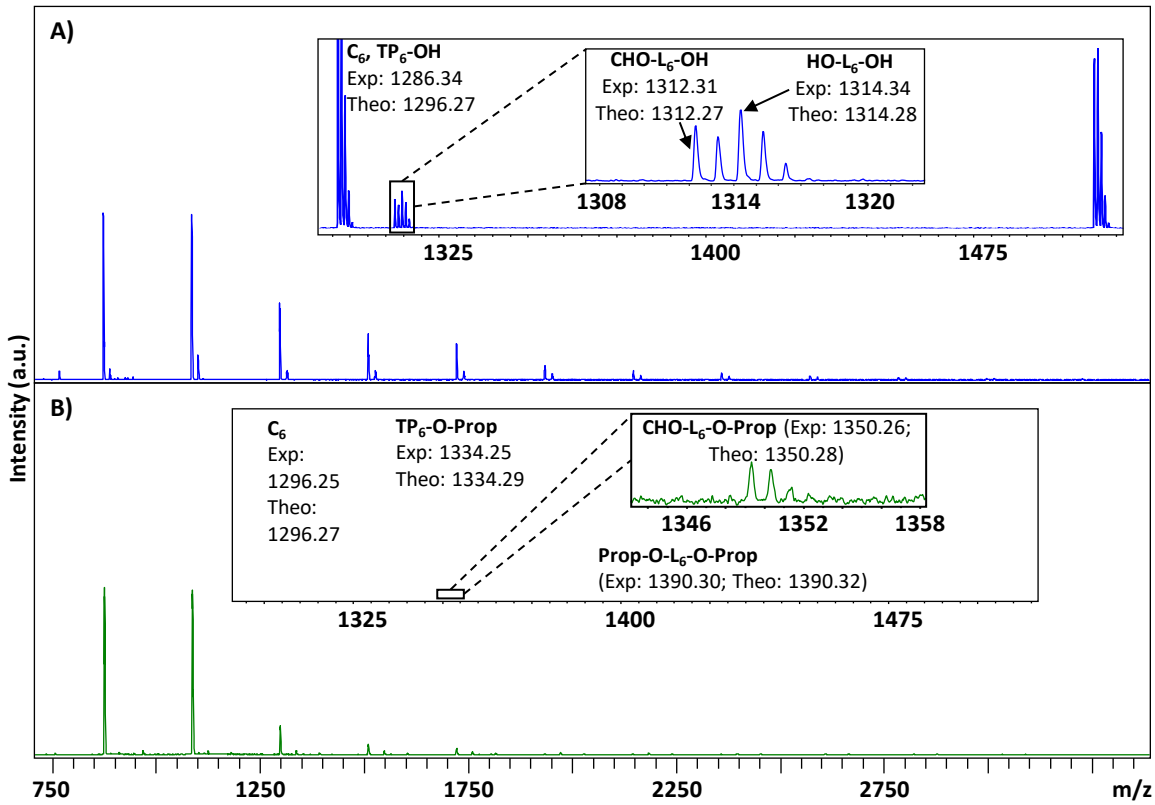

Figure C6. MALDI-ToF mass spectra of crude poly(ETD) (A) and propargylated poly(ETD) (B). Identification of signals is based on the end group functionalization. The spectra were acquired in positive reflector mode, and all signals represent the sodiated adducts.

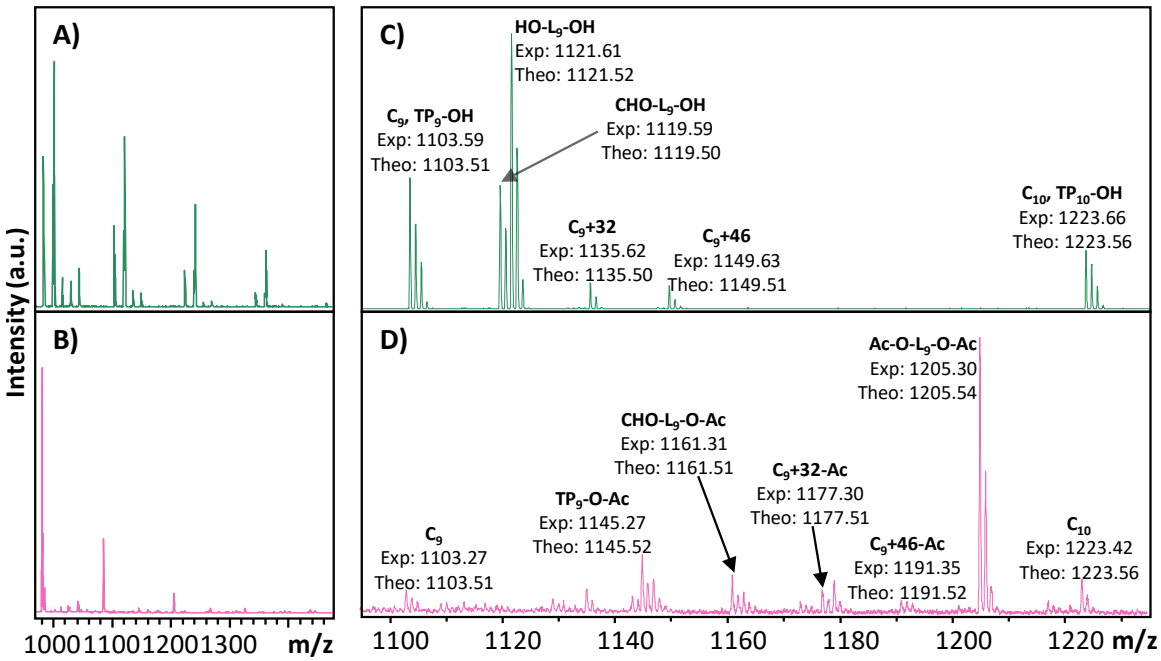

Figure C7. MALDI-ToF mass spectra of the low molecular poly(SO) fraction before (A,C) and after acetylation (B, D). Identification of signals is based on the end group functionalization. The spectra were acquired in positive reflector mode, and all signals represent the sodiated adducts.

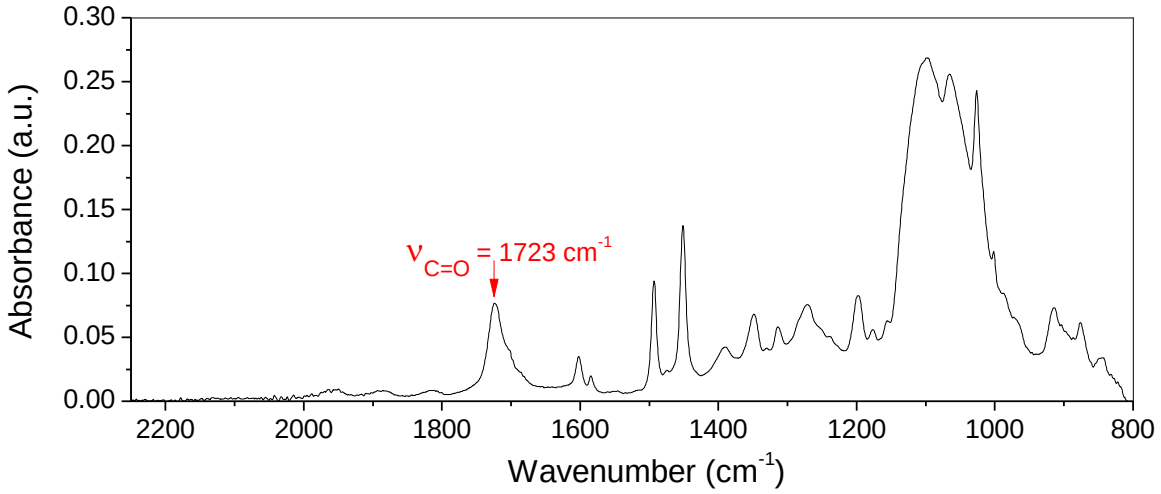

Figure C8. FTIR data of poly(SO) indicating the formation of carbonyl groups in the SO polymer series resulting from the initiation of polymerization with phenylacetaldehyde.

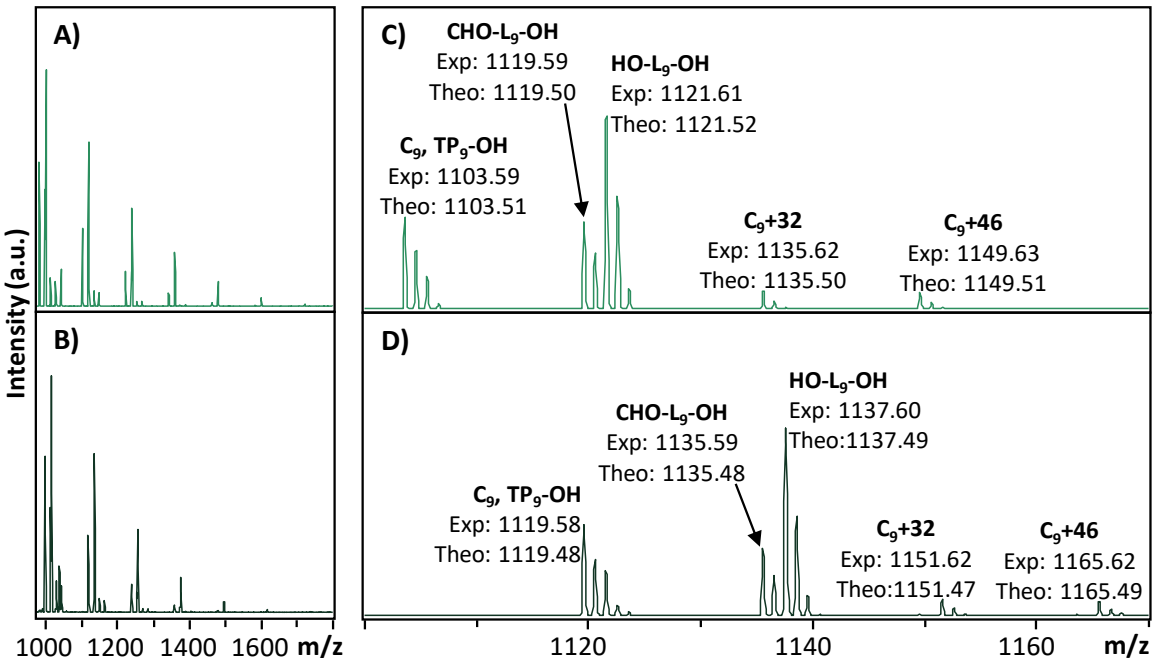

Figure C9. MALDI-ToF mass spectra of the low molecular poly(SO) fraction collected using Na+ as a cation (A, C) and K+ as a cation (B, D). All signals shift by a nominal mass of + 16 m/z from the Na+ (C) to K+ (D) spectra, confirming the assignment of signals is based on the proposed structure plus the added cation source.

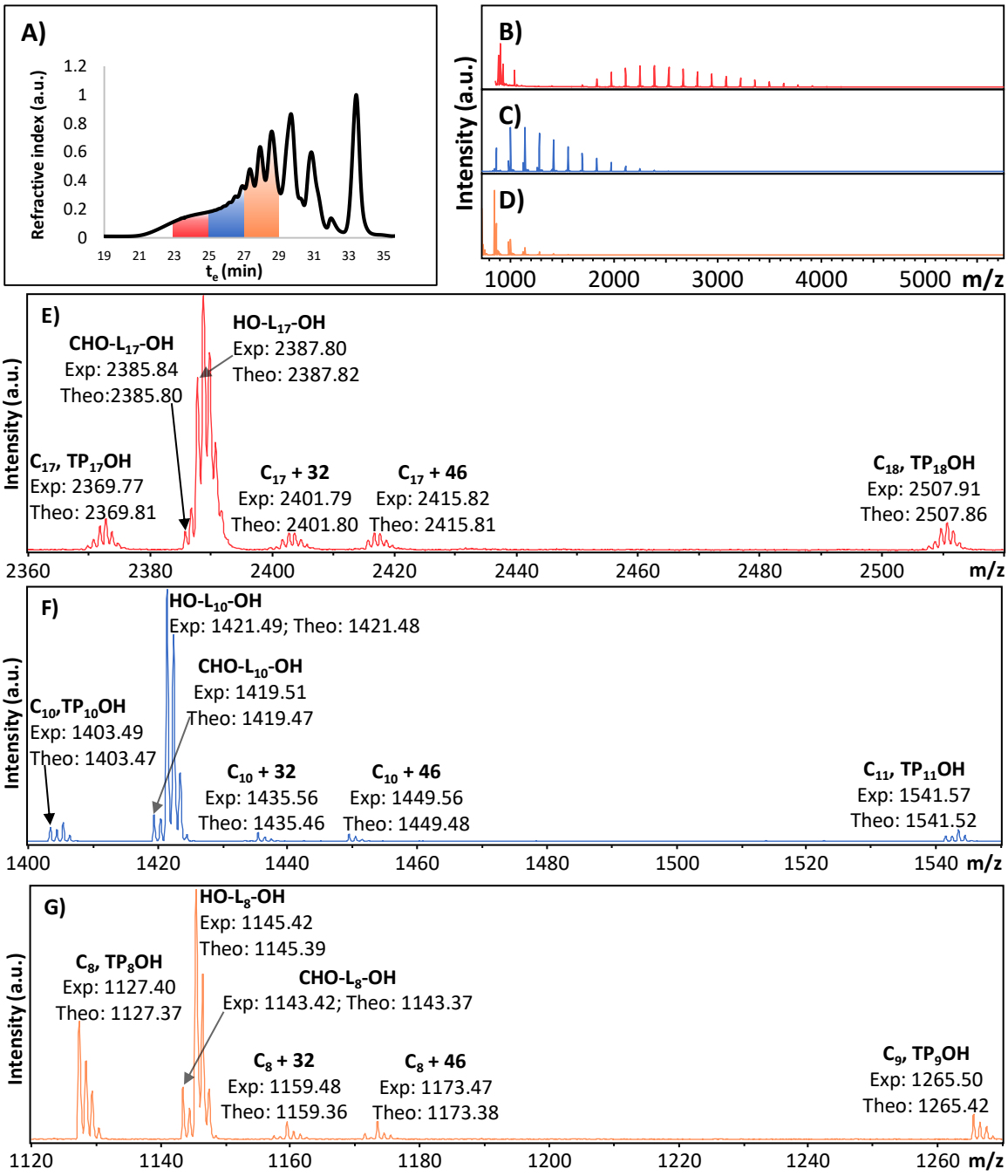

Figure C10. MALDI-ToF mass spectra of poly(F-SO) fractionated via SEC. The spectra were acquired in positive reflector mode, and all signals represent the sodiated adducts.

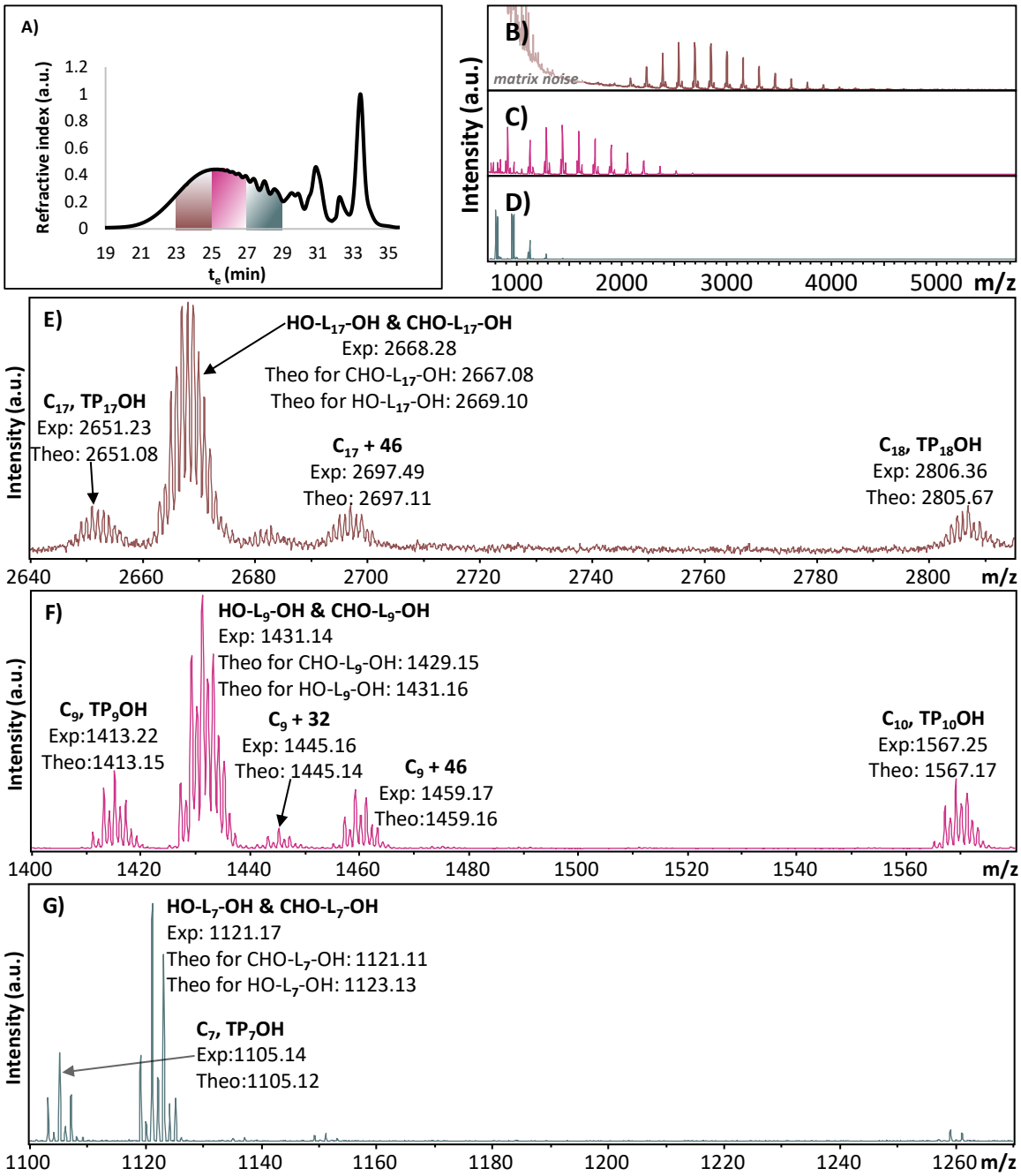

Figure C11. MALDI-ToF mass spectra of poly(Cl-SO) fractionated via SEC. The structure assignments were based on the isotopic peak of maximum intensity based on calculating the isotopic distribution using enviPat Web 2.4.[4] Normally structure assignments are made based on the M+ signal, however, the M+ signal for poly(Cl-SO) is very weak in intensity due to its minimal abundance. Furthermore, HO-L-OH and CHO-L-OH cannot be differentiated from each other due to their overlaying isotopic distributions and only having a m/z difference of + 2 m/z. Consequently, both theoretical values are listed for what is assumed to be a signal representing two different structures. The spectra were acquired in positive reflector mode, and all signals represent the sodiated adducts.

Table C1. Calculated ΔH (kcal/mol) values for all species and substituents required for the formation of complexes C_1, C_1' and C_1'' during the polymerization of X-PGE, where X = H, Cl, NH2, and CN.

	X=H	**X=Cl**	**X=NH₂**	**X=CN**
React	0.00	0.00	0.00	0.00
C_1	-12.79	-12.96	-14.28	-12.31
C_1'	-3.32	-2.52	-6.45	0.27
C_1''	-8.61	-9.76	-9.46	-9.62

Table C2. Relevant bond distances (in Å) for the C_1, C_1' and C_1'' complexes for H, all X-PGE, where X= H, Cl, NH_2, and CN. (See Figure C2 for atomic labels)

	X=H				**X=Cl**			
	X-PGE	**C_1**	**C_1'**	**C_1''**	**X-PGE**	**C_1**	**C_1'**	**C_1''**
B-O1	-	1.661	-	-	-	1.664	-	-
B-O2	-	-	1.719	4.356	-	-	1.734	4.442
O1-C1	1.453	1.472	1.440	1.443	1.448	1.472	1.440	1.443
O1-C2	1.451	1.495	1.439	1.447	1.445	1.495	1.438	1.446
O2-C3	1.445	1.427	1.492	1.439	1.441	1.428	1.493	1.443
O2-C4	1.380	1.383	1.440	1.373	1.371	1.379	1.433	1.377
	X=NH₂				**X=CN**			
	X-PGE	**C_1**	**C_1'**	**C_1''**	**X-PGE**	**C_1**	**C_1'**	**C_1''**
B-O1	-	1.654	-	-	-	1.668	-	-
B-O2	-	-	1.698	-	-	-	1.818	4.463
O1-C1	1.448	1.473	1.440	1.443	1.448	1.472	1.440	1.443
O1-C2	1.446	1.499	1.439	1.447	1.443	1.493	1.438	1.445
O2-C3	1.436	1.424	1.490	1.436	1.446	1.433	1.491	1.446
O2-C4	1.383	1.394	1.444	1.381	1.361	1.370	1.419	1.360

Table C3. Cartesian coordinates for the following reactants: X-PGE and $B(C_6F_5)_3$, where X = H, Cl, NH_2, and CN.

$B(C_6F_5)_3$			
B	0.000000	0.000000	-0.001379
C	0.388562	1.297114	-0.782327
C	1.093349	3.651556	-2.197950
C	1.149815	1.263809	-1.960563
C	0.000000	2.575012	-0.352357
C	0.324507	3.737960	-1.038677
C	1.515269	2.406319	-2.660504
C	0.000000	0.000000	1.561889
C	0.000000	0.000000	4.397856
C	0.977783	0.671407	2.311321

C	-0.977783	-0.671407	2.311321
C	-1.001719	-0.672281	3.699923
C	1.001719	0.672281	3.699923
C	-0.388562	-1.297114	-0.782327
C	-1.093349	-3.651556	-2.197950
C	-1.149815	-1.263809	-1.960563
C	0.000000	-2.575012	-0.352357
C	-0.324507	-3.737960	-1.038677
C	-1.515269	-2.406319	-2.660504
F	-0.089866	4.937676	-0.601613
F	-0.756813	2.714723	0.756044
F	1.425316	4.761006	-2.865087
F	2.265041	2.327107	-3.771194
F	1.596045	0.085890	-2.444455
F	-1.596045	-0.085890	-2.444455
F	0.756813	-2.714723	0.756044
F	0.089866	-4.937676	-0.601613
F	-2.265041	-2.327107	-3.771194
F	-1.425316	-4.761006	-2.865087
F	-1.971414	-1.309713	4.374789
F	0.000000	0.000000	5.734387
F	1.977920	1.326480	1.685548
F	1.971414	1.309713	4.374789
F	-1.977920	-1.326480	1.685548

H-PGE			
C	-2.213427	0.353280	0.262320
H	-1.630725	1.064483	0.846689
C	-3.332687	-0.330217	0.918373
H	-3.652895	-1.302773	0.548168
H	-3.555267	-0.116465	1.961643
C	-1.523764	-0.273491	-0.927664
H	-1.210918	0.484816	-1.655110
H	-2.206673	-0.969410	-1.419995
O	-0.396780	-1.072195	-0.521343
C	0.793654	-0.440763	-0.248928
C	3.318045	0.628109	0.334762
C	1.846453	-1.285552	0.128964
C	1.002917	0.940500	-0.332904

C	2.266874	1.461700	-0.041026
C	3.097204	-0.750473	0.418160
H	1.663813	-2.354343	0.187798
H	0.203630	1.615785	-0.616616
H	2.419771	2.535361	-0.108226
H	3.905384	-1.415682	0.709550
H	4.294971	1.043552	0.561833
O	-3.573558	0.771709	0.010333

Cl-PGE			
C	-2.162483	1.211261	0.316625
C	-2.519887	-0.110787	0.047231
C	-1.570831	-1.032288	-0.380408
C	-0.241995	-0.634792	-0.543746
C	0.126849	0.689114	-0.279760
C	-0.840909	1.606907	0.151785
O	1.394978	1.193036	-0.416726
C	2.443119	0.312169	-0.867359
C	2.978728	-0.532200	0.265826
O	4.291090	-1.085461	0.024410
C	4.130363	-0.077532	1.051665
H	2.281198	-1.228555	0.730072
H	4.586017	0.883864	0.820572
H	4.262636	-0.440293	2.068697
H	2.086594	-0.307971	-1.698216
H	3.231566	0.971432	-1.236363
H	-0.542354	2.630897	0.353093
H	0.483108	-1.370398	-0.871896
H	-1.857935	-2.058207	-0.583809
H	-2.910213	1.922613	0.650016
Cl	-4.186287	-0.615006	0.255012

NH_2-PGE			
C	-2.613144	1.032209	0.339269
C	-2.943762	-0.318774	0.134270
C	-1.924163	-1.189194	-0.270604
C	-0.617653	-0.735880	-0.470037
C	-0.305826	0.610686	-0.267534
C	-1.315643	1.488745	0.142107

O	0.944456	1.175415	-0.444864
C	2.014950	0.324387	-0.883019
C	2.609267	-0.456500	0.267316
O	3.932284	-0.982338	0.013675
C	3.767022	0.063285	1.001861
H	1.946015	-1.152706	0.779441
H	4.187538	1.026892	0.718621
H	3.938017	-0.251491	2.029252
H	1.670247	-0.344690	-1.681405
H	2.771843	0.996470	-1.294691
H	-1.069612	2.534341	0.302661
H	0.137773	-1.450685	-0.777064
H	-2.147289	-2.241163	-0.432632
H	-3.383145	1.732748	0.653960
N	-4.272202	-0.762371	0.259437
H	-4.828374	-0.218552	0.911153
H	-4.357810	-1.752973	0.462390

CN-PGE			
C	-2.296112	1.198637	0.322171
C	-2.675486	-0.132922	0.059120
C	-1.706089	-1.052579	-0.371326
C	-0.383366	-0.660598	-0.538372
C	-0.014784	0.667642	-0.277852
C	-0.980879	1.591923	0.154503
O	1.244339	1.166349	-0.417349
C	2.302148	0.289470	-0.868612
C	2.845256	-0.542628	0.269186
O	4.166375	-1.073340	0.032272
C	3.986666	-0.067216	1.058001
H	2.157136	-1.249741	0.731341
H	4.427206	0.901183	0.827371
H	4.120586	-0.427145	2.075680
H	1.946009	-0.334886	-1.695401
H	3.080993	0.956903	-1.241622
H	-0.675369	2.614320	0.351047
H	0.343665	-1.394239	-0.865225
H	-1.991295	-2.079845	-0.572245
H	-3.039939	1.914480	0.655551

C	-4.028640	-0.542883	0.230319
N	-5.135284	-0.876884	0.370184

Table C4. Cartesian coordinates for complexes C_1 and C_1' that result from $B(C_6F_5)_3$ coordinating with the epoxide oxygen and the glycidyl ether oxygen, respectively, in X-PGE, where X = H, Cl, NH_2, and CN

		C_1-H	
B	-0.489299	-0.148560	0.297479
C	-0.808451	1.402576	-0.099192
C	-1.560169	3.984475	-1.057470
C	-1.322270	1.622919	-1.381325
C	-0.699058	2.553525	0.681045
C	-1.058090	3.822898	0.227246
C	-1.694273	2.865953	-1.874838
C	0.780906	-0.817229	-0.459432
C	3.065893	-2.052555	-1.651998
C	1.657964	-0.130529	-1.308512
C	1.117256	-2.161347	-0.264119
C	2.227207	-2.784399	-0.817904
C	2.768425	-0.720718	-1.908753
C	-1.909247	-0.948932	0.247923
C	-4.529694	-2.079809	0.102029
C	-2.978574	-0.511940	1.039801
C	-2.248180	-1.956715	-0.661752
C	-3.517824	-2.525073	-0.741298
C	-4.258011	-1.054245	1.001530
F	3.557755	-0.011393	-2.733749
F	1.468539	1.171080	-1.613127
F	4.146338	-2.626186	-2.201239
F	2.492068	-4.079658	-0.565381
F	0.324600	-2.951816	0.514903
F	-1.445402	0.570963	-2.230903
F	-2.168933	3.001314	-3.127430
F	-1.910761	5.201492	-1.505115
F	-0.927808	4.895864	1.032467
F	-0.234206	2.513968	1.956774
F	-1.353028	-2.413406	-1.564493
F	-3.777738	-3.494776	-1.637021
F	-5.754637	-2.622358	0.040256

F	-5.229352	-0.593566	1.811077
F	-2.795734	0.519624	1.907464
C	-0.586566	-0.648746	3.088278
H	-0.778352	0.107343	3.841676
H	-1.377557	-1.362572	2.887619
C	0.786392	-1.022940	2.732670
C	1.980876	-0.459516	3.446904
H	1.859774	0.606726	3.661372
H	2.062584	-0.996555	4.398207
O	3.196457	-0.743079	2.755724
C	3.643084	0.138668	1.789059
C	4.767291	1.794061	-0.161239
C	4.810490	-0.256567	1.126318
C	3.026234	1.350481	1.472054
C	3.601704	2.172785	0.499463
C	5.365567	0.570846	0.155709
H	5.265334	-1.208018	1.384316
H	2.105731	1.662312	1.949622
H	3.113697	3.111012	0.252393
H	6.268083	0.254865	-0.359564
H	5.198507	2.434436	-0.923974
H	0.927471	-1.987283	2.262052
O	0.016370	-0.069093	1.877444

	C_1'-H		
C	3.265600	-2.043435	-0.702269
C	3.970958	-1.196940	-1.552951
C	3.395069	0.007112	-1.937379
C	2.122630	0.343527	-1.477738
C	1.360283	-0.481052	-0.646782
C	2.002961	-1.664908	-0.271301
B	-0.067696	-0.094291	0.015958
C	-0.808401	1.242024	-0.550106
C	-1.126313	1.240262	-1.913461
C	-1.847573	2.239933	-2.551364
C	-2.312195	3.319842	-1.805827
C	-2.049261	3.359555	-0.442926
C	-1.323936	2.329487	0.156856
F	-3.011462	4.303261	-2.395296

F	-0.721671	0.198870	-2.684355
F	-1.153486	2.448456	1.495354
F	-2.506249	4.389030	0.295709
F	-2.103087	2.174921	-3.871602
F	5.197809	-1.532020	-1.979355
F	1.399345	-2.500753	0.615956
F	1.672828	1.558986	-1.863587
F	4.077449	0.848434	-2.735881
F	3.822188	-3.198007	-0.289881
C	-1.220828	-1.250477	0.008016
C	-1.216589	-2.373714	-0.830763
C	-2.292353	-3.251958	-0.950011
C	-3.455777	-3.028241	-0.224005
C	-3.529083	-1.910293	0.599805
C	-2.436945	-1.054554	0.678764
F	-4.494486	-3.869945	-0.324099
F	-0.161251	-2.659622	-1.624099
F	-2.597650	0.033834	1.472695
F	-4.650448	-1.662594	1.300499
F	-2.215761	-4.313561	-1.772930
O	0.433887	0.210495	1.631317
C	0.036775	-0.652593	2.781549
C	1.739601	0.800869	1.769598
C	2.812618	0.031029	2.206252
C	4.072786	0.622868	2.285861
C	4.250545	1.958698	1.924989
C	3.158323	2.708520	1.491975
C	1.888383	2.134048	1.416554
H	2.691249	-1.013631	2.465840
H	4.916365	0.026945	2.619737
H	5.235297	2.411399	1.982253
H	3.283554	3.749634	1.211924
H	1.040439	2.715300	1.086658
H	0.727185	-1.495592	2.823808
C	0.032517	0.132188	4.054804
H	-0.956465	-1.006704	2.536052
C	-0.951620	-0.211143	5.093445
H	0.980372	0.568950	4.364050
H	-0.695846	-0.036799	6.136127

H	-1.683284	-0.994314	4.902200
O	-1.110894	0.973097	4.289918

		C_1-Cl	
C	5.029240	-0.454951	0.454242
C	4.639385	0.860337	0.197438
C	3.541505	1.417405	0.842311
C	2.815234	0.654871	1.758360
C	3.205480	-0.658304	2.027116
C	4.310217	-1.212485	1.370826
O	2.586770	-1.491926	2.935245
C	1.387497	-1.053638	3.575486
C	0.170063	-1.370449	2.755471
O	-0.376422	-0.254023	1.925206
C	-1.147868	-0.799589	3.053419
B	-0.788724	-0.165992	0.315179
C	-2.342316	-0.633720	0.156807
C	-3.335748	-0.015228	0.925962
C	-4.697616	-0.261053	0.795240
C	-5.131845	-1.153462	-0.179429
C	-4.192813	-1.767088	-1.001045
C	-2.837092	-1.496604	-0.827380
F	-6.439363	-1.409540	-0.331724
F	-2.983548	0.902049	1.866284
F	-2.009641	-2.097166	-1.710326
F	-4.603409	-2.610398	-1.965492
F	-5.591566	0.358309	1.587758
C	-0.740659	1.429554	-0.024617
C	-1.090992	1.796577	-1.328203
C	-1.152500	3.105806	-1.785391
C	-0.855512	4.142778	-0.905650
C	-0.508508	3.835894	0.403526
C	-0.462837	2.504954	0.818981
F	-0.905205	5.420345	-1.316638
F	-1.365619	0.823277	-2.233778
F	-0.129860	2.326233	2.124101
F	-0.225267	4.829047	1.269345
F	-1.484154	3.380071	-3.060745
C	0.345592	-1.074209	-0.405794

C	1.404187	-0.576574	-1.175764
C	2.390063	-1.383453	-1.740953
C	2.362659	-2.756296	-1.532487
C	1.330255	-3.306064	-0.779092
C	0.358319	-2.465193	-0.254565
F	3.317838	-3.541780	-2.050271
F	1.529686	0.742909	-1.431056
F	-0.636122	-3.077135	0.450262
F	1.279966	-4.635130	-0.574527
F	3.372881	-0.844146	-2.482040
H	-1.271450	-0.069676	3.845851
H	-2.026247	-1.359765	2.752491
H	1.425866	0.003016	3.857850
H	1.321410	-1.653350	4.489093
H	4.595468	-2.237160	1.586423
H	1.950057	1.100814	2.231386
H	3.235424	2.434417	0.624116
H	5.881113	-0.883193	-0.062217
Cl	5.532839	1.812735	-0.967773
H	0.191061	-2.315447	2.228384

C_1'-Cl			
C	2.138878	1.748881	0.881559
C	1.758872	0.525757	1.415112
C	2.698566	-0.417839	1.818277
C	4.053605	-0.133597	1.672636
C	4.440154	1.086121	1.118943
C	3.495298	2.030455	0.725887
O	0.357984	0.231939	1.494987
C	-0.058473	-0.383859	2.789972
C	0.278475	0.518698	3.934072
O	-0.602832	1.633833	4.155040
C	-0.616742	0.548850	5.101639
B	-0.397229	-0.149633	-0.018721
C	-1.756202	-1.008721	0.252355
C	-2.092571	-2.192978	-0.418448
C	-3.333840	-2.816906	-0.306828
C	-4.322888	-2.257585	0.493126
C	-4.056611	-1.064377	1.156002

C	-2.809363	-0.470029	1.005873
F	-1.229290	-2.794120	-1.265599
F	-3.585691	-3.955328	-0.977581
F	-5.518114	-2.851989	0.614783
F	-5.003552	-0.494181	1.922420
F	-2.637905	0.711590	1.650177
C	0.830941	-0.920682	-0.740169
C	1.656744	-0.381757	-1.730223
C	2.777162	-1.037196	-2.238798
C	3.126108	-2.288389	-1.746543
C	2.351465	-2.860386	-0.741054
C	1.247706	-2.168446	-0.264998
F	2.695649	-4.055321	-0.225742
F	4.204629	-2.929442	-2.219035
F	3.532376	-0.459865	-3.190393
F	1.431094	0.851656	-2.235871
F	0.584251	-2.744602	0.773329
C	-0.898547	1.244502	-0.693232
C	-1.366135	1.156182	-2.009899
C	-1.931234	2.211002	-2.712996
C	-2.068497	3.446043	-2.085311
C	-1.645011	3.583486	-0.769931
C	-1.086885	2.493913	-0.100543
F	-1.280812	-0.031235	-2.661687
F	-2.347172	2.052591	-3.983232
F	-2.609752	4.485680	-2.740252
F	-1.785133	4.767138	-0.143138
F	-0.736934	2.726342	1.187605
H	2.400363	-1.375943	2.226106
H	4.798551	-0.861294	1.973186
Cl	6.137297	1.432454	0.916497
H	3.808550	2.978185	0.303561
H	1.398710	2.476720	0.584252
H	0.433468	-1.353635	2.874836
H	-1.128559	-0.522414	2.699107
H	1.332402	0.745042	4.085676
H	-0.195422	0.776432	6.078166
H	-1.525843	-0.049910	5.097131

C_1-NH_2			
C	4.979909	-0.072435	0.248961
C	4.544418	1.198876	-0.162867
C	3.535867	1.825280	0.582966
C	2.974416	1.208410	1.699077
C	3.418552	-0.053899	2.091797
C	4.420031	-0.693362	1.360163
O	2.965742	-0.722124	3.228162
C	1.635640	-0.459162	3.662639
C	0.616557	-1.086576	2.746914
O	-0.219163	-0.149120	1.928295
C	-0.826241	-0.977909	2.983319
B	-0.608205	-0.154286	0.320260
C	-2.136067	-0.718655	0.209976
C	-3.143624	-0.157589	1.003495
C	-4.489216	-0.495331	0.916642
C	-4.891342	-1.430808	-0.031254
C	-3.937545	-1.998336	-0.868662
C	-2.598455	-1.635637	-0.739353
F	-6.183349	-1.775060	-0.140334
F	-2.823266	0.786856	1.926857
F	-1.753890	-2.211075	-1.624089
F	-4.317823	-2.889773	-1.802373
F	-5.399691	0.075243	1.727406
C	-0.660354	1.422861	-0.096569
C	-1.044876	1.707579	-1.411188
C	-1.191274	2.987718	-1.927466
C	-0.953375	4.080798	-1.099384
C	-0.581118	3.856541	0.219434
C	-0.449796	2.551623	0.696019
F	-1.084903	5.332814	-1.568450
F	-1.271603	0.679356	-2.268113
F	-0.103721	2.456704	2.004533
F	-0.355974	4.904816	1.036379
F	-1.549849	3.181337	-3.210956
C	0.550777	-1.039498	-0.389219
C	1.544505	-0.548639	-1.243172
C	2.535693	-1.350279	-1.806503
C	2.580488	-2.706512	-1.512401

C	1.613911	-3.249063	-0.671199
C	0.634639	-2.415122	-0.149510
F	3.543832	-3.483083	-2.030112
F	1.589807	0.753088	-1.597132
F	-0.293500	-3.012915	0.651766
F	1.635076	-4.562568	-0.379006
F	3.453136	-0.821751	-2.637119
H	-1.203187	-0.370680	3.799504
H	-1.476376	-1.758025	2.602940
H	1.432658	0.608145	3.805248
H	1.556529	-0.955654	4.634819
H	4.755374	-1.678841	1.669291
H	2.193050	1.725084	2.242988
H	3.170783	2.803220	0.279702
H	5.753940	-0.585094	-0.316620
N	5.140266	1.844392	-1.254461
H	0.972019	-1.936011	2.176739
H	5.534413	1.212921	-1.943771
H	4.546063	2.534446	-1.701801

C_1'-NH_2			
C	2.101727	1.941414	1.114248
C	1.800099	0.656081	1.539758
C	2.806686	-0.234103	1.899890
C	4.134281	0.167053	1.822569
C	4.474314	1.456962	1.371605
C	3.432530	2.335998	1.026234
O	0.417718	0.237681	1.542161
C	0.017188	-0.477878	2.785827
C	0.229015	0.390148	3.985523
O	-0.782515	1.376347	4.260202
C	-0.673011	0.239671	5.137928
B	-0.225954	-0.130611	0.014738
C	-1.533593	-1.099573	0.172074
C	-1.758097	-2.264070	-0.575053
C	-2.955406	-2.977490	-0.551728
C	-4.013663	-2.533757	0.231670
C	-3.859717	-1.364099	0.967683
C	-2.652328	-0.678587	0.905049

F	-0.821112	-2.757769	-1.414030
F	-3.097896	-4.092161	-1.292234
F	-5.168166	-3.215257	0.268369
F	-4.875901	-0.903126	1.719809
F	-2.592240	0.474859	1.616933
C	1.079253	-0.778679	-0.700606
C	1.903122	-0.129761	-1.623395
C	3.085827	-0.677198	-2.118010
C	3.501817	-1.928203	-1.681055
C	2.730394	-2.607513	-0.742815
C	1.563498	-2.019764	-0.277134
F	3.137474	-3.804620	-0.278110
F	4.641282	-2.467204	-2.141522
F	3.836216	0.003781	-3.003990
F	1.611369	1.112458	-2.072075
F	0.903274	-2.698410	0.700374
C	-0.810959	1.244796	-0.639495
C	-1.206418	1.176347	-1.980607
C	-1.820071	2.212032	-2.671570
C	-2.087746	3.404719	-2.005719
C	-1.741742	3.518651	-0.665880
C	-1.130487	2.449169	-0.010455
F	-0.995061	0.028964	-2.674570
F	-2.159352	2.074821	-3.967552
F	-2.679406	4.425553	-2.647971
F	-2.008797	4.660290	-0.001937
F	-0.867685	2.655257	1.302675
H	2.578919	-1.240884	2.229967
H	4.917490	-0.533269	2.098697
N	5.800500	1.826985	1.213525
H	3.665151	3.340459	0.684418
H	1.316443	2.633953	0.849298
H	0.600781	-1.397712	2.845076
H	-1.030762	-0.717883	2.653169
H	1.246692	0.732054	4.164729
H	-0.292340	0.454550	6.133959
H	-1.503761	-0.461780	5.082199
H	5.989525	2.821490	1.188656
H	6.481439	1.309836	1.755803

		C_1-CN	
C	5.115413	-0.361644	0.455875
C	4.714878	0.963090	0.193733
C	3.587209	1.484957	0.844379
C	2.865105	0.705803	1.740384
C	3.277941	-0.605285	2.000317
C	4.402410	-1.137491	1.352628
O	2.663744	-1.455682	2.880828
C	1.468609	-1.036693	3.551766
C	0.243274	-1.360658	2.748191
O	-0.310096	-0.248069	1.920865
C	-1.071310	-0.788581	3.058757
B	-0.731771	-0.163559	0.309238
C	-2.277874	-0.653933	0.157370
C	-3.277112	-0.049100	0.929959
C	-4.635687	-0.315105	0.804869
C	-5.060526	-1.214534	-0.167568
C	-4.115957	-1.814645	-0.992922
C	-2.763724	-1.524164	-0.824846
F	-6.364523	-1.489938	-0.314368
F	-2.934419	0.874651	1.867545
F	-1.930796	-2.111697	-1.711244
F	-4.517918	-2.663965	-1.955418
F	-5.535352	0.291654	1.600346
C	-0.706053	1.432537	-0.027960
C	-1.067808	1.795453	-1.329662
C	-1.150577	3.104110	-1.785227
C	-0.863751	4.144493	-0.906000
C	-0.504629	3.841491	0.400912
C	-0.437747	2.511007	0.814539
F	-0.934140	5.421256	-1.315223
F	-1.332319	0.818718	-2.234385
F	-0.092914	2.335055	2.117538
F	-0.229883	4.837429	1.265948
F	-1.493114	3.374525	-3.058116
C	0.415480	-1.054391	-0.412953
C	1.467627	-0.538724	-1.180053
C	2.464249	-1.329160	-1.749709

C	2.454786	-2.703649	-1.549700
C	1.430292	-3.270994	-0.798246
C	0.447844	-2.445945	-0.267938
F	3.419877	-3.473210	-2.071682
F	1.578171	0.784431	-1.424427
F	-0.535555	-3.074507	0.436846
F	1.398177	-4.601187	-0.600269
F	3.442069	-0.771612	-2.484027
H	-1.187536	-0.055850	3.849602
H	-1.951539	-1.351331	2.768554
H	1.504197	0.017181	3.841826
H	1.430580	-1.646789	4.459451
H	4.698334	-2.159347	1.565228
H	1.985075	1.127596	2.207424
H	3.264210	2.498997	0.635615
H	5.980888	-0.773276	-0.051831
C	5.439960	1.761664	-0.737144
H	0.258011	-2.308617	2.225992
N	6.033895	2.413620	-1.496525

C_1'-CN			
C	2.177076	1.658406	0.926150
C	1.796258	0.454023	1.509255
C	2.739091	-0.444775	2.004659
C	4.089360	-0.130829	1.912523
C	4.491989	1.075630	1.319083
C	3.527323	1.968108	0.825861
O	0.410642	0.149073	1.543028
C	-0.044833	-0.556964	2.774560
C	0.216681	0.273260	3.991607
O	-0.722113	1.328845	4.261844
C	-0.714537	0.177188	5.126742
B	-0.353700	-0.136067	-0.081188
C	-1.665109	-1.063031	0.142775
C	-1.935318	-2.237325	-0.574504
C	-3.145031	-2.924624	-0.498547
C	-4.166125	-2.443904	0.312786
C	-3.964920	-1.265179	1.023595
C	-2.747886	-0.604566	0.908400

F	-1.035276	-2.759302	-1.434746
F	-3.336260	-4.046804	-1.213836
F	-5.330723	-3.099861	0.400917
F	-4.943710	-0.774612	1.803806
F	-2.634651	0.552405	1.606308
C	0.921485	-0.796126	-0.813847
C	1.707941	-0.177556	-1.790758
C	2.854586	-0.754916	-2.333725
C	3.275441	-2.001914	-1.888372
C	2.543707	-2.650275	-0.896783
C	1.407965	-2.038055	-0.388766
F	2.955582	-3.842465	-0.429214
F	4.380911	-2.566318	-2.392054
F	3.567604	-0.104797	-3.269820
F	1.412167	1.058975	-2.248811
F	0.776489	-2.692943	0.620429
C	-0.884441	1.298660	-0.621838
C	-1.377004	1.298574	-1.932480
C	-1.965972	2.394518	-2.547196
C	-2.100423	3.580034	-1.829445
C	-1.650511	3.628605	-0.516345
C	-1.068732	2.500501	0.063089
F	-1.287989	0.160763	-2.667110
F	-2.405381	2.323154	-3.816708
F	-2.663869	4.657731	-2.397070
F	-1.788154	4.762951	0.195003
F	-0.692775	2.642390	1.356109
H	2.445800	-1.391000	2.441012
H	4.831970	-0.826259	2.287023
C	5.880707	1.391925	1.216907
H	3.834424	2.901756	0.368476
H	1.434455	2.345043	0.547635
H	0.455986	-1.524643	2.818118
H	-1.107216	-0.705967	2.627017
H	1.253589	0.535170	4.195368
H	-0.335459	0.350878	6.131174
H	-1.593829	-0.459728	5.047418
N	7.011752	1.647714	1.133226

Table C5. Calculated bond lengths (R in angstroms) and ΔH (kcal/mol) values for all species and substituents required for the formation of complexes C_1 and C_1' during the polymerization of ECH.

	PGE	**C_1**	**C_1'**
ΔH	-	-9.38	-4.33
B-O	-	1.649	-
B-Cl	-	-	3.335
O-C1	1.449	1.479	1.442
O-C2	1.446	1.473	1.441
Cl-C3	1.820	1.806	1.823

Table C6. Cartesian coordinates for ECH reactant and complexes C_1 and C_1' that result from $B(C_6F_5)_3$ coordinating with the epoxide oxygen and the chlorine heteroatom, respectively, in ECH.

ECH			
H	2.189900	1.584800	0.402900
C	1.644000	0.858000	-0.194600
H	1.440500	1.138700	-1.226600
O	2.067200	-0.515600	-0.012500
C	0.766800	-0.108700	0.471100
H	0.678100	-0.078900	1.556200
C	-0.382000	-0.737200	-0.265400
H	-0.211100	-0.739400	-1.341800
H	-0.594400	-1.746400	0.088300
Cl	-1.894900	0.229000	0.032600

C_1			
C	3.571581	2.797670	0.075422
C	3.533699	1.748312	0.987591
C	2.398493	0.947889	1.052235
C	1.255226	1.139712	0.267872
C	1.355132	2.193796	-0.645800
C	2.474940	3.015617	-0.751205
F	2.506440	4.017706	-1.648883
F	0.352356	2.463113	-1.511584
F	4.654925	3.584481	-0.010372
F	4.591785	1.512684	1.785806
F	2.444743	-0.082080	1.937174
F	-1.195316	2.690292	0.798538

F	-3.557027	3.547079	-0.128070
F	-5.141910	1.884834	-1.625342
F	-4.297062	-0.658847	-2.170610
F	-1.957102	-1.538060	-1.276144
C	-1.411263	0.553018	-0.239905
C	-1.915653	1.831063	0.026589
C	-3.141705	2.302254	-0.423567
C	-3.514881	0.169780	-1.456820
C	-2.276740	-0.259710	-0.980566
C	-3.950908	1.460132	-1.181175
B	0.023292	0.075155	0.346563
C	0.578044	-1.353675	-0.209316
C	0.960373	-1.396664	-1.553770
C	1.509352	-2.508207	-2.178771
C	0.793412	-2.542833	0.489474
C	1.343061	-3.683173	-0.097476
C	1.705180	-3.670005	-1.438193
F	0.474690	-2.672156	1.800487
F	1.527671	-4.801677	0.631182
F	2.235231	-4.762673	-2.012466
F	0.771515	-0.296449	-2.326895
F	1.844877	-2.476214	-3.482446
O	-0.236211	-0.182841	1.954917
C	-1.453485	0.096348	2.747734
C	-0.193278	0.792136	3.058083
H	0.440877	0.444209	3.866117
H	-0.074677	1.818795	2.731778
H	-2.202852	0.644204	2.185830
C	-1.938660	-1.076920	3.534917
H	-2.576099	-0.735271	4.352405
H	-1.114313	-1.676882	3.917869
Cl	-2.946679	-2.144449	2.484139

		C_1'	
C	0.838350	-2.481949	0.185036
C	1.638258	-3.601633	0.369101
C	2.976596	-3.555291	-0.014720
C	3.493530	-2.387441	-0.569715
C	2.667609	-1.279563	-0.714177

C	1.313001	-1.270786	-0.342171
F	3.228073	-0.187993	-1.276279
F	4.778332	-2.345367	-0.958159
F	3.757906	-4.628786	0.141327
F	1.135587	-4.728041	0.901280
F	-0.450100	-2.603549	0.564906
C	-1.083155	-0.082785	-0.907067
C	-2.040486	0.861570	-0.491180
C	-3.383704	0.787395	-0.840388
C	-3.819328	-0.255452	-1.654743
C	-2.908322	-1.203838	-2.114919
C	-1.575675	-1.102841	-1.738629
F	-0.738920	-2.030733	-2.247661
F	-3.326346	-2.194472	-2.920299
F	-5.107264	-0.339072	-2.004917
F	-4.260806	1.710669	-0.422626
F	-1.683713	1.892909	0.292583
C	1.086451	1.421583	-0.297051
C	0.814715	2.499276	-1.151203
C	1.396003	3.752225	-1.005408
C	2.281591	3.973009	0.047210
C	2.583486	2.935074	0.925867
C	2.000719	1.689205	0.731222
F	2.338457	0.720393	1.608339
F	-0.025035	2.338734	-2.197195
F	1.115598	4.748497	-1.861813
F	2.844203	5.175774	0.210089
F	3.437322	3.147382	1.940902
B	0.423272	0.012284	-0.492593
H	-2.333422	-1.245533	1.634239
C	-2.109550	-1.053619	2.682626
H	-1.936742	-1.990888	3.212897
H	-3.019050	0.025055	4.376874
C	-3.180708	-0.238296	3.332612
O	-3.737358	0.825060	2.535710
C	-4.561676	-0.321130	2.830056
H	-5.387831	-0.135200	3.513081
H	-4.781432	-0.956023	1.973102
Cl	-0.512641	-0.173805	2.703450

REFERENCES

1. Kanazawa, A.; Kanaoka, S.; Aoshima, S. Rational design of oxirane monomers for efficient crossover reactions in concurrent cationic vinyl-addition and ring-opening copolymerization with vinyl ethers. *Macromolecules* **2014,** 47 (19), 6635-6644.

2. Kanazawa, A.; Kanaoka, S.; Aoshima, S. Concurrent cationic vinyl-addition and ring-opening copolymerization using $B(C_6F_5)_3$ as a catalyst: copolymerization of vinyl ethers and isobutylene oxide via crossover propagation reactions. *Journal of the American Chemical Society* **2013,** 135 (25), 9330-9333.

3. Haque, F. M.; Alegria, A.; Grayson, S. M.; Barroso-Bujans, F. Detection, quantification, and "click-scavenging" of impurities in cyclic poly(glycidyl phenyl ether) obtained by zwitterionic ring-expansion polymerization with $B(C_6F_5)_3$. *Macromolecules* **2017,** 50 (5), 1870-1881.

4. Loos, M.; Gerber, C.; Corona, F.; Hollender, J.; Singer, H. Accelerated Isotope Fine Structure Calculation Using Pruned Transition Trees. *Analytical Chemistry* **2015,** 87 (11), 5738-5744.

BIOGRAPHY

Farihah M. Haque was born in Big Rapids, Michigan on February 10, 1992 but spent much of her childhood in Lake Charles, Louisiana. She received her high school diploma from Louisiana School for Math, Science, and the Arts in May 2010, graduating with Distinction for her work, *A Photographic Essay: An Environmental Study of Urban Bangladesh*. Farihah continued onto Loyola University New Orleans pursuing a chemistry degree, developing a love of organic chemistry through many research opportunities, including her research under Dr. CJ Stephenson at Loyola and Dr. Valerie Ashby at UNC Chapel Hill (through an REU program). As a senior, she took physical organic chemistry at Tulane University, where she was introduced to Dr. Scott Grayson. Upon completion of her B.S. in chemistry in May 2014, she enrolled at Tulane University for her PhD in chemistry in Fall 2014 to join Scott's group. During her time here, she earned two awards: the Arlo Harris Fellowship Award for exemplary record as a PhD student (September 2015) and the Best Poster Award at the ACS PMSE poster session (March 2018). Farihah's PhD has been focused on the synthesis and characterization of cyclic polymers while also collaborating with many research groups to understand their unique physical properties, yielding 8 publications (4 first author).

During Farihah's time at Tulane University, she has furthered her interests in graduate and undergraduate education, which includes focusing on issues of diversity and inclusivity in academia. To this end, Farihah worked with the Graduate Students Studies Association from 2015-2017 as a Chemistry Department Representative and Treasurer to be a voice for graduate students. In 2016, she joined Women in Science and Engineering, inspired by all the strong and empowered women working to make Science a more inclusive and accepting space. Finally beginning in November 2017, in light of the potential taxing of graduate student tuition waivers, Farihah joined Solidarity Tulane, a group working with the university administration to provide improved and affordable healthcare to fellow graduate students.

As a graduate student and resident of New Orleans, Farihah has attended countless marches and rallies to fight for marginalized groups and those without voices. In April 2017, she attended the March for Science in DC, inspired by all the people who came together to fight for Mother Earth, who desperately needs our help. In September 2018, she joined Citizens' Climate Lobby (CCL). With a few of her team members, she went to Capitol Hill in November 2018 to lobby for CCL's carbon fee and dividend legislation by meeting with nearly the entire Louisiana congressional delegation.

Upon completion of Farihah's doctorate, she is moving to Minneapolis, Minnesota to work as a postdoctoral fellow in the Center for Sustainable Polymers at the University of Minnesota under the direction of Dr. Marc Hillmyer. She is very excited for her new research prospects towards tackling some of today's biggest consumer concerns by researching new sustainable, biodegradable, and recyclable materials using renewable resources to replace current industry standards that continue to pollute our planet. She hopes to continue to maintain her educational and climate advocacy interests by addressing these as dual scientific and social justice issues.